Observation-Based Conceptual Site Modeling Framework Combining Surface Geophysical, Direct Push-Based, Hydrogeochemical and Stable Isotope Methods

Dissertation

der Mathematisch-Naturwissenschaftlichen Fakultät

der Eberhard Karls Universität Tübingen

zur Erlangung des Grades eines

Doktors der Naturwissenschaften

(Dr. rer. nat.)

vorgelegt von

M.Sc. Ahamefula Udume Utom

Geboren am 18.09.1985, aus Ubam Ugwuegu (Afikpo), Nigeria

Tübingen

2018

Tag der mündlichen Qualifikation:	11.02.2019
Dekan:	Prof. Dr. Wolfgang Rosenstiel
1. Berichterstatter:	Prof. Dr. Peter Grathwohl
2. Berichterstatter:	Prof. Dr. Peter Dietrich

Acknowledgements

First of all, I sincerely thank Prof. Dr. Peter Dietrich for the immense opportunity to work on this project. His supervision, mentoring and continuous support throughout the last 4 years was great and will never be forgotten. I am equally grateful to Dr. Ulrike Werban, who worked hand-in-hand with Prof. Dr. Peter Dietrich to ensure that I enjoyed the most serene and highly motivating work atmosphere offered by the Department of Monitoring- and Exploration Technologies (MET), Helmholtz Centre for Environmental Research (UFZ), Leipzig, Germany. I am thankful for the opportunities given to broaden my horizon via conferences, and short courses.

I appreciate the many creative suggestions by Dr. Carsten Leven (Center for Applied Geoscience (ZAG), Eberhard Karls Universität Tübingen). It was an honor to have had the opportunity to receive advice from Dr. Carsten Leven. I also thank Prof. Dr. Christiane Zarfl for accepting to serve as a member of my doctoral oral examination committee.

Equally responsible for narrating and elucidating the nitrate plume side of the story that sparked my attention was Prof. Dr. Peter Grathwohl (ZAG), during a short field visit in 2014. I would like to thank Dr. Marc Schwientek (ZAG) for sharing historic data, and insightful preliminary results. In the same vein, I thank Dr. Thomas Wendel (ZAG) for taking time to analyze the groundwater samples for the bicarbonate species.

I can never forget that the identification of anomalous resistivity paradigm discussed in this dissertation was made possible by the resilient nature of my great friend of heart of gold Constantin Vogt (of blessed memory) who passed away in an avalanche accident near Lauenen in Switzerland in late February 2018.

I would also like to express my gratitude to Dr. Kay Knöller (Department of Catchment Hydrology, UFZ, Halle), who did not hesitate to offer me the opportunity to use his laboratory for Stable Isotopes Analyses. I am indebted to Dr. Christin Müller who gave me all the necessary assistance during the evaluation of the stable isotope analytical results. I appreciate the effort of Petra Blümel and Martina Neuber in the stable isotopes analyses.

I thank Dr. Sibylle Mothes, Ines Volkmann, and Heidrun Paschke, of the Department of Analytical Chemistry (UFZ, Leipzig) for their assistance during major ions concentration measurements.

I also thank Dr. Carsten Vogt (Department of Isotope Biogeochemistry, UFZ, Leipzig), for accepting to critique some parts of this thesis.

Without the help of several people in MET, UFZ (Leipzig), a smooth start from field studies to evaluation of data would have been impossible. I benefitted a lot from the field geophysical experience of Marco Pohle. The operation of the direct push tools would not have been fun without the technical assistance of Helko Kotas and Andreas Schoßland. To evaluate refraction seismic and electrical resistivity imaging results, Dr. Hendrik Paasche and Dr. Claudia Schütze provided immense support. Thanks to Dr. Steffen Zacharias for putting me through geostatistical variogram analysis. Many thanks are due to colleagues (former and present) at the MET Department for stimulating and fruitful discussions.

A big thank you to my wonderful friends in the UFZ, Leipzig and Germany at large for making me feel at home.

My gratitude also goes to Profs. Benard I. Odoh, Anthony U. Okoro and Boniface C.E. Egboka, of the Nnamdi Azikiwe University, Awka (Nigeria) for their scientific guidance, and preparing me for this doctoral studies. Their moral advice was highly rewarding.

German Academic Exchange Service/Deutscher Akademischer Austauschdienst (DAAD) majorly financed this doctoral work. This work was also partly supported by the German Research Foundation (DFG). Special thanks also go to the "Society of Exploration Geophysicists (SEG)" Foundation for the 2013 – 2014 educational program scholarship awards. The "Helmholtz Interdisciplinary GRADuate School for Environmental Research (HIGRADE)" provided exciting courses, career development possibilities and travel grants during the doctoral research period.

Most importantly, I am deeply grateful to my family, in particular to my wife, Chisom Rosemary for her support and patience. This dissertation is also dedicated to my wife and little boy Benjamin who endured my absence from many family occasions with smiles.

Summary

Initial environmental and analytical data quality plays an important role in the cost-effective and successful cleanup of impacted soil and groundwater systems. In the absence of complete subsurface data, mathematical models are commonly developed to simplify complex dynamic interactions of natural processes. However, ecosystem functions are beset with high uncertainties that are too poorly understood to permit good modeling with a generalized numerical code. Due to sparse subsurface information and lack of flexibility, traditional methods of observation also lack sufficient uncertainty management characteristics. To capture significant contributors to data uncertainty and minimize faulty conclusions, an adaptive conceptual site model (CSM) approach of site investigation is therefore required to test hypotheses. The approach differs from the traditional methods in terms of the strategic work plan, targeted sampling, and the ability to minimize irrelevant field mobilizations. Under the framework of the CSM approach, carefully selected multimethods tend to iteratively leverage each other's strengths. This dissertation examines the combined use of surface geophysical, direct push, and laboratory analytical tools in the evaluation of a subsurface CSM at the Wurmlingen study site (between Rottenburg am Neckar and Tübingen), southwest Germany. The general objective of this study was the assessment of the subsurface conditions in an attempt to quantify solute sources, fluxes, fate and transport at the nitrate plume scale. Geoelectrical resistivity measurements identified the presumable distribution of the subsurface structures and revealed a linearized anomalous low-resistivity feature aligned with the northwest – southeast trend of the investigated nitrate plume. Seismic refraction in conjunction with the direct push-based reverse vertical seismic profiling evaluated the subsurface structural integrity in relation to the bedrock structure. A channelized low P-wave velocity zone was detected and associated with the identified low-resistivity feature. Direct push-based soil electrical conductivity signatures and soil lithostratigraphy corroborated the channelized structure as an alluvium-bedrock interface capable of promoting groundwater exchange between the channelized deeper aquifer compartment and the surrounding shallower aquifer compartment. On the floodplain part of the study site, solute concentrations of groundwater samples collected using a direct push-based multilevel sampling device revealed steep geochemical gradients indicating higher fluxes of solutes associated with the channelized structure, which appears to represent a preferential flow path and a potential chemical hotspot within the nitrate plume. Stables isotope ratios also indicated that the source of the nitrate transported from the land surface through recharging water into the aquifer has been biogeochemically transformed and distinctly partitioned into soil organic nitrogen in the shallower compartment and animal (manure)/septic waste in the deeper flow compartment. It is observed from the combined evaluation of the groundwater chemical and dual stable isotope data that a diffusion-limited hydrologic transport mechanism created by the channelized aquifer system coupled oxic nitrate removal process in the shallower compartment depleted in the dual isotopes of nitrate to nitrate source admixture and remineralization processes in the deeper channelized compartment enriched in the dual isotopes of nitrate. Nevertheless, I hypothesize that explicit consideration of the role played by microbes in cycling the nitrogen nutrients transferred to them will lead to a clearer understanding of these alternative nitrogen-cycling pathways. A key finding emerging from this study is that there is a major shift in the nitrogen-cycling routes commonly associated with the canonical theories of oxic nitrification and anoxic denitrification. Another major finding is that the geohydrology of the area exerted dominant control on the complex nitrogen biogeochemical transformation pathways. In particular, the observation of anoxic nitrification in the deeper aquifer compartment appealed to field evidence for the resolution of the occurrence of what Granger and Wankel (2016) (see Supplementary Information - S1) reported as the "freshwater conundrum." The complexities in the identified hydrobiogeochemical pathways suggest that the understanding of nitrogen-cycling processes in aquifer systems is far from complete and requires further research. This study highlights the necessity of realistically acknowledging the high degree of aquifer physical and biogeochemical heterogeneity, as well as varying solute source origins in the CSM evaluation procedure. Logical incorporation of nitrogen-processing information into the resolution of aquifer structural conditions not only allows for a better definition of mobility, persistence and transformation pathways of nitrate and other dissolved constituents but also alleviates concerns regarding the transparency of decision-making.

Zusammenfassung

Die Qualität der anfänglichen Umwelt- und Analysedaten spielt bei einer kostengeffizienten und erfolgreichen Sanierung verunreinigter Boden- und Grundwassersysteme eine wichtige Rolle. Sollten vollständige Daten zum Untergrund fehlen, werden im Allgemeinen mathematische Modelle zur Vereinfachung der komplexen dynamischen Wechselwirkungen entwickelt. Allerdings sind Ökosystemfunktionen mit einer Vielzahl von Unsicherheiten verbunden, die kaum verstanden werden, um mit verallgemeinerten Zahlen eine gute Modellbildung zu ermöglichen. Aufgrund spärlicher Informationen zum Untergrund und mangelnder Flexibilität verfügen traditionelle Beobachtungsmethoden auch nicht über ausreichende Unsicherheitsmanagementmerkmale. Um wesentliche, zur Datenunsicherheit beitragende Faktoren zu erfassen und fehlerhafte Schlussfolgerungen zu minimieren, ist für Standorterkundungen ein adaptiver, sprich anpassungsfähiger, konzeptioneller Standortmodell- (CSM) Ansatz erforderlich, um Hypothesen zu testen. Der Ansatz unterscheidet sich von den traditionellen Methoden im Hinblick auf den strategischen Arbeitsplan, die gezielte Beprobung und die Fähigkeit, irrelevante Feldmobilisierungen zu minimieren. Im Rahmen des CSM-Ansatzes neigen sorgfältig ausgewählte Mehrfachmethoden dazu, iterativ jeweils von den Stärken des anderen zu profitieren. Bei dieser Dissertation wurde am Untersuchungsstandort Wurmlingen (zwischen Rottenburg am Neckar und Tübingen), im Südwesten Deutschlands, in der Auswertung eines konzeptionellen Untergrund-Standortmodells (CSM), der kombinierte Einsatz von oberflächen-geophysikalischen, Direct-Push- und Laboranalysewerkzeugen untersucht. Das allgemeine Ziel dieser Studie bestand in der Beurteilung der Untergrundverhältnisse und dem Versuch, im Rahmen einer Nitrat-Schadstofffahne die Ursprünge gelöster Substanzen, Ströme, den Verbleib sowie den Transport zu quantifizieren. Geoelektrische Resistivitätsmessungen ermittelten die voraussichtliche Verteilung des Untergrundaufbaus und offenbarten bei der untersuchten Nitrat-Schadstofffahne eine von Nordwesten nach Südosten verlaufende, geringe linearisierte anomale Resistivität. Mittels Refraktionsseismik in Verbindung mit Direct-Push-basierten entgegengesetzten vertikalen seismischen Messungen wurde die strukturelle Integrität des Untergrunds in Bezug auf die Struktur des Grundgesteins untersucht. Es wurde eine kanalisierte geringe P-Wellengeschwindigkeitszone festgestellt und mit der ermittelten geringen Resistivität in Verbindung gesetzt. Die Direct-Push-basierten Signaturen der Leitfähigkeit des Bodens und die Boden-Litho-Stratigraphie bekräftigten die kanalisierte Struktur als eine Schwemmstoff-Grundgesteinsschnittstelle, die in der Lage war, einen Grundwasseraustausch zwischen der kanalisierten tieferen, grundwasserführenden Kammer und der umliegenden seichteren, grundwasserführenden Kammer zu fördern. Im Vorland des Untersuchungsstandortes offenbarten die löslichen Konzentrationen der, mit Hilfe eines Direct-Push-basierten mehrstufigen Probenahmegerätes gesammelten Grundwasserproben steile geochemische Gradienten, die in Verbindung mit der kanalisierten Struktur auf höhere Ströme gelöster Substanzen hinwiesen, was für einen bevorzugten Strömungsweg zu stehen scheint und einen potentiellen chemischen Hotspot innerhalb der Nitrat-Schadstofffahne. Stabile Isotopen-Verhältnisse wiesen auch darauf hin, dass die Quelle des Nitrats, das von der Landfläche über neuausgebildetes Wasser in die Grundwasserleiter befördert wird, bio-geochemisch umgewandelt und in der seichteren Bodenkammer deutlich in organischen Stickstoff sowie in der tieferen Strömungskammer in tierische (Gülle) /septische Abfallstoffe unterteilt wurde. Bei der kombinierten Auswertung der chemischen und zweifachen stabilen Isotopen-Daten des Grundwassers wurde festgestellt, dass ein diffusionslimitierter hydrologischer Transportmechanismus, der durch den, mit dem kanalisierten Grundwasserleitersystem gekoppelten oxischen Nitratabbauprozess in der seichteren Kammer geschaffen wurde, in der die zweifachen Nitratisotope zu Nitratbeimischungs- und Remineralisierungprozessen verbraucht wurden, in der tiefer kanalisierten Kammer in den zweifachen Nitratisotopen angereichert wurden. Nichtsdestotrotz gehe ich davon aus, dass eine explizite Berücksichtigung der Rolle, die Mikroben bei dem an sie übertragenen Stickstoffkreislauf haben, zu einem deutlicheren Verständnis dieser alternativen Stickstoffkreislaufpfade führen. Eine zentrale Erkenntnis aus dieser Studie besteht darin, dass es eine erhebliche Verschiebung bei den Stickstoffkreisläufen gibt, die im Allgemeinen mit den kanonischen Theorien der oxischen Nitrifikation und anoxischen Denitrifikation verbunden werden. Ein weiteres wesentliches Ergebnis besteht darin, dass die Geohydrologie des Gebietes die komplexen bio-geochemikalischen Stickstofftransformationspfade beherrschend kontrolliert hat. Insbesondere die Beobachtung der anoxischen Nitrifikation in der tieferen grundwasserführenden Kammer bietet den Nachweis für die Schlussfolgerung dessen, was Granger und Wankel (2016) als „Frischwasser-Rätsel“ beschrieben haben (siehe Zusatzinformationen - S1). Die Komplexität der festgestellten hydro-bio-geochemischen Pfade lässt vermuten, dass das Verständnis der Stickstoffkreislaufprozesse in den Grundwasserleitersystemen bei Weitem noch nicht

abgeschlossen ist und weiterer Forschung bedarf. Diese Studie zeigt die Notwendigkeit auf, im CSM-Bewertungsverfahren realistisch den hohen Grad an physikalischer und bio-geochemischer Heterogenität der Grundwasserleiter als auch die unterschiedlichen Ursprünge gelöster Substanzquellen anzuerkennen. Die folgerichtige Einbindung der Informationen zur Stickstoffverarbeitung in die Schlussfolgerung über die strukturellen Wasserleiterbedingungen ermöglicht nicht nur eine bessere Bestimmung der Mobilität, Langlebigkeit und Transformationspfade von Nitrat und anderen gelösten Bestandteilen, sondern nimmt auch Bedenken bezüglich der Transparenz von Entscheidungsfindungen.

Table of contents

List of figures

List of figures

List of figures

List of figures

List of figures

List of tables

"*I consider it certain that we need a new conceptual model, containing the known heterogeneities of natural aquifers, to explain the phenomenon of transport in groundwater*"
Charles V. Theis (1967)

Chapter 1
General introduction

1.1 Background and scope of study

Cost-effective, efficient, defensible, and successful cleanup of impacted soil and groundwater systems depends on the initial environmental and analytical data quality (Ritzi et al., 2004; Cypher and Lemke 2009). However, the limited data regarding subsurface conditions have failed to sufficiently capture all major contributors, representing data uncertainty. This has invariably hampered contaminated site assessment, environmental management, and remediation efficacy. Scale and heterogeneity have been identified as the major causes of data uncertainty (Engdahl et al., 2010; Dogan et al., 2011; Sudicky and Illman 2011; Gazoty et al., 2012; Berg and Illman 2013). On the one hand, upscaling or downscaling requires adequate understanding or good knowledge of processes occurring at the smaller or larger scales (Zyvoloski et al., 2003; Tetzlaff et al., 2010; Gentine et al., 2012; Chien and Mackay, 2013) in the natural system. The extrapolation of such understanding to a smaller or larger scale may require additional knowledge of small- or large-scale variability. If this need for additional knowledge is not recognized, then an implicit assumption of "scale invariance" is made, and if this assumption is false, the interpretation of measurements or model evaluation exercises and assumptions may be erroneous (Halm and Grathwohl, 2005). On the other hand, inability to quantify contaminant heterogeneity associated with the distribution of pollutant release and physical mechanisms that control their migration can also lead to major decision errors (Taylor et al., 2005; Ouellon et al., 2008; Li et al., 2011; Tang et al., 2014; Han et al., 2014). Moreover, because the subsurface is not an ideal homogeneous and isotropic medium, inhomogeneities in the spatial distribution of geologic and hydrogeologic properties can alter the groundwater flow regime and, consequently, contaminant transport velocity (Bermejo et al., 1997). Deficient understanding of these conditions produces misleading pictures of contamination if data uncertainties are not controlled, unless the decision-maker develops and tests predictions and assumptions regarding where elevated chemical constituents of concern would be, if present (Crumbling, 2004).

In the absence of extensive field data and observations regarding subsurface conditions, "verification" or "validation" of conceptual site models has been carried out by employing numerical modeling (Bain et al., 2000; Davies et al., 2004; Bredehoeft, 2005; Jankovic et al., 2006; Cirpka and Valocchi, 2007; Barazzuoli et al., 2008; Akber Hassan and Jiang, 2012). Although numerical models are able to represent processes that simplify the understanding of transient flow and transport in complex natural systems, they do not restore confidence in their results due to either possible uncertainties in the choice of model parameters and characteristics or sparsity of data, including a deficient account of the heterogeneity required to adequately initialize the model (Miles, 2007; Sousa

et al., 2012; Nordstrom, 2012; Tremblay et al., 2014). Where such knowledge of uncertainty is unavailable, environmental scientists and engineers are encouraged to develop and evaluate conceptual site models (CSMs) to facilitate the thought process regarding which actions to prioritize as part of a site characterization and modeling process (Nikolaidis and Shen, 2000).

A CSM plays a major role in the development of hypotheses, identification of data gaps and management of uncertainty (Burger et al., 2006; Matott et al., 2009; Siontorou and Batzias, 2012; Greenberg et al., 2014). A well-developed CSM could also assist in the design of long-term solute concentration monitoring programs. A CSM as a planning tool is generally the result of the problem formulation phase ("conceptual exposure model") of soil and groundwater risk assessment (Crumbling et al., 2001; Thornton and Wealthal, 2008). It characterizes the physical, chemical, and biological system existing at a site by determining CSM elements such as: (1) hypothesized sources of the release of constituents of concern, including the extent, location, concentrations and chemical form(s); (2) their pathways, including not just the physical pathways of migration that facilitate the transport of the constituents but also the biogeochemical transformation pathways; and (3) environmental receptors' exposure to the constituents of concern, including understanding of the receptor location and site-specific conditions. Investigators have demonstrated the importance of developing and evaluating CSMs in fate and transport, as well as in remediation programs, and the associated pitfalls (Mackay et al., 1996; Crumbling et al., 2003; Woll et al., 2003; Crumbling et al., 2004a; Almasri, 2007; Canter, 2008).

This study emphasizes nitrogen processing in an alluvial aquifer. Nitrogen is a major constituent of the Earth's atmosphere and occurs in many different forms, such as elemental nitrogen, nitrate (NO_3^-) and ammonia (NH_3). Whereas ammonium (NH_4^+, that is, the ionic form of NH_3) is quickly absorbed by the rock matrix of the soil, NO_3^- is not bound and can move with soil water and therefore has the potential to be lost through leaching from the soil zone into the aquifer system. Nitrate is highly bioavailable and is the dominant nitrogen component delivered to the aquatic systems. Increases in nitrogen inputs from geogenic/natural sources and/or fixation by nitrogen-fixing bacteria in soil and root nodules of leguminous plants (Holloway et al 1998; Lowe and Wallace 2001; Atkins and Jones 2010), nitrogen oxide emissions and atmospheric depositions (Murdoch and Stoddard, 1992) and land-use changes and other various forms of anthropogenic inputs (Galloway et al., 2008) have resulted in environmental problems, such as nitrogen saturation (Stoddard, 1994), eutrophication (Diaz and Rosenberg, 2008) and groundwater contamination (Spalding and Exner, 1993; Burow et al., 2010). Due to these increases in nitrogen inputs and their effects, there is growing interest in methods and processes that can remove the various forms of nitrogen from ecosystems (e.g., Stelzer and Bartsch, 2012; Lansdown et al., 2012) through different scales of studies (e.g., network-scale and/or continental-scale) (e.g., Alexander et al., 2009; Hall et al., 2009).

Böhlke et al. (2006) highlighted the necessity to evaluate the physical and biogeochemical processes before the movement and fate of nitrogen compounds in contaminated or uncontaminated aquifers can be rationalized or predicted. It is well known that transformation, retention and removal processes of available nitrogen occur in upland soils (Seitzinger et al., 2006), riparian zones (Duff et al., 2008), hyporheic zones, where groundwater and surface water mix (Zarnetske et al., 2011), and the surface water of streams and rivers (Heffernan et al., 2010). However, compared to these other environments, such as surface soils, streams, rivers and the open ocean, much less is known about nitrogen processing in the terrestrial subsurface below the water table. According to Smith et al. (2006),

detailed studies on groundwater nitrification as a process are lacking. How the process interacts with the physical environment and biogeochemical turnover present in an aquifer to control the transport and attenuation of nitrogen is still open to further investigation. Most of the many barriers to accurate assessment of biogeochemical processes (a major control of dissolved oxygen and nitrogen concentrations and speciation) have been attributed to the inaccessibility of the subsurface and the spatiotemporal heterogeneity and deficient parameterization of the system's physical, chemical and biological processes. While representative cores can be difficult and expensive to obtain and may yield overestimates during laboratory-based bench-scale control rate studies (Chapelle et al., 1993), field tracer tests (Krueger et al., 1998) can also have shortcomings due to the slow nature of subsurface microbial processes, particularly in pristine environments, which can make the rates of activity difficult to measure (Ghiorse et al., 1988). Moreover, some tracers, such as NH_4^+, are not transported conservatively.

To evaluate the CSM of the subsurface in the context of nitrogen processing in an alluvial aquifer, the challenges lies in adequate representation of the nutrient's sources and sinks, as well as identification of key interfaces/connectivity that influence the nutrient cycling within the aquifer system. The capability to resolve these challenges signals that there is a good understanding of how the system works, which can be translated into the following key questions:

a) Through which hydrological pathways is the nutrient physically transported?
b) What is the origin of the nitrogen nutrient, and where at the site are its source areas?
c) What are the effects of the parent materials and development of the hydrologic pathways on the nitrogen nutrient cycling, and what biogeochemical processes are likely to occur?

These key questions and unknowns to be investigated basically express and constitute the components of an initial CSM evaluated from the problem scoping process involving the site history review in terms of the existing information on the site boundary, historic and current site conditions, source release histories and potential chemical constituents of concern, area(s) of release, and site-specific and/or regional information (geology, hydrogeology, and hydrogeochemistry) to help identify surface and subsurface transport pathways (e.g., Ehrlich, 1988).

Due to the invisibility of the subsurface, CSMs will always be evaluated based on assumptions and data interpretations. Because no single line of evidence can answer key CSM questions, attention is often turned to combining multiple lines of evidence from different testing and multiple investigation methodologies to balance the degree of uncertainty. However, conventional approaches to site characterization provide answers to the questions in disaggregated forms. This means that management decisions on the nitrogen nutrient sources and transport mechanisms could therefore prove more difficult. The CSM approach acknowledges the unique strengths of different methods of investigation. Organization of available evidence under the flexible and adaptive CSM approach is more reliable, resulting in a better understanding of the dynamic processes that characterize the nutrient cycling behavior. This is because the different investigation methods are most effective when combined. During the initial CSM testing and evaluation, any line of evidence that is challenged is iteratively upgraded using additional features from the newly acquired data. An updated CSM is then expected to have proved or disproved and/or filled data gaps from the initial or sketchy CSM. By being able to create a CSM, one can tell a "story" of a site in a format that is easy to read, see and understand, as well as identify uncertainties in the model that require further assessment. Thus, the CSM serves as a

risk communication tool for the public and for efficient environmental decision-making.

To augment the framework of a CSM by describing a site, including its geology, hydrogeology and pathways of migration of NO_3^- (and other groundwater solutes), sources of release, and fate mechanisms, this study evaluated data from complementary, corroboratory and confirmatory surface geophysical, direct push-based and laboratory analytical (chemical and stable isotope) methodologies. A literature review of the methods indicates that these methods have different strengths in relation to the aforementioned CSM questions. For instance, whereas surface geophysical techniques could potentially map large-scale physical heterogeneities as well as finer-scale structures (including potential hydrologic pathways), follow-up direct push investigations define the target features delineated by the surface geophysical studies in a much higher resolution. Because an individual approach is not sufficient to unambiguously identify and localize processes, the surface geophysical and direct push approaches are combined to leverage each other's strengths. Irrespective of the potential successes of the surface geophysical and direct push approaches in evaluating a subsurface CSM, one formidable challenge remains in the end: how to develop an understanding of, for example, nitrogen nutrient sources and the cycling, transport or fate of redox-active constituents and integrate such process knowledge into the subsurface model. This requires gaining detailed insight into the physical mechanisms and biogeochemical interactions from multilevel groundwater chemical and dual-stable isotope data measured and analyzed in the field or laboratory to complement the surface geophysical and direct push observations. The necessity for such further studies arises from the fact that several determinants obscure the reconstruction of the geochemical characteristics of solute sources. For instance, mixing processes, which are mostly localized at the interface between two distinct geohydrologic media, could have consequences for biogeochemical turnover of the solute. Mixing-controlled biodegradation is frequently proven via numerical simulations and bench-scale laboratory experiments (Cirpka et al., 1999). Additionally, complex CSMs for reactive transport modeling have been appropriately defined and successfully developed at laboratory scale (Davies et al., 2004). The same cannot be said for CSM development at field scale. This is due in large part to conventional approaches for characterizing complex subsurface conditions, which are unable to adequately capture heterogeneous/preferential flow paths and the location of transition zones that control steep biogeochemical gradients. Hence, by evaluating closely spaced solute concentration data and stable isotope information across mixing interfaces defined by surface geophysical and direct push investigations, it is possible to develop an enhanced predictive and mechanistic understanding of nitrogen fate and transport in an aquifer system. This approach couples independent constraints of aquifer physical and biogeochemical heterogeneity and their impact on nitrogen sources, fate and transport while providing insight into uncertainties that mar the accurate depiction of field-scale CSMs.

1.2 Objectives

This dissertation is based on a study with two major objectives:

1. Use of surface geophysical measurements in combination with the direct push tools to evaluate subsurface structural variability in an attempt to gain knowledge of fluid and solute flow pathways;
2. Determine, from field/laboratory chemical and multi ('dual')-stable isotopic measurements, the sources of solutes and associated nitrogen nutrient transformation pathways using aquifer groundwater collected based on a high-resolution direct push multilevel groundwater sampling technique.

A case study is presented using the agriculturally impacted Wurmlingen study site where a plume of NO_3^- was previously described in an alluvial aquifer setting (Schollenberger, 1998), thereby illustrating the potential benefit of utilizing the CSM approach for efficient subsurface characterization and evaluation.

1.3 Dissertation outline

This work is organized into five chapters. The first chapter addresses the general introduction of the study, scope of the study, and objectives and structure of the dissertation. In the second chapter, the motivation of the CSM approach is described. Chapter two also illustrates an observation-based CSM approach, including the target-oriented site characterization and laboratory analytical tools employed.

The third chapter presents the application of surface geophysical and direct push investigation methods. This chapter is subdivided into two parts. (Part 3A) Description of the study site location, geohydrology and relevance. Part A of Chapter three also describes the study site-specific CSM and brief information regarding an earlier attempt at characterizing the NO_3^- plume in question. (Part 3B) Combined interpretation of surface geophysical and direct push-based ground-truth data for the characterization of subsurface structural heterogeneity and geometry. In Part 3B, two-dimensional (2-D) electrical resistivity imaging and refraction seismic tomography investigations of specific survey profiles were motivated by a large-scale preliminary field screening of the subsurface conditions based on Schlumberger resistivity depth sounding surveys. The field screening test provided a rough estimation of subsurface structural variations in terms of the apparent resistivity distribution and served as the basis for the development of further investigation methods. The 2-D electrical resistivity imaging results not only confirmed the interpretation of the vertical electrical sounding results but also helped overcome the limitations of the 1-D nature of the vertical electrical sounding surveys, which are based on the assumption of intra-stratigraphic homogeneity. Despite visually apparent discrimination of subsurface structures in terms of the resistivity variations, the electrical resistivity imaging results had difficulty resolving the aquifer substratum on the floodplain part of the study site, possibly due to the poor vertical resolution of the deeper subsurface. Direct push-based reverse vertical seismic profile data assisted in enhancing the credibility of the refraction seismic tomography result, which delineated the unresolved bedrock surface. The noninvasive surface geophysical tools preceded minimally

invasive direct push-based techniques and assisted in the selection of suitable locations for these intrusive investigations. Correlations between the surface geophysical response and the direct push-based soil electrical conductivity and lithological logs were used to evaluate the reliability of the subsurface geometry and architectural pattern.

Chapter four is particularly consequential in the assessment of changes in geochemical and stable isotopic tracers and footprints, which track water movement and fluxes in relation to the aquifer structural patterns interpreted in Part B of Chapter three. In addition, this chapter significantly improves the conceptual understanding of the hydrogeochemical evolution, origin and fate of solutes. Chemical data was used to assess the water-rock interactions and redox conditions with regards to the NO_3^- dynamics. Dual stable isotopes were not only useful in determining groundwater recharge origin and solute sources but also valuable in evaluating the physical and biogeochemical processes that influence the fate of the NO_3^-.

Following this, Chapter five presents a general discussion, conclusions, and the scientific impact, as well as recommendations regarding future studies.

Chapter 2

Observation-based conceptual site modeling and site investigation methodologies

Chapter summary

Although mathematical/ numerical modeling is able to simplify assumptions of transient flow and solute transport, due to sparsity of data and deficient understanding of all of the factors that influence the heterogeneity of complex environmental systems, it is unable to restore confidence in their results. Moreover, due to rigid workplans, spatially limited and invariably time-consuming and cost-intensive investigation strategies, conventional approaches developed independently of each other are also often unable to fill data gaps required to make predictions. This chapter discusses the need for an observation-based conceptual site modeling framework, including the work flow for selecting and employing target-oriented site characterization and laboratory analytical techniques. The target-oriented site investigation methodologies consist of multidisciplinary tools that are iteratively integrated to leverage each other's strength. Consequently, in particular, data acquired under the flexible and adaptive observation-based conceptual site modeling framwork could restore reliability in mathematical modeling studies.

2.1 Introduction

Without an adequate identification of the physical and biogeochemical processes providing different end-member solute sources (i.e., natural and anthropogenic), the management practices for groundwater resources and other environmental media are fraught with uncertainties. To model these processes, many mathematical methods and numerical modeling approaches have emerged as powerful tools of great significance. In groundwater systems, for instance, such modeling methods are able to represent processes to simplify and approximate the present understanding of transient subsurface fluid flow in addition to solute fate and transport by integrating existing knowledge into a logical framework of rules, relationships and governing equations, each of which is solved through the use of numerical or analytical techniques (Christakos and Hristopulos, 1996; Rolle et al., 2011; Maier et al., 2013). It is widely argued that developing a mathematical model is advantageous to developing an observational model; for example, experimentation within a real system is costly and time-consuming or even impossible, while mathematical model simulations are repeatable and can generate easy-to-

interpret, quantitative results (Zeigler, 1976; Ziegler, 2006). Such results can then be generalized, thereby resulting in new models that can be subsequently validated for similar situations elsewhere (Kapur, 2015). However, the development of such models can be challenging, and the corresponding results often lack confidence due to an incomplete conceptual understanding (Oreskes and Belitz, 2001; Hassan, 2004; Tetzlaff et al., 2008) and due to uncertainties associated with limited site-specific data on subsurface features and processes (Moradkhani, 2005). That is, any imprecision in the conceptual model rigorously influences the outcome of the mathematical model and its reliability. Additionally, the complex factors that govern the movement and behaviors of groundwater contaminants in natural settings for most environmental and ecosystem modeling studies are poorly understood (Ellsworth, 1996; Corwin, 1999). In this context, the sole reliance on mathematical modeling can be dangerous and would provide little to no contribution to the effective communication of impending environmental risks.

Models have been termed "verified" or "validated" to prove that the accuracy and predictive capabilities of those mathematical models lie within the acceptable limits of error determined through tests independent of the calibration data. Nonetheless, Oreskes et al. (1994) suggested that models of natural systems cannot be verified/validated simply because a model could be calibrated regardless of whether an observation is poorly predicted, following which the cause of a natural process would not be properly known, and thus, the results cannot be regarded as the absolute truth. Thus, uncertainties are inevitable when creating a model (Konikow and Bredehoeft, 1992; Walker et al., 2003; Beven, 2009). This usually leads one to question the effectiveness or usefulness of models for decision-making purposes. Conceptual uncertainties, which are uncertainties in the conceptualization of a model attributable to an inadequate representation of physical and biogeochemical processes, an incomplete understanding of the subsurface geological framework, and an inability to properly explain most available observations of state variables (Pathak et al., 2015), are often used to quantify the usefulness of a model. Further efforts to quantify and minimize such conceptual uncertainties have focused on the use of multiple models under different uncertainties (Li and Tsai, 2009; Troldborg et al., 2007). Some investigators (e.g., Neuman, 2003; Ye et al., 2005) employed a multi-model approach to demonstrate how well different models represent the behaviors of a system by believing that only one conceptual model for a particular site could lead to poorly informed decisions (Neuman and Wierenga, 2003). To address such conceptual uncertainties, Bayesian model averaging (BMA) is commonly implemented (Rojas et al., 2008; Singh et al., 2010) to aggregate the outputs from competing models. In an integrated BMA framework, posterior model weights are obtained for a set of alternative (i.e., conceptual) models based on the relative ability of an individual model to reproduce the behavior of the system. Usually, these weights are determined by evaluating how well different models match the available data composed of predictive variables using Bayesian probability theory (Leube et al., 2012; Wöhling et al., 2015). Exemplarily, in an effort to detect initial groundwater contamination in a 3-D heterogeneous alluvial aquifer, Storck et al. (1997) present a Monte Carlo-based monitoring well network design optimization strategy. At an existing landfill site, the authors revealed the success of the method in determining whether the existing well network is suboptimal or optimal with respect to the considered objective. However, due to the assumption that goes into the building of a complex subsurface model, the authors did not fail to mention the need for siting larger number of wells in order to increase the expected contaminated volume of the detected plumes. Based on the notion that

it is difficult, if not impossible to obtain complete and detailed distribution of a heterogeneous subsurface domain in another example, Cadini et al. (2012) also applied a novel particle tracking scheme to estimate the extent and timing of solute transport through a preferential pathway. Although these approaches are famed for their abilities to produce models with respectable diagnostic and predictive capabilities, they still exhibit limitations insomuch that the assignment of the prior weights remains subjective even with the available data. This means that the credibility of the model structure depends entirely upon the degree of the measurement accuracy and the uncertainty associated with that accuracy (Thomsen et al., 2016).

CSMs represented either pictorially or in written form are greatly helpful for identifying surface and subsurface transport pathways. The use of a CSM at contaminated sites is well-established (US EPA, 2002). The standard guide for establishing a CSM effectively illustrates how to overcome the challenge of data insufficiency based on the traditional use of field/laboratory methods and strategies (ASTM Standard E1689-95, 2014). Even though traditional observation techniques have embraced modernization, which has led to fast and inexpensive computing, the lack of flexibility and the uncertainty in the management characteristics associated with traditional approaches means that the acquired data (even if they possess high spatial and temporal resolutions) are not scaled relative to the strengths of those different techniques. When combined, such disparate datasets are unlikely to properly address the posed research questions. Thus, in conjunction with traditional CSM guidelines, fact modelers often base their decisions on the appropriateness of the available information and subjective judge the scale of the model, and thus, these modeling approaches remain flawed. A typical example of this situation was demonstrated by Hassan et al. (2002) and Hassan and Chapman (2006) as cited in Benning et al. (2009). In Amchitka Island's subsurface, Hassan et al. (2002) used hydraulic conductivity, recharge, fracture porosity, dispersivity, and other heat driven flow uncertainties to develop a 2D radionuclide transport model. The study was aimed at determining travel times and potential seepage locations in an effort to improve risk assessment. On the incorporation of additional data from bathymetric and magnetotelluric (MT) survey results regarding the depth of the transition zones and effective porosities, Hassan and Chapman (2006) revised the 2002 statistical groundwater model and found that for all realizations, the travel times were greater than the 2,200 year modeled time scale. The main lesson from this illustration is that a model should not be justifiably modeled without complementary phenomenological experimentation.

Much of the present-day discussion on the integration of data in environmental science has focused on the value of information analysis linked to specific problems; that is, the primary goal is to collect not only high-resolution data but also representative data and to interpret results appropriately given the questions being asked. Accordingly, this paper explores how an adaptive, observation-based CSM approach could be used to identify the key components of a CSM and the extent to which those components control the variables that could obscure the data interpretation and lead to faulty conclusions. This approach is not new or dissimilar to traditional approaches with regard to the applications of field and laboratory tools. Instead, the proposed approach is different from traditional methods because of its uncertainty management and improved decision-making characteristics, high-resolution/targeted sampling approach, and time-/cost-efficient and flexible work plan, all of which result in a system based on feedback between the field/laboratory practices and the policies/objectives of the program. Under the observation-based CSM framework, the initial CSM is directly tested and

updated in an iterative manner based on field/laboratory evidence of confirmed observations from multidisciplinary investigation approaches. These observations fill existing data gaps without triggering irrelevant field mobilizations. In the wake of growing trends within modeling studies conducted on problems characterized by incomplete data, this approach encourages a procedure for an adequate conceptualization of the subsurface. This conceptualization should instead be considered a hypothesis against which the performance of a mathematical model can be tested and evaluated in accordance with protocols for effective modeling to avoid suspect rendering models and what Refsgaard and Hansen (2010) described as modeling nightmares. The emphasis on such a strategic observation-based conceptualization is to promote a continuous appreciation of the vital role played by observations in the formulation of models. According to Livingston et al. (2000), it is unfortunate that long-term, integrated, interdisciplinary research remains a scientific rarity today. The adopted approach is considered to be somewhat related to the "Triad" approach, which was carefully crafted and demonstrated in Crumbling et al. (2003), Crumbling et al. (2004a) and Crumbling et al. (2004b), and the ModelPROBE strategy (Kästner and Cassiani, 2009; French et al., 2014).

2.2 Observation-based conceptual site model approach

The modeling process required to sufficiently elaborate upon the CSM assumptions regarding the chemical constituents of interest and their pathways as well as the spatiotemporal distributions of receptors involves two main stages: (a) conceptualization, and (b) mathematical formalization (Carrera, 1992; Jorgensen and Fath, 2011). Conceptualization (as illustrated in this study), which is the first stage of the modeling process, is arguably the most important step since it forms the foundation of the mathematical model and is consequently the basis for the generation of computer codes used for simulations (NRC, 2001). Efficient conceptualization allows for the distillation of a bewildering variety of emerging issues into a few essential core designs with easily understood features while accounting for the predominant processes occurring at varying scales of interest. With regard to limited site-specific data and the need to ensure the reduction of uncertainties in modeling, risk assessments, predictions and remediation actions, it is therefore desirable to create a reliable CSM (i.e., a simplified approximation of the real system of interest) based on observations to operationally precede model building, even though the elements of observations and mathematical models are mutually supportive.

The conceptualization stage illustrated in this study proceeds through three main steps: (1) the development of an initial CSM; (2) experimentation based on target-oriented site characterization and laboratory analyses; and (3) an evaluation of the observation outcome through collaborative data analyses (i.e., the confirmation/validation of a CSM). The role and approach of the observation-based conceptualization is illustrated in Figure 2.1.

Given that every successful modeling process begins with some initial perception of a field problem (i.e., a perceived real system of interest) and that any model is an instrument designed for a specific purpose, it is necessary to explicitly define the objectives of the modeling endeavor to provide a guide for the type of model chosen. The degree and scale of the undertaken modeling complexities should be consistent with the complexities of the site, available data, and the problem being addressed or the questions to be resolved (Gerhard et al., 2014) within the limits of the study area. Thus, the first

step in the conceptualization stage is to develop the initial CSM, which constitutes the collection and assessment of uncertain (but testable) assumptions/hypotheses, algorithms (particularly when performing mathematical modeling) and relationships and the determination of whether the available data are sufficient to describe the real system under consideration. The initial CSM forms the basis upon which both mathematical modeling and observation acquisition can be performed. At this step, the conceptualization is typically highly subjective, and thus, the selection of the CSM features requires some level of creativity and selective perception. That is, contrasting opinions about the system under investigation, its environment and the different possible scenarios within the system could lead to drastically different versions of the model and consequently to different degrees of errors (Oreskes and Belitz, 2001). As noted earlier, this is usually the primary source of uncertainty when creating a CSM. Although subjectivity can greatly affect scientific interpretations, some researchers (e.g., Polson and Curtis, 2010; Bond et al., 2012) have argued that the existence of subjectivity in the formation of hypotheses does not necessarily imply a lack of scientific rigor and can also lead to the advancement of novel hypotheses. However, in an effective manner, a well-crafted initial CSM is expected to clearly propose salient questions and provide information about the expected size of the target(s) and the geometry of the investigation site as well as the surrounding ground conditions. The development of the initial CSM therefore constitutes an important aspect of the project planning and affects the successful completion of the experiment. From this perspective, beginning the evaluation of a CSM without prior knowledge of the initial CSM could be incredibly costly since it would inevitably result in the selection of the inappropriate equipment and techniques, and therefore, the evaluation process will be compromised (Crumbling et al., 2003).

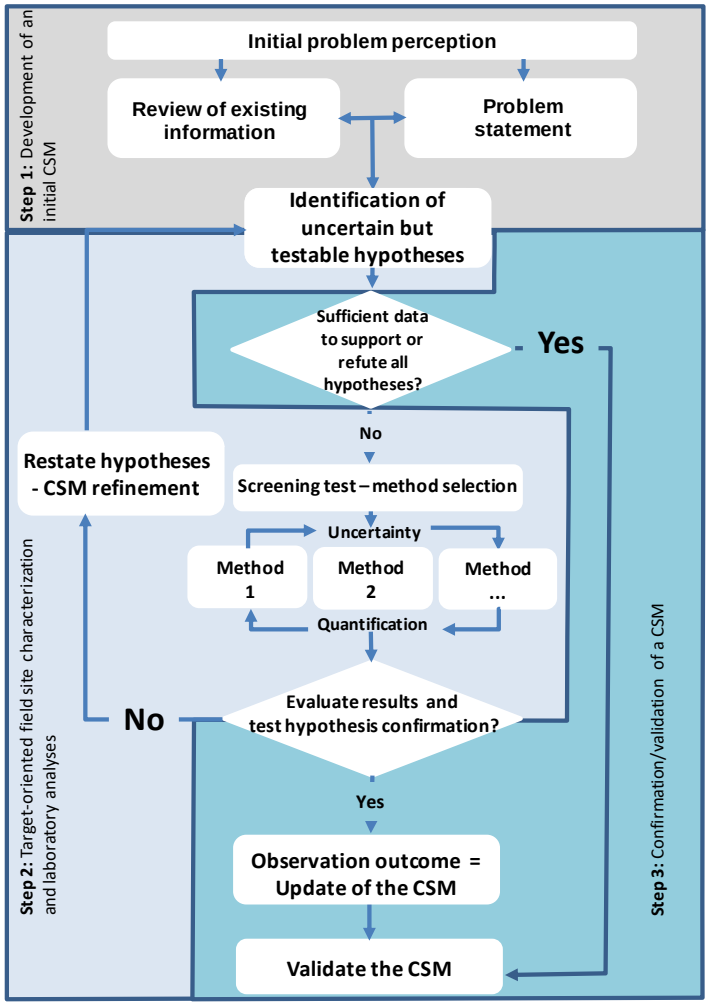

Figure 2.1. Observation-based conceptual site modeling process.

Following the final selection of the hypotheses, the second step is to conduct experiments through target-oriented site characterization and laboratory analyses. The advantage of the adopted approach is that the inferences and conclusions drawn from the perception of processes occurring at the specific site are derived directly from field and laboratory data and integrated as sub-models that address special stratigraphic, hydrogeological and geochemical questions at any stage during the modeling. The CSM is a multi-compartmental model in which the representative unit of a site (e.g., groundwater) can be associated with decision process models to handle these highly specialized questions (Jakubick and Kahnt, 2002). Hence, the iterative manner of establishing the compartments will help to better understand the geology and hydrogeology of the subsurface in addition to how they impact the groundwater flow conditions and solute fate.

To assist with the observational studies, it is essential to perform a preliminary field screening and initial site characterization (which could consist of aerial or ground mapping/remote sensing exercises) to re-establish the limit of the search area(s) and to determine the specific hypotheses that form the basis of the investigation program before the application of detailed, follow-up measurement methods. The preliminary identification of the search area(s) can provide ample hints demonstrating

the feasibility of the project concept and the certain usage of follow-up confirmative and collaborative methods. The information flow during the target-oriented site characterization and laboratory analyses (Figure 2.1) employs the reasoning related to new observations and associated cause-and-effect phenomena to produce new updates to the CSM. Accordingly, evidence based on field and/or laboratory data can then be used to infer the sub-model characteristics and subsequently determine the next level, type and nature of additional data to be collected. These decisions are mostly aided by the ability to recognize typical patterns, following which the limitations related to the representativeness of the sampling results (that is, the data uncertainties) can be further evaluated and supported by newer data and observations while managing the decision-making uncertainties at an accepted level. The underlying rationale for this strategy is that a model that iteratively leverages and tightly couples data derived from the application of different types of site characterization and laboratory analytical techniques can be utilized with an increased level of confidence (ITRC, 2003; Crumbling et al., 2004a). In this way, data gaps can be systematically identified and filled; this represents the "uncertainty quantification" cycle shown in Figure 2.1.

The third step is to collaboratively analyze the experiments or observation studies and the associated multiple lines of evidence that characterize the CSM compartments and then evaluate the interrelations between the heterogeneous results from various tests employed to investigate and confirm the existing or initial CSM. From an analysis of the experimental results, the previous hypotheses can be reformulated or discarded if they are not confirmed; moreover, the site investigation concept can be adapted (i.e., CSM revision and refinement). By traversing the CSM revision and refinement process, an effective cycle is initiated that engenders an improved CSM and a better understanding of the behaviors of the system under consideration. Philips (2001) describes a case study in which processes that were neglected in the initial CSM were later found to be of fundamental importance, leading to a substantial revision of the CSM. Philips (2001) also noted that such revisions are particularly expected in complex environments where often poorly understood physical, chemical, and biological processes interact. In the event that the hypothesis is confirmed, an observation outcome (that is, updated CSM) is produced.

A discussion on mathematical conceptual site modeling (which literally follows the same principles as observation-based modeling) is beyond the scope of this study. However, once an accepted version of an observation-based model is reached such that only a single "*valid"* hypothesis remains (i.e., the hypothesis is well corroborated or the bias is confirmed with greater empirical meaning and understanding), the outcomes from the observation-based conceptualization can then be transformed into concise model features and parameters that are more directly useful for a comparison with the mathematical modeling simulation results (Thacker et al., 2004). Subsequently, the simulation outcome may be hopefully "validated" through a quantitative comparison if the agreement between the simulation outcome and the observation outcome is acceptable, thereby constituting the next real system of interest (Oreskes et al., 1994). At this point, it should be clear that the logical conclusions reached if the conceptualization process was successful are as valid and rigorous as the mathematical techniques employed. This is because the model results are a direct consequence of the hypotheses and concepts defined in the conceptualization phase (Torres and Santos, 2015). If the agreement is unacceptable, the model or the experiment (or both) can still be revised depending upon the judgment of the model developer and experimenter. As already shown (Figure 2.1), a revision to the experiment

will involve modifying the experimental test design, procedures, or measurements to better understand the behaviors of the investigated system or to improve the agreement with the simulation outcomes. A revision of the mathematical model will involve changes to the basic assumptions, structures, parameter estimates, boundary values, or initial conditions of the model to improve the final agreement with experimental outcomes. Nevertheless, it is crucial to emphasize that there is a lack of consensus on the definition of "validation" (NRC, 2001), and thus, whether a model can be validated remains the subject of debate. While certain authors (e.g., Konikow and Bredehoeft, 1992; Oreskes et al., 1994) have maintained that models cannot be validated because scientific hypotheses are fundamentally unprovable, a "well-corroborated/confirmed" CSM can merely be reduced to an "as-yet-not-refuted" CSM, and one cannot be entirely sure that the initial group of hypotheses is exhaustive. Meanwhile, other scientists (e.g., Jarvis and Larsson, 2001) argued that a "validated" model could be considered a model that is acceptable for its intended use.

For the purpose of this discussion, I have focused our attention on an affirmative answer to the question "Are the conceptual models comprising resolved unknowns and associated supporting data adequate for achieving the stated purpose" and how that answer would help to formulate a confirmative observation rather than on whether a hypothesis implies that observable effects indicate either verification or validation. Based on the adaptive nature of the proposed observation-based CSM approach, the confirmation of observations constitutes the recognition that data are never complete (and that the model response is uncertain) with the intent that the observation responses will be closely interpreted, and those observations can then be employed to update the measurement programs iteratively, leading to substantial improvements in the modeling process (e.g., Marker, 2007; Kosso, 2010). In this way, the burden on mathematical modelers to demonstrate the degree of reliability between their model and the real system of interest being represented is significantly minimized. Thus, the constructed models are able to elucidate discrepancies in the strength of evidence required to corroborate a hypothesis and identify the further needs of a study.

2.3 Target-oriented site characterization and laboratory analyses

As highlighted in the previous section, the purpose of the observation-based CSM approach (once the initial CSM has been developed) is also to provide an iterative strategy for site characterization endeavors and laboratory analyses with smart feedback loops between different activities. Figure 2.2 schematically shows how the observation-based CSM approach can be used to update a CSM by combining different site investigation methodologies (see the discussion below). Although the purpose of each independent method is to improve upon the initial CSM, noninvasive surface geophysical techniques typically pave the way for minimally invasive direct push probing systems and subsequent groundwater chemical and dual stable isotope analyses. In the workflow shown in Figure 2.2, surface geophysical techniques serve one major purpose, namely, to screen and identify target features for a site investigation prior to invasive/minimally invasive sampling techniques. Whereas surface geophysical and direct push techniques provide subsurface information regarding the structural conditions of aquifers, groundwater chemistry data combined with multi-stable isotopes analyses provide additional information about hydrogeochemical evolution processes and solute

source apportionments as well as inferences about the hydrological and biogeochemical processes influencing the behaviors of the solutes.

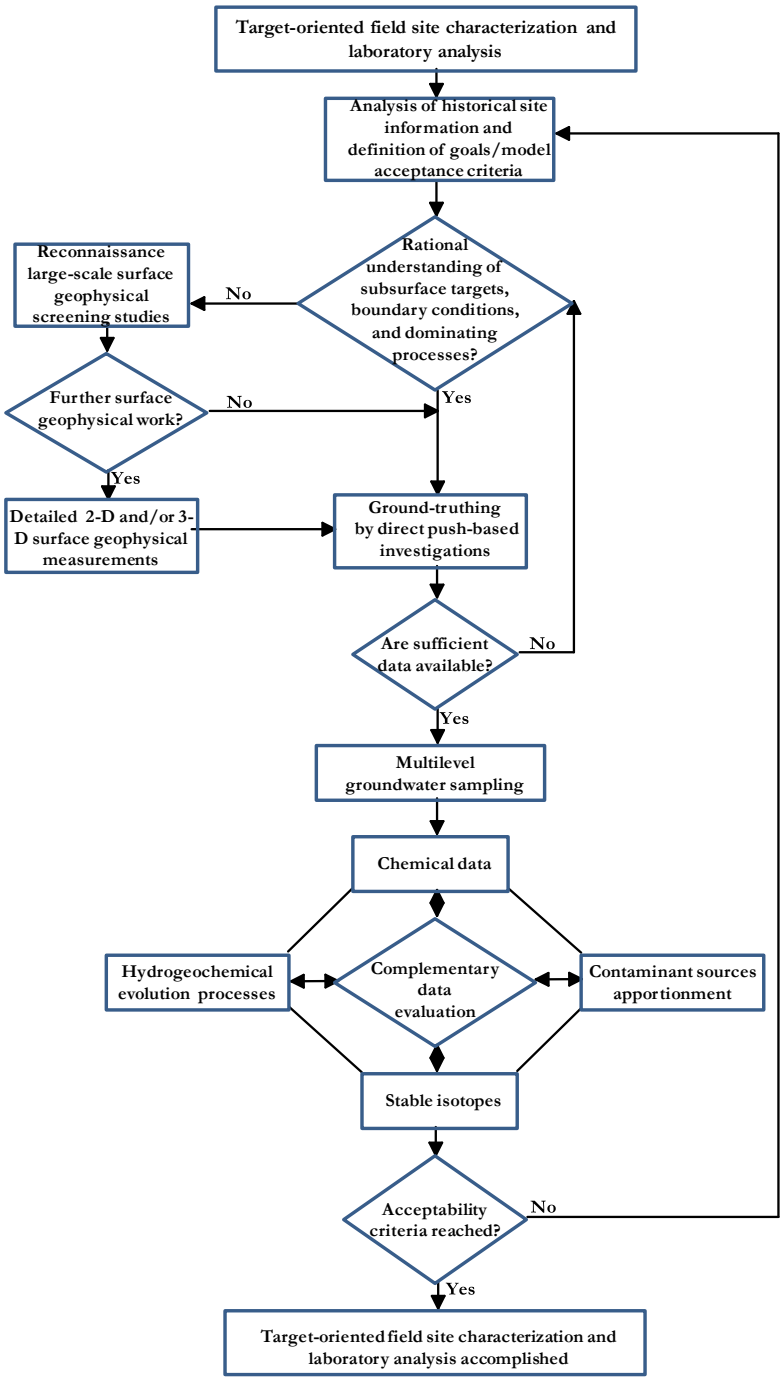

Figure 2.2. Generalized workflow of the target-oriented site characterization and laboratory analysis approach used in the observation-based conceptual site modeling.

2.3.1 Noninvasive ground-based near-surface geophysical methods

Here, it is remarked that although the geophysical measurement spectrum can be broken down into three major categories: airborne-, ground- and borehole-based, for the purposes of this documentation, emphasis is placed on the ground-based geophysical techniques (hereafter referred to as surface geophysical techniques - that is, observation of geophysical parameters as measured at the ground surface) for near-surface investigations/applications. Discussion on borehole-based geophysical techniques is reported under section 2.3.2, which treats direct push-based investigation tools. Also, some surface geophysical methods have been described as invasive (e.g., Parsekian et al., 2015) because parts of the instrument sets are driven into the ground to create contacts for the generation of strong signals. Here however, surface geophysical measurements are described as noninvasive because I did not consider driving instrument sets only a few centimetres into the ground as far enough to designate them as invasive.

Geophysical techniques have become increasingly important for developing conceptual models of subsurface processes and characterizing hydrogeological properties (Moysey et al., 2012). Given the need for reliable and site-specific boundary conditions during groundwater and contaminant transport modeling, relatively quick and noninvasive surface geophysical surveys can provide substantial information about subsurface hydrogeological conditions. Moreover, to account for the sparsity of data sets commonly associated with conventional site assessments, surface geophysical investigations (in addition to airborne/remote sensing techniques) can function as tools for conducting field reconnaissance surveys and can be performed faster than traditional drilling methods, which require the drilling of a large number of boreholes; thus, surface geophysical methods provide a greater spatial coverage (Maliva, 2016). Field reconnaissance surveys and preliminary field screening are performed immediately thereafter to investigate the site history and inform us about the required extent of the sampling density. Although airborne studies exhibit a major and undeniable advantage insomuch that they are vital in areas that are not accessible or at least difficult to access for ground surveying, ground investigations are highly preferable, particularly in relatively small areas or for problems of local interest with limited spatial extents that must be explored. By covering large subsurface regions in a relatively short time using surface geophysical reconnaissance (which may nevertheless yield results that are in one-dimension (1-D)), favorable areas of primary interest can be distinguished from those that appear unpromising with respect to groundwater flow- and solute transport-influencing features. Surface geophysical survey and reconnaissance methods are therefore useful for strategically placing wells, thereby enabling investigators to avoid relatively costly "trial-and-error drilling" techniques. Hence, it is advantageous to execute reconnaissance surface geophysical surveys not only to delineate subsurface structures and select sites for further detailed investigation but also to guide the optimum selection of suitable methods and instrumentation for detailed surveys. In most cases, detailed surface geophysical studies, which typically cover much smaller areas, may be performed to acquire 2-D and 3-D data along closely spaced profiles with dense measurements. It is highly essential that such detailed survey layouts be situated along straight lines with a significant coverage perpendicular to the strike of the investigated target feature. This underscores the need to first conduct a reconnaissance (i.e., quicker and more reliable) survey to delineate a target feature. Hence, it is highly important to account for issues of scale during geophysical field surveying to match the scale of variations in hydrogeological properties with

the geophysical response due to the shape, size and depth of the target feature. In particular, if the measurement scale is greater than the scale of variations in the hydrogeological/geochemical/geotechnical properties, the heterogeneities could be averaged out during data acquisition and processing, thereby obscuring the geophysical response from the investigated target feature.

Different geophysical methods depend upon considerably different geophysical properties (e.g., electrical resistivity, seismic velocities, density, susceptibility, potential differences, and permittivity; Knödel et al., 2007). These different geophysical properties are obviously sensitive to changes in hydrogeological/geochemical/geotechnical parameters such as the mineral matrix, fluid content, porosity, permeability, degree of water saturation, water salinity, volumetric clay content, cation exchange capacity, pore water temperature and total dissolved solids (Lagmanson, 2005; Loke et al., 2013). Thus, in addition to the measurement scale, obtaining a recognizable geophysical response from a target structure depends upon whether its geophysical properties contrast sufficiently with those of the surrounding matrix and the characteristics of the overburden. Moreover, an adequate analysis and evaluation of the acquired surface geophysical data requires the professional experience of the users and their appreciation of the emerging significance and applicability of the methodology to the evaluation of different problems. Nonetheless, the problem of non-uniqueness is often encountered during the interpretation of surface geophysical data, thereby requiring the combination of different methods to effectively process the subsurface information. Regardless of the geophysical tools chosen, the most comprehensive data sets are collected through the collaborative interpretation of different physical properties through a combination of various geophysical techniques. The general intent is to ensure that each method leverages the strengths of the other techniques while enhancing the overall quality of the CSM. No single geophysical tool can satisfactorily deliver the desired information, since different geophysical methods are sensitive to different physical properties of an anomalous target and its surrounding materials. Hence, an integrated interpretation strategy is necessary for reliably capturing common target anomalies, controlling the interpretation, refining the CSM and reducing the associated ambiguities (Chandra, 2015). Of course, there are an ever-expanding number of geophysical techniques suitable for various near-surface primary and secondary applications. The literature provides a well-documented and comprehensive discussion of the background information regarding the near-surface applications of surface geophysical techniques and their modes of operation for environmental and engineering issues (e.g., Telford et al., 1990; Butler, 2005; Burger et al., 2006; Knödel et al., 2007; Reynolds, 2011; Milsom and Eriksen, 2011; Parsekian et al., 2015). It is commonly acknowledged that CSMs can greatly vary from one site to another. Thus, following concerns regarding the instrument availability and the expertise of an investigator, the rationale for selecting the most appropriate geophysical tools is dependent upon site-specific considerations such as the existing knowledge of the investigated problem and the hydrogeological site conditions. In relation to the scale and the boundary conditions of the target, such conditions make it possible to acquire the most valuable information on the subsurface conditions (McLachlan et al., 2017).

Surface electrical resistivity (that is, reciprocal of conductivity) methods are sensitive to changes in texture, mineralogy and water saturation. The surveying approach is concerned with observing earth resistance by measuring the potential field set up on passing electric current between specific surface locations (Habberjam, 1979). Computing advances and the user-friendly nature of field resistivity

systems (particularly multielectrode electrical resistivity imaging systems in 2-D or 3-D) have launched them as a standard investigatory and commercially-available tool to measure lateral and vertical variations in the subsurface resistivity, yielding interpretable information about subsurface conditions. Electrical resistivity imaging has proved successful in the evaluation of geohydrologic and geochemical CSMs relevant to the management of environmental issues. Notable environmental applications of the technique include mapping of contaminant plumes from urban sites (see Vaudelet et al. 2011), searching for and localizing sources of leachate leaking from landfills (see Reynolds, 2011) and their effect on the environment as well as detecting landfill boundaries and hidden buried valley aquifer systems that compromise the interpretation of groundwater chemical information (Kirsch et al., 2006). High-resolution time-lapse information assessed from electrical resistivity imaging systems has widened its scope of application with regards to monitoring changes in geophysical geoelectrical resistivity properties. Together with the demerits of the conventional 1-D resistivity depth sounding technique, which is that individual resistivity depth sounding data do not take lateral changes in the subsurface resistivity field into account, it is generally thought that the dense sampling of the subsurface by the "faster" 2-D resistivity imaging technique is far better. However, as already discussed in relation to site reconnaissance, except in urban areas, conventional 1-D resistivity soundings can be very useful and employed in the early survey phases as a reconnaissance field survey tool for rapidly covering large survey areas and identifying anomalous regions before a 2-D or 3-D resistivity modeling focused on the identified anomalous regions are undertaken to gain a better understanding of the subsurface. Although the resistivity technique works very well and has been more extensively described and applied compared to other surface geophysical techniques, the exact definition of the geometry of a target structure may not be ascertained by the resistivity technique alone. This is due to inherent overburden conductance, equivalence and suppression constraints and variables that cause non-uniqueness in interpretation and decreased depth resolution of subsurface features. Thus, the support of complementary surface geophysical techniques is highly necessary in situations that vitiate geoelectrical resistivity measurements and interpretation.

If an electrically conductive feature is very distinct, intense and homogeneous with characteristic physical properties of its own, for instance, the velocity of seismic waves propagated through such a zone/feature can be generally reduced in comparison to the velocity of surrounding less conductive materials. Therefore, it is possible to map such a feature of interest by seismic methods. Seismic methods, which can be subdivided into reflection, refraction or surface wave methods generate/record wave fields on geophone and rely on the fact that the travel times of seismic waves can be used to infer the mechanical properties of the subsurface in the form of velocities contrasts and attenuation of seismic waves in different rock and sediment units. In each method, major wave types are considered. For example, compressional / P-wave velocities are estimated from refraction seismic surveys. Also, reflected seismic energy can be used to detect velocity changes at sharp boundaries and delineate density contrasts, whereas velocity of shear/surface waves that bends through velocity gradients, and waves that propagate along the surface ('ground roll') are estimated from the surface wave method (Parsekian et al., 2015). Detailed description and distinction of these methods, including the mode of data acquisition, analysis and interpretation of results can also be found in Socco and Strobbia (2004) and Rabbel (2010).

For near-surface applications, refraction seismic is particularly useful. Refraction seismic

method is able to yield near-accurate information about lithological boundaries including the bedrock configuration and depths of the subsurface geologic units. Due to both the intrinsic limits of resolution of refraction images and the overlap in velocity between sedimentary rocks with high initial porosity (such as alluvial deposits), Parsekian et al. (2015) stated however, that refraction seismic does a relatively poor job of identifying lithological boundaries in sedimentary units. Also, because it is time-consuming to conduct refraction seismic surveys, applying the method requires much better planning, and specific skills in data processing and interpretation. Such planning may include earlier reconnaissance phases and resistivity imaging surveys (as described previously) to estimate adequate coverage of a target feature. Thus, like other geophysical methods, an understanding of the volume of the investigated feature (lateral and horizontal extent and thickness) is necessary for appropriate design and implementation of the refraction seismic surveys. In a nutshell, and depending on the site-specific conditions, a combination of resistivity and refraction seismic surveys, focusing particularly on a common anomaly that was identified from an initial/reconnaissance surveys is highly recommended.

2.3.2 Minimally-invasive direct push-based investigation techniques

Although surface geophysical measurements help to fill information gaps in the lateral and vertical directions, particularly between boreholes, their vertical resolution decreases with the depth for physical reasons (Dietrich and Leven, 2009). Moreover, geophysical methods indirectly measure the distribution of subsurface properties (e.g., Parsekian et al., 2015) and therefore require direct confirmation. Direct push technology (DPT) (e.g., Dietrich and Leven, 2009) is invaluable for performing direct site investigations and for overcoming the limitations of surface geophysical measurements.

DPT employs direct push (DP) machines (e.g., Geoprobe®) to push tools and sensors attached to the end of a probe (i.e., a steel rod) into the ground, creating a path for the tools without drilling (http://geoprobe.com/direct-push-technology). DP machines rely on a small amount of static (i.e., vehicle) weight combined with percussion to serve as the energy source to push the tool string into the ground. With a broad range of available sensors and probes at its disposal, DPT is much more promising for effective and rapid sampling/imaging and data collection from unconsolidated sediments at depths of typically less than 30 m below the ground surface than the conventional drilling approach. The sediment properties (e.g., grain size and stiffness), however, may vary with the investigation depth. Despite the fact that both conventional and DP methods provide point investigation data, DPT has comparative advantages over traditional drilling methods in terms of its measurement speed, time/cost effectiveness, field accessibility, and onsite decision-making ability (Leven et al., 2011).

As a minimally invasive sampling procedure, DPT minimizes the disruption of near-surface sediment structures and anoxic microsites, leading to the preservation of the natural hydrological flow path through the aquifer. Testing with the DPT not only results in good sampling results but also a high reproducibility of the measurement of small-scale variabilities. Recent developments in DPT have also led to the successful deployment of multi-parameter probes. Through continuous/discontinuous measurements, the devices (i.e., sensors, filter or samplers) used for the acquisition of soil, soil gas, and groundwater samples as well as for direct imaging and logging help provide high-resolution subsurface

geophysical, hydraulic/lithological, geochemical, and geotechnical information (Leven et al., 2011). The operation of DP machines may also provide an avenue for the deployment of external tools and gadgets that are not readily attachable to probe tools.

DPT is being increasingly utilized during the installation of observation wells (either temporary or permanent). Such wells are intended for numerous applications, such as electrical conductivity (EC) and resistivity logging and cone penetrometer testing for hydrostratigraphic profiling and estimating geotechnical properties, aquifer hydraulic conductivity profiling, pumping tests and slug testing, aquifer biogeochemical heterogeneity definitions through direct hydrogeochemical imaging and multilevel groundwater sampling (followed by laboratory assays), in situ soil color logging, and vertical seismic profiling (both conventional and reverse), to better understand the rock/sediment properties. Among these many applications, tracer testing is increasingly being used for aquifer characterization and geotechnical investigation programs. In several occasions, these DP tools may be combined, making it possible to confidently match changes in the investigated parameters to changes in the subsurface conditions.

DP-based activities commonly result in the acquisition of high-resolution vertical profiles of the investigated parameters. Unfortunately, just as the results of surface geophysical measurements can be marred by a poor vertical resolution, DP-based data acquired along 1-D vertical profiles also exhibit shortcomings and problems. As mentioned previously, DP-based data suffer the same fate as conventional drilling data; that is, important information is lacking in the lateral directions between 1-D vertical profiles/boreholes. The combination of surface geophysical measurements and DP investigations is useful for imaging in greater detail and verifying obscure, complex subsurface structures. In particular, such a combination of methods (both qualitatively and quantitatively) offers immense opportunities to explore scale issues in subsurface heterogeneities critical for the understanding of solute fate and transport processes. Moreover, by combining surface geophysical measurements with DPT-based information, the dominant obstacles in the installation of new wells (i.e., knowing the exact conditions of the subsurface and finding the most suitable locations for new wells) are avoided. This is because surface geophysical measurements can guide the selection of optimal locations for the installation of wells. Consequently, the presence of strategically placed wells presents a unique opportunity to gauge formation depths accurately, abate the occurrence of subsurface attenuation, and evaluate a target feature more closely with different parameter measurements. Moreover, since it is more goal-oriented, this approach also drastically reduces the cost of installing new wells. In addition, DPT can offer great opportunities for tomographic measurements and representations in both 2-D and 3-D, thereby addressing vertical and lateral resolution issues resulting from the independent application of either surface geophysical measurements or DP surveys based on 1-D vertical profiling. A wealth of literature is available regarding the applications of DPT to environmental and geotechnical engineering issues (Schulmeister et al., 2003; Sellwood et al., 2005; Wilson et al., 2005; Paasche et al., 2009; Schütze et al., 2012; Vienken et al., 2012).

2.3.3 Groundwater chemistry and multi ('dual')-stable isotope assays – tools for fingerprinting solute sources and bioavailability assessments

Over the last 30 years, the term bioavailability, which has long been used in pharmacology, toxicology and agricultural sciences, has gained substantial traction in environmental science disciplines. This is primarily due to a growing awareness of the varying degrees to which soils and sediments bind various chemicals, thereby altering their availabilities to other environmental media (e.g., water, soil, and air) and living organisms (microbes, plants, invertebrates, wildlife, and humans), and the understanding that such processes are crucial for effective risk assessment and remediation activities (NRC, 2003). Although the characteristic hallmark of bioavailability research is to provide clearly articulated and well-justified risk assessment and management decisions so that they can be readily understood by nonprofessionals, the ambiguous definition of bioavailability resulting from numerous complex issues, including a deficient understanding of bioavailability and the difficulty associated with measuring relevant environmental and human health indicators of bioavailability, has limited its application (Ehlers and Luthy, 2003; Naidu et al., 2015; Ortega-Calvo et al., 2015). In this discussion, the concept of bioavailability is considered in terms of biodegradation (i.e., the extent to which a contaminant is available for biological conversion), which is a function of the biological system, the physical and chemical properties of the contaminant and the environmental factors (Maier, 2000). Although the consideration of processes affecting transformation pathways that drive nutrient bioavailability should represent an integral component of the risk assessment and management of a contaminated site during a CSM evaluation, such considerations are often neglected in standard CSM guides due to a perceived greater burden of proof for incorporating bioavailability into decision-making endeavors (NRC, 2003; Sorell and McEvoy, 2013).

Groundwater chemical approaches conventionally measure the concentrations of the chemical constituents of interest in groundwater monitoring wells or piezometers positioned along specific flow paths to predict the attenuation of those concentrations. Knowledge of the groundwater chemistry, which can be applied to better understand water quality problems such as groundwater potability and applicability for different purposes, is directly affected by the concentrations and speciation of various chemicals. Additionally, such knowledge of the groundwater chemistry can be used to trace fluxes across water reservoirs throughout the hydrological cycle. However, even though the water chemistry is routinely measured during regional monitoring studies to identify the zones in need of remedial action, the monitoring of solute concentration trends alone is insufficient for tracking the solute sources of origin. A common technique used to assess the impacts of a particular chemical constituent within pore water is to theoretically match the dissolved solute concentration levels to a certain quality reference and toxicity assessment criteria; however, such measurements do not translate to information about the site-specific bioavailability of that particular chemical constituent. Furthermore, although solute concentration gradients can provide clues for the kinetics and thermodynamic driving forces of reactions, it is not always sufficient to simply characterize a site by analyzing the concentrations of chemical compounds because they can be biologically transformed (i.e., biotransformation). Biotransformation that is controlled both by the biochemical activities of microorganisms that recycle the chemical compounds and by the mass transfer of those chemical compounds to the microorganisms (Bosma et al., 1997) can limit the bioavailability. Thus, the bioavailability of a particular

chemical constituent is tightly linked to its origins and its utilization by microorganisms, and it is not readily reflected in the aquifer groundwater chemical composition, which is easily altered and controlled by physical-chemical processes such as advection/diffusion, sorption/desorption, and oxidation/reduction (including cation exchanges with aquifer solids) (Shen et al., 2015).

Compound-specific stable isotope analysis has become an increasingly important quantifying tool for a straightforward assessment of pollutant biodegradation. Biodegradation results in shifts in the stable isotope ratios of contaminants. In particular, patterns in stable isotope signatures can be used to infer microbial activities along biogeochemical gradients (i.e., over spatiotemporal scales). Stable isotopes have been proven to be a transformative tool in the environmental sciences and beyond, as they have been utilized to promote studies ranging from biogeochemical cycling across scales, ecological food web and resource partitioning, and microbial nutrients and forensics (Whitman and Lehmann, 2015). Nonetheless, in the context of contaminant biodegradation in the field, an assessment of the bioavailability using an individual stable isotope system may lead to an inconclusive, unrepresentative and problematic interpretation as well as an underestimation of the biodegradation processes. This difficulty stems from a deficient understanding of the mass transfer limitations and an overlap of coupled processes due to isotopic fractionation. In the worst-case scenario, a discrepancy in the estimation of biodegradation processes between other available methods (e.g., chemical and toxicity testing) and stable isotope fractionation may highlight the relevance of considering mass transfer limitations in the unmasking of information hidden within the stable isotopic labeling technique. Accordingly, compared with the use of individual stable isotopes of an element, an evaluation of the simultaneous fractionation of two elements (i.e., 2-D or dual isotope approaches) can assist with the better recovery of mechanistic information regarding how isotope fractionation varies in the presence of mass transfer, biogeochemical transformations or limited bioavailability (Elsner, 2010). In general, the use of a greater quantity of isotopes is better. This is because multi-isotope studies have better chances of answering the posed questions. Under aquifer (i.e., field) conditions, the limiting factors of the bioavailability are influenced by the geometry (i.e., size and shape) of the system. This geometry governs the movement of microbes and the steepness of the redox and microbiological gradients; moreover, the system geometry ultimately drives the rate of diffusive transfer and the desorption mechanism of high-affinity chemical uptake in the presence of electron acceptors/donors and the capability of the microbes to impact the availability of chemical compounds (Thullner et al., 2013). Consequently, the system being modeled must be effectively characterized using site investigations tools such as surface geophysical techniques and DPT as described in the previous sections in order for groundwater chemistry and multi-isotope methods (the best results are achieved when the two approaches are combined) to be reliably applied to uncouple complex reactive transport processes (Barth et al., 2005) and interpreted as tools for an assessment of the bioavailability.

2.3.4 Interdisciplinary considerations

It is thought that because sediment texture, mineralogy and mineralogy, which influence geophysical attributes, play a crucial role in controlling biogeochemical processes, geophysical surveys could assist in the development of biogeochemical models (Lendvay et al., 1998; Binley et al., 2015).

Atekwana and Atekwana (2010) showed that some physical, chemical, and/or biogeochemical transformations may generate geophysical signals. The potential of geophysical techniques to map hot spots of biogeochemical activity has also been demonstrated (e.g., Wainwright et al., 2016). However, the capability of the geophysical techniques to image complex biogeochemical interactions at the field scale remains limited. Because of the dynamic coupling of hydrologic and biogeochemical processes, a present and significant challenge for geophysical techniques is posed by their inability to sense, isolate the effect of these coupled processes and quantify their contributions to changes in geophysical signatures (which vary over a wide range of spatiotemporal scales) (Atekwana and Atekwana, 2010). Advances in geophysical technologies, nevertheless continue to improve the way and manner in which these challenges are being addressed.

In the context of predicting the fate of aquifer groundwater solutes and their bioavailability (section 2.3.3), the methods of surface geophysics and DPT previously described in sections 2.3.1 and 2.3.2, respectively are applied under the framework of the developed CSM approach to guide the selection of factors that adequately define subsurface geohydrologic conditions wherein biogeochemical processes could be interpreted. By acknowledging the contrasting dynamics of the different processes that account for the heterogeneity of source areas and different flow pathways, the interpretative limitations associated with the traditional approach of constructing a subsurface CSM can be avoided. This is best achieved by following the proposed adaptive observation-based CSM approach, which integrates the understanding of many disciplines, including geology, microbiology, hydrogeology, geophysics, and the chemistry of solute fate and transport. In spite of individual disciplinary uncertainties, these iteratively combined multidisciplinary tools uniquely provide a certain degree of flexibility and reliability for the subsurface representation of contamination and the complex behaviors of dissolved constituents. In this way, an adaptive observation-based CSM that more holistically accounts for a wide range of different physical, chemical and biological processes will improve the predictive powers of mathematical/numerical modeling methods.

Chapter 3

Application of surface geophysics and ancillary direct push methods in the investigation of subsurface structures

Chapter summary

Chapter three describes the structural variability of the subsurface based on the developed CSM framework in Chapter two, using the Wurmlingen study site as a case example. This chapter is subdivided into two parts (A and B):

- Part 3A describes the study site and the relevance of an alluvial aquifer study in understanding dissolved solute/nutrient processing. The initial CSM that embodies the investigated shallow groundwater nitrate source hypotheses is also contained in this Part A.
- Following the development of the initial CSM, Part 3B employs surface geophysical tools and ground-truthing direct push data to identify subsurface structures and aquifer compartments as critical hydrologic features that may control nutrient cycling.

Part 3A – Field site descriptions

Chapter 3

3.1 Introduction

Following the development of the observation-based conceptual site modeling framework in Chapter two, I will now introduce the Step I of Figure 2.1, which articulates the problems with perception to be addressed. Components of this study's research problem include the following:

1) Description of the study site's location, review of site's geohydrology, and relevance of performing the study within the alluvial valley aquifer (section 3.2);
2) Description of the initial CSM based on the regional distribution of nitrate concentrations, which includes identification of uncertain but testable hypotheses (section 3.3); and
3) Traditional attempt at evaluating the nitrate plume, its boundary and dominating processes (section 3.4)

By emphasizing N processing in an alluvial aquifer, I examine the physical (hydrological), chemical and biological controls on N cycling. Such a study could have implications on the sustainable N management and water resources protection.

3.2 Study location, geohydrology, and relevance

Situated in southwest Germany (in the region of Baden-Württemberg), approximately 5 km from Rottenburg am Neckar in the southwest, 7 km from Tübingen in the east-northeast, the Wurmlingen study site (Figures 3.1 and 3.2) lies between 48.498° and 48.503° north latitude and between 8.968° and 8.974° east longitude, covering about 0.273 km^2. The area is a relatively flat plain to undulating uphill. On the hill slope are wine farms and cover trees. The plain is also covered by farmland segmented and partitioned into squares and rectangles for growing crops, and feed. The regional geology of the study area is typical of the sedimentary rock formations of the Triassic, southwest Germany (e.g., Ziegler 1990; Kozur and Bachmann, 2005; Palermo et al 2010; Beyer, 2015).

The surficial geology of the area is generally regarded as the spatially-distributed Neckar valley young Terrace sediments. The uppermost layer of the valley sediments (that is, the floodplain sediments, which cover the gravel body) typically consist of alluvial silty clay materials with a thickness of ~ 3 m and an organic topsoil thickness of up to 0.5 m on average (inclusive). Below this unit is an unsaturated sand and gravel layer with a thickness of ~ 2.5 - 3 m (Kostic and Aigner, 2007). Below this layer, is the local aquifer - generally referred to as the Quaternary sand and gravel unit. Sands, which primarily constitute the matrix between the gravels, were mainly derived from the Triassic sandstones (Kleinert, 1976; Kostic and Aigner, 2007). As a part of the study site, Figure 3.1 also shows an inferred border zone between Lettenkeuper (Ku) and Gipskeuper (km1) below the gravel fillings of the Neckar valley. On a local scale, groundwater is thought to flow predominantly northwest (NW) - southeast (SE) into stream(s), which ultimately join the Neckar river, located approximately 2.5 km from the study site (Figure 3.1).

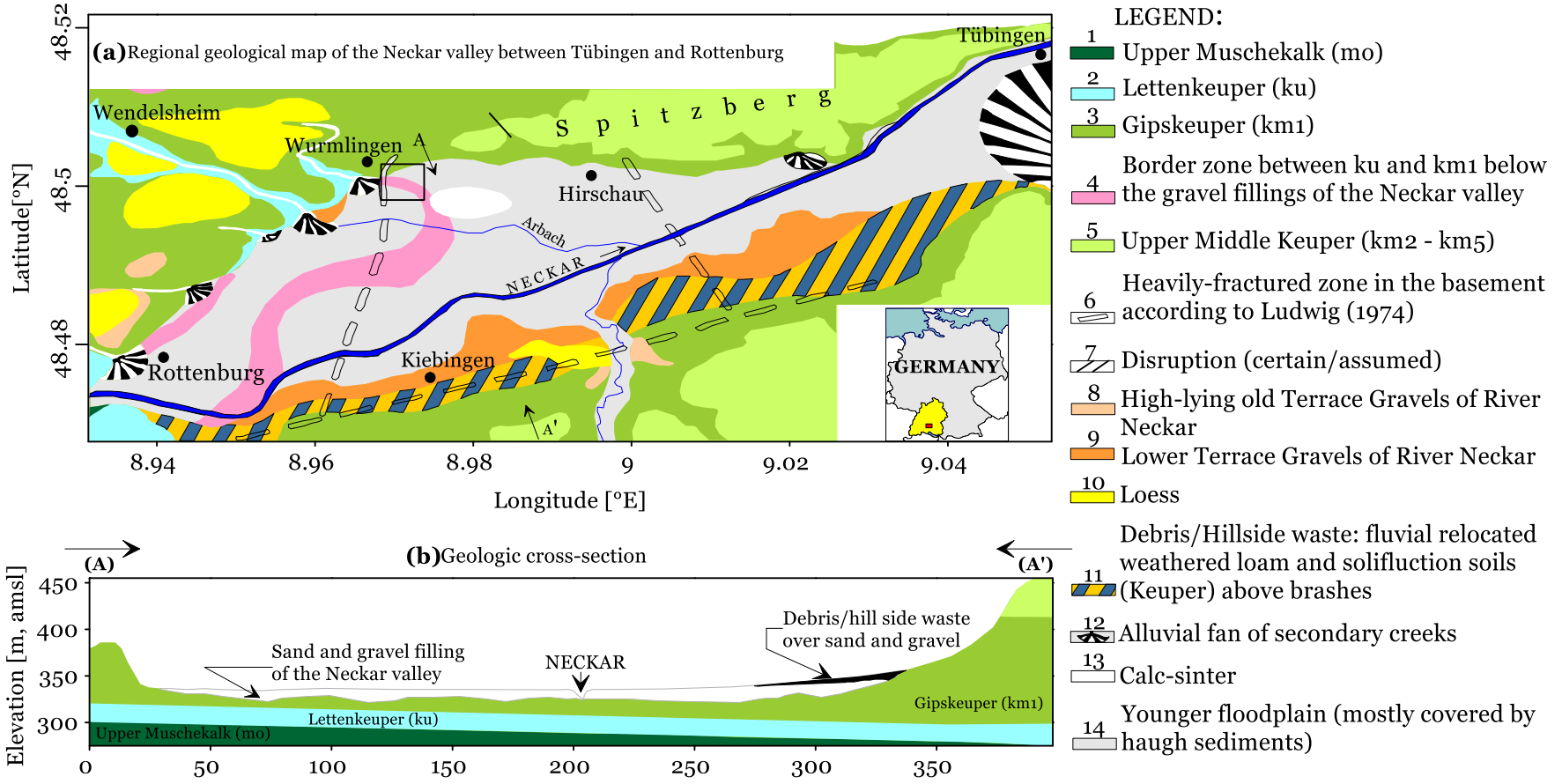

Figure 3.1. (a) Regional geological map of the Neckar valley between Tübingen and Rottenburg: (1) – (7) Pre-quartenary basement (bedrock) – (1) Upper Muschelkalk (mo), (2) Lettenkeuper (ku), (3) Gipskeuper (km1), (4) Border zone, ku/km1 below the gravel fillings of the Neckar valley, (5) Upper Middle Keuper (km2 – km5), and Lias (L), (6) Heavily fractured, (7) Disruption (certain/assumed); (8) – (14) Quartenary – (8) High-lying old Terrace gravels of River Neckar, (9) Lower Terrace, (10) Loess, (11) Debris/hillside waste: fluvial relocated weathered loam and solifluction soils of Keuper over gravels, (12) Alluvial fan of secondary creeks, (13) Calc-sinter, (14) Younger floodplain (mostly covered by haugh sediments) (After Hahn and Schädel, 1973; Kleinert, 1976). (b) A geologic cross section showing the schematic interpretation of the rock/sediment layers along traverse line A – A' shown in Figure 3.1(a).

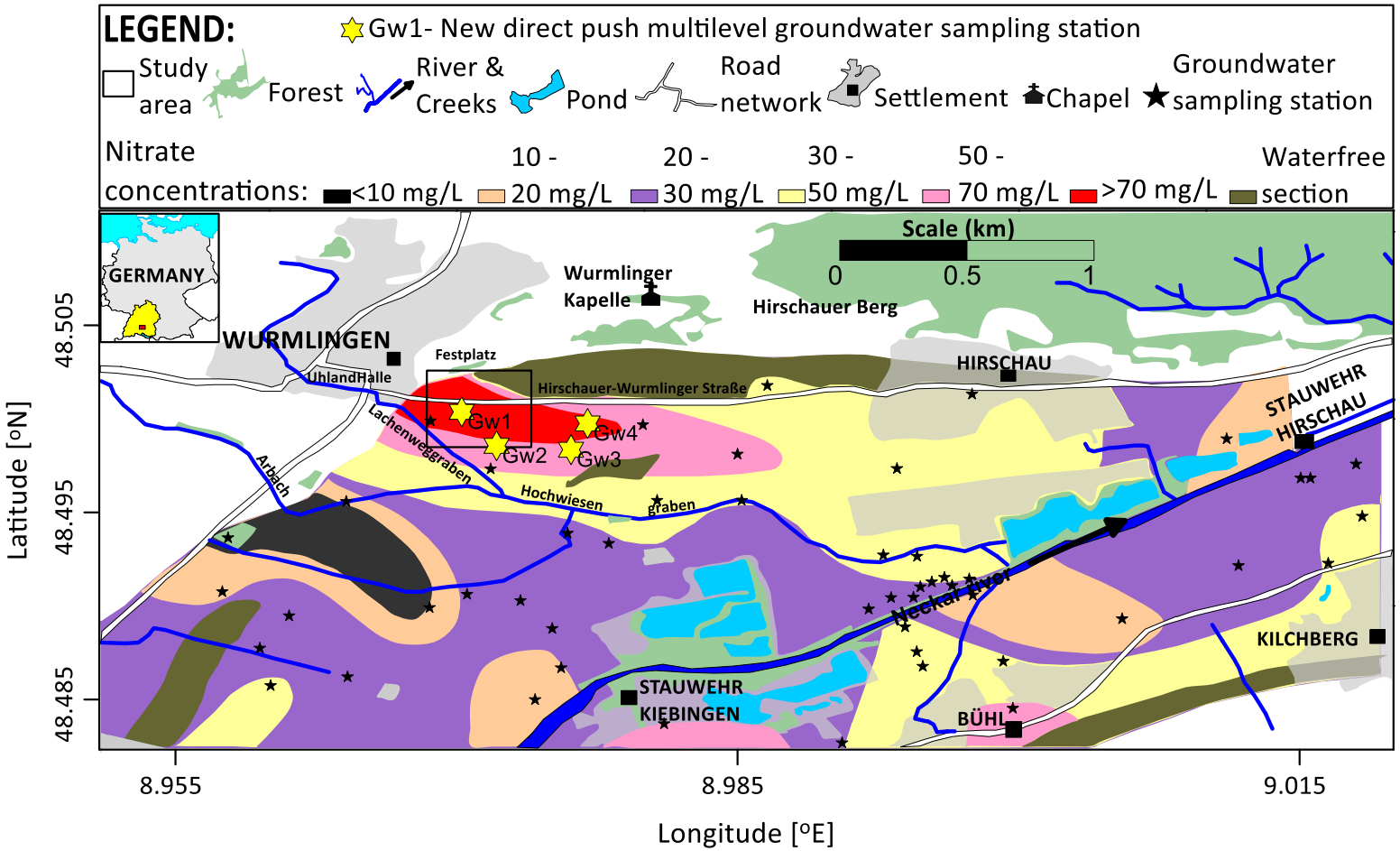

Figure 3.2. Regional distribution of the nitrate concentrations showing the location of the Wurmlingen study site (between Rottenburg am Neckar and Tübingen), southwest Germany. The selected section of the studied nitrate plume is also shown as a small black rectangle. The map shows lateral extension of an elevated nitrate concentration zone with a plume-like structure that appears to originate from the Wurmlingen settlement and trends northwest (NW) - southeast (SE) (Schollenberger, 1998). Note the sparse coverage of the groundwater sample wells represented as black stars from the previous work by Schollenberger (1998), indicating high uncertainty in the physical context upon which the chemical data should be interpreted. Four new direct push multilevel groundwater sampling wells sited close to/within the indicated plume are also shown as yellow stars.

Owing to the hydrological importance attached to the groundwater within alluvial valley aquifer (e.g., Bowling et al., 2005; Baillieux et al., 2014; Lamontagne et al., 2015; Käser and Hunkeler, 2016), this site may be of considerable research value. In particular, the distribution of the alluvial aquifer sediments influences the variability of hydraulic functions that limit the deliverability of water to wells, biogeochemical activities and solute mobilization processes (e.g., Andriashek and Atkinson, 2007; Rayner and Rosenthal, 2008). However, the contributory role of alluvial aquifer systems remains unclear. Schollenberger (1998) made an effort to use hydrogeochemical and hydrogeological data to study chemical composition and dynamics of groundwater in the Neckar River valley. A plume-like zone of high NO_3^- concentration trending in the NW - SE direction around the Wurmlinen study site (see Figure 3.2) was identified in the work of Schollenberger (1998). Of relevance is the extent to which the existence of preferential flowpaths, which influence the rate of water-related solute transport and residence times, exerts dominant hydrologic controls on water chemistry and isotope patterns and imparts solute attenuation mechanisms within the aquifer system (e.g., Krzeminska et al., 2014; Bethune et al., 2015). Adequate evaluation of hydraulic and geologic heterogeneities such as preferential flow zones is one major drawback in hydrogeology which however is necessary for efficient site characterization and reliable planning of site remediation. Although the shallow groundwater at the study site is not exploited for drinking purposes, incorporation of hydrologic flowpath dynamics is critical to the understanding of the transport of point and nonpoint source pollutants (Peters, 1994) and in producing reliable chemical models (Robson et al, 1992). Insights gained through the incorporation of flowpath information in the interpretation of chemical and isotope data can be transferred to a wide spectrum of hydrologic systems.

3.3 Description of the initial conceptual site model

Along the larger stretch of the Upper Neckar river valley between Rottenburg and Tübingen, in the region of Baden-Wurttemberg, southwest Germany a water balance and chemistry study focusing on the nature and the renewal of groundwater has been conducted (Kleinert, 1976). This study laid the framework for a critical understanding of the groundwater chemical characteristics. Over the course of time, it seemed appropriate to edit the hydrogeology of the area. This was due to a number of expected modifications resulting from changes in the groundwater regime, shifts in the boundary of land affected by high sulfate and NO_3^- concentration levels, and changes in groundwater recharge rate, and among other things, given a variety of threats to the groundwater and partly competing ideas about the future land use. As a follow-up study, the work of Schollenberger (1998) was intended to provide additional information on the chemical composition and flow dynamics of the gravel ("kies") aquifer groundwater based on the conventional drilling, and sampling approach. Pertinent findings reported by Schollenberger (1998) around the Wurmlingen settlement (toward the northwestern portion of the Upper Neckar valley) as addressed in this study are as follows. There is a strong influx of the sulfate-dominated groundwater from the so-called Gipskeuper ("Gypsum Keuper") into the groundwater from the northern border of the Upper Neckar Valley and the presence of the groundwater chloride and NO_3^- is predominantly anthropogenic. Emanating from the Wurmlingen settlement area is a NO_3^- plume structure with concentration reaching 70 mg/L and trends northwest – southeast (Figure 3.2).

According to Schollenberger (1998), the NO_3^- plume is the resultant effect of land use practices (primarily agricultural) (Kanz, 1977). Schollenberger (1998) postulated that 80 - 95 % of the NO_3^- originate from nitrogen (N) fertilizer in the form of NH_4^+. However, considering that the groundwater NO_3^- plume can be consistent with a localized source of NO_3^- controlled by the local hydraulic gradient (Hinkle, et al., 2007) and based on informal face-to-face communication with older farmers, an emerging perception is that a hypothetical landfill site (HLS) situated toward the Wurmlingen settlement (possibly around the Festplatz arena) may have contributed to the elevated concentration of NO_3^-.

I thought that if the application of N fertilizer in the form of NH_4^+ on the agricultural soil was responsible for the elevated NO_3^-, there should have been a more diffuse or widespread distribution of the NO_3^- in the so-called heterogeneous aquifer system rather than a structurally-controlled plume. Otherwise, the source of the NO_3^- may be from a point source such as the hypothetical landfill site. On a second thought, the zone of elevated NO_3^- may have been caused by the presence of an unknown preferential flow structure into which the solutes composed of either of the two/both sources of NO_3^- emptied themselves and from which the groundwater samples may have been collected by the previous study described. Thus, given the disparity in the understanding of the NO_3^- sources and the influence of subsurface hydrologic system, it was necessary to track the sources of the nitrogen loading to the aquifer. There were also concerns about the hotspot of the NO_3^- plume, where reaction rates are expected to be disproportionately higher than the surrounding aquifer matrix (e.g., Morse et al., 2014).

Based on the groundwater monitoring programme by the State Institute for Environment, Measurements and Nature Conservation Baden-Württemberg (LUBW, 2015), groundwater NO_3^- concentration levels in the region of Baden-Wurttemberg are on a consistent and gradual decline (Figure 3.3) driven, in part, by the sustainable nitrogen management in the region. Given that the concentration levels of the studied NO_3^- plume as at 1998 (based on Schollenberger, 1998) is way above the warning value stipulated in Figure 3.3, another interesting question is whether NO_3^- still persists in the aquifer and how the ubiquity of the NO_3^- presence and its behavior at different depths in the aquifer is influenced by the subsurface geohydrology. Soluble NO_3^- can be mobile in groundwater with abundant dissolved oxygen, but may be lost through different biogeochemical transformation pathways under distinct conditions. Also, given the gypsiferous carbonate environmental geochemistry of the study area and the thermodynamic considerations that microbial NO_3^- reduction is energetically more favorable than sulfate (SO_4^{2-}) reduction (Lovley and Chapelle, 1995; He et al., 2010); there is a strong need to understand the extent of nitrogen biodegradation by microbial communities in the aquifer with some degree of certainty. Thus, for such an aquifer system, investigating the biogeochemical conditions in the light decreasing (or increasing) chemical constituents are a useful measure of their mobility and persistence (e.g., McMahon, 2001; Böhlke et al., 2002) and attenuation mechanisms of the loaded anthropogenic nitrogen (e.g., Nakaya et al., 2007; Ibrahim et al., 2010). In addition, to what extent that the fate of NO_3^- is controlled by the distribution of subsurface aquifer structure remains poorly studied. Although in previous hydrogeological studies, the occurrence of buried channel features was defined in different parts of the regional alluvial-valley system by independent methods like refraction seismic (mentioned in Kleinert, 1976), the existence of such an alluvial architecture is unknown in the vicinity of the NO_3^- plume around the Wurmlingen study site.

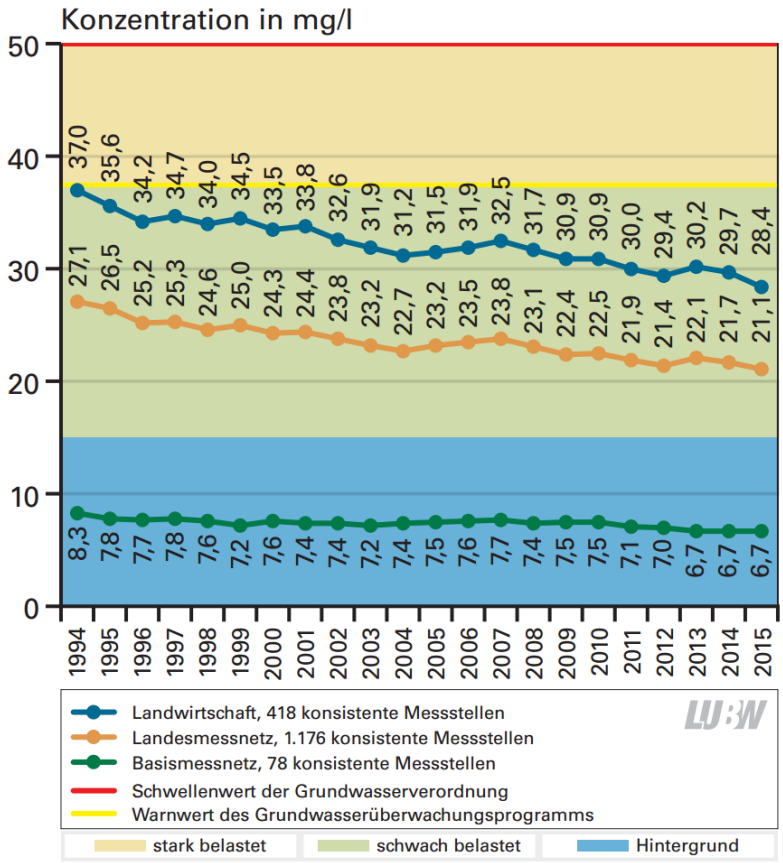

Figure 3.3. Medium-term trends of mean nitrate concentrations for the overall measuring network observed annually in autumn - Inside and outside water protection areas in the region of Baden-Württemberg (LUBW, 2015).

The descriptions given above constitute the initial view of the study site, which I used as the working hypotheses for the purpose of arriving at the conclusions drawn in this study. These initial working hypotheses constitute the unknowns and unanswered questions with regards to nitrogen processing in the alluvial aquifer system and will be checked against the collaborative analyzes of the observed data characteristics in order to establish whether the proposed sources of NO_3^- are in tune with the real (experimentally-determined) sources of NO_3^-. Other hypotheses worth considering regarding the origin of the groundwater NO_3^- plume are as follows. The general strike direction of the Mesozoic layers in the area is toward the Neckar valley, and an intrusion of sulfate-rich water found at the northern boundary of the Neckar valley aquifer indicates that the southernmost part of the Ammer valley (adjacent to the Neckar valley) infiltrates into the Neckar valley aquifer (Cirpka et al., 2017); by implication, the groundwater NO_3^- may also originate from the hillslopes via the fractured bedrock (P. Grathwohl, personal communication, June 2018). Similarly, Kortunov et al. (2016) advanced that agricultural NO_3^- applied to the Neckar valley soils does not reach the groundwater and that the groundwater NO_3^- in the Neckar valley aquifer may have largely emanated from NO_3^- applied to the hillslopes underlain by fractured oxidized mudrock transported to an unknown extent by groundwater recharge in the Ammer valley. This hypothesis is also predicated on the assumption that both Ammer and Neckar floodplains contain Holocene sediments relatively high in organic carbon that potentially reduced agricultural NO_3^-. However, my opinion in this present study is that opportunity should also be given to hydrologic leaching and infiltration of NO_3^- as a potential physical pathway for the introduction of NO_3^- into Neckar valley aquifer from the agricultural soils in the Neckar valley. Overall, in this present study, I placed

emphasis on a section of the investigated NO_3^- plume (see Figure 3.2) in the Neckar valley, hoping to define patterns and provide new opportunities to explore the poorly-understood hypotheses in relation to the origin of the NO_3^- plume and physical (hydrological) and biogeochemical factors controlling the concentration distribution of the NO_3^- solute.

3.4 Earlier attempt at the nitrate plume characterization

Earlier in this study, before the application of the observation-based CSM approach presented in Chapter two, new multilevel groundwater samples were collected at four selected points (see Figure 3.2) adjudged to manifestly conform to the statistical assumption of a high-NO_3^- population target using a high-resolution DP multilevel sampling technique. The multilevel sampling technique was a step ahead of the conventional and solute concentration-averaging drilling technique by Schollenberger (1998), which does not clearly recognize or account for aquifer heterogeneity. However, the chemical data analysis results in terms of the major ions (Table A1) were uniformly distributed across depth profiles and did not signal the possibility of having delineated an anomalous "high hit" region within the plume. In this situation, given the sparse distribution of the sampling points it is most likely that the physical reality of the subsurface in relation to the distribution of the NO_3^- violates the model assumptions of spatial statistics. This means that the distribution of the new groundwater sampling locations did not form a pattern in space that could be linked to the NO_3^- plume. Thus, the sample representativeness was highly uncertain; that is, mismatches between the scale of decision making and the scale of sampling/analysis was certainly not addressed (e.g., Crumbling et al., 2004b). As a consequence, the targeted NO_3^- plume is poorly defined. It was soon realized that characterizing the subsurface structural pattern and the hydrological system (including their geometry and potential pathway of flow) associated with the distribution of the groundwater solutes (Marker, 2007) would require a much more densely deployed sampling plan. Because time-constraints and high cost associated with populating the study site with substantial multilevel well placements grossly defeat the purpose of developing a smart CSM, the CSM evaluation exercise was started off using a preliminary field screening test followed by detailed subsurface imaging based on noninvasive surface geophysical characterization and by DP investigations to offer rapid insight into the subsurface physical context in which the distribution of groundwater solutes should be assessed (see Part B of this Chapter three for details). Figure 3.4 shows locations of the surface geophysical measurements and DP investigations discussed in this dissertation text.

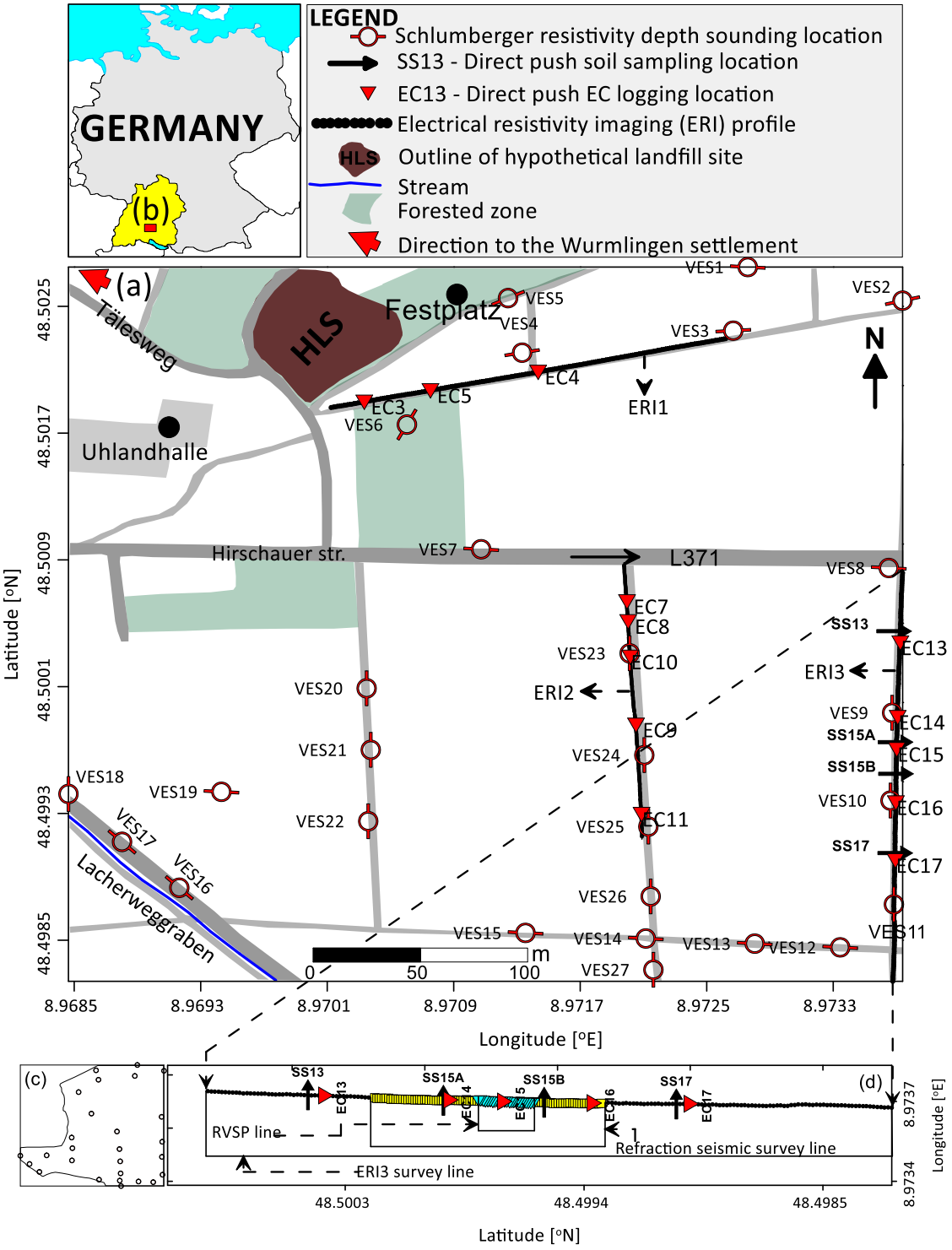

Figure 3.4. Site-specific map of the Wurmlingen study site (a) showing the locations of some of the surface geophysical techniques and direct push investigation methods discussed in the dissertation texts within the region of Baden-Wurttemberg, southwest Germany (b). Outline of the distribution of the preliminary Schlumberger resistivity depth sounding survey locations is shown in (c). (d) Cross section showing coincident surface geophysical and direct push methods described under the combined interpretation strategy in section 3.7.6.

Part 3B – Combined and strategic interpretation of surface geophysical imaging and direct push-based ground-truthing data for the characterization of subsurface structural heterogeneity and geometry

3.5 Introduction

Now that the initial CSM has been developed, I will now describe the variability in subsurface structures using surface geophysical and direct push investigations. This refers to the Step II and some parts of Step III of Figure 2.1, as well as Part I of Figure 2.2.

In developing conceptual groundwater flow and solute transport models, adequate description of the variability in the spatial coverage and thickness of subsurface internal structures as well as the geometry of the soil-bedrock boundary is required (e.g., Dagan et al., 1989; Gupta et al., 2012). Studies indicate that subsurface geologic and hydraulic heterogeneities could exist in various discrete forms such as fractures, faults, dykes, buried channels or lenses (e.g., Neumann, 2005; Grapes et al., 2006). Their occurrence however may not be easily discernible from surface expressions (e.g., Hou and Mauger, 2005; Jiang et al., 2014). Whereas straightforward approximation of groundwater flows is possible once hydraulic head data become available, Mohamed et al. (2015) noted that this is not always the case with the structures given their heterogeneities in hydraulic properties (e.g., porosity and permeability) and the expectation of fluid flow along preferred pathways. Gish et al. (2002), Anderson and McCray (2011), and Tremblay et al. (2014) also concluded that subsurface structural heterogeneity not only controls the physical transport of contaminants or groundwater solution contents but also influences chemical fluxes and reactions. Hubbard et al. (2001) highlighted the importance and control of physical heterogeneity of aquifer sediments (including hydrogeological and chemical heterogeneity) on field-scale bacterial transport. However, the subsurface is rarely mapped to a sufficient detail to capture the spatial distribution of subsurface matrix and associated complex groundwater flow pathways and interactions (e.g., Robinson et al., 2009; Kalbus et al., 2009; Power, 2014; Bethune et al., 2015). Thus, there is need to characterize the distribution of subsurface structures to elucidate information about physical controls on the internal hydrological processes and complex pathways of flow (Zheng and Gorelick, 2003; Ronayne et al., 2008; Händel and Dietrich, 2012).

The main obstacle to the achievement of this goal is linked to the fact that subsurface hydraulic and geologic properties tends to be quantified at spatially limited borehole and well geological log scales that is, in 1-D profiles (from millimeter to meter scale, (Krásný, 2002; Burkholder et al., 2008)) using the classical drilling, sampling and hydraulic testing techniques. Anderson (2007) highlighted that the estimation of subsurface hydraulic properties directly from small-scale measurements is one of the critical unresolved problems in groundwater hydrology (see also Chen et al., 2010). Apart from the associated cost, refusal depth limitations, and localized nature of these measurements, borehole-based sampling can lead to disturbance induced to samples (Vignoli et al., 2012). Additionally, the quality of geologic logs and their ability to resolve fine-scale features varies greatly with the sampling technology (Schulmeister et al., 2003). Given the scale variant nature, the spatio-temporal heterogeneity associated with the subsurface combined with high degree of equivalence in inverse hydraulic modeling, Crook et al. (2008) suggest that localized measurements cannot provide the required data density to adequately characterize large uncertainties in the continuity of the heterogeneous subsurface structures.

de Marsily et al. (2005) noted that subsurface imaging can assist in the description of a heterogeneous system. Rubin and Hubbard (2005) in several illustrations exemplified how geophysical imaging methods can be used to remotely examine subsurface heterogeneity and prediction of flow. Although most quantitative hydrogeophysical imaging studies have been demonstrated at the local scale (~ 10 m), where the scale disparity between direct/wellbore and

indirect/geophysical measurements is often not sufficient, the relatively quick and noninvasive surface geophysical tools have shown obvious potentials in the characterization of subsurface heterogeneities over scales relevant to the management of contaminant plumes and water resources (Koch et al., 2009; Ward et al., 2014; Mendes et al., 2014) than has hitherto been the case in conventional drilling. Surface geophysical techniques can also be an effective tool for reducing the number of drilling positions during geological and hydrogeological studies (Balia et al., 2003; Watson et al., 2005).

Different geophysical tools depend on different physical principles or processes, differ in scales of investigation, and tend to be sensitive and limited to certain intervals of interest and changes in the properties of rocks, soils, sediments, and pore fluids within it in the context of their imaging capacity. These key considerations, can be reconciled in a complementary geophysical methods combination or integration (that is, in a quantitative-based joint inversion process and/or qualitative combined interpretation strategy) allowing for a more focused probing of the collocated or coincident subsurface zone. The central goal is to provide a reliable picture of the subsurface. Studies have shown the usefulness of simultaneous and complementary combination of several independent geophysical observations when investigating a hydrological question (Gallardo and Meju, 2003; Falgàs et al., 2011; Leibundgut and Seibert, 2011; Moorkamp et al., 2013; Hausmann et al., 2013; Gabàs et al., 2014). If the different methods provide seemingly comparable results, more general conclusions can be drawn leading to reduced uncertainties. Yet still, because the inherent degree of uncertainty resulting from differences in properties and scales between different geophysical data and the problem of ambiguity due to the way that these data are processed by different software packages, cannot be easily circumvented (Kearey et al., 2002), successful interpretation of geophysical data and the development of site-specific relationships remains undermined. Thus, rather than just using geophysical methods in the one-time contribution for usual site characterization, surface geophysical measurements can be correlated with high resolution ground-truth imaging and sampling data derived from the DPT. Interestingly, the DPT has become a widely used and attractive alternative to the conventional drilling methods (see Dietrich and Leven, 2009). DPT allows for a cost-effective, rapid imaging, sampling and data collection from unconsolidated sediments or soils. Even though surface geophysical methods indirectly complement direct measurement, such direct observations as that from DPT are encouraged and used to calibrate geophysical approximations of structures and processes.

I present the fundamental role of two surface geophysical methods, namely 2-D electrical resistivity imaging and refraction seismic tomography in evaluating a northwest (NW) - southeast (SE) trending near-surface feature of low apparent resistivity identified from a prior wide area investigation based on Schlumberger resistivity depth sounding surveys (see section 3.6). This feature was delineated at a section of the Wurmlingen study site (Figure 3.2), where higher levels nitrate in an alluvial aquifer was identified (Schollenberger, 1998). How the feature relates to structural controls on the NO_3^- concentration distributions is unaddressed. Because resistivity sections from unconstrained inversion suffer from the inherent low vertical resolution and the depth to features of interest may be uncertain, if evaluated with care alongside seismic data, which detect with a better resolution, the geometry of bedrock depth, a reasonable amount of confidence can be injected into the interpretation process. By co-rendering the electrical resistivity and refraction seismic tomography results, the correlation between seismic velocity structures and resistivity variations has been used to draw inferences on the structure of the subsurface (Meju et al., 2003). However, the underlying question remains: what is the cause of the resistivity variations

and the implication of the delineated subsurface structures? A comparison of the interpreted geophysical data (that is, observed variations in seismic and resistivity attributes) and ground truth information from the DP-based investigations could therefore inject greater confidence in the results of the geophysical studies and reveal underlying aquifer structures that influence fluid properties and the dynamic behavior of processes occurring within the aquifer system.

The primary and immediate goals of this study were to: (1) characterize the main features of the near-surface structure such as the presence of and depth to bedrock as well as the lateral and spatial extent of the alluvial-aquifer sediments. (2) demonstrate how complementary usage of the surface geophysical and DP-based data can systematically leverage the effectiveness and strength of each method in providing the spatial coverage and resolution required to image subsurface properties and processes. These serve to improve the conceptual understanding of the subsurface architectural patterns. With such knowledge of structural controls, fluxes, exchange and interaction of solutes and gases at critical ecohydrological compartments can be quantified.

3.6 Initial spatially dense coverage of the subsurface region by resistivity depth soundings

Here, an initial spatially dense coverage of the subsurface region was made by resistivity depth soundings. As earlier noted, such surface geophysical measurements offer greater measurement support volume advantage over many traditional subsurface observational approaches (e.g., drilling techniques). In particular, the use of the resistivity depth soundings is illustrated here as an interesting reconnaissance surface geophysical tool because it will be highly cost-intensive and time-inefficient to obtain enough data density required to investigate a section of the NO_3^- plume using the preliminary direct push multilevel groundwater sampling highlighted in Section 3.4. Most importantly, an approach to define presumable nature of the subsurface conditions was required to faster target-oriented site characterization process.

It is highlighted in section 3.4 that scaling up the limited volume of hydrogeochemical data from the multilevel groundwater sampling to understand the processes that govern the evolution of the NO_3^- plume could be statistically biased. Nonetheless, based on the average major chemistry analysis, the groundwater electrical conductivity was found to be more sensitive to the sulfate ion, which, among other major ions is approximately 50 percent of the groundwater electrical conductivity (Figure 3.5). Thus, by assuming that the sulfate - saturated aquifer system with uniform porosity (e.g., Archie, 1942) has considerable and geoelectrically-mappable ionic strength, I elected to use or try out the resistivity method as a suitable geophysical tool to distinguish contrasting subsurface features (e.g., Nyquist et al., 2008; Jiang et al., 2014). The NO_3^- level was too low to induce measurable response from the resistivity instruments. Granted that, I also expect that the ability of the resistivity mapping exercise to localize the distribution of the subsurface structures in relation to the groundwater ionic strength associated with the sulfate concentration levels would ultimately influence the understanding of the origin and behavior of NO_3^- solute. This is because in principle the terminal steps of anaerobic microbial sulfate removal would be expected to take place sequentially after NO_3^- removal, unless there are other potential electron acceptors such as iron and manganese (Whitmire and Hamilton, 2005). Evidently, therefore, there are linkages between the sulfur and nitrogen cycles such that the amount of sulfate produced varies relative to

the NO_3^- removed from diverse set of freshwater environments (Burgin et al., 2007).

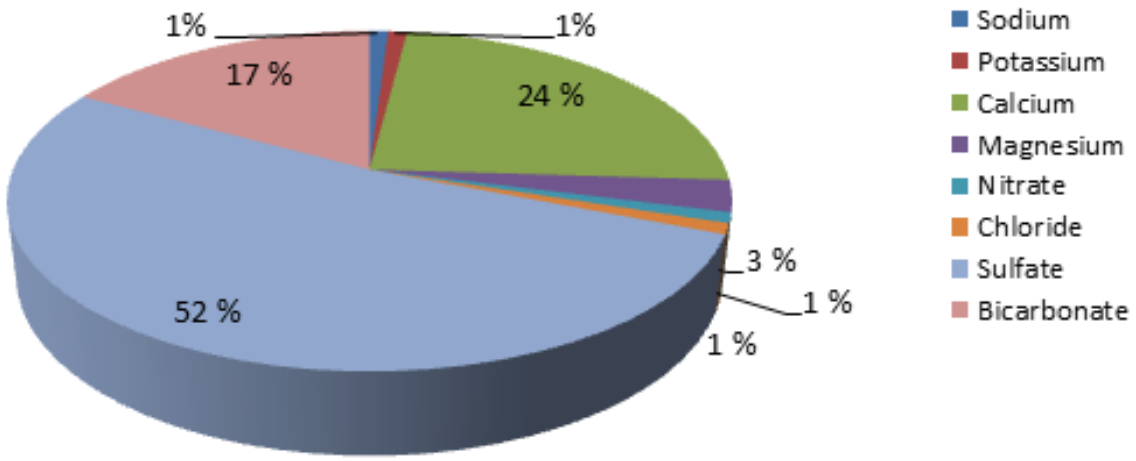

Figure 3.5. Percentage contribution of the major ions to the groundwater electrical conductivity. Average concentrations of the major ions from the four new multilevel groundwater sampling locations shown in Figure 3.2 have been used in this computation.

3.6.1 VES data acquisition, processing and inversion

27 ground-based resistivity depth soundings (that is, vertical electrical sounding, VES) were acquired based on the traditional four-electrode Schlumberger configurations (Hermana, 2001). Because lateral heterogeneities are well emphasized, the Schlumberger array is preferred. Under the framework of the developed CSM approach, the VES surveys constitute a preliminary field screening test aimed at providing a rough estimation of the presumable distribution of subsurface geoelectrical target structures with a more detailed data coverage over larger areas in a short period of time than would have been accomplished by siting multilevel sampling wells across the site. Basically, for a resistivity survey, a voltmeter, an ammeter, a battery or other power supply source(s) and four metal stakes are used (Figure 3.6). The VES resistivity surveys were conducted using a Syscal-R1 resistivity meter (IRIS Instruments, France) at a section of the study site where I expected highest NO_3^- concentrations based on Schollenberger (1998) (Figure 3.2). The outer two current electrodes (A and B) are used as current (source) to inject current (I) into the subsurface while the inner two electrodes are used as potential electrodes (M and N) to measure the voltage (electric potential difference, V_{MN}). For each sounding, the current electrodes position is moved outwards by the same distance from the centre of the profile in order to increase the depth of penetration of the sounding, taken as AB/2. The AB/2 values in meters used include 1.5, 2.5, 4, 6, 8, 10, 12, 15, 20, 25, 25, 30, 40, 60 with a corresponding MN values of 1, 1, 1, 1, 1, 1, 1, 1, 1, 1,10,1,10,10,10. Overlap measurements were taken with every change in MN spacing and the MN distance was increased to improve the signal strength in the resistivity measurements with increased AB spacing and to ensure a potential difference large enough to be measured with accuracy. For Schlumberger sounding, Keller and Frischknecht (1966) have shown that it is desirable to keep the apparent resistivity within an error limit of 5 %, translated as measurements taken with $MN/2 \leq 0.435\ AB/2$.

The resulting apparent resistivity can be estimated as:

$$\rho_a = \frac{V_{MN}}{I} K \tag{3.1}$$

For the Schlumberger array sounding,

$$K = \frac{\pi}{2}\left[\frac{(AB/2)^2 - (MN/2)^2}{MN/2}\right] \tag{3.2},$$

is the geometric factor that will acquire a particular ρ_a value for a given electrode spacing. Thus, the ρ_a value depends on the apparent resistance (V/I) according to the Ohm's law and the K values. The employed resistivity meter had the internal capacity to calculate the geometric factors and outputting the apparent resistivity parameter.

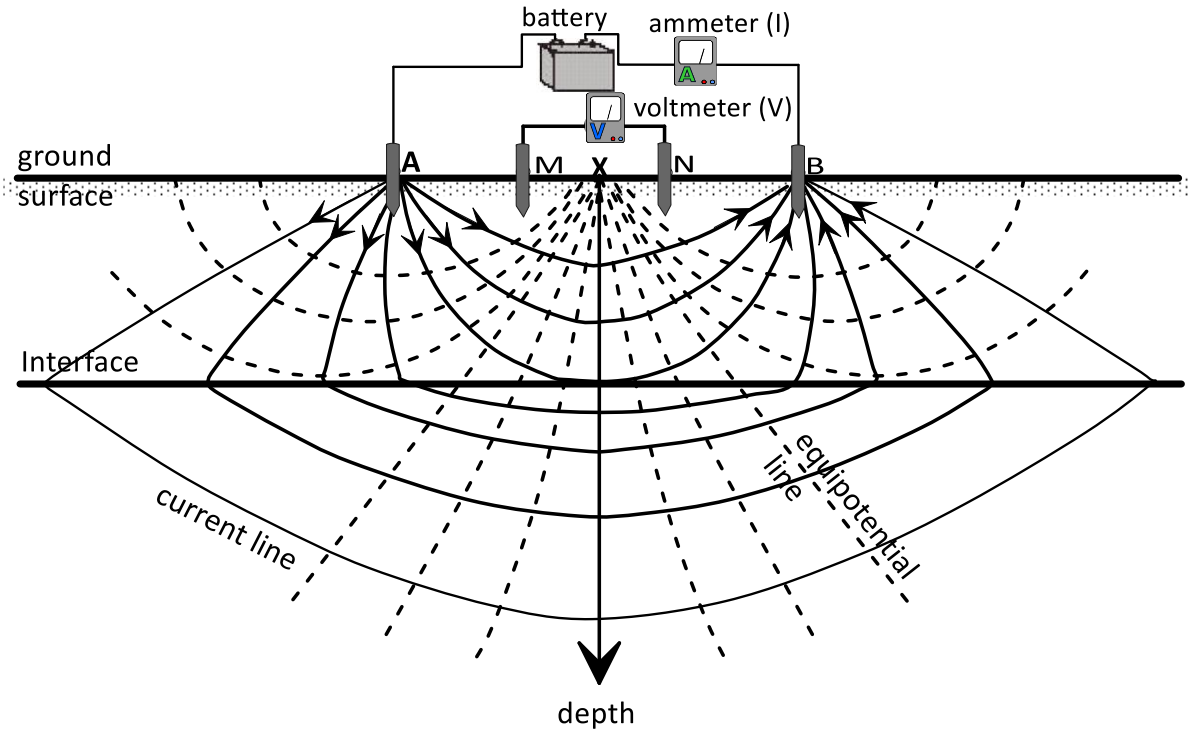

Figure 3.6. Typical four surface electrodes configuration in linear resistivity surveys. Equipotential and current flow lines are shown. The A and B electrodes inject a current into the ground whereas the M and N electrodes measure the difference in voltage across the earth. X represents apparent resistivity measurement location.

Two common aspects of data processing, analysis and interpretation (that is, qualitative and quantitative) were considered. First, by quantitative interpretation of the electrical resistivity soundings, I used an automatic, iterative procedure to invert the observed data into 1-D layered earth models. In this study, the inversion process was carried out using Interpex IX1Dv2 program. Forward modeling and the automated inversion processes produced best fit curves and parameters that best explained the observed data based on the modeler's best judgement. Typically, if the discrepancies in the curve-fitting error (that is, an estimation of the difference between the

measured and calculated apparent resistivity) are large, it is required that the structure of the inversion is re-modified until the root mean square error (RMS) drops below 10%. Unreliable depth models may be obtained. However, by incorporating auxiliary information such as depth to the water table from nearby/adjacent wells into the inversion procedure, it was possible to construct estimate of subsurface geologic structures with good confidence. Depths to the water table obtained from previously drilled wells at the site ranged between 5.08 and 5.95 m. Thus, for quantitative interpretation of the VES data, it is convenient to conduct a VES survey near a known stratigraphic column for better calibration of the acquired data (e.g., López Loera et al., 2015) and to confirm that the solution of the final forward model agrees with known geologic information. Second, by qualitative interpretation, visual analysis of apparent resistivity maps (popularly called isoresistivity maps) constructed from the measured/raw apparent resistivity data help to decipher areas of different subsurface resistivities. At a given measurement station, measured apparent resistivity data sample volume located beneath the station at a depth level equal to the array spacing (AB/2). The distribution of apparent resistivity data is a useful concept for initial quick scan interpretation and quality checks in the field, because it represents the resistivity properties of the subsurface better than the raw data (e.g., van der Kruk et al., 2000).

3.6.2 Interpretation and discussion of the VES results

Figure 3.7 (a, b and c) shows typical Schlumberger resistivity depth sounding curves at the study site. Most of the sounding curves are typical of type K ($\rho_1 < \rho_2 > \rho_3$) and of type A ($\rho_1 < \rho_2 < \rho_3$). The shapes of the curve of apparent resistivity versus electrode spacing potentially reflect subsurface heterogeneity and the vertical resistivity contrasts at boundaries. For instance, it is shown at VES-8 (type A curve), that there is a progressive increase in the apparent resistivities with the electrode spacing. This indicates that there is hardly a conductive discontinuity in the current flow path. Conversely, VES-9 and VES-13 with type K curve show that deeper in the subsurface the current approaches a potential conductor, resulting in a decrease in the apparent resistivity function. Nevertheless, it is clear that the range of apparent resistivity values at the VES-13 location is larger than those at the VES-9 location. On the apparent resistivity maps that will be shown later, there is confirmation that the VES-9 survey center invariably located within or near a conductive anomaly compared to the VES-13 survey center. The presence of such a conductive feature may be helpful in the approximation of the position and the size of the lateral heterogeneity along a given profile. Although VES-13 appear similar to VES-9 in terms of type K curve, a remarkable difference between the two VES curves can be observed from the nature of the shifts in the overlapping segments of the apparent resistivity curves between AB/2 values of 20 and 30 m. The degree of the shifts without a "tie" shows extent of the local lateral heterogeneities that exist near the potential electrodes. Figure 3.7a shows that there is no significant discrepancy between the theoretical sounding curve and the field data whereas Figure 3.7b also did not show significant discrepancy between theoretical sounding curve and the field data except at the overlapping segments wherein the curves do not tie-in. On the contrary, Figure 3.7c showed noticeable discrepancies between the theoretical and field curves. It can also be seen that the extent of the shifts at the overlapping segments in Figure 3.7c is more pronounced than in Figure 3.7b. Possible causes of such discrepancies include the presence of features not receptive to interpretation as horizontal layers, cultural effects from buried structures such as drainage ditches, pipes, and current

leakage from the resistivity equipment, among others factors that may result in resistivity contrasts between layers in the stratified earth.

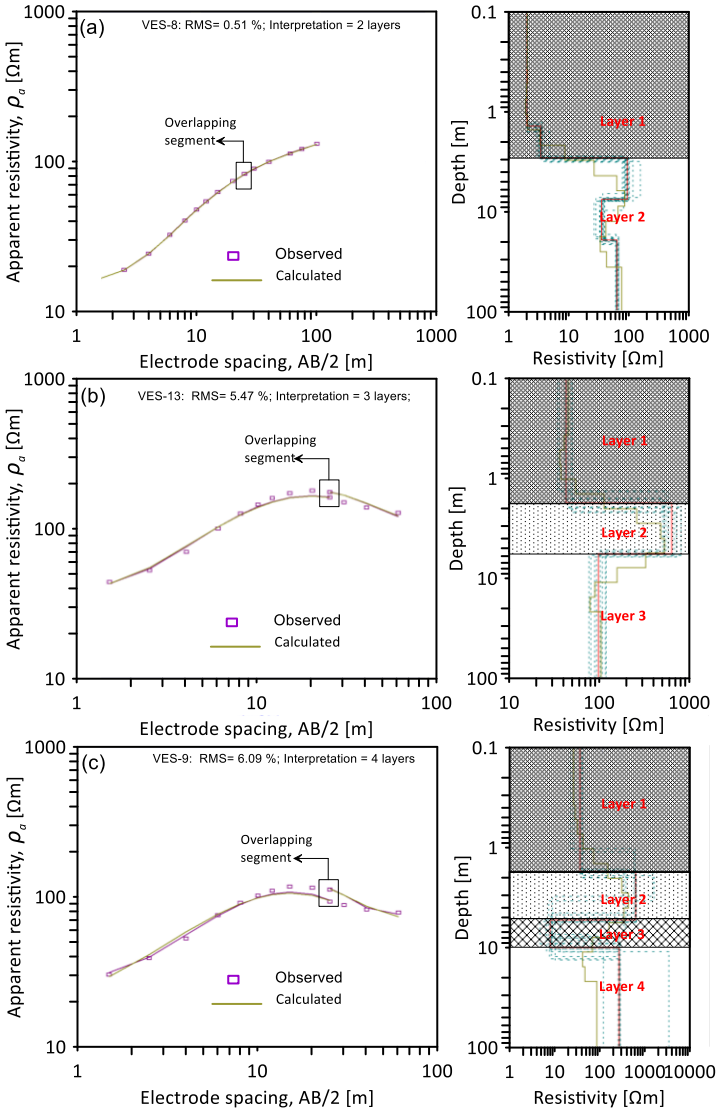

Figure 3.7. 1-D inversion of apparent resistivity data for: (a) VES-8, (b) VES-13, and (c) VES-9. Modeled typical VES type curves of the study site are shown on the left hand pane whereas inverted 1-D layered models are shown on the right hand pane (solid red color). Estimated smooth model (solid green color) and equivalent models (broken lines) are also shown on the right hand pane. As indicated on the model VES curves, the relationship between the observed and calculated apparent resistivity data portray the level of subsurface heterogeneity. It can also be imagined that the greater the heterogeneity, the greater the shift in the overlapping segment observed on the curves.

The interpretation models of VES-8, VES-13, and VES-9 consist of 1-D horizontal layers derived from the quantitative interpretation technique. The resistivity of the first layer was as low as 12 Ωm, 40 Ωm and 30 Ωm for VES-8, VES-13 and VES-9 with thicknesses of circa 2.95 m, 1.8 m and 1.75 m, respectively. VES-8 curve type shows only two interpretable layers. The second layer of VES-8 reaches a resistivity value of 200 Ωm. In VES-13 and VES-9, the depths to the second layer are 5.5 and 5.2 m, respectively. These values correspond to the average groundwater level at that part of the site. The characteristic difference in the inverted 1-D resistivity models between VES-13 and VES-9 lies in the number of layers. VES-13 has three interpretable layers

while VES-9 has four layers. The resistivity of the second layer for VES-13 and VES-9 was found to be around 600 Ωm. The higher resistivity second layer of VES-13 is overlain a 95 Ωm lower resistivity third layer. Comparatively, in VES-9, the higher resistivity second layer is overlain a third layer with a much lower resistivity value of 7 Ωm. Also, the third layer in VES-9 is overlain the fourth layer characterized by a resistivity of ~ 250 Ωm.

Benson et al. (1997) highlighted that interpreted resistivities should provide a much more accurate picture of resistivity as a function of depth compared to representing apparent resistivity values as isoresistivity maps from most studies have shown (Foster et al., 1987; Burger, 2006). According to Benson et al. (1997), this is because apparent resistivity values collected in the field are affected by the thickness and fluid content of each of the subsurface layers. Nonetheless, because modeling errors in conventional 1-D resistivity soundings result when representing the true resistivity and/or thickness of the interpreted layer (Loke, 2001), it is difficult to proceed from surface observations to derive an unambiguous spatial continuity in the subsurface resistivity distribution. Thus, at the stage of the 1-D resistivity soundings, one of the best approaches is to interpolate the acquired apparent resistivity sounding data.

Isoresistivity maps for electrode spacings equal to 4 m, 20 m, 40 m and 60 m (Figure 3.8; see Table A2 for the VES survey location coordinates and the complete apparent resistivity data for electrode spacings 1.5, 2.5, 4, 6, 8, 10, 12, 15, 20, 25, 30, 40, and 60 m) were generated using block kriging with a linear variogram model. Using the Schlumberger electrode configuration, Roy and Apparao (1971) computed depth of investigation ranges from 0.125 of the maximum electrode spacing (AB, that is, the distance between the current electrodes) to a limit of 0.29AB (Apparao and Rao, 1974; Szalai et al., 2009). Thus, the range of depths of investigation for the isoresistivity maps are 1 – 2.32 m, 5 – 11.6 m, 10 – 23.2 m and 15 – 34.8 m for electrode spacings equal to 4 m, 20 m, 40 m and 60 m at the various resistivity sounding station centers. Apart of the survey arrangement, the investigation depths depend on the resistance of the subsurface materials to allow current pass through it. Figure 3.8a illustrates a northeast – southwest trending low apparent resistivity pattern at AB/2 equals 4m. Subtly, the pattern of apparent resistivity variations at this electrode spacing bulges out and follows closely the surface topography contours. This pattern is also interpreted to be broadly similar to the near-surface structures at that depth. Figure 3.8b reveals, however, that at AB/2 of 20 m, nearly half of the study site toward the hillslope up North is covered with lower apparent resistivity materials compared to relatively higher apparent resistivity materials on the floodplain area down South. The pattern of the isoresistivity map in Figure 3.8c is remarkably different from those of Figures 3.8a and 3.8b. Compared to Figure 3.8b, Figure 3.8c shows that the low apparent resistivity feature on northeastern part of the map cleared up and was replaced by a relatively higher resistivity feature. It was also observed that the low apparent resistivity feature from the northwestern part of the area extended almost linearly to the southeastern part. The apparent resistivity map shown in Figure 3.8d further depicted a linearized and well-defined anomalous low apparent resistivity zone. The anomaly is also a NW – SE trending feature defined by a 70 – 90 Ωm contour. Immediate vicinity around the delineated feature, however, remained characterized by higher resistivities of > 90 to <145 Ωm. As earlier noted, the location of VES-9 near/ within the linearized low apparent resistivity feature indicate that the feature could be responsible for the degree of shifts observed on the depth sounding curves (see Figures 3.4 and 3.8).

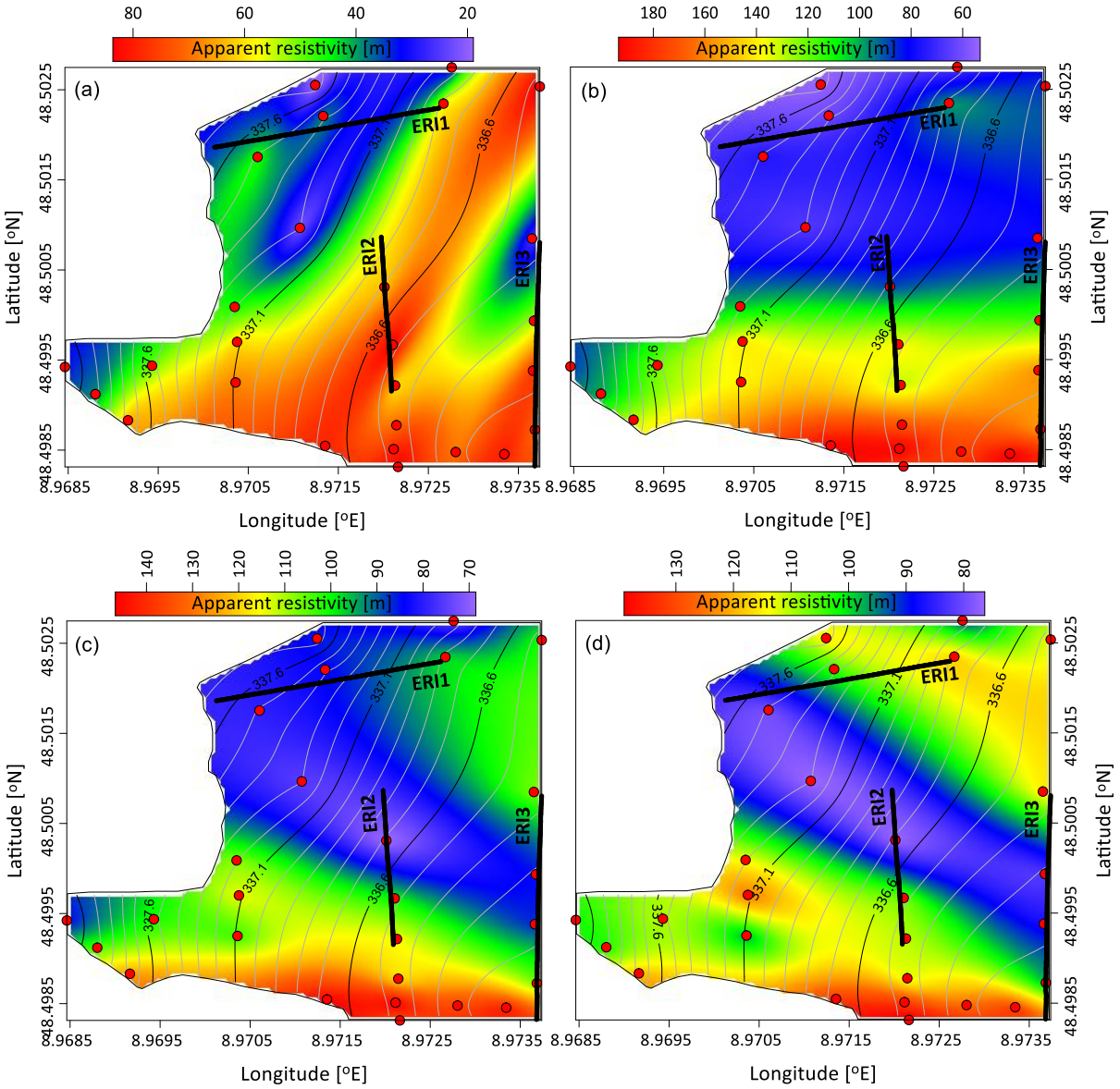

Figure 3.8. (a), (b), (c) and (d) Apparent resistivity distribution maps of the subsurface at electrode spacings of 4m, 20m, 40m, and 60 m, respectively. Also superimposed on the map are surface elevation contours in metres and the confirmatory electrical resistivity imaging (ERI) profiles. Data points used for the construction of the maps are also shown as solid red circles.

Although the most likely conclusion is that the investigated NO_3^- plume (Figure 3.2) is controlled by the delineated NW – SE trending low apparent resistivity feature (Figure 3.8d), there was no readily available subsurface geological information to the explain the anomaly. Interpretation that rests rather on the distribution of apparent resistivities rely on the fact that recognized signatures might reveal complex and substantial resistivity structures, which endure regardless of the interpretation purposes. The only danger in such an approach is that an observer may postulate the likely nature of a target, while in actuality his proposal may not be in existence. For instance, based on the assumption made during the selection of the resistivity mapping tool, it might be tempting to hypothesize that the anomalous low apparent resistivity feature relates to the presence of a local groundwater system, with sufficiently higher groundwater electrical conductivity influenced by the sulfate concentration compared to the surrounding environment. However, it is also worth acknowledging that resistivity anomalies can be driven by variations in grain size,

mineralogy, and water saturation. Thus, because of insufficient data, it was quite premature to make conclusions on the cause of the low apparent resistivity anomaly.

3.7 Surface geophysical 2-D imaging surveys and direct push investigations along transects

To reduce the inherent degree of non-uniqueness and ambiguity in the interpretation process of the VES data (see section 3.6) and to avoid misrepresentation of subsurface geologic anomalies (e.g., Polson and Curtis, 2010; Knight et al., 2012), I decided to confirm the existence of the delineated apparent resistivity features (e.g., Hodlur and Dhakate, 2010; Zarroca et al., 2011) by conducting further investigations. It was borne in mind that the identified low apparent resistivity anomaly (Figure 3.8d) serves particularly as a target feature. Also, constraining geophysical interpretations of the feature with other geological and hydrogeological information help build more robust subsurface conceptual models (e.g., Ryan et al., 2013). Standard surface geophysical 2-D imaging methods (two-dimensional (2-D) electrical resistivity imaging (ERI) and refraction seismic tomography (RST)) were employed along transects to gain more reliable information on the distribution of subsurface structures than the 1-D sounding and lateral mapping techniques. At strategic locations selected on the basis of the surface geophysical investigations, information from DP investigations such as reverse vertical seismic profiling (RVSP), soil electrical conductivity (EC) logging and lithological soil sampling (SS) were used to ground-truth the surface geophysical results. The locations of these techniques are shown in Figures 3.4 and 3.8

3.7.1 2-D electrical resistivity imaging (ERI)

As a consequence of the marked trends on the apparent resistivity distribution maps (Figure 3.8), electrical methods (in particular, resistivity tools) are adjudged suitable to detect, localize and characterize the distribution of the subsurface structures at the study site in terms of the resistivity variations.

The tomographic variants of the electrical method (e.g., electrical resistivity imaging, ERI) have become the most universally applicable. 1-D methods such as the vertical electrical soundings (VESs) presented in section 3.6 are based on the assumption of horizontally homogeneous subsurface conditions (that is, intra-stratigraphic homogeneity) (Khalil and Santos, 2013). Given that lateral variations along the survey line can affect results significantly and individual anomalies will not show explicitly in the results, ERI help surmount the difficulty of the VES data in resolving more subtle, complex and/or small-scale features. Interpreting heterogeneous subsurface conditions using 2-D inversion schemes provides more accurate subsurface resistivity models (Daily et al., 2004; Zarroca et al., 2011).

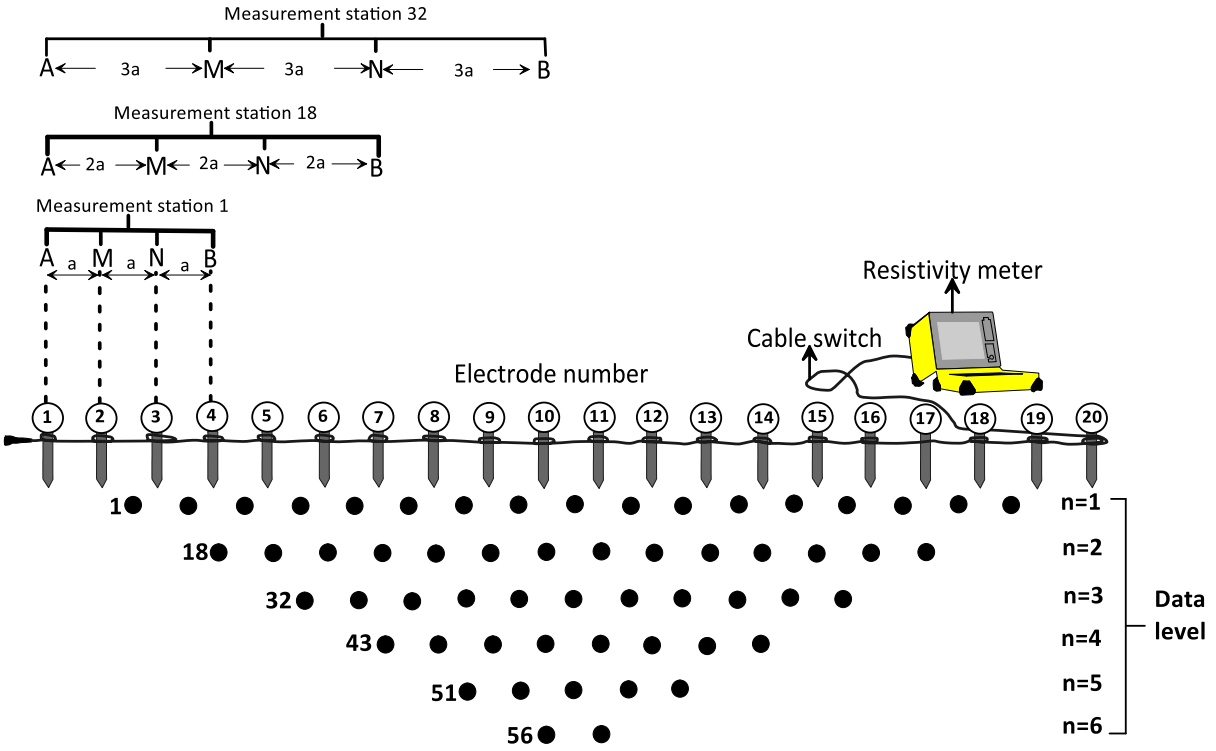

Figure 3.9. Sequence of measurements for creating a 2-D resistivity pseudo-section based on Wenner array. Wenner array makes use of equally spaced electrodes at a specific data acquisition level.

Nevertheless, in the same way as the VES, during ERI surveys, the spatial variation of electrical resistivity is estimated using four electrodes. Any combination of the electrodes can be used for current injection and voltage measurements to obtain resistance values, which when multiplied together with the appropriate geometric factor (a function of distance between the four electrodes) permits the determination of the so-called apparent resistivity. Multiple single apparent resistivity measurements with different electrode spacings and midpoints can then be acquired as tomographic data. Thus, the pseudosection, which represents the distribution of apparent resistivity measurements taken from electrodes arranged along a survey line form the basis of the tomographic investigations (Tassone et al., 2010). Because this approach is time consuming and require more field personnel, the ERI is usually implemented using an array of electrodes (that is, based on the multi-electrode resistivity imaging system), which combines aspects of both sounding and profiling to provide 2-D images of the heterogeneous subsurface structures (Figure 3.9).

3.7.1.1 ERI data acquisition, processing and inversion

In this study, ERI data were acquired using a RESECS multi-electrode device (Geoserve, Germany) along three survey profiles (ERI1, ERI2, and ERI3), aligned across the identified low apparent resistivity feature (Figure 3.8). Toward the Wurmlingen settlement (Northwest) and the hillslope environment (up North) of the study area, ERI1 is aligned SW – NE while on the floodplain area, ERI2 and ERI3 are aligned parallel to each in the N – S direction. Wenner-alpha array/electrode configuration was adopted due to inherent advantages of good signal-to-noise ratio (Revil et al., 2005) and good resolution of horizontal layers, however has moderate rating for the

resolution of steeply deeping structures (Wyatt et al., 1996). I used 192 electrodes between the current and voltage electrodes for each profile at 1 m spacing for ERI1 and ERI2 and at 1.5 m spacing for ERI3. A total of 4365, 3339, and 4830 measurements with initial maximum depths of investigation of 17.8, 16.1, and 38 m, respectively were generated for ERI1, ERI2, and ERI3, assuming theoretical relationships between electrode spacing and geometry for ideal homogeneous subsurface conditions (e.g., Loke, 2001). Although, ideally, the resulting apparent resistivity image or map would be a good first approximation to the actual subsurface resistivity, requiring no assumption about the nature of the subsurface in advance (Caldwell and Bibby, 1998), interpretations made only from the raw unprocessed resistivity field data (pseudosection) can be challenging. Therefore, potentially more reliable information can be obtained from data processing, and subsequently, the processed is then subjected to inversion. Rather than the apparent resistivity presented in the pseudosection format, inversion procedure accounts for variables such as the arrays and suggests true resistivity values.

Apart from taking care of inherent subsurface characteristics such as layers of loose boulders and air voids that can cause misfit points, ERI data processing would generally involve editing according to some criteria such as determining which minimum voltage/current levels are physically realistic, identifying noise (usually due to high contact resistance between the electrode and earth) and deleting data points due to poorly coupled/malfunctioning electrodes. Data error and voltage error estimated using default values of 3% noise and a voltage of error of 0.1 mV were used to account for the variable quality of the individual data. Such steps help to reduce error in the final tomogram.

Just as in every geophysical modeling process, ambiguity of different models/solutions that satisfy a single data is a looming problem. That is, a model (m) is sought for, that explains the measured/observed data (d) to a certain degree by minimizing error $(e) = d - f(m)$ (that is, producing acceptable misfit) in a least square series – where $f(m)$ is the model response (Günther et al., 2006). Thus, the main objective of the modeling process is to minimize a weighted data misfit. Inversion algorithms are generally used to model the acquired ERI data by converting field-measured (observed) apparent resistivity data to calculated (predicted) apparent resistivity data. Misfits – deviations from the model's solution at individual data points can be calculated as (Greer et al., 2017):

$$\text{Misfit} = \frac{\left| d_{observed,i} - d_{predicted,i} \right|}{d_{predicted,i}} \tag{3.3}$$

In this study, the inversion procedure was implemented in DC2DInvRes based on a Gauss-Newton type minimization with a smoothness-constrained explicit regularization as described by Günther et al. (2006). During the nonlinear iterative resistivity data inversion process, the DC2DInvRes software compares the resulting predicted data from a forward model to the observed data and iteratively varies the inverse model resistivities to decrease the misfit between the model result and the measured data. The inversion process solves an optimization problem in order to obtain an optimal model. Objective function (Φ) of a mathematical programme is used by the optimization procedure to measure the size of the model and to select better model over poorer model. Φ consists of an error-weighted data misfit (Φ_d) plus the model roughness/norm (Φ_m) weighted by the regularization/tuning/Tikhonov parameter (λ) as expressed in Eqn (3.4):

$$\Phi = \Phi_d + \lambda \Phi_m \tag{3.4}$$

$$\Phi_d = \sum_{i=1}^{N_d} \left(\frac{d_{obs,i} - d_{pred,i}}{\varepsilon_i} \right)^2 \tag{3.5}$$

where N_d is the number of measurements, d_{pred} is the predicted data, $d_{obs}$is the measured data, and ε_i is the standard deviation of the measured data. Φ_d measures the minimized discrepancy between predicted and observed data according to a certain norm, that is, the ℓ_2 - Norm (or least least square – that is the sum of the weighted squared data errors for the entire survey):

$$\ell_2 - \text{Norm} = \frac{\sum_{i=1}^{N_d} \left(\frac{d_{obs,i} - d_{pred,i}}{W_i} \right)^2}{N_d} \tag{3.6}$$

where W_i is the weight factor assigned to each data point via the data weighting matrix, a function of assumed data error (Binley et al., 1995).

Φ_m contains information that characterize the model's closeness to a reference model, and the amount of structure in the spatial direction. With basically an unkown value when the inversion begins, λ would serve the purpose of controlling the relative importance attached to obtaining a small misfit and reducing the value of the model norm.

The error-weighted Chi-squared fit/statistic (χ^2) and the root mean square (RMS) error are also available to measure data fit during the iterative inversion procedure. $\chi^2$is related to Φ_d as,

$$\chi^2 = \Phi_d / (N_d - 1) \tag{3.7}$$

Under the assumption of a Gaussian distribution of data errors, the smoothness-constrained inversion finds the smoothest model whose response fits the data to the a-priori χ^2 as the convergence criterion. In general, $\chi^2 = 1$ means a perfect fit, good convergence to the solution, and indicates that the data are appropriately weighted (Holbrook et al., 2014) given the actual noise and data noise is normally distributed (Johnson et al., 2012). The RMS error corresponds to the difference between the measured and calculated apparent resistivity, in percent, given by

$$RMS = \sqrt{\frac{\sum_{i=1}^{N_d} \left(\frac{d_{obs,i} - d_{pred,i}}{d_{pred,i}} \right)^2}{N_d}} \; x100 \tag{3.8}$$

As another suitable parameter for measuring the goodness of the fit, RMS error evaluates the spatial variability of the electrical resistivity. A large RMS indicates that the electrical resistivity is highly variable. This could indicate the presence of several abnormal data points. Possible solution is to delete the abnormal data points and restart the inversion process so as to achieve model convergence.

The roughness of the models was tuned using the smoothness constraints of 2nd order due to its usefulness in delineating boundaries of small bodies such as the linearized low apparent resistivity feature idenitified in Figure 3.8d. Because the smoothness model constraint can result in slower convergence, significant improvement in the convergence speed was ensured (in

combination with line search and global regularization). To account for significant outliers in the ERI data that often lead to poor data fits; robust modeling, an $\ell_1 - \text{Norm}$ minimization scheme based on iteratively reweighted least squares (see Günther et al., 2006) was selected. Because the $\ell_1 - \text{Norm}$ adds a penalty function that minimizes the absolute deviation (residual) between observed and theoretical response, it effectively downgrades the role of outliers in the measurements. On the other hand, ℓ_2 - Norm may not work in the presence of outliers. This is because the square of the deviation between the theoretical and observed response would weigh disproportionately on the penalty function. As a result, the outcome of the inversion using the ℓ_2 - Norm biases towards the outliers. Even though the outliers may present themselves as noise in any conductive feature, they are difficult to identify. Therefore, choosing the more appropriate penalty function is an important recommendation irrespective of one's preconception about the geometry of a conductive structure. It was however, highly dignifying to have initially observed and assessed the systematic outliers in the data given that one can easily loose resolution. Ideally, resulting misfit plots should represent uncorrelated random distributions. But when robust modeling results in low resolution, some systematic layering might show on the plot hinting that some information still remain. In this regard, the vertical weight (z-weight) of 1 was set to improve interpretations related to the layering associated with vertical contrast in the misfit function. Overall, λ played a key role in controlling the strengths of the smoothness. Trial-and-error approach was used to select a fittingλ, starting with a higher value. For the data from the three ERI profiles, $\lambda = 10$ was selected during the full inversion process for keeping the χ^2 value within a reasonable limit. At a very large χ^2, the error estimates were also increased to keep the χ^2 within limit.

3.7.1.2 Interpretation of the ERI results

Figure 3.10 (a, b and c) shows that the forward response of the inverted models fit well with the observed data, except at few spots that have low data coverage. The RMS data misfit values of 8.06, 3.54, and 4.47 % were obtained for the smoothness-constraint inversion aborted with the χ^2 values of 1.60, 0.08, and 0.46 for the final ERI1, ERI2, and ERI3 resistivity models, respectively. The recorded RMS misfit values represent the expectations on data quality and the number of observations as well as the number of parameters to which the model is constrained. According to Brody et al. (2015), while an RMS error value of < 5 % is ideal for processing, RMS values of < 10 are generally deemed acceptable. Also in Figure 3.10, the low-certainty inversion region is shown as the completely blanked out region whereas high-certainty region is imaged without shading. This follows the inversion sensitivity coverage, a measure of the model cell resolution. Overall, these indicators evaluate the robustness of the ERI survey results.

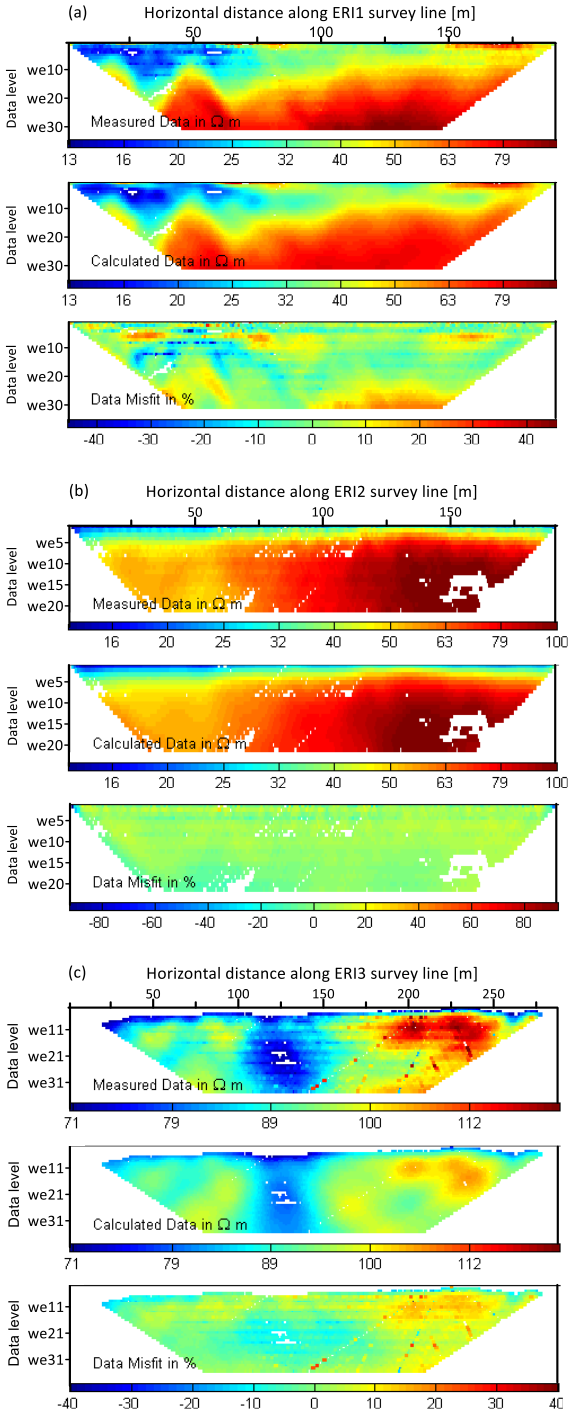

Figure 3.10. Measured data, calculated data and data misfit between the observed and predicted data for (a) ERI1, (b)ERI2, and (c) ERI3. The predicted data appear reasonably consistent with the observed data except at areas of low data coverage.

Figure 3.11 (a, b and c) shows the inverted resistivity models (ERI1, ERI2 and ERI3) of the measured apparent resistivity data. ERI results reveal strong variations in the resistivity values along the profiles. ERI1 profile (Figure 3.11a) displays two distinct zones: a 5 to 7 m thick layer of low resistivity, which was quickly identified as alluvium sediments, overlain well-defined and potentially high resistivity bedrock. Within the alluvium, patches of relatively higher resistivity features near the surface could indicate the presence of distinctly coarser-grained sediments compared to other finer-grained sediments. Although the alluvium-bedrock boundary appears nearly horizontal, it is apparent that the alluvium thickness is lower and the bedrock shallows

toward the higher elevation zone on the left (SW) than to the right (NE). Also, along horizontal distance between 20 and 45 m, the bedrock seems to be deeply scoured.

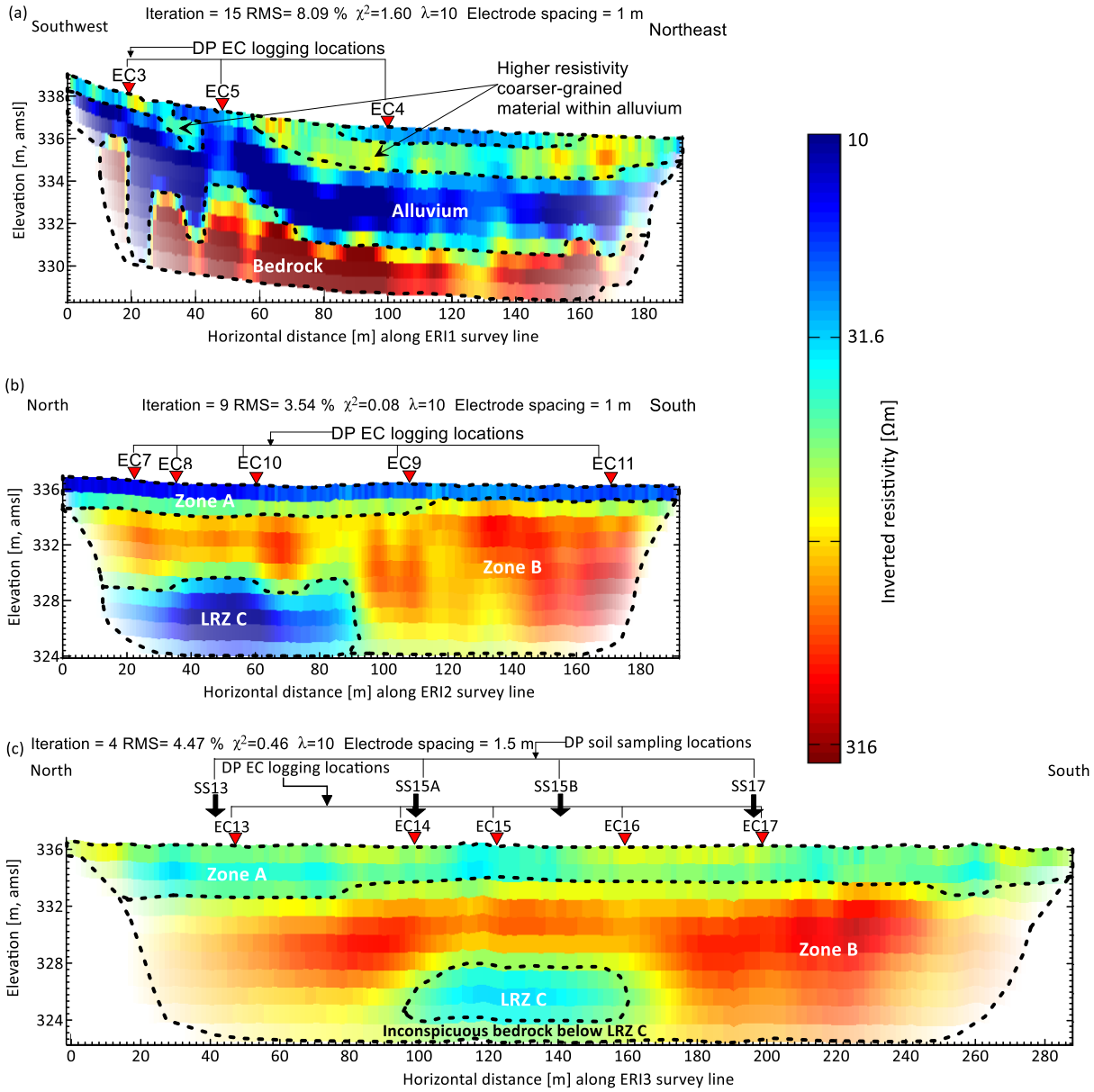

Figure 3.11. Electrical resistivity tomography models for the Wenner electrode configuration along (a) ERI1, (b) ERI2 and (c) ERI3 profiles. Dashed black lines are resistivity interfaces that demarcate zones identified in the subsurface. Respective locations from where the ground-truthing data (DP-based soil EC logging and lithologic sampling (SS)) were acquired are also shown.

In contrast to ERI1(Figure 3.11a), both ERI2 (Figure 3.11b) and ERI3 (Figure 3.11c) delineated three main resistivity zones. The uppermost zone A near the surface is characterized by an electrically conductive layer. Below zone A lies a relatively high resistivity zone B. Zone B appears to enclose a confined low resistivity zone ('LRZ') C. The low resistivity zone C spans from the horizontal distance of ~30 to 90 m along the ERI2 survey line and from ~ 90 to 160 m along the ERI3 survey line. Noticeably in ERI2, there is no clear presence of a resistive bedrock feature underneath 'LRZ' C like that highlighted along ERI1 profile. The implication is that the clarity of such bedrock interface along ERI2 profile is simply not within the model region of inversion. Along ERI3 profile, a potential bedrock feature underlain the 'LRZ' C is present but inconspicuous.

Comparing the ERI2 and ERI3 profiles results, it is possible that longer ERI3 profile would have imaged deep-seated bedrock features better. Also, the closeness of the ERI1 profile to the hillslope and the depositional sequence of sediments in the area (that is, shallower transition from alluvium to the bedrock) would have facilitated the easy imaging of the alluvium-bedrock interface unlike in ERI2 and ERI3 profiles on the floodplain - farther away from the hillslope.

Overall, as expected of the ERI results, the smeared boundaries between the 'LRZ' C and the surrounding high resistivity zones can also result from ambiguities and non-uniqueness problems inherent in the geoelectrical methods (e.g., Hoffmann and Dietrich, 2004). The regularization constraints introduced to address problems of ill-posed, non-unique solutions by minimizing the roughness of an image (in particular, resistivity inversion routine) often smooth out fine-scale geophysical structures (e.g., Tarantola, 2005; Binley et al., 2015), unequivocally resulting in the difficulty to demarcate the bedrock features (Hirsch et al., 2008; Hsu et al., 2010). The observed poor resolution in depth is also probably controlled by the high resistivity zone B, which may have restricted deeper penetration of the injected current. Thus, just as with geophysical techniques, the resulting resistivity models are not unambiguously dependent on data quality, measurement geometry and the choice of inversion parameters (Hauck et al., 2007).

Prominent feature on the ERI2 and ER3 models is the presence of the confined 'LRZ'C. Here, connecting the 'LRZ'C feature on ERI2 and ERI3 profiles with the feature identified between the horizontal distance of 20 and 45 m on ERI1, it seems clear that the ERI results confirmed the pronounced and linearized low apparent resistivity feature at electrode spacing equals 60 m (Figure 3.8d). Although the electrical resistivity method appears to have successfully and independently mapped the distribution of subsurface resistivities, which could relate to the variability and dynamics of subsurface hydrological structures (e.g., Parsekian et al., 2015), interpretations of the bedrock structure (particularly on the floodplain area) suggest the need for combined, more elucidatory and complementary interpretations with other geophysical tools.

3.7.2 2-D refraction seismic tomography (RST)

In a bid to detect a bedrock surface, which may have been less confidently-resolved by the ERI data due to the problem of decreased resolution with depth, I also conducted a refraction seismic survey aimed at delineating subsurface layers of differing velocities. In refraction seismic studies, the depth of sediment/alluvium between the water table and basement, which is necessary for a successful water-table estimation, may hinder precise determination of the alluvium-bedrock interface. This problem is often encountered in deeper alluvium-bedrock interface. Hence, factoring in such a scenario is always advised when planning refraction seismic surveys. In this study's refraction seismic survey setup, the transect length, and orientation (e.g. Haeni, 1988), was aligned to cross the identified low resistivity target structure along ERI3 survey profile (Figure 3.8d) in a manner that ensured good coverage and to minimize the influence of one of the common problems of refraction seismic just highlighted.

3.7.2.1 Refraction seismic data acquisition

The refraction seismic method involves transmitting seismic energy into the ground and recording the arrival of the direct and refracted compressional-waves (P-waves) at preset distances along the ground surface (Figure 3.12). The refraction seismic data were acquired using a 24-channel Geometrics Geode Seismic Recorder and 14 Hz P-wave geophones. The energy source was provided by the equivalent of 7.5 kg sledgehammer striking stainless steel plate. Geophones were laid out and buried in a way to improve energy coupling over a distance of 95 m from position 70 to 165 m along the ERI3 survey line. The geophone spacing was 1m and a total of 20 shots were fired at 5 m spacing between the two ends (inclusive) during the survey. The data were sampled at 62.5 μs interval using a recording length of 0.25 s, a low cut filter of 15 Hz to take out low frequency noise and a notch filter equal to 50 Hz to handle any powerline-related noise frequency. To enhance the P-wave arrivals (onset of the signal) during picking, the signals were processed minimally using only a 50-100-300-500 Hz bandpass filter to remove low frequency cultural noise (e.g., Zollo et al., 2003). Typically, the data were of good quality and clear P-wave arrivals can be identified for picking, as an example shot gather in Figure 3.13 illustrates.

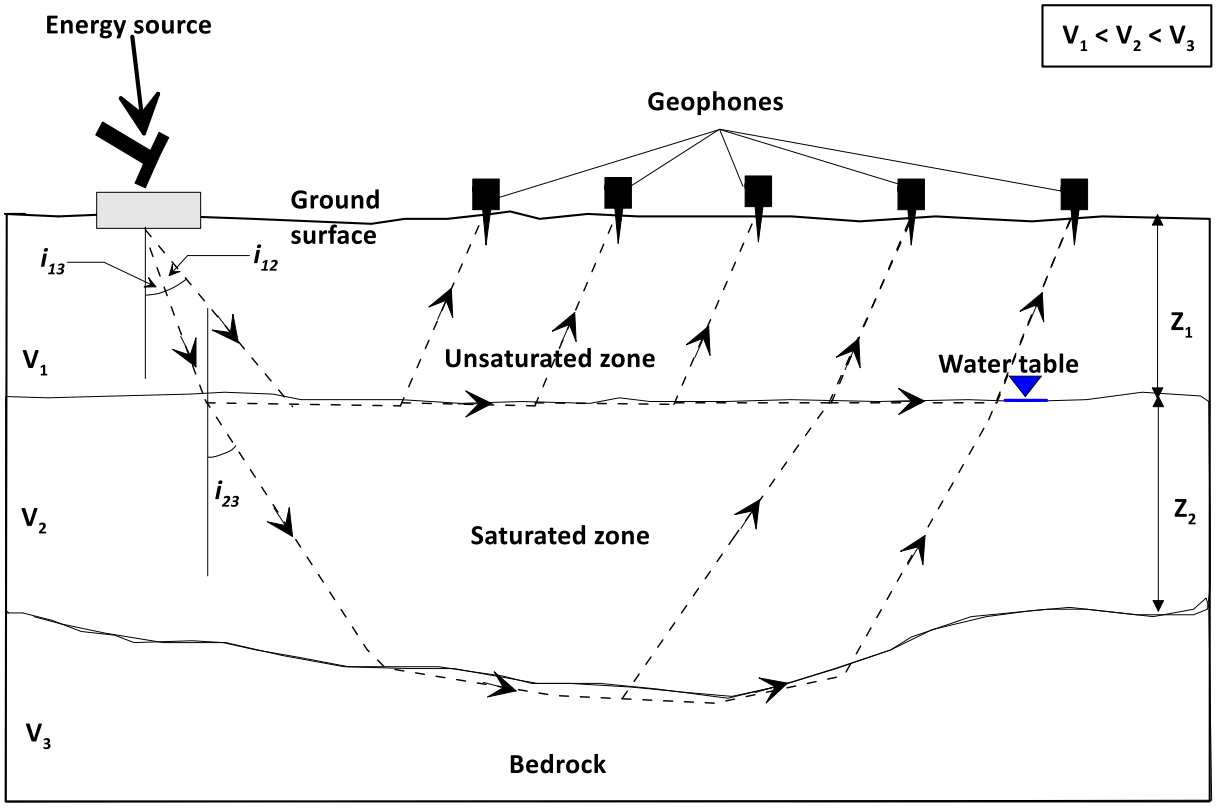

Figure 3.12. A typical three-layer field refraction seismic geometry and layout. Surface refraction seismic ray paths are also shown.

3.7.2.2 Travel times and pick uncertainty

The P-wave first arrivals were picked manually with the Reflexw, version 7.5 software (Sandmeier, 2012). The accuracy of the refraction seismic interpretation methods and final solution depends on using consistent first break arrival times. Picking individual traveltimes can be time-

consuming, and prone to error even with relatively simple, high-quality data (Biondi, 2007). Therefore, assigning prior uncertainties to the first arrival picks is necessary, especially when inverse modeling to avoid over- or under-fitting the data (Zelt, 1999). To estimate pick uncertainties, certain guidelines have been issued: uncertainties are often assigned qualitatively by inspection, taking into account the data's S/N ratio and frequency content (Zelt and Forsyth, 1994), time difference of reciprocal times (that is, travel time reciprocity) (Zelt et al., 2006) or where two profiles intercept (Park et al., 2007), and by estimating picking uncertainties as part of an automated picking routine (Toomey et al, 1994). In this study, the approach of repeated picking was applied to obtain a number of arrival time values for each trace (e.g., Bauer et al., 2010). By repeated traveltime determination, mispicks are not used as single data values in the inversion but are statistically averaged. Individual data errors can be derived directly from the picking process without statistical assumptions and used for data weighting in the tomographic inversion.

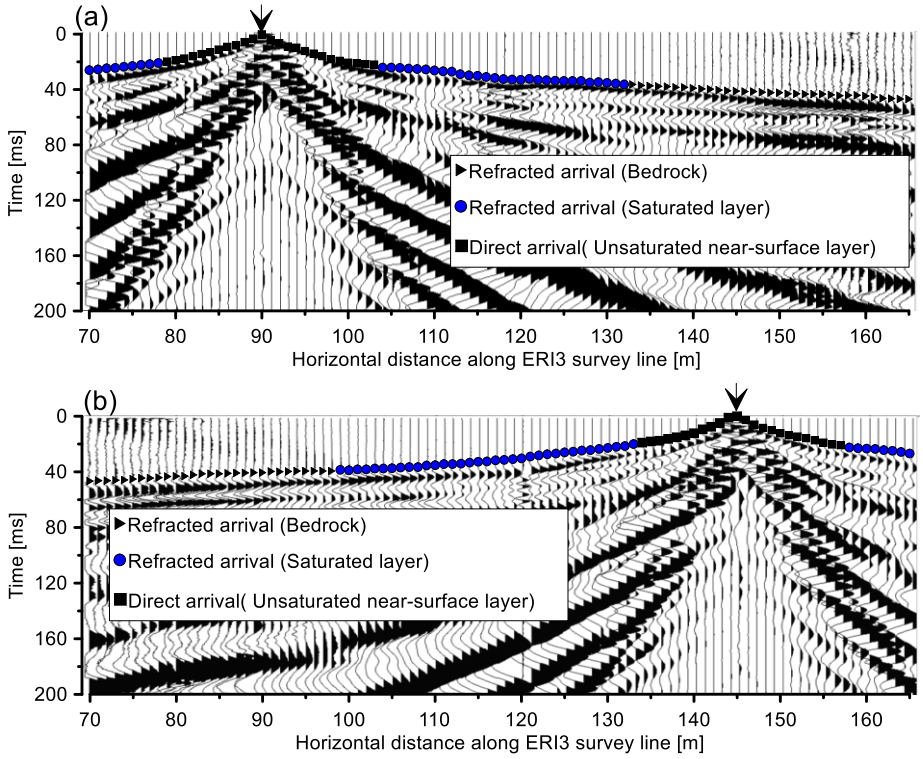

Figure 3.13. Example of shot gather from the surface refraction seismic surveys recorded at shot location (a) 90 m, and (b) 145 m along the ERI3 survey line. Picked first arrivals are also shown. The arrow pointing down shows the shot location on the ground surface.

The average traveltime, $\overline{t_i}$ determined for each trace (i) from a number of picks N_i with traveltimes t_{ik} can be expressed as:

$$\overline{t_i} = \frac{1}{N_i}\sum_{k=1}^{N_i} t_{ik}, \tag{3.9}$$

where N_i is basically 5 – 10 (that is, I picked the onset of each trace randomly about 5 - 10 times). The standard deviation, S_i accounted for the relatively small number of values per trace, and was used to provide unbiased parameter estimation for pick uncertainty as:

$$s_i = \sqrt{\frac{1}{(N_i - 1)} \sum_{k=1}^{N_i} (t_{ik} - \bar{t}_i)^2} \tag{3.10}$$

Figure 3.14 (a and b) shows an overview of all and reduced average traveltime values, respectively as a function of the source and receiver locations. As noted by Bauer et al. (2010), the plot with reduction velocity of 4000 m/s reflect the variations of the traveltime function along the profile for specific offsets and related penetration depths. The standard deviation calculated from repeated determination of the first arrival travel times are also shown as a function of source and receiver locations in Figure 3.14c. Shown in Figure 3.14d (that is, the distribution of the standard deviation in a histogram), it was observed that about ninety-two percent of the travel times were picked with standard errors 0.19 - 0.665 ms. This value approximates a quarter period corresponding to the dominant frequency of the filtered data, which is roughly 376 - 1315 Hz.

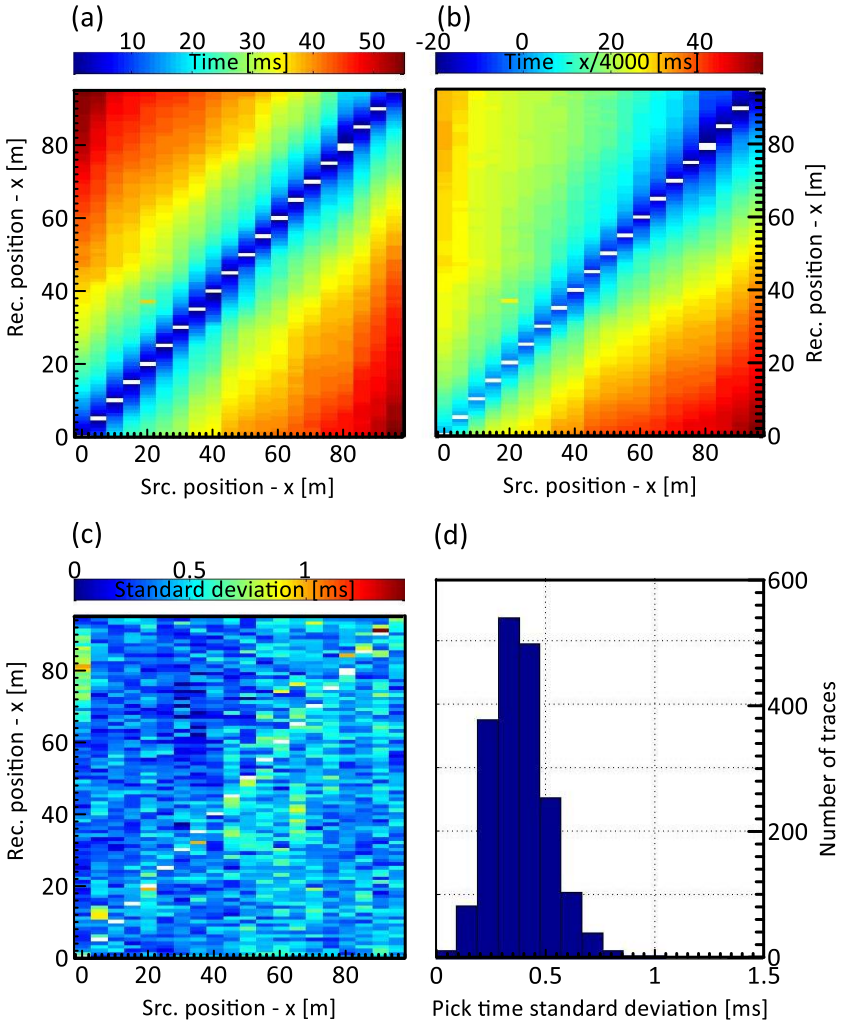

Figure 3.14. First arrival travel times: (a) Unreduced, and (b) Reduced with a 4000 m/s reduction velocity as a function of the source and receiver location. (c) Standard deviation of first arrival times determined from repeated picking (varying between 5 and 10 times) as a function of the source and receiver location. (d) Histogram of the travel time standard deviation presented in Figure 3.14c.

According to Zelt et al. (2006), a rule of thumb for picking accuracy is that an arrival can be identified at best to within one-quarter of the dominant period because if two waves arrive within this interval, they will add constructively and cannot be distinguished from one another. To weight the traveltime data during the tomographic inversion, picks were assigned an uncertainty in the range 0.19 – 0.665 ms.

3.7.2.3 Estimation of layer velocities based on delay time analysis

Raypath propagation of seismic waves is definitely influenced by the initial model of the P-wave velocities and associated gradients. Thus, incorporating preconceived structures and layer velocities in the initial model not required for model parameterization may diminish the overall credibility of the final objective travel time tomographic model (Zelt and Forsyth, 1994). These are subjective choices that can be largely addressed by estimating the minimum model structure required by the least subjective portion of the traveltime data thereby guaranteeing a higher degree of certainty and differentiation from a structure that is merely consistent with the data. Travel times of first arrivals can be analyzed individually for various shot gathers to derive a number of 1-D velocity-depth profiles along a refraction seismic survey profile (Sain and Kaila, 1996; Vijaya Rao et al., 2007). Subsequently, the 1-D models are assembled to obtain the gross subsurface structure representing the pseudo 2-D velocity model that is used as a starting model for 2-D travel time tomographic inversion (Lanz et al., 1998). However, the approach of using 1-D reference models may not clearly capture low velocity structures or those features that are important to geological interpretation. In this sense, refraction seismic interpretation techniques usually based on simple planar geologic layered models commonly restricted to two or three layers, may be of limited use for heterogeneous subsurface structural conditions. Like the ERI technique, RST inversion schemes can be employed for reliable 2D interpretations. The RST assessment is not intended to supersede the minimum-structure models. This is because the minimum-structure model is typically better resolved and more interpretable except in very complex cases. Moreover, the travel times tomographic approach does not make limiting assumptions, but provides only a smoothed version of the minimum-structure models (Watson et al., 2005). In this study, I used the conventional approach based on the delay time interpretation technique, wherein simplifying assumptions, such as constant velocity, lateral homogeneity within layers, or strictly increasing layer velocities with depth were made to approximate the minimum-structure model of the subsurface. The aim was to determine a simple, but representative subsurface structure that predicts the observed travel time data as accurately as possible without biasing the results during subsequent 2-D traveltime tomography. Delay time is the time taken by a pulse to travel upward and downward a layer. If the delay time beneath a geophone is known, then the depth to the refractor interface can be estimated. The delay time interpretation method can be very effective in mapping non-planar/irregular velocity interfaces.

Assuming that the depths at the shot point and detector are not equal, because of either surface elevation changes or dip changes (and the errors resulting from neglecting dips are negligible for dips of up to 10^{o}, and also not serious for dips as great as 25^{o}), the travel time (t) for a pulse from the shot to any detector beyond the critical distance for a three-layer case is given by

$$t = \frac{x}{\mathrm{V}_3} + \frac{\mathrm{Z}_{s2}\cos i_{23}}{V_2} + \frac{Z_{d2}\cos i_{23}}{V_2} + \frac{Z_{s1}\cos i_{13}}{V_1} + \frac{Z_{d1}\cos i_{13}}{\mathrm{V}_1} \tag{3.11}$$

where x is the horizontal distance from the shot point to the detector, V_1 is the velocity of the first layer, V_2 is the velocity of the second layer, V_3 is the velocity of the third layer (refracting bedrock) and i is the critical angle of incidence ($sini_{23} = V_2/V_3; sini_{13} = V_1/V_3$), Z_s and Z_d are the depths below the shot point and detector, respectively measured normally to the refracting interface. Eqn (3.11) can be re-written as:

$$t = \frac{x}{V_3} + \frac{2Z\cos i_{23}}{V_2} + \frac{2Z\cos i_{13}}{V_1} \tag{3.12}$$

The latter two terms of Eqn (3.12) are the sum of the delay times terminating at the shot point and any detector respectively for layers 1 and 2. At zero offset ($x = 0$), the expression is identical to the intercept time. Palmer (1981) defined the delay time as the "generalized half-intercept time" if the shot depths ($\leq$ 0.5 m) are negligible. This is to say that the delay time interpretation method involves partitioning intercept times into shot and receiver delay times (Barry, 1967). According to Lawton (1989), however, this is easily accomplished for reciprocal records but is more difficult if only end-on records are available. As shown in Eqns (3.11) and (3.12), the sum of the delay times for the shot and any detector for the first and second layers can be determined by subtracting x/V_3 from the detector arrival times of critically refracted arrivals. Because the delay time for the shot point remains constant for any spread, any variations in the delay time for detectors are proportional to variations in depths to the refractors beneath those detectors. The depth beneath the detector to the top of the refractor can then be calculated as:

$$Z_1 = \frac{\Delta \mathrm{T}_1 \mathrm{V}_1}{\cos(\sin^{-1}\mathrm{V}_1/\mathrm{V}_2)} \tag{3.13}$$

$$Z_2 = \frac{(\Delta T_{13} - \Delta T_1)V_2}{\cos(\sin^{-1}V_2/V_3)} \tag{3.14}$$

where Z_1 and Z_2 represent the thicknesses of the first and second layers. ΔT_1 and ΔT_{13} represent the 1st layer and combined layers 1 and 2 delay times, respectively. The second layer delay times (ΔT_2) as shown in Eqn (3.14) is calculated by subtracting ΔT_1 from ΔT_{13}.

From the set of travel time picks, five shots (Figure 3.15a) were selected for applying the delay-time method as described by Pakiser and Black (1957), Redpath (1973), and Dentith and Mudge (2014). The following describe the steps taken in the delay time interpretation method (by graphical analysis):

1 Cautiously delineate arrival times that belong to refractions from the same layer following change in slope at the crossover point and assign various layer velocities (Figure 3.15a). The intermediate shots at positions 90, 115, and 145 m have been included to enable proper resolution of the near-surface layers. The resulting apparent velocity from this procedure indicate that there is a three-layer case: a first layer with a velocity of 556 to 705 m/s, a second layer with a velocity of 1571 to 2187 m/s, and the last third layer (bedrock) with a velocity that lies between 2444 and 4248 m/s. I computed the harmonic means of shots

for the first and second layers on both the northern (N) and southern (S) halves of the survey line and averaged the values for those layers. The computational process for the harmonic mean (HM) values is illustrated below:

$$V_{1(HM)N-S} = \frac{4}{(1/705)+(1/607)+(1/559)+(1/595)} = 612\,m/s$$

$$V_{1(HM)S-N} = \frac{4}{(1/577)+(1/592)+(1/556)+(1/592)} = 579\,m/s$$

$$V_{2(HM)N-S} = \frac{4}{(1/1716)+(1/2187)+(1/1718)+(1/1695)} = 1808\,m/s$$

$$V_{2(HM)S-N} = \frac{4}{(1/1571)+(1/1871)+(1/1802)+(1/1614)} = 1705\,m/s$$

The average velocity values of the first and second layers were found to be 596, and 1757 m/s, respectively;

2 Estimate the true velocity of the refracting horizon (V_3) that is, the third layer velocity using the travel time difference method. This is determined using differences in critically refracted arrival times from end-shots. As shown in Figure 3.15b, both arrivals, which must be refracted from the same layer, were added to the added arbitrary Y-axis line of 70. The resulting velocity value of 2477 m/s defines the velocity function, which comprises a line whose slope is $2/V_3$. Changes in slope might be indicative of lateral changes in velocity, in which case a series of straight-line segments may be fitted to the data. The calculated V_3 velocity value of 2601 m/s was found to be in reasonable agreement within the range of the nominal velocities of 2444 and 4248 m/s estimated in Figure 3.15a.

3 Calculate the delay times. For the three-layer case considered, I computed the delay times for layer 1 (ΔT_1), and layer 2 ($\Delta T_2 = \Delta T_{13} - \Delta T_1$). For the end-shots (Figure 3.15b), the intercept times (T_{int2}) emanating from the second layer were halved to represent ΔT_1. Half intercept times are also available at the intermediate shot positions 90, 115, and 145 m. The delay times at the remaining receiver/geophone stations, were obtained by interpolating between the half-intercept times. From the travel time curves for opposite ends of a reversed spread (Figure 3.15b), a line is drawn through the origin whose slope is equal to the known velocity of the refractor (V_3) determined using the approach described in step 2. The ΔT_{13} values (Figure 3.15c) are then determined by scaling the time difference between each arrival time (beyond the critical distance) and the corresponding position on the sloping line. This is equivalent to subtracting x/V_3 from the recorded detector arrival times and halving the results. Also, according to Eqns (3.11) and (3.12), the intercept times emanating from the third layer (T_{int3}) is sum of the delay times at the shot and detector combined for layers 1 and 2. The observed vertical offset in the two delay time curves, shows that the depth to the refracting horizon is greater at Shot 1 than at Shot 2 up to the horizontal distance of 144 m and vice-versa.

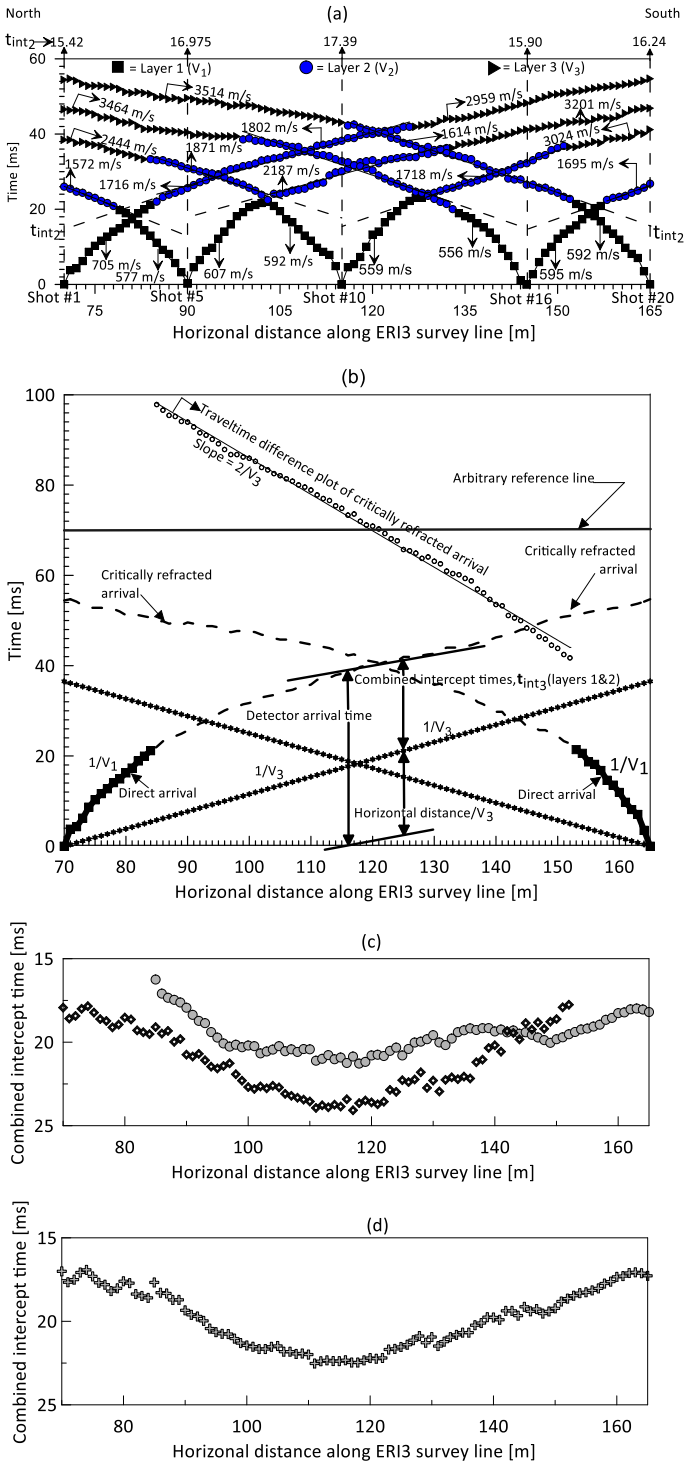

Figure 3.15. Delay time analysis for a three layer case. (a) Selected travel time plots used for identifying subsurface layers by apparent velocities (and changing slopes) and determining intercept times for the first layer. (b) Computation of the third layer velocity (V_3) by travel time difference method and estimation of the intercept times layers 1 and 2 (combined) (c) Combined intercept times for each detector beyond the critical distance. (d) Delay times in (c) adjusted vertically for the best fit.

4 Adjust the computed total delay times (ΔT_{13}), which is the half-intercept times (T_{int3}) from opposite ends vertically for the best fit (Figure 3.15d) using the difference between the times for the overlapping zones and average of the difference for the non-overlapping

zones.

5 Based on the estimated delay times, compute the layer thicknesses, Z_1 and Z_2, using Eqns (3.13) and (3.14).

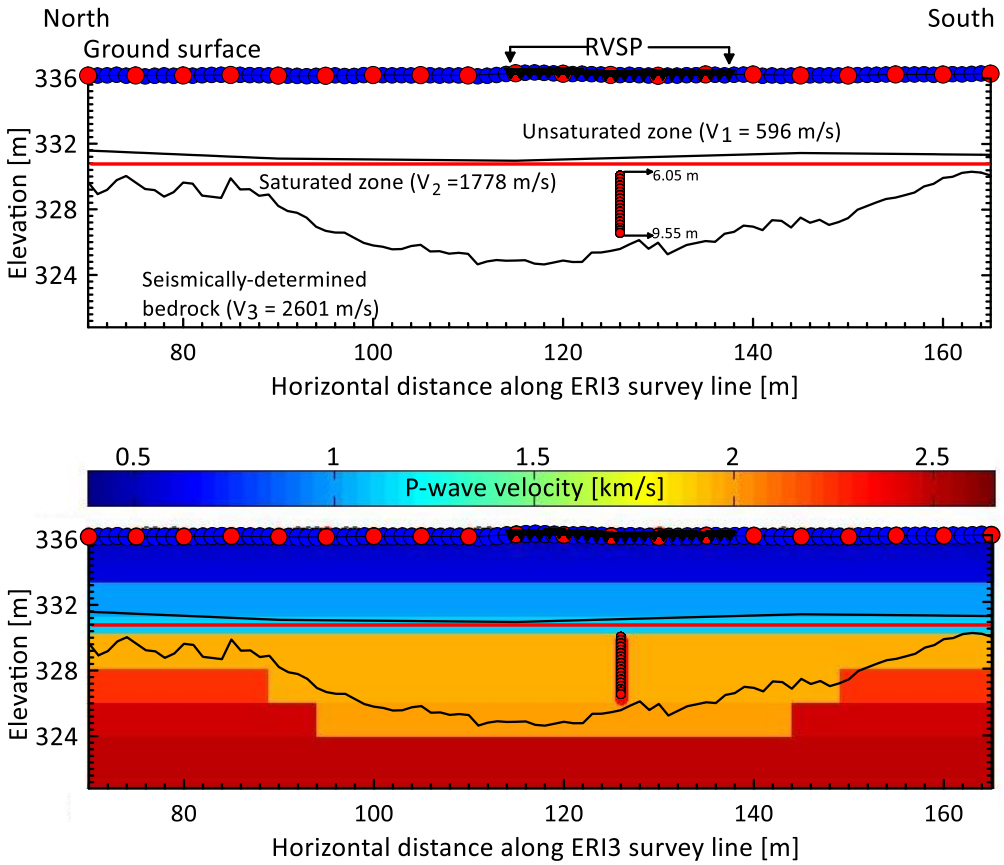

Figure 3.16. (a) Resulting interpretation of the time-distance graph of Figure 3.15. The interpreted refraction seismic cross section indicates the presence of a depression on the surface of the seismically-determined bedrock. (b) Initial model for the tomographic inversion of P-wave travel times. North and South refer to the spatial orientation of the survey section along the ERI3 survey line. The closed red circles are surface refraction seismic and downhole reverse vertical seismic profile shot points. The closed blue circles represent the surface refraction seismic receivers while the inverted black triangles are the reverse vertical seismic profile receivers. The red horizontal line indicates the groundwater table.

3.7.2.4 Model parameterization for refraction seismic tomography

Figure 3.16a shows the interpreted subsurface velocity cross-section model from the observed travel times based on the delay time analysis. From Figure 3.16a, the 2-D starting velocity model (Figure 4.16b) for the travel time tomography was parameterized. This initial 2-D velocity model represents a velocity field with values on discrete mesh of grids or cells. The model spans 95 m horizontally, from 70 m to 165 m along the ERI3 survey line and 18 m vertically, from 0 to 18 m (elevation above mean sea level was attached to these depths ranges), creating a 96 by 19 grid nodes for the forward step and a 95 by 18 grid of 1710 cells for the inversion. Because the ray density and number of crossing rays generally decrease with increasing depth (e.g., Lanz et al., 1998;

Krautblatter and Draebing, 2014), to account for the resulting decreases of resolution with depth during the inversion, it was also appropriate to increase model cell size with depth as shown in the initial model. In this sense, I used a uniform-grid model of relatively small cells and larger model cells in the shallow and deeper regions of the model, respectively for the forward travel time calculations and inversion.

Several inversion routines for the seismic travel time tomography have been developed, many of which have become commercially available over time. Sheehan et al. (2003) evaluated a number of the refraction tomography codes for near-surface applications. For the travel times tomographic inversion, I employed a MATLAB-based isotropic finite-difference travel time inversion program (Paasche et al., 2008). This inversion program uses a damping and a smoothness constraint based on ray tracing algorithm. Horizontal smoothness constraints of 100 evaluated how similar the neighboring raypaths are, in the horizontal direction while a high damping constraint of 10,000 ensured that the model remain unchanged by suppressing fluctuating high or low values in the model. I assumed that the contact between the first layer and the second layer represents the unsaturated layer and the saturated zone boundary. Thus, I allowed sharp velocity contrast in the inversion by disabling vertical smoothness constraints at a depth of 6 m below the ground surface. The idea behind the refraction seismic travel times tomographic inversion is that the velocity values on the grids or cells that will best fit the observed travel times will be sought after. In the process, the discretized initial velocity model is modified through an iterative process to yield smoothed model with the minimum amount of required structure that fit the observed data adequately. The trial- and-error process of forward modeling was used to compute the model travel times for all traced raypaths based on the initial constraining estimates of the near-surface velocity model. Just as in every geophysical modeling process, the inverse modeling then compares the computed (synthetic) travel times to the measured (observed) ones and the difference (travel time residual) applied for velocity corrections and ultimately used to produce an updated velocity model. A total of 1919 averaged P-wave travel time data for each trace picked, were inverted to retrieve the final P-wave velocity of the investigated subsurface.

3.7.2.5 Interpretation of the RST results

Four iterations in total, reduced the RMS of the travel time residual (Figure 3.17) from 1.53 to around 1.26 ms for the final surface refraction seismic tomography (RST) model. At 95 % confidence interval, my picks uncertainty ranges lie within this travel time residual. Figure 3.18a shows the final P-wave velocity model. Unlike ERI results, the computed standardized coverage for the RST is either 0 or 1 depending on whether a ray crosses a model cell or not. Here, the blanked region without ray crossing is represented by 0 whereas the regions with ray crossing are represented by 1. The P-wave velocities in the model increase gradationally with depth from ~ 250 m/s to about 700 m/s near the surface (depths 0 - 3.5 m). Higher P-wave velocity values (up to 950 m/s) are observed in the lower zone from depths 3.5 to 5.75 m. This range of velocities (250 – 950 m/s) is compatible with the expected P-wave velocity values in the heterogeneous unsaturated sediments (e.g., Knight and Endres, 2005). The inversion results showed that at position x = ~ 90 – 160 m and y = ~6 – 12 m, the subsurface takes a concave up/trough-like shape. This deeper trough-like structure appears to be filled with sediment materials that exhibit lower P-wave velocities in the range of 1500 to 2000 m/s compared to the base and flanks with

higher P-wave velocities. This range of P-wave velocity values is consistent with typical seismic velocities of floodplain alluvium (e.g., Brody et al., 2015). The observed trough-like low P-wave velocity structure within the middle portion of the profile suggests the existence of a strong velocity gradient. The low P-wave velocity structure is followed by a visible transition into a higher velocity layer (over 2500 m/s) that runs underneath the low P-wave velocity structure and to the both sides of the structure.

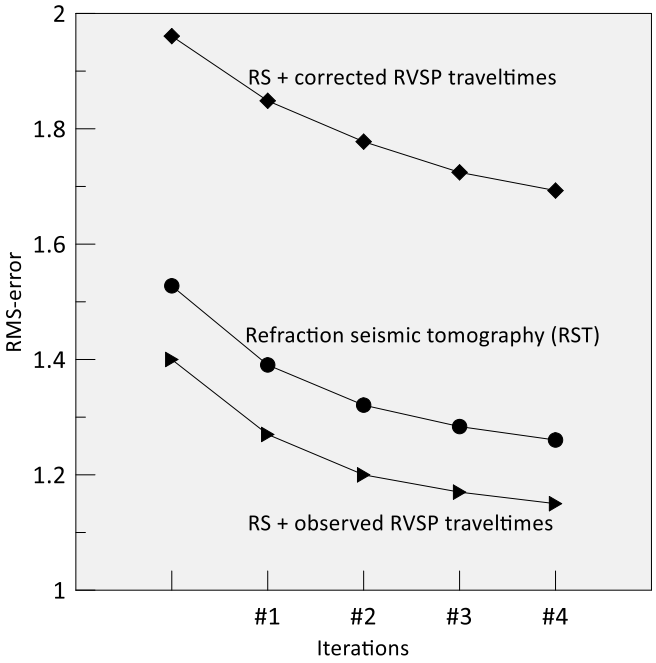

Figure 3.17. Root-mean-square (RMS) error as a function of the number of iterations of the inversion algorithm. The three curves signify inversions for the refraction seismic (RS), RS plus observed reverse vertical seismic profile (RVSP) travel times, and RS plus corrected RVSP travel times.

Displayed in Figure 3.18b, the spatial distribution of the color-coded travel time residual values (that is, observed travel times minus calculated travel times) as a function of the source-receiver offsets provides an indication of how well the travel time inversion predicted the observed travel times. In general, smaller and uncorrelated travel time residuals show that the assumption on the linear approximation of the relationship between the velocity model and the travel times is not violated during the inversion process. Negative residuals represent fast travel times whereas positive residuals represent slow travel times. There appear to be some inversion resolution problems at some source-receiver positions (see small arrow indications in Figure 3.18a). The ray coverage (Figure 3.18c) measured the hit count and angular coverage of all traversing raypaths. By examining the raypaths, information about regions of accuracy in the model is evaluated. The introduction of the localized channel feature in the initial model has been recognized by some studies (e.g., Lanz et al., 1998) to contradict the assumption of continuous constant layers. In this regard, it is proposed that there may be absence of rays passing through certain parts of the final models thereby exacerbating the problems of using RST to study such features. This is also because; the presence of such a feature may likely hinder the passage of refracted seismic energy into the bedrock and back to the detectors on the ground surface in measurable amounts. However, this may not always apply and was not the case in this study wherein ray coverage through the

channelized zone was quite dense. This indicates that the refraction seismic survey coverage of the area of interest was reasonably enough and practical. The observation of dense ray coverage demonstrates that the subsurface velocity model is likely well-constrained against diffuse raypaths which could suggest that the model is less well determined.

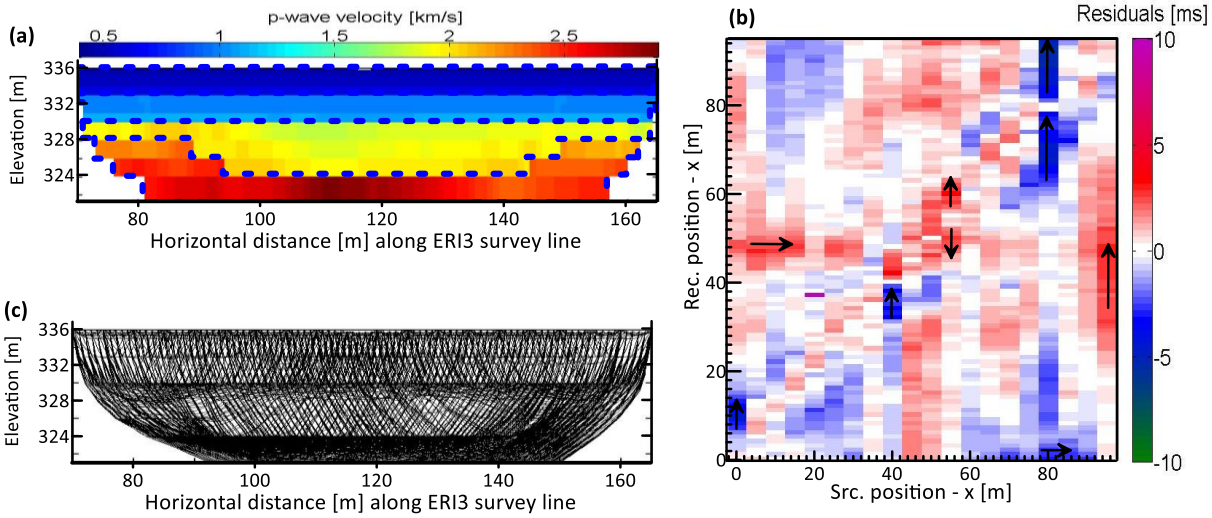

Figure 3.18. Surface refraction seismic tomography results. (a) Final 2-D velocity model obtained from the inversion of the surface refraction travel times along a segment of the ERI3 survey line. The areas with empty information represent the cover zones with ray coverage < 0. Distinct P-wave velocity interfaces are shown as the dashed blue lines. (b) The travel time residuals presented as 2-D functions of the source and receiver locations. (c) Ray diagram for the surface seismic refraction profile. The ray coverage density appears to be relatively high even in the channelized zone. In general, low ray coverage would indicate reduced resolution and reliability possibly resulting in a poorly-constrained model.

3.7.3 Evaluation of the RST results based on the reverse vertical seismic profiling concept

The emergence of the reverse vertical seismic profiling (RVSP) technique, in which energy sources are placed along the borehole and the receivers laid at intervals at the ground surface using various acquisition technologies has become widely accepted as a seismic methodology based on the accessibility of a borehole. It is a useful tool for reservoir/aquifer delineation, producing high resolution images over relatively small zones of illumination. The RVSP configuration is considered to be quite similar to the conventional VSP geometry in terms of the ray paths travelled, but the orientation of the receivers and the sources are reversed (Chen et al., 1990). However, at the heart of the RVSP concept lays some key strengths and advantages over the conventional VSP surveys (wherein energy sources are generated at the ground surface and receivers/detectors placed at intervals along the borehole). For instance, compared to the conventional VSP, the RVSP gives relatively better coupling/resolution and can solve a major noise problem in seismic studies. Also, the placement of seismic energy sources in wellbores overcomes the logistical limitations of the multiple surface energy sources needed in some VSP surveys, thereby minimizing cost (Shehab et al., 2008). Furthermore, in contrast to the surface refraction seismic method in which the near surface materials' attenuation properties changes the character of the seismic wave that passes through the subsurface, leading to non-elastic deformation, velocity dispersion and absorption and

greatly decreased resolution of the travel time data, there is less attenuation associated with the RVSP due to the shorter ray path from source to receiver. Therefore, modeling the first arrival data of the surface refraction seismic based on travel time fits alone may not provide a complete set of solution without quantifying the uncertainties of the estimated model parameters. In particular, variations in vertical velocities from the RVSP survey provide information on the existence of a low-velocity layer. To ensure a reliable reconstruction of the near-surface P-wave velocity variations, structural redefinition of the starting velocity model and evaluate the performance of refraction seismic tomographic modeling, travel time data from the RVSP survey were incorporated.

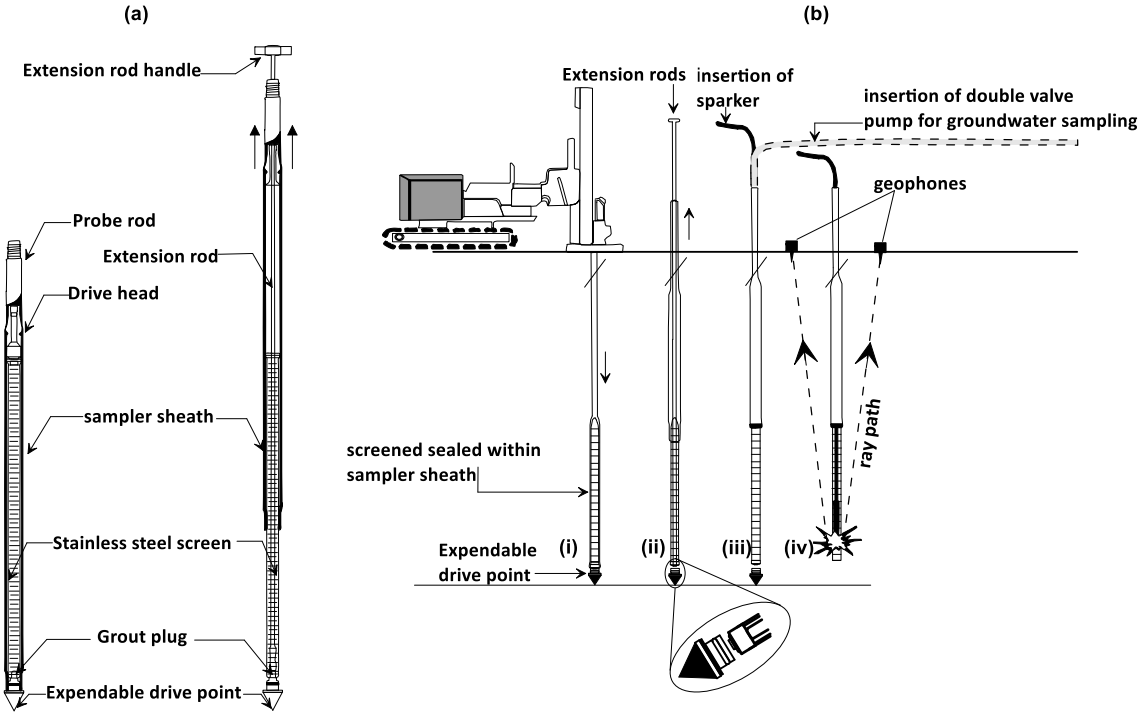

Figure 3.19. (a) Typical screen point (SP) 16 sampler (https://geoprobe.com/sp16-groundwater-sampler). (b) Steps in driving in the groundwater sampling device to the desired depth for acquiring the reverse vertical seismic profiling data using the direct push technology (e.g., Paasche et al., 2009; see dissertation text in Chapter four (section 4.2 for a detailed description of the multilevel groundwater sampling technique).

3.7.3.1 RVSP data acquisition

The applicability of the RVSP was initially limited as source power placed along boreholes can get the borehole damaged. However, advances in the usage of different near surface RVSP data acquisition approaches have bettered the employability of the method. As one of the ways of getting around this limitation, Dietrich and Leven (2009) suggest the use of the DPT to perform RVSP measurements. Based on this approach, a high-voltage (> 4 kV) seismic sparker source was used in combination with the DPT (Figure 3.19). To deploy the sparker source, a Geoprobe® DP machine was used to drive a groundwater sampling system with a screen length of 0.5 m to a total depth of 9.55 m in the saturated zone (see section 4.2 for a more detailed description of the multilevel groundwater sampling approach). At this total depth position, sufficient seismic signals were generated for stacking by firing a 3-string of shots using the sparker source inserted into the borehole within a zone screened for groundwater sampling. The sparker source power is triggered

from the remote unit of an electric surge generator. The downward radiation caused by the sparker is steered by its electrode housing. The collapsing bubbles produce broadband (50 Hz – 4 kHz) pulse that penetrates the subsurface. Once the original string of shots had been fired, an extra charge was prepared and fired at the next retracted depth. The reader is also referred to Paasche et al. (2009) for a comprehensive detail about this tool. In this study, shots were fired at a total of 19 source locations as the rod string was retracted at 0.20 m intervals (from depth 6.05 to 9.25 m) and at 0.15 intervals (from depth 9.25 to 9.55 m) up to a depth of not less than 30 cm below the groundwater level. Taking RVSP shots substantially within the saturated zone ensures that high resolution direct arrivals are recorded. The same acquisition system as for the hammer source-based surface refraction seismic was used to record the RVSP data. The shot location was on the horizontal distance 126 m along the ERI3 survey line (Figures 3.4d and 3.16). Twenty-four P-wave geophones were laid north-south on a spacing of 1m apart with twelve geophones on the either side of the shot location. The two closest geophones on the either side of the shot location were located 0.5 m each from the shot location. Each shot produced a 24 trace record. For these records, trace 1 is the most northerly receiver, trace 24 the southernmost.

3.7.3.2 Picking of the RVSP arrival times and tomographic inversions

The onset of the direct arriving energy was clear for picking (Figures 3.20) and required minimal processing. For the purpose of velocity determinations, only the pre-processing steps of gathering to common receiver domain and first break picking were applied to the shot gather. I used the Geogiga VSP 8.3 – vertical seismic profiling software (www.geogiga.com/en/vsp.php) to sort the plotted raw data into common receiver gathers, apply 50 ms automatic gain control (AGC), and to pick the direct arrival times (Table A3). The common receiver grouping was intended to strengthen the signal and minimize random noise. Ground roll noise caused by the source support equipment is noted to be randomized in common-receiver gathers (Krasovec, 2001).

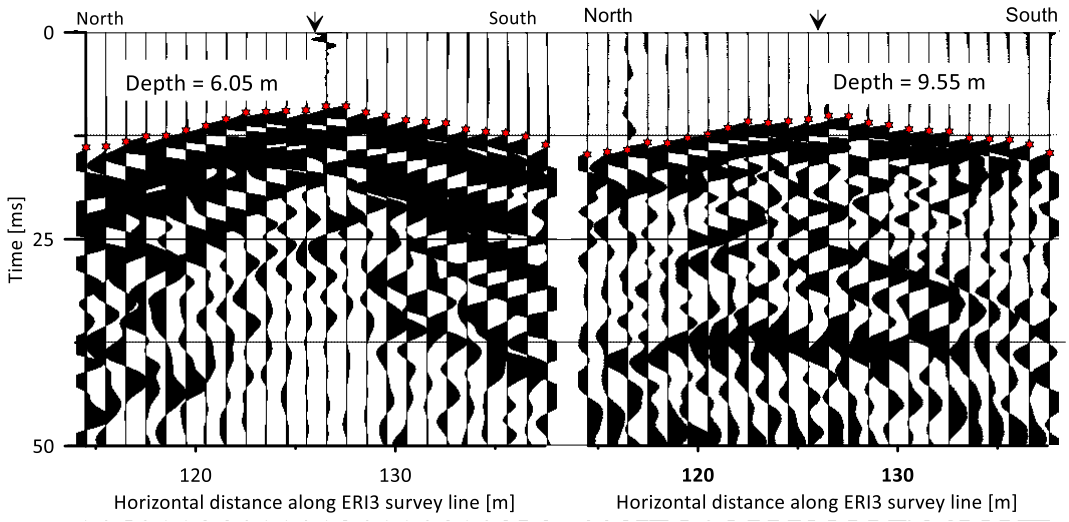

Figure 3.20. Shot gathers of reverse vertical seismic profiling along ERI3 survey line at the shot depths of 6.05 and 9.55, respectively.

Using the RVSP direct arrival times differences between source locations at different depths, velocity variations with depth can be determined. The resolution of the vertical velocity

structure increases with decreasing RVSP source location spacings in the borehole. However, source location-to-location interval velocities can become increasingly sensitive to arrival time picking errors as source location spacing decreases (Lizarralde and Swift, 1999; Moret et al., 2004). To provide more travel time information, through the upper layers, delineate abrupt and lateral velocity changes away from the well, a reverse multi-offset VSP travel time tomography was designed. This approach is better appreciated than the conventional uphole survey analysis in which only picks from near-offset are directly applied in the estimation of velocities. Because only one well was used in this study (see Figure 3.16), a major setback of this approach is that in certain velocity fields (far from the well), some of the cells are not crossed by raypaths. Hence, velocity information obtained in those cells may not be reliable. To solve this problem, studies have employed crosshole and multi-well reversed multi-offset VSP travel time tomography (Clement et al., 1999; Dietrich and Tronicke, 2009). In this study, however the aim was to test the sensitivity of the travel times and to evaluate how reasonably-consistent the subsurface velocity estimates and variations from the surface refraction seismic first arrival picks are.

To parameterize the starting model for the combined refraction seismic and DP downhole shots travel time tomography, I estimated the weathered and subweathered layer velocities from the RVSP data for comparison to existing layer velocity information from refraction seismic. Here, the weathered zone velocities represent the velocities above the water table while the subweathered layer velocities represent the zone below the water table. From the plot of the shot depth versus observed direct arrival time for various offset receivers (Figure 3.21), the interval velocities were determined as the inverse of the slope of the graph. Just as in the refraction seismic, the calculated velocities represent only apparent velocities and not the true velocities of the subsurface. This is because for some recorded distances from the well/shot location and the depths, most energy does not propagate vertically. The straight-ray path approximation neglects the effects of refraction at interface. For example, at the water table, where high velocity contrast between the saturated and unsaturated zones is expected, ray paths originating at DP shot locations in the aquifer are refracted strongly and cross to the unsaturated zone almost vertically (Paasche et al., 2009). Schuster et al. (1988) noted that at offset/depth ratio greater than zero but less than one, straight-ray geometry is a valid assumption. Parry and Lawton (1994) also observed that at shot depths greater than 5 m at 2 m offset, the straight-ray assumption becomes invalid. Beyond this offset, times can be compensated for, by reducing the recorded or picked travel times by the factor cos θ; where θ is the angle between the well and a straight line drawn from shot to receiver. This correction factor represents the ratio of the shot depth to the slant distance from the shot depth to the receiver. Figure 3.21 also shows the plot of the shot depth versus corrected direct arrival times for the various offset receivers and the associated interval velocities. It is clear from Figure 3.21 that there is little appreciable time compensation for shot depths greater than 6.55 m at 2.5 m offset or less. Such existing differences between the observed and corrected RVSP travel times were exploited to quantify the uncertainty in the travel time data used for the surface RST.

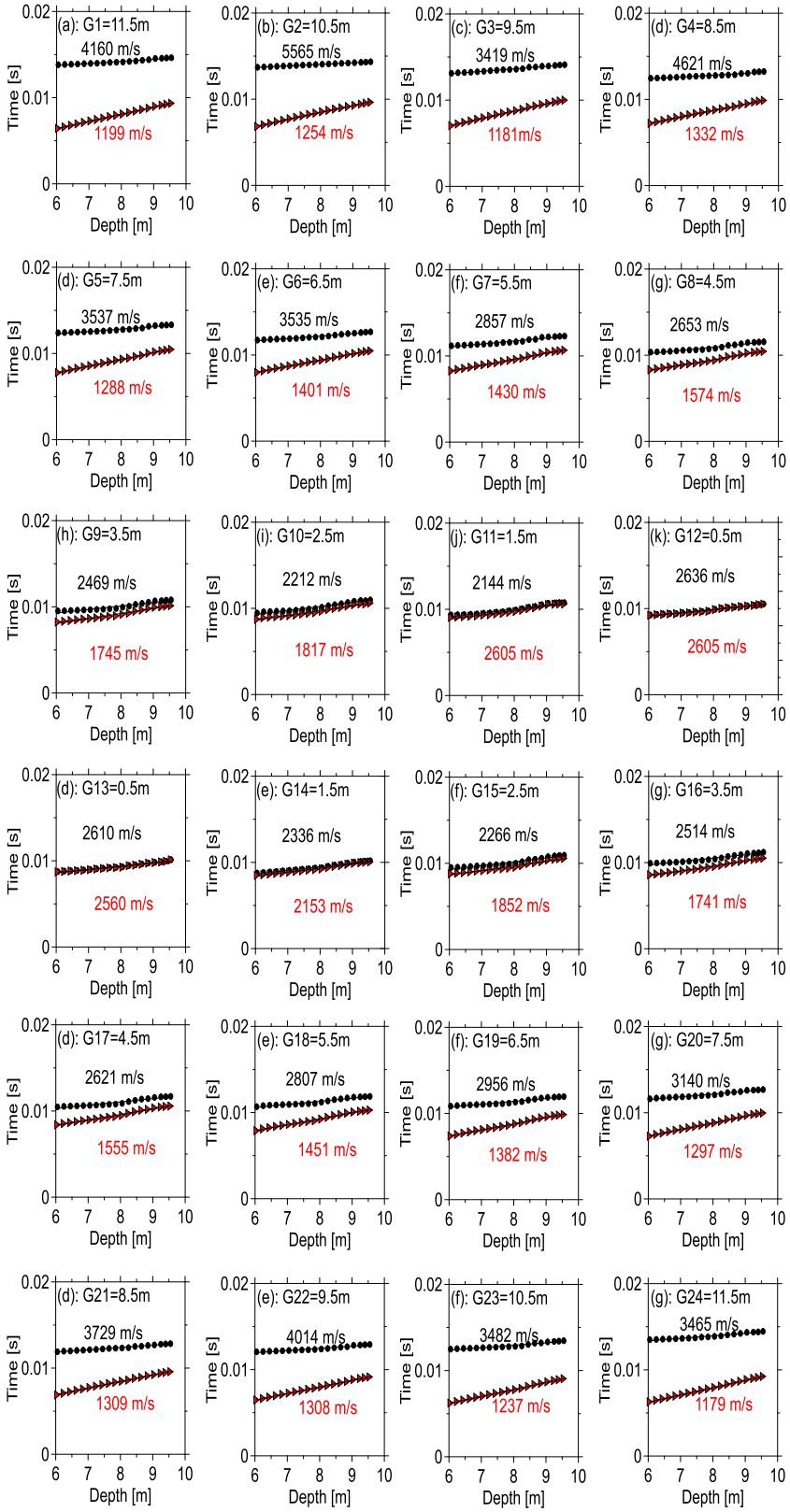

Figure 3.21. (a) Time/depth plots for receivers (represented as G) at various offsets (= offset location) from the shot location on the surface. Data points represented as closed black circles are the observed travel times while the closed red triangles represent the corrected travel times assuming a straight ray path. The interval velocities obtained as the inverse slope of the shot depth/direct arrival plot are shown on both sides of the observed and corrected travel times.

For the RVSP travel time tomography, the initial model presented in Figure 3.16 was retained. Because the measured static groundwater level was in the same range as the depth to the first layer, the vertical smoothness constraints from the RST was retained as well. Also, I did not alter the smoothness and damping constraints used for the RST. The observed and calculated travel times from the downhole shots were added separately into two files containing the surface refraction seismic travel times and then inverted in the same manner as the RST.

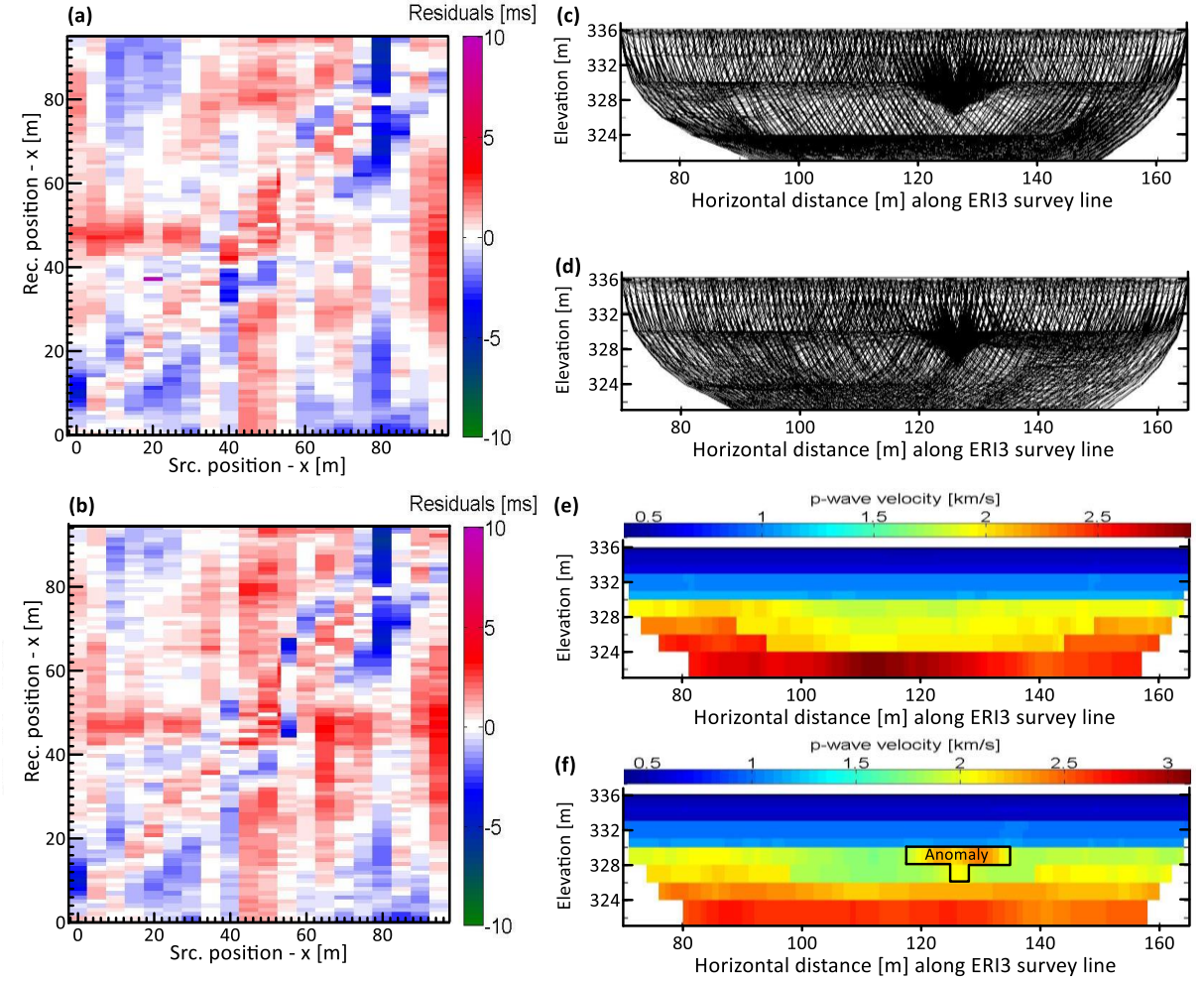

Figure 3.22. (a) and (b) Travel time residues on the incorporation of the observed and corrected RVSP travel times, respectively during the travel time tomographic inversion. (c) and (d) Ray diagrams on the incorporation of the observed and corrected RVSP travel times, respectively. (e) and (f) Subsurface velocity models produced from the travel time tomographic inversion on the incorporation of the observed and corrected RVSP travel times, respectively.

3.7.3.3 Interpretation of the combined RVSP and RST results

Plot of the travel time residuals in relation to the source-receiver pair (Figure 3.22a) from the combined tomographic inversion of the surface refraction seismic and observed RVSP travel time data indicate that the larger travel time residuals from the RST inversion (Figure 3.18a) significantly reduced to near zero around the RVSP shot depths. In contrast, the combined refraction seismic and corrected RVSP travel time inversion (Figure 3.22b) indicate small travel time residuals for receiver offsets close to the shot location whereas large residuals were observed

for receiver offsets away from the shot location. Unlike the tomographic inversion performed with the observed RVSP travel times (Figure 3.22a), which closely resembles the RST (Figure 3.22a), it is clear from the travel time residuals (Figure 3.22b) that the introduction of the corrected RVSP travel times effected remarkable changes across the source-receiver domain. Comparison between Figure 3.22 (c and d) is an indication of larger ray density for the observed travel times and smaller ray density for the corrected travel times around shot location. As explained earlier, large ray densities imply well-constrained model parameters at the grid cells and vice-versa.

Furthermore, the comparison of the P-wave velocity tomograms (Figures 3.22e and 3.22f) re-echoes that the surface RST inversion seems well-constrained with the observed RVSP traveltimes compared to the tomographic inversion performed with the corrected RVSP traveltimes. Although the incorporation of the corrected RVSP travel times showed a relatively denser ray coverage within the channelized low P-wave velocity structure than when the observed RVSP travel times are incorporated into the inversion process, the smaller ray density around the shot location (Figure 3.22d) indicated that significant velocity anomaly (Figures 3.22f) is associated with the corrected RVSP travel times. This is also reflected in the RMS error values (Figures 3.17) for the combined RST and corrected RVSP travel times inversion, which resulted in misfits that are a lot larger than those of the RST and RST plus observed RVSP travel times. Basically, these illustrations are aligned with the study's aim of performing the RVSP. The purpose of acquiring the RVSP data was to evaluate the performance of the refraction tomography inversion using the observed and corrected RVSP travel times to image the sensitivities and residuals for each inversion. In general, I demonstrate that combining surface refraction seismic with borehole shots/surface receivers spreads can result in a better resolution of the lateral variations in the subsurface P-wave velocities.

3.7.4 Soil electrical conductivity logging and lithological sampling

The DP electrical conductivity (EC) logging tool (Figure 3.23) was employed for the calculation of subsurface apparent EC. Compared to other EC logging methods (e.g., Keys, 1989), the DP EC logging does not require pre-existing wells or borehole. Without compromise originating from drilling mud, borehole fluids of phenomenally high ionic conductivity or changes in borehole diameter (Schulmeister et al., 2003), the DP EC logging tool provides a high-resolution segregation of fine-grained sediments of high EC values from low EC dry sands or gravels. Mixtures of fine-, medium-, and coarse-grained sediments can also be interpreted from the EC log signatures. Basically, the main rational behind this is that every soil conducts electricity differently and depends on the primary factors of soil type such as grain size, mineralogy and pore fluid. During the DP EC logging, a sensor/EC log probe attached to the end of a steel pipe is driven into the subsurface using a hydraulically driven percussion probing machine. The sensor configuration consists of a four-electrode Wenner array with an inner-electrode spacing of 0.025 m. The small electrode spacing allows the sensor to resolve thin units (Beck et al., 2000). As the EC probe is advanced into the subsurface, EC is calculated from the current applied to the two outer electrodes and the voltage measured across the two inner electrodes to produce a log of EC versus depth. The signals from both the conductivity probe and string pot (which measures the depth and the speed of advancement of the probe) are carried to the instrumentation box by a cord set. A field laptop connected to the instrumentation box and the Direct Image software provides

a real time display of the conductivity signal, probe depth, and speed of advancement are tracked by a spring pot mounted on the mast of the DP unit as logging is conducted.

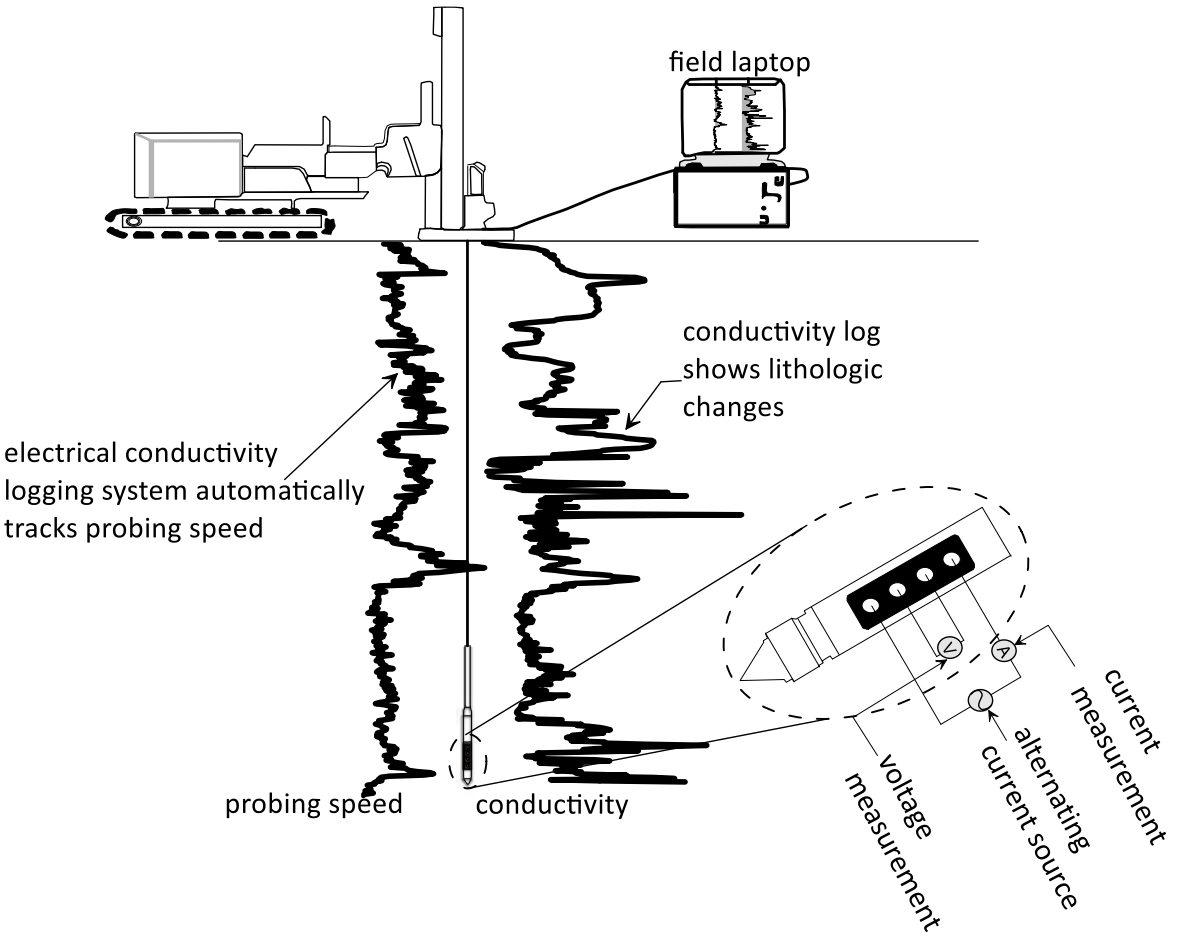

Figure 3.23. Example soil electrical conductivity logging using the direct push tool.

In comparison to conventional drilling, DP soil sampling techniques are less laborious, guarantee quicker setup time, and generate less drill cuttings. Two categories of DP samplers are distinguishable for soil lithological sampling (US EPA, 2002): (1) open barrel, and (2) closed barrel (piston) samplers. The open barrel samplers remain open as they are pushed to the target depth while the closed barrel samplers remain closed until reaching the target depth. Also, the rod systems exist in two forms, namely: (1) single tube, and (2) dual tube. Although these two rod systems can be used in several of the same environments, they have varying degrees of strengths and shortcomings. As the name sounds, whereas the single tube rod system uses a single string of rod to connect the sampling tool to the rig, the double tube system makes use of two sections (an outer tube, or casing and a separate inner rod attached to the sampler for sample recovery and insertion). Unlike in the single tube system, the outer tube in the dual tube system provides stabilization and a sealed hole from which soil samples may be recovered without the threat of cross contamination and collapse. Typically, these devices make it possible for continuous or discrete soil sampling to be conducted with ease. For more detailed comparison of the sampling tools, rod systems, their merits and demerits as well as the overview of the DP-based soil sampling systems (http://geoprobe.com/soil-sampling-overview), readers are also referred to Dietrich and Leven (2009), Zschornack and Leven (2012), and Haussmann et al. (2013). The dual tube rod system was used to perform the soil sampling. Before embarking on this operation, the soil sampling system

components (that is, the tool string) (Figure 3.24a) were properly assembled. As shown in Figure 3.24b, the following summarize the steps taken in deploying the tool string: (i) Position the DP machine well enough for drive the tools string into the ground surface to fill inner liner with soil; (ii) Adjust the DP machine hammer to have access to the top of the sample. Remove the drive cap and thread an additional light-weight center rod onto the centre string with an adjustable rod clamp in position to keep the center rods from falling when they are removed. Retrieve the sample with the inner rod string. At this point, the filled liner and the liner retainer can be removed from the Sample Sheath. The liner is also is covered with a pair Vinyl end caps and labeled for subsequent analysis and description of the subsurface lithology; (iii) For consecutive sampling or filling of the liner with soil, a new liner and additional lengths of inner rod and outer casing (clean sample sheath) are added to tool string; (iv) Advance the tool string down the previously opened hole to the top of the next sampling interval; (v) Again, retrieve the sample with inner rod string as demonstrated in step (ii). This process is repeated until the desired sampling depth is reached. When the last sample has been retrieved, the outer casing is removed and bottom-up grouting can be performed.

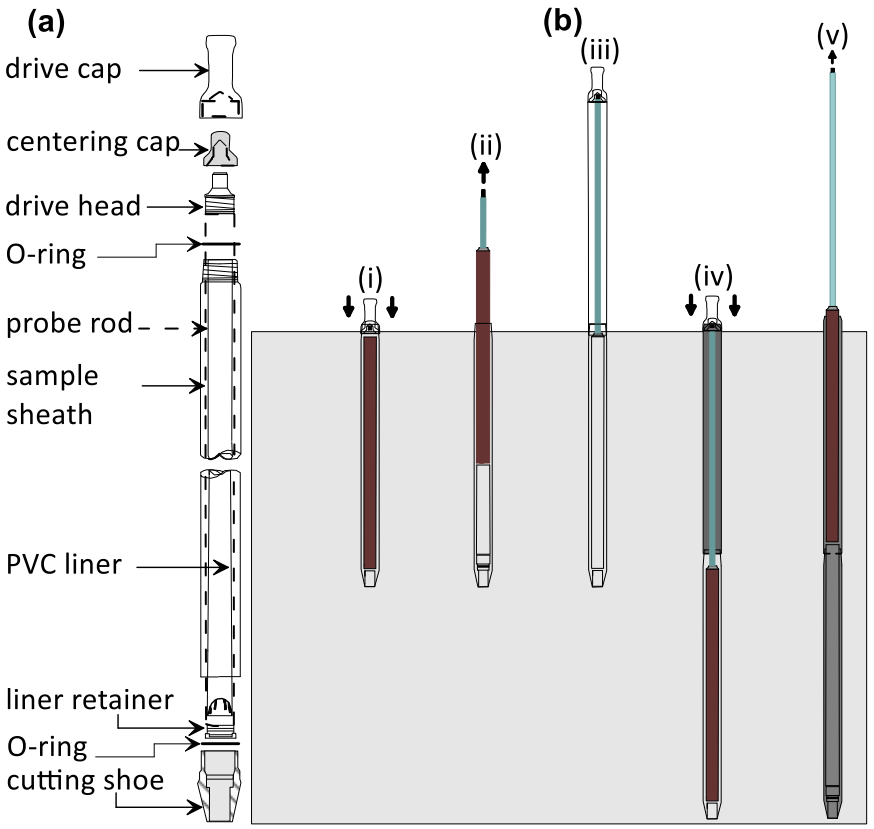

Figure 3.24. A typical DP tool string (a) for soil sampling (b).

The DP EC logging was conducted at seventeen (17) locations (see Table A4 for the location coordinates of the EC logging). However, for the purpose of ground-truthing and "calibrating" the results of the surface geophysical measurements along transects, only EC logs from thirteen (13) locations are discussed in the dissertation text (see Figure 3.4). A total of four (4) DP-based soil sampling was conducted at the site (see also Table A4 and Figure 3.4 for the soil sampling locations) mainly along the ERI3 survey line. Although the DP EC logs are used to infer lithologic variations and characterize subsurface geological structures, the relevance of the information obtained from the DP EC logs can be strengthened by comparing the EC logs with

the lithologic data from the soil sampling. Figure 3.25 shows an example of such comparison. The soil samples were visually described and classified in terms of the observable change in lithology (and texture). Six unconsolidated materials were defined: clay, gravelly sandy clay, gravelly clayey sand, silty sand, sand with gravel, clayey sand and classified into three main units: (1) Alluvial silty clay, (2) Unsaturated sand and gravel, and (3) Quaternary aquifer.

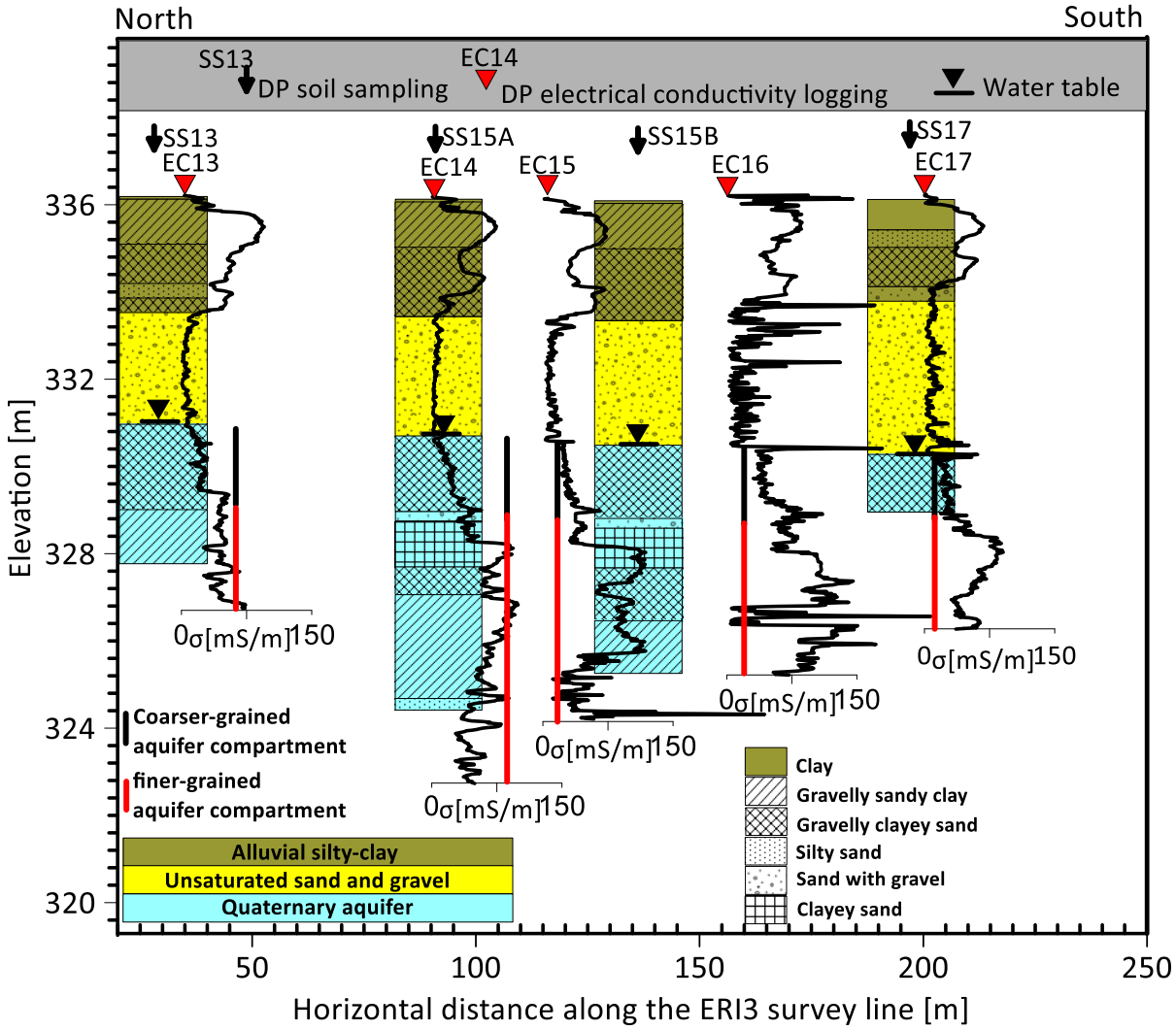

Figure 3.25. Comparison of the DP EC log data to the soil lithologic log data along the ERI3 survey line.

Higher EC values in the uppermost 3 m of the profiles were interpreted to represent the alluvial silty-clay materials with an organic top. Abrupt decrease in the EC between ~3 and 5.91 m is expected in the case of absence of electrically conductive materials, such as unsaturated sand and/or gravel layers. Below this horizon is a further increase in the EC values with a coarsening-upward sediment sequence. Distinctively, coarser-grained (homogeneous) sediments (consisting of majorly sand and gravel) immediately below the groundwater table are distinguishable from the deeper finer-grained (highly heterogeneous) sediments (little quantity of sand and silt with majorly clay/mud-rich materials). The horizon also corresponds to the saturated Quaternary aquifer zone. The groundwater level stood at ~ 5.38 – 5.91 m and separates the unsaturated layer from the saturated zone. Notable features on EC logs also include the relatively higher EC spikes, which might be indicative of thin lithological intervals with higher proportions of finer-grained sediments.

The competent bedrock was determined by the length of the DP EC log probe pushed until it reached refusal. However, caution guided mistaking cobbles for bedrock. Soil samples were collected up to the depths of 8.44 m, 10.54 m, 11.76 m and 8.42 m for the locations labeled as SS13, SS15A, SS15B, and SS17, respectively. Remarkably, the estimated depths to bedrock were up to 3 m deeper for the middle part of the ERI3 survey line than the depth to bedrock of adjoining areas. Although there is an inferred border zone between Lettenkeuper and Gipskeuper within the study area (Figure 3.1), the bedrock referred to, on the floodplain is inferred and not categorically Lettenkeuper or Gipskeuper except toward the hillslopes where the bedrock is noticebly made of Gipskeuper. Because I do not want to be speculative on whether the bedrock is of Lettenkeuper or Gipskeuper, further studies on the bedrock geology, particularly those on the classification of rocks and their formation are highly recommended.

3.7.5 Correlation of the interpreted DP EC logs along the ERI transects

The application of the high-resolution DP EC imaging and soil lithologic sampling tools was not only for providing first stratigraphy-based indication of boundaries of subsurface lithologic structures (e.g., Weaver and Wilson, 2000; Wilson et al., 2005) which can greatly enhance investigation decisions and the conceptual model of a site (e.g., Griesemer, 2001), but also for subsequent corroboration of the surface geophysical data. Interpretive subsurface geologic model cross sections were produced from correlating the EC logs along ERI1, ERI2 and ERI3 survey lines (Figure 3.26). The EC log signatures along ERI1 in general exhibited irregular trends describing high variability in the alluvial silty clay lithologies. Here, intervals of higher EC values are interpreted to be closely related to the clayey components whereas the lower EC values relate to the silty materials. Nonetheless, at the EC4 location, a coarsening upward lithologic sequence was observed on the EC log signature. The upper parts appear to contain more of silty sand materials and clayey materials at the lower parts. Correlating this information with the resistivity cross section in Figure 3.11a, it is not surprising that a relatively higher resistivity feature was observed at the upper parts of the ERI1 model between the horizontal distance of 60 and 180 m. Although the high resistivity bedrock feature in Figure 3.11a shallows toward the higher elevation region in the northwest, the EC log probe at the EC3 and EC5 locations appear to have detected a deeper competent bedrock structure. The geostratigraphic cross sections along the ERI2 and ERI3 survey lines (Figure 3.26 (c and d)) on the floodplain valley were characteristically different from that along the ERI1 survey line near the hillslope. Unlike the stratigraphic cross-section described along ERI1 profile with two distinct layers (consisting of the alluvium overlain the competent bedrock), the subsurface stratigraphy along ERI2 and ERI3 profiles shows three successive layers overlain the inferred bedrock consisting of alluvial silty clay, unsaturated sand and gravel layer and the Quaternary aquifer. The Quaternary aquifer system on the floodplain valley (interpreted along ERI2 and ERI3) coarsens predominantly upward. Accordingly, two compartments of the aquifer are identifiable as highlighted in Figures 3.25 and 3.26 (c and d).

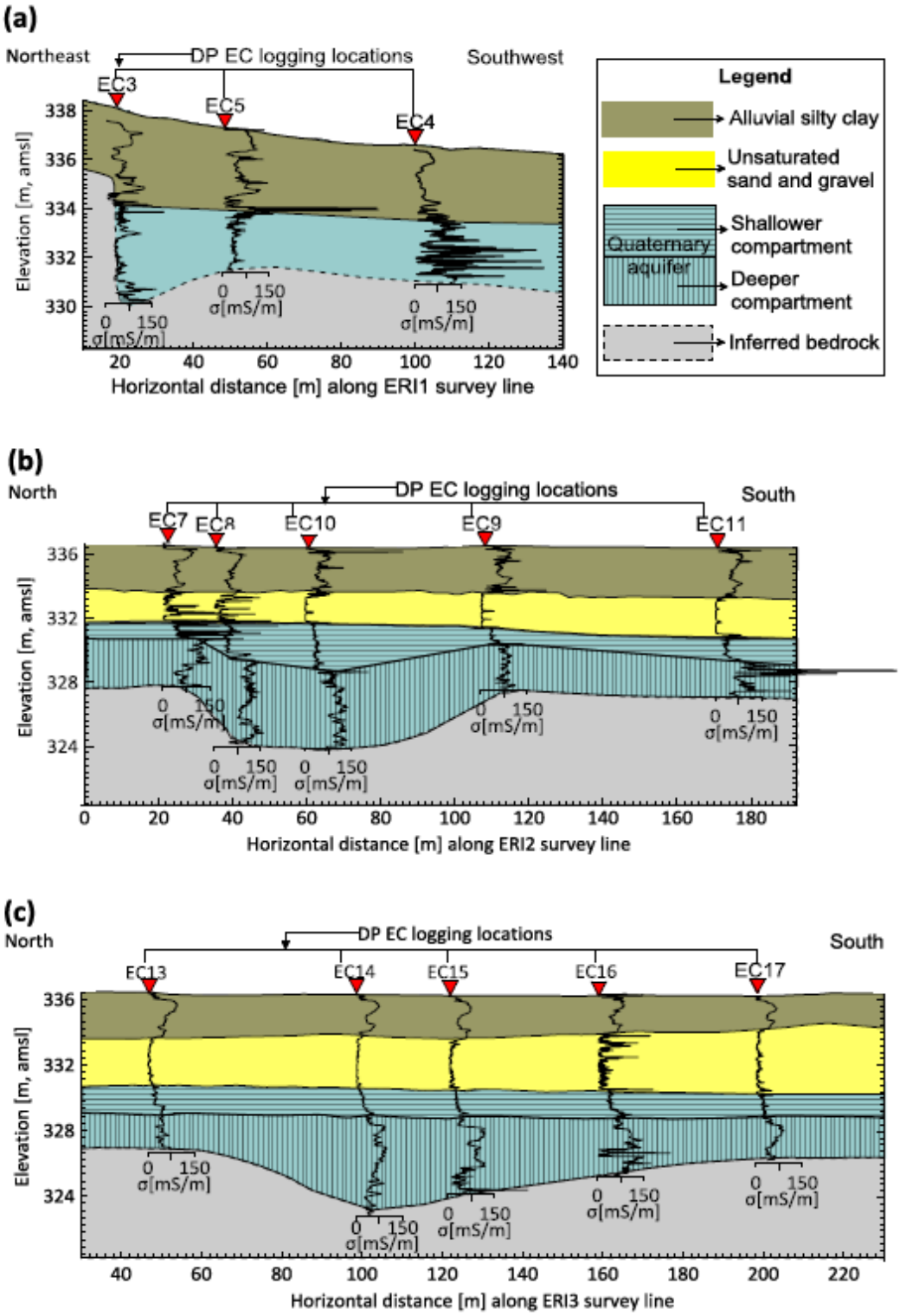

Figure 3.26. A simplified, interpretive subsurface geologic model of the site on lines of cross- section: (a) along ERI1, (b) along ERI2 and (c) along ERI3 profiles. The interpretation given here is that the ERI1 profile toward the hillslope area has geostratigraphic units that are distinctively different from ERI2 and ERI3 located on the floodplain area. On the floodplain area, the Quaternary aquifer is shown to be partitioned into coarser-grained shallower and finer-grained deeper compartments.

3.7.6 Combined interpretation of coincident RST (plus RVSP) and ERI profiles with DP soil EC- and litho-logs

In order to interpret fairly, the conceptual model of the subsurface, the reliability of the detected low resistivity feature and the channelized near-surface low P-wave velocity structure was checked by comparing the interfaces of the geophysical imaging results with the structural and lithologic information estimated from the DP-based EC- and litho-logs along the ERI3 survey profile. From the combined information (Figure 3.27), it is observed that although the 2-D resistivity imaging result supplied useful information on the overall distribution of the subsurface resistivity structure, it was particularly weak at defining deeper lithological boundaries. In contrast, the sharp changes/increases in the P-wave velocities allows for the different layer boundaries to be delineated. Comparison of the resistivity imaging and the refraction seismic tomography inversion results suggests that the channelized low P-wave velocity structure correlates the confined low resistivity zone identified along the ERI3 survey line. It is most likely that the channel-like bedrock feature detected using the RST represents the almost elusive bedrock structure in the ERI3 result. Thus, the RST was helpful in reducing of the uncertainty associated with estimating the alluvium-bedrock interface on the floodplain area.

The collocation of the low resistivity feature with the channelized low P-wave velocity zone also lend credence to the hypothesis that porosity/saturated water content may be a key determinant in evaluating the P-wave seismic velocity-resistivity relation (Mazac et al.,1988; Marion et al., 1992; Meju et al., 2003). From laboratory measurements on cores, Mazac et al. (1988) observed that resistivity decreases with increasing saturated permeability. Based on the works of Marion et al. (1992) and Meju et al. (2003), it is also shown that increases in water saturation would theoretically decrease and increase seismic velocities in clay and in sand, respectively illustrating corresponding interparticle stresses in these media (Shen et al., 2016). In this respect, the integration of in-situ measurements of porosity/saturated water content into a jointly inverted P-wave seismic velocity-resistivity relation obtained from surface geophysical measurements could be considered as an important topic for further research. The channelized structure was not immediately evident from inspection of the area's relatively flat surface topography and has not been documented by previous investigations in the study area. Using self-potential signatures combined with electrical resistivity profiles and borehole data, Revil et al. (2005) also detected the presence of such channel-like subsurface structure (however of high resistivity) at a Méjanes site, South-East of France. Based on the channelized geometry of the feature, the authors indicated that the channelized feature reflects area of relatively strong hydraulic transmissivities. Overall, given the geometry of the detected bedrock surface and the thickness of the deposited sediments assessed from the surface geophysical measurements and DP-based ground-truthing techniques, it is also interpreted here that the linearized low resistivity feature and low P-wave velocity structure may not be unconnected to a relic stream channel that has become buried over time and may preferentially influence groundwater flow and solute transport . Detailed studies regarding the extent of the structure beyond the present study site boundary on the floodplain valley are also recommended.

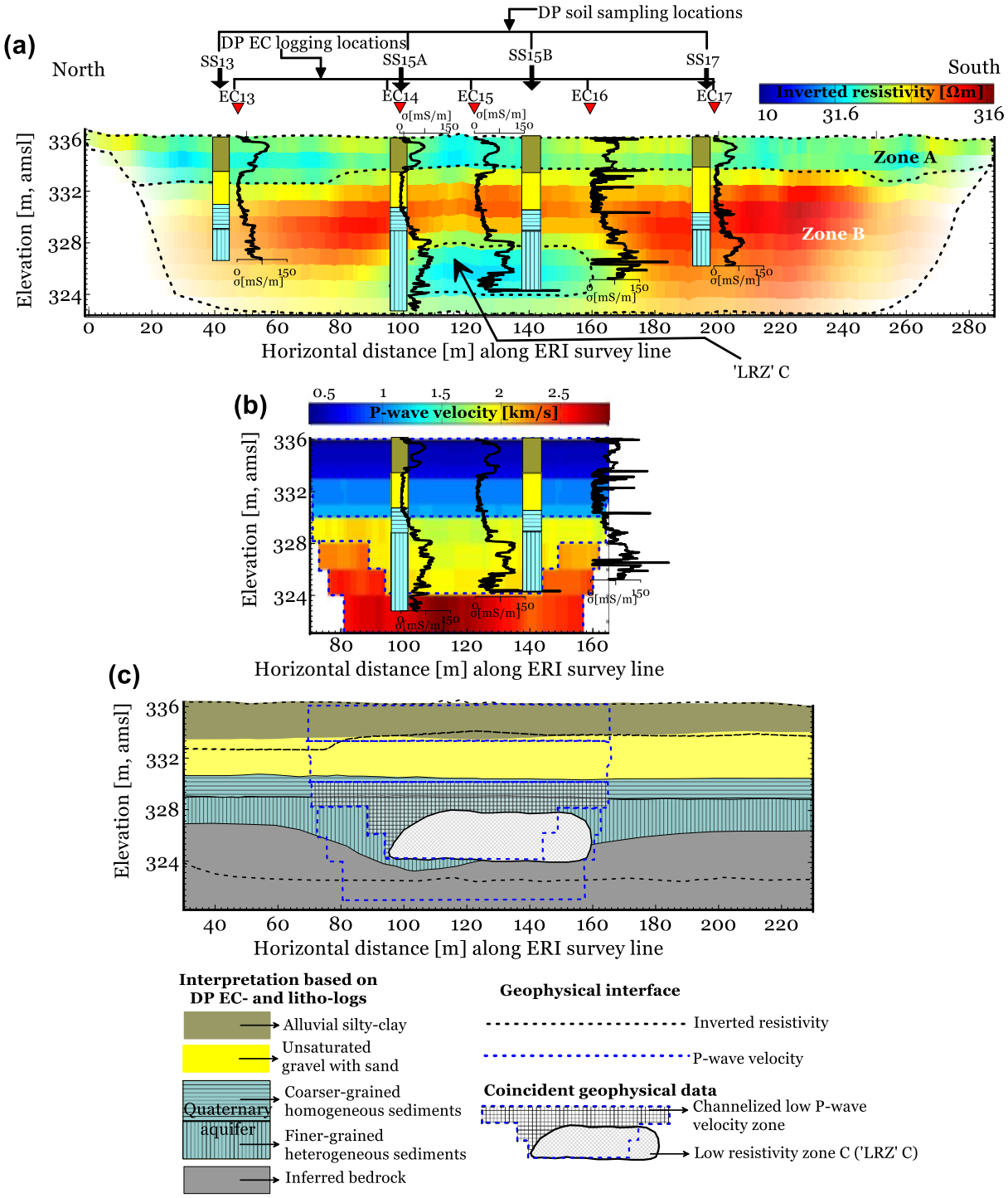

Figure 3.27. Comparison between interfaces based on ERI (a), and RST (b) along the ERI3 survey line and the interpretation of the geostratigraphic units with the DP EC- and litho-log data (c). Subsurface P-wave velocity and resistivity models produce images with distinct areas of sensitivity. In conjunction with the geostratigraphic information from the DP EC- and litho-logs, a coincident portion of the surface geophysical data has been interpreted as an indicator of similar subsurface feature.

3.8 Discussion and conclusions

At the Wurmlingen site (between Rottenburg am Neckar and Tübingen), southwest Germany, there exist a NO_3^- plume defined by a sparsely distributed groundwater sampling

stations. This created a considerable gap in the understanding of how hydrological processes and distribution of subsurface structures control groundwater flow and NO_3^- concentration variations. To avoid missing a significant physical migration pathway that can induce biogeochemical nitrogen fluxes within the studied alluvial aquifer system, I acquired complementary surface geophysical data, including ERI and RST, which were later ground-truthed by the DP-based RVSP, soil EC logging and sampling to explore the distribution of an anomalous low subsurface apparent resistivity structure preliminarily delineated using the Schlumberger array-based resistivity depth sounding surveys. The linearized low apparent resistivity feature was found to be aligned with the investigated NO_3^- plume. The most important point outlined in this study is that the scale of all geohydrologic investigations is of utmost importance and data should be acquired with high spatial density over large areas to strengthen the working hypothesis used as the basis for combined consideration of data sets from different investigation methods. In this study, wider coverage apparent resistivity data obtained using Schlumberger vertical electrical sounding of geoelectrical resistivity method opened up the possibility for the application of the above-mentioned combined methods.

The ERI results confirmed the distribution of the subsurface apparent resistivity distribution from large-scale preliminary field screening test (based on the VES surveys) but were weak at resolving the deeper subsurface stratigraphy of the area. In particular, detecting the potential bedrock surface on the floodplain area was not possible with the ERI tool. Inversions of the surface refraction seismic travel times (with the RVSP travel times) seem to have resolved a channelized low P-wave velocity feature–high P-wave velocity competent bedrock boundary that appears to have eluded detection by the geoelectrical resistivity imaging surveys. The surface geophysical results were helpful in ultimately guiding the selection of the locations for DP soil EC logging and lithological sampling used to ground-truth the geophysical data. DP-based soil EC- and lithologic-logs evaluated the subsurface internal structures and important information about the site's stratigraphy. A combined interpretation of the surface geophysical results and the DP-based ground-truth data indicate that the low resistivity feature aligned with the investigated nitrate plume coincided with the channelized low P-wave velocity structure. Given the orientation of the bedrock structure in relation to the NO_3^- plume, it is suggested here that groundwater flow and solute transport in the area may be largely controlled by the configuration of the aquifer bedrock topography. The uncovered anomalous subsurface channel structure is a new, unequivocal pattern at the study site that calls into questions the control of the NO_3^- plume only by the local hydraulic gradients associated with the local flows in the commonly described sand and gravel aquifer in the Neckar valley.

This approach of gathering a large amount of information about aquifer structural heterogeneity and geometry relevant to geohydrologic investigations was successful. The use of this strategy for making decisions on groundwater vulnerability and how the structure/geometry of an aquifer system influences the migration/transport pathways of recalcitrant chemical constituents of concern is highly recommended.

Against the success of this strategy, it may be argued that investigations involving the collection of such a large amount of geophysical information are time-consuming and cost-intensive. However, studies as the one highlighted above, wherein iterative investigations involve the employment of methods that leverage each other's strength are way better than the conventional approaches to large scale site assessments in relation to subsurface contamination characterization and management. Executing surface geophysical investigations with spatially

denser data coverage is more economically advantageous than siting few unsuccessful boreholes (Christensen and Sorensen, 1998), especially in highly heterogeneous aquifer systems. When the cost of not having acquired surface geophysical studies is reviewed, it becomes very clear that the conventional (drilling) approaches would hardly succeed (cost- and time-effectively) without surface geophysical survey(s) (reconnaissance and along transects). Because no single technique can confidently resolve the heterogeneity of subsurface features, a strategy such as that illustrated in this study, which could iteratively combine confirming observations from different methods presents a cost- and time-saving alternative.

Despite the progress made in understanding the physical heterogeneity of complex aquifer systems by the highlighted studies, attempts to detect and predict processes that moderate the relation between the structural and sediment heterogeneity, the development of pore water flows, and overall controls on fluid and solute fluxes remain a challenge. Channelized/buried valley aquifer structures such as that delineated in this study can be associated with mixing interfaces. Geochemical reactions in mixing zones that serve as factors of effective mass flux estimation and solute fate and transport are often unaccounted for. The existence of such mixing interface has been noted to influence changes in water chemistry and deepening in the level of the oxidation-reduction (redox) front, formed when oxidizing groundwater penetrates into the reduced sediments (Kirsch et al., 2006). In particular, the presence of muddy/clayey (finer-grained heterogeneous) deeper aquifer compartment may be hypothesized to provide adequate stagnant zone wherein denitrifiers could have enough time to drastically reduce NO_3^-. However, to provide a detailed understanding of the internal aquifer structures and decipher the invisible subsurface flow patterns as well as links to dynamic processes governing aquifer system's behavior for improving predictive physically-based groundwater hydrology models, further studies would require the examination of a suite of geochemical and isotopic tracers in groundwater. Results of such studies could shed more light on the essence of adequate subsurface structural characterization, which is critical for a correct observation of mixing processes, and aquifer water-rock interactions. In particular, I hypothesize that the interface between the two aquifer compartments inferred in this study may be useful to those interested in monitoring reactive processes, mechanisms of nitrogen nutrient exchanges and biogeochemical transformations at these mixing transition zones.

Chapter 4

Use of depth-specific chemical and multi ('dual')-stable isotope analyses to constrain an alluvial aquifer groundwater recharge origin, sulfate and nitrate fate

Chapter summary

In this chapter, chemical and multi ('dual')-stable isotope data were used to evaluate the origin of the alluvial aquifer recharge as well as the fate of the groundwater sulfate and nitrate. Emphasis is also placed on representative groundwater sampling, which involves understanding the subsurface structures and flow path as defined in Chapter three and from which part of the aquifer system to collect groundwater samples in order to foster reliable interpretation of the hydrogeochemical evolution, and evaluate nitrate source hypotheses/biotransformation processes. It was also necessary to perform depth-specific groundwater sampling in order to capture the physical (hydrological) and biogeochemical heterogeneity that characterize different aquifer zones.

4.1 Introduction

With a view to determining how subsurface features, described in Chapter three, particularly in the aquifer system govern net NO_3^- fate and solute concentrations, depth-specific analysis of groundwater chemical and stable isotope data was performed. This refers to the Step II and some parts of Step III of Figure 2.1 and Part II of Figure 2.2.

It is essential to understand and evaluate the origin of the groundwater recharge and the fate of groundwater solutes in order to provide insights into contaminants that might enter the aquifer with the recharge water and potentially reach groundwater wells as well as quantify the natural and anthropogenic factors influencing the groundwater solutes (e.g., Eberts et al., 2013; Miao et al., 2013; Murgulet and Tick, 2013). Such an understanding and evaluations may be enhanced by the use of geochemical and stable isotope approaches. The interest in hydrogeochemistry stems from the fact that ions leached from different anthropogenic sources may impact groundwater quality and increase solute concentrations above natural background levels. Moreover, with hydrogeochemical analysis, more light can be shed on the groundwater geochemistry as a function of the mineral contents of the aquifer rock through which it flows and anthropogenic influences, controlled by the regulatory mechanisms of weathering, precipitation, dissolution, ion-exchange, evaporation and contact time with the host rock (Schwartz and Zhang,

2003; Van der Weijden and Pacheco, 2006; Elango and Kannan, 2007; Jiang et al., 2009; Ma et al., 2011; Valle et al., 2014; Devic et al., 2014; Ma et al., 2014). However, adequate understanding of these regulatory mechanisms is limited. In addition, classical chemical data do not guarantee unambiguously the contribution of different solute sources and the biogeochemical transformations that the solutes have undergone. To offer considerable elucidations, stable isotopic tools have also become invaluable in identifying sources of groundwater recharge, sulfate and nitrate as well as associated transformation processes in both shallow and deep groundwater systems (Ofterdinger et al., 2004; Blasch and Bryson, 2007; Kendall et al., 2007; Wankel et al., 2009; Mattern et al., 2011; Liu and Yamanaka, 2012; Wong et al., 2014; Samborska et al., 2013; Zhang et al., 2015; Filippini et al., 2015).

The basic idea behind the use of stable isotopes is that every time a chemical constituent of concern transforms from one end-member source to the other, the processes and reactions that characterize the diagnostic shifts (that is, the so-called kinetic reaction) in isotopic composition is unidirectional, and occurs in quite reliably predictable pattern (not random). This is also because biological fractionation tends to use lighter isotopes preferentially as it takes less energy leaving behind heavier isotopes, making it easier to estimate the occurrence of the processes and their reaction rates. Remarkably, independent or individual isotope data also do not always permit conclusive establishment of solute sources and their fate, except on local scales wherein groundwater can be directly tied to specific events and land use types. The major issue here appears to be the overlapping isotope signatures and biological fractionation processes that modify the isotope ratios (Lohse et al., 2009). Thus, dual isotopic techniques are often used to provide distinctive means for testing hypothesis about pathways of biogeochemical cycling. The dual isotope procedure takes advantage of the fact that compounds consist of several elements, many of which can be easily analyzed for their isotopic ratios (Hosono et al., 2013), and when used as a dual-isotope reflects and tracks isotopic changes associated with kinetic fractionation events. The novel procedure of measuring the dual isotopic composition (e.g., an isotope of an element and its oxygen isotope counterpart) has expanded the use of isotopic techniques in tracing different solute (for example, NO_3^-) sources and transformations (e.g., Casciotti et al.,2002; Ohte et al., 2004; Elliott et al., 2009). Such a combination of oxygen and nitrogen isotope of NO_3^- can help distinguish atmospheric and synthetic fertilizer sources from organic fertilizer and septic sources (Kendall et al., 1998). Also, attenuation calculations show that where input of oxygen isotope-enriched atmospheric NO_3^- is negligible (Parfitt et al., 2006), the advantage of incorporating oxygen isotope of NO_3^- is that it is less impacted by source mixing than its nitrogen isotope associate (Barnes and Raymond, 2010). Hence, dual-isotopes not only act as fingerprints of solute origins, but also as inference about solute biogeochemical transformations. Although coupling oxygen isotopes of the analyzed individual elements in dual mode helps to better identify solute sources as well as constrain and distinguish processes overprinting each other, wide variations in the isotopic composition of the sources, mixing, and biological cycling still greatly obscure these values. Using multi-isotopic species offer opportunity to explore a wide range of possibilities for reaching conclusions about solute fate mechanisms due to changes in isotopic compositions (Wells et al., 2016). The more isotopes the better the chances of confronting questions with suitable answers.

Even though this study places emphasis on the use of chemical and stable isotopes in groundwater systems, how and where samples to be analyzed are collected is equally very important. This includes knowing which part of the groundwater system to sample from and the appropriate sampling protocol, which is essential for collecting representative water samples for

elemental composition and stable isotope assays. Thus, data quality is more than just chemical and stable isotope analyses. A perfect groundwater chemistry and stable isotope analyses with non-representative sample(s) equals "bad data". For these reasons, it is expected in this study that chemical data and a good knowledge of the investigated groundwater system combined with multi ("dual")-isotopic" compositions should be able to provide a much more comprehensive interpretation of processes affecting the fate and transport of the groundwater solutes in aquifers (Mengis et al., 1999; Dogramaci et al., 2012; Kim et al., 2014; Gurumurthy et al., 2015). In particular, just as flow paths drive changes in solute chemistry, reduction-oxidation (redox) chemical reactions have a strong effect on isotope fractionations so that chemical and hydrologic data are useful and necessary complementary elements for a credible interpretation of stable isotope data in relation to solute fate and transport mechanisms (Griffiths et al., 2016).

The technique of depth-specific/multilevel sampling (MLS) of groundwater based on the DPT (Dietrich and Leven, 2009) has become a widely-accepted and alternative means of collecting groundwater samples with a clear advantage over the traditional drilling approach. Smith et al. (1991) illustrate how a conventional groundwater sampling approach could not clarify biogeochemical processes related to nitrogen nutrient cycling in an aquifer system and how a subsequent MLS technique was able to realize the existence of informative steep vertical geochemical gradients in a contaminant plume. It also allows for flexibility in sampling, fine spatial resolution of chemical and isotope tracer heterogeneity, and generally lower cost (Einarson and Cherry, 2002; Amos and Blowes, 2008). By targeting and focusing on a known or defined subsurface hydrologic system, a substantial minimization in the interpretive uncertainty associated with quantifying the origin and processes of groundwater solute and recharge can be guaranteed. Such knowledge of the existence of defined flowpaths can provide a valuable parameterization tool for biogeochemical modeling.

The goal of this study was to build upon previous investigations by providing new information on the following: (1) enhanced conceptual understanding of hydrogeochemical evolution, and (2) processes that control groundwater recharge, sulfate and nitrate concentrations within an alluvial aquifer. It is posited here that such studies will contribute to a better groundwater quality assessment and a more effective implementation of environmental management measures.

4.2 Multilevel sampling of groundwater

As an integral part of determining the overall hydrogeological condition of a site, a DP-based MLS of groundwater was operated in order to provide a clearer picture of the distribution of the groundwater solutes (e.g., Lane, 2012). The adopted MLS approach was designed to overcome the inability of the traditional long-screen wells to resolve biogeochemical heterogeneity (Topinkova et al., 2007), the limited sampling depths shortcomings of MLS short-screen wells such as nested piezometers and cluster wells (Einarson, 2006) and to reveal the complexities of plume behaviour. It is particularly useful in aquifers where knowledge on vertical mixing is limited and steep gradients in chemical concentrations and isotopic signatures are expected (Cozzarelli et al., 1999; Schulmeister et al., 2004; Winderl et al., 2008; Ducommun et al., 2013). Typically, numerical modeling and laboratory experiments are often performed to identify and validate the driving force of mixing of reactants (Prommer et al., 2006; Olsson and Grathwohl, 2007). Nowadays, the hidden dynamics of mixing-controlled biogeochemical process have become glaring via high-resolution

depth-specific sampling of groundwater in well-characterized aquifer systems (Anneser, 2008).

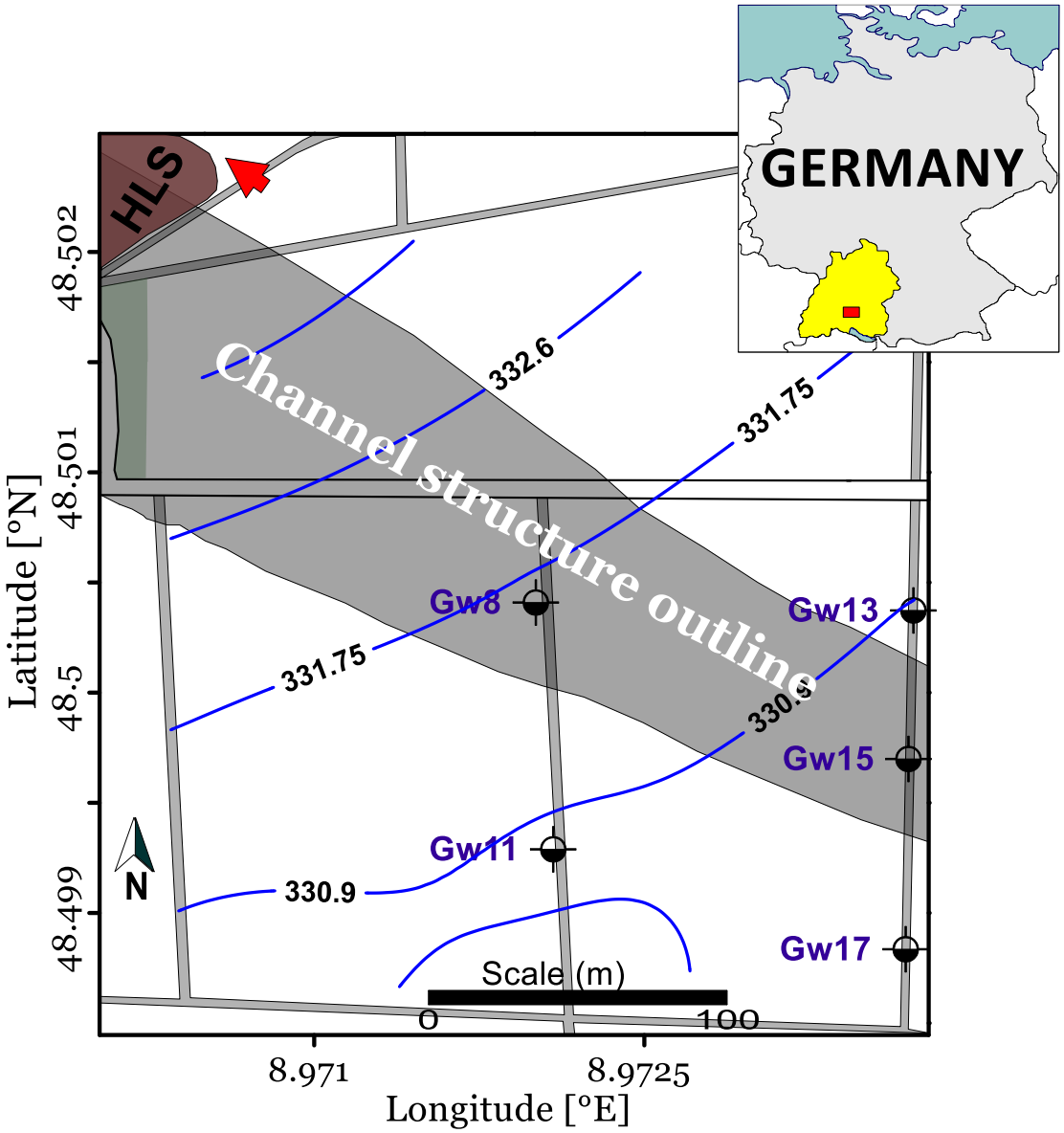

Figure 4.1. Wurmlingen study site, showing the targeted multilevel groundwater sampling locations (Gw8, Gw11, Gw13, Gw15, Gw17) and the outline of a buried channel structure inferred as a hydraulically transmissive zone from the combined surface geophysical and direct push investigations. Also superimposed on the map is the groundwater table elevation at an interval of 0.85 m and brown-colored outline of a hypothetical landfill site (HLS). The red arrow points northwest to the Wurmlingen settlement.

The specific locations for the MLS are based on the findings from the combined interpretation of the surface geophysical studies and the DP investigations presented in Chapter three. Shown in Figure 4.1, the previous study inferred a hydraulically transmissive zone because of the discrete nature of the buried channel structure compared to the surrounding environment. As interpreted in Chapter three, the structure could have an overarching control on groundwater flow and solute transport. Groundwater table elevation measured after seventeen (17) prior DP-based soil electrical conductivity logging show that the transmission of fluid by the channelized feature could follow the local hydraulic gradient. Nevertheless, it is also possible from the distribution of the groundwater table elevation contours that the channel structure may serve not

only as a flow convergence zone, but also as a flow divergence zone. The sampling depths and design was carefully set on the basis of the location of the detected channelized structure to ensure that if the feature is a flow path that it is possible to predict the geochemical and isotopic responses fairly correctly. The deepest parts of the aquifer are within the channel structure. Consequently, the base of the aquifer structure controlled the maximum depth of the multilevel groundwater sampling – that is, wells Gw8, and Gw15 located within the channel feature were relatively deeper than wells Gw13, Gw17, and Gw11 located in the areas surrounding the channel feature. Remarkably, two distinct aquifer compartments consisting of shallower coarser-grained and deeper finer-grained were interpreted from the performed DP-based soil electrical conductivity logging and lithological sampling (see Chapter three, sections 3.74, 3.75, and 3.7.6). As this study also sought to investigate, it is conceptualized that the interface that connects the compartments could have implications as a critical hotspot for changes in physical or biogeochemical properties of solutes (Krause et al., 2017).

During groundwater sampling (Dehnert et al., 2010), the DP machine is used to drive an assembly of screen point 16 (SP16) sampler of ~ 0.5 m in length within a sealed , steel sheath (Figure 3.19a to the desired total sampling depth (Figure 3.19b(i)). The sampler assembly is advanced with Geoprobe rods that are added incrementally. Extension rods with a screen push adapter added incrementally and carefully are lowered inside the probe rod until the adapter contacts the bottom of the screen (Figure 3.19b(ii)). Some reasonable length of the extension rod is allowed to protrude from the probe rod for easy retraction of the tool string while physically holding the screen in place. The screen starts to dangle inside the sheath once the extension rod is given a slight knock to dislodge the expendable point (Figure 3.19b(iii)). Typically, the screen sheath forms a mechanical annular seal above the screen interval. At the point of raising the hammer and tool string, the screen head will contact the necked portion of the sampler sheath and the extension rods will rise with the probe rods. Thus, as the protective outer rod is retracted, the screen is exposed allowing groundwater inflow into the sampler chamber under the hydraulic head condition that exists at that depth. Upon removing the top extension rod and top probe rod and then finally, extracting all extension rods, groundwater samples were collected. Or as demonstrated in section 3.7.3.1, the seismic sparker source or some other external devices can be deployed into the hole for the measurement of desired parameters. The sampler is afterward retracted upward to the next sampling depth.

Prior to water sampling, up to twelve liters of water were evacuated from each sampling port using a peristaltic pump based on standard procedures and established protocols (e.g., Barcelona et al., 1985). Parallel measurements of the temperature (Temp.), pH, groundwater electrical conductivity (EC), oxidation-reduction (redox)/electrode potentials (Eh), and dissolved oxygen (DO) were made using electrodes (WTW, Weilheim, Germany) while water was being pumped through flow cell chamber to minimize atmospheric interactions. Table 4.1 shows method of preservation of the groundwater samples collected in the field for laboratory chemical and stable isotope analyses and laboratories where the analyses were carried out.

Table 4.1. *Summary of preservation methods of the groundwater samples used for the analysis of hydrogeochemical and dual stable isotopic constituents.

Hydrogeochemical and dual stable isotopic constituents	Method of preservation
$^{+}NO_3^-$, NO_2^-, NH_4^+, SO_4^{2-}, Cl^-	-40 ml glass bottle with cap; filtered -Storage condition: at about 4°C -No preservatives
$^{+}Ca^{2+}$, Mg^{2+}, Na^+, K^+, Mn^{2+}	-50 ml white plastic bottle; filtered -Storage condition: at room temperature -2-3 drops (0.5 ml) 65 % Suprapur® Nitric Acid (HNO_3)
$^{+}Fe^{2+}$	-40 ml brown glass bottle with cap; filtered -Storage condition: normal cooling temperature -3 drops of 3M 30 % Suprapur® Hydrochloric Acid (HCl)
$^{+}$DOC	-100 ml schott brown glass -Room temperature storage is enough No preservatves
$^{++}HCO_3^-$	-500 ml glass bottles- air tight; unfiltered -Storage condition: normal cooling temperature is alright, but not absolutely necessary
$^{+++}$Dual isotopes of NO_3^- ($\delta^{15}N$-NO_3^- and $\delta^{18}O$-NO_3^-) and water isotopes (δ^2H and $\delta^{18}O$)	-60 ml HDPE plastic bottles; filtering is important - From 3 to 5°C (ice packed during longer transportation to avoid microbial denitrification) -No preservatives
$^{+++}$Dual isotopes of SO_4^{2-}($\delta^{34}S$-SO_4^{2-} and $\delta^{18}O$-SO_4^{2-})	-250 ml HDPE plastic bottles; filtering not necessary -Storage condition: at room temperature, although not necessary -Zinc Acetate (for potential stabilization of hydrogen sulfide, H_2S)

*The chemical and dual stable isotopic analyses of the groundwater samples were performed at the laboratories of the $^{+}$Analytical Chemistry Department (UFZ - Helmholtz Centre for Environmental Research, Germany), $^{++}$Centre for Applied Geosciences (Eberhard Karls Universität Tübingen, Germany), and $^{+++}$Catchment Hydrology Department (UFZ - Helmholtz Centre for Environmental Research, Germany).

4.3 Laboratory (chemical and stable isotopic) analyses

At the Analytical Chemistry Department (Helmholtz Centre for Environmental Research - UFZ, Leipzig Germany), hydrogeochemical constituents such as calcium (Ca^{2+}), magnesium

(Mg^{2+}), sodium (Na^{+}), potassium (K^{+}), and manganese (Mn^{2+}) were determined by atomic emission spectroscopy with inductively coupled plasma (ICP-AES) (Spectro Ciros CCD, Spectro Analytical Instruments) (e.g., Martin et al., 1994). Nitrate (NO_3^-), nitrite (NO_2^-) ammonium (NH_4^+), and ferrous iron (Fe^{2+}) were determined by the photometric method (Gallery Plus, Thermo Fisher Scientific) (e.g., Rastetter et al., 2015). Sulfate (SO_4^{2-}), and chloride (Cl^-) were determined using ion chromatography (DX 500, Thermo Fisher Scientific) (e.g., Jackson, 2004). DOC contents were analyzed by the difference method with a total organic C/total N analyzer (multi N/C® 3100, Analytik Jena AG, Thuringia, Germany) (Yan et al., 2017). Analysis for HCO_3^- by titration was performed at the Centre for Applied Geosciences (Eberhard Karls University of Tübingen, Germany) - the procedure involves adding four drops of methyl orange to 100 mL of the groundwater sample being analyzed, if the pH is < 8.5 and titrating against 0.1 mol/L hydrochloric acid (HCl) until the color changes from yellow to pink.. The choice of the selected analytes is predicated upon the general field conditions based on the results of the site history investigations (Kleinert, 1976; Schollenberger, 1998).

I checked the analytical data quality of the major ions by comparing the sum of the equivalents of the cations with the sum of the equivalents of the anions (Hounslow 1995). The considered ions include: major cations - Ca^{2+}, Mg^{2+}, Na^{+}, and K^{+} and anions - NO_3^-, HCO_3^-, SO_4^{2-}, and Cl^-. Freeze and Cherry (1979), the percent charge-balance error (CBE) is calculated as:

$$\%CBE = \frac{\sum cations - \sum anions}{\sum cations + \sum anions} x100\% \quad (4.1)$$

As shown in Figure 4.2, ionic balance values in this study ranged from -10.4 to 2.6 %. A positive result means that both an excess cations or insufficient anion exists, and a negative result means the opposite. For a freshwater system, ionic balance is assumed to be good if it is within the range of ± 10 % (Rice et al., 2012). Charge-balance error values beyond this limit could be an indication of error resulting from unaccounted analyte(s).

Stable isotope analyses were also performed at the Catchment Hydrology Department (UFZ, Halle, Germany). The dual stable isotopes of water ($\delta^{18}O$-H_2O, $\delta^{2}H$-H_2O) were analyzed by laser-based analyzer (L1102-I, Picarro Inc.) with a measurement precision of 1.0 and 0.3 ‰ for deuterium ($\delta^{2}H$) and oxygen ($\delta^{18}O$), respectively. Isotopic composition of sulfate ($\delta^{34}S$-SO_4^{2-}, $\delta^{18}O$-SO_4^{2-}) was determined by elemental analyzer (continuous flow flash combustion technique) coupled with an isotope-ratio mass spectrometer (delta S, ThermoFinnigan, Bremen, Germany) after the conversion of $BaSO_4$ and Ag_2S to gaseous SO_2 with an analytical error of better than ±0.3 ‰. Dual nitrate isotopes ($\delta^{18}O$-NO_3^-, $\delta^{15}N$-NO_3^-) were assayed by a mass spectrometer DELTA V Plus in combination with a GasBench II from Thermo Scientific. NO_3^- isotopic signatures were measured with the denitrifier method by using bacteria strains of *Pseudomonas chlororaphis* (ATCC #13985) after Sigman et al. (2001) and Casciotti et al. (2002). The analytical precisions for the nitrogen (N) and oxygen (O) isotope measurements of NO_3^- are 0.4 and 1.6 ‰, respectively. For calibration, international standards (USGS32, USGS34, USGS35 and IAEA NO3) were used. Unlike N_2, which requires avoidance of atmospheric contact, the advantage of analyzing NO_3^- is that its stability is maintained against chemical or biological degradation where samples cannot be analyzed immediately after collection (Mariotti et al., 1988).

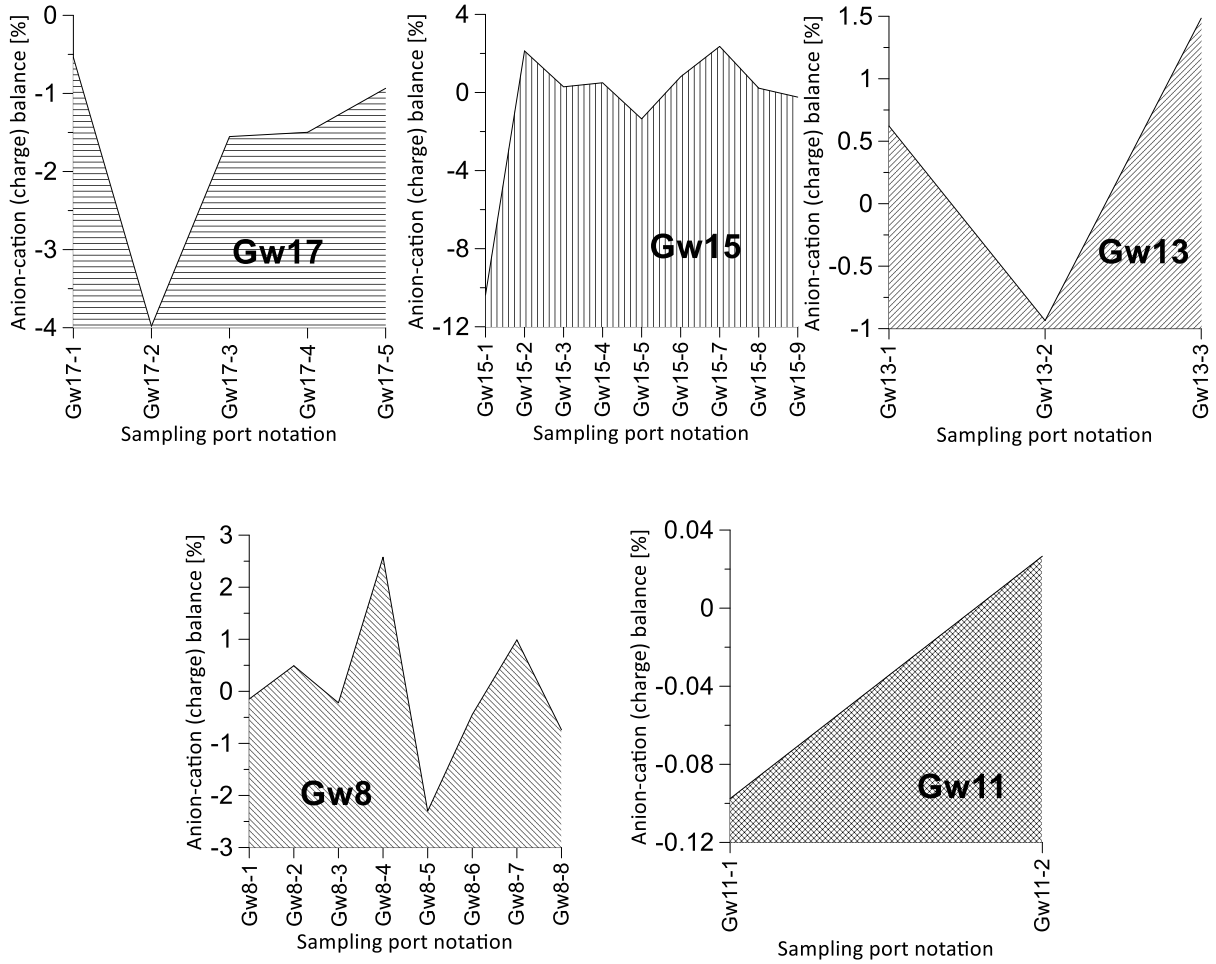

Figure 4.2. Charge balance error (CBE) based on the concept that all ions in water are charge-balanced.

All stable isotope analysis data are reported in standard delta (δ) notation as the relative abundance in a per mil (‰) basis, defined as:

$$\delta(‰) = \left[\left(\frac{R_S}{R_R}\right) - 1\right] x\ 10^3 \quad (4.2)$$

where R is the isotopic ratio of abundance of the heavy isotope to abundance of the light isotope of a sample (R_S) and a reference (R_R) material (for example, $\delta^{15}N$ values are reported with respect to standard atmospheric (AIR) nitrogen, N_2 for the nitrogen isotopes, $\delta^{18}O$ values are reported with respected to Vienna-Standard Mean Ocean Water, V-SMOW, whereas $\delta^{34}S$ values are reported with respect to Vienna-Canyon Diablo Troilite, V-CDT).

Analysis of the groundwater chemistry and isotopic data was useful in identifying flow and solute transport mechanisms in the aquifer. These groundwater sampling and laboratory (chemical and stable isotopic) analyses were a strategic attempt to provide additional confirmation constraints for evaluating the geochemical conditions and sources of groundwater solutes and to understand the consequences of the aquifer heterogeneity on biogeochemical processes. Specifically, the relevance of the stable isotope study is that, though a large proportion of the total mass/or concentration of solutes in the aquifer depletes over time and distance from the source, the stable isotope ratio of the residual material, closely resembles the ratio in the original material (Komor and Anderson,1993).

4.4 Results and discussion

The analyzed hydrogeochemical parameters and dual stable isotopic signatures are summarized in Table 4.2. Tables A6 and A7 provide detailed hydrogeochemical and dual (stable) isotope data of the sampled groundwater including parameters such as NH_4^+, Fe^{2+}, NO_2^- and DOC that registered some concentration levels below the detection limit.

4.4.1 Major ion hydrogeochemical evolution mechanisms and anthropogenic influence

Figure 4.3 shows boxplots that summarize the measured major ion hydrogeochemical constituents including physical parameters. The recorded groundwater temperature ranges from 13.7 to 20.4°C (M=17.00, MD=16.9, SD=1.50, CV=8.75 %). Average daily temperature values of 26°C, 27°C, and 27°C were also noted for the sampling periods of 2, 3 and 4 June 2015, respectively. The sampled shallow groundwater is characterized by relatively/near neutral pH values, ranging from 6.72 to 7.2 (M=6.98, MD=37.9, SD=0.11, CV=1.56 %). The range of pH values appears reasonably optimum for maintaining reactions such as conventional nitrification and denitrification. Based on this study, mineralization of the groundwater samples did not show wide variations, with the groundwater EC ranging from 2330 to 2670 μS/cm (M = 2439.63, MD=2450, SD = 71.63, CV = 2.95 %). The Eh ranged from -109.6 to 117.1 mV (M = 42.20, MD=37.9, SD = 47.60, CV = 112.86 %). Traditionally, as Eh increases, the solution becomes more oxidizing. Hence, geochemists often measure Eh based on thermodynamic considerations for different reactions. However, a meaningful redox measurement can be derived if and only if (see Rose and Long, 1988) (1) chemical and electrochemical equilibriums exist within the solution and (2) all the redox reactions between the redox couples occur reversibly. These conditions are rarely met because of the irreversibility of biologically mediated redox reactions. For these reasons, measuring DO as an important component of water-quality monitoring and assessment studies is considered more reliable. Nevertheless, the existence of a good correlation between the recorded DO and Eh values (Figure 4.4) suggests reasonable predictability for the redox potential based on the DO concentration levels, which ranged from 0.14 to 4.07 mg/L (M = 1.80, MD=1.62, SD = 1.06, CV = 58.70 %).

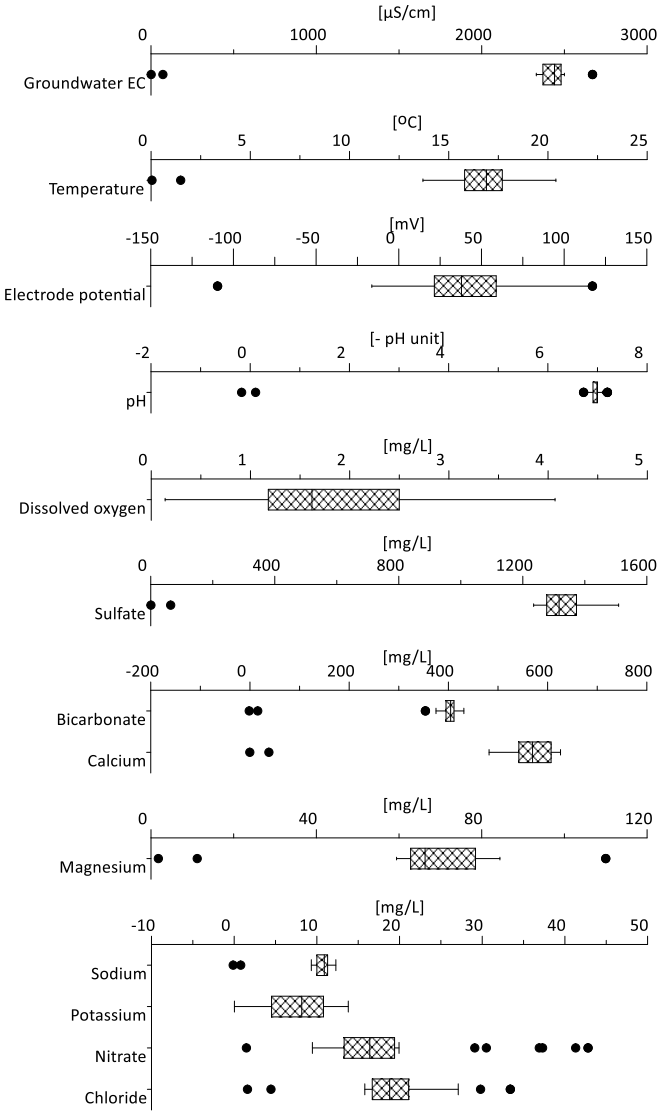

Figure 4.3. Boxplots of groundwater electrical conductivity (EC), temperature, electrode potential, pH, dissolved oxygen, and major ion concentrations (sulfate, bicarbonate, calcium, magnesium, sodium, potassium, nitrate, and chloride). The median (middle quartile) is denoted by the vertical line that divides the rectangular box into two parts. Start and end of the rectangle represents the lower and upper quartiles, respectively. Start of the left whisker and end of the right whisker represents the lowest and highest values that are not outliers. Solid black circles show outliers outside 10th and 90th percentiles.

Table 4.2.*Summary of the hydrogeochemical and dual isotope data, with basic statistics. Note: n = number of samples, M = mean, MD= median, SD = standard deviation, Min = minimum, Max = maximum, CV = coefficient of variation

Parameters	N	M	MD	SD	Min	Max	CV(%)
Temp.	27	17.00	16.9	1.50	13.7	20.4	8.75
pH	27	6.98	7	0.11	6.72	7.2	1.56
EC	27	2439.63	2450	71.98	2330	2670	2.95
Eh	27	42.20	37.9	47.60	-109.6	117.1	112.86
DO	27	1.81	1.62	1.06	0.14	4.07	58.70
Ca^{2+}	27	569.60	571	38.10	482	626	6.70
Mg^{2+}	27	71.20	66.3	11.20	59.4	110	15.71
Na^{+}	27	10.80	11	0.80	9.3	12.3	7.29
K^{+}	27	7.90	8.3	3.20	3.3	13.8	40.02
SO_4^{2-}	27	1333.60	1317	64.20	1235	1509	4.81
HCO_3^{-}	27	404.06	408.21	15.67	353.59	431.09	3.88
NO_3^{-}	27	19.90	16.9	9.50	12	42.8	47.45
Cl^{-}	27	20.20	18.8	4.50	15.8	33.4	22.09
Mn^{2+}	27	0.074	0.057	0.056	0.011	0.198	75.93
^{18}O-H_2O	25	-8.50	-8.50	0.10	-8.7	-8.3	-1.18
^{2}H-H_2O	25	-62.00	-62.1	0.38	-62.5	-61.3	-0.62
d-excess	25	6.00	6.06	0.65	4.60	7.10	10.77
^{34}S-SO_4^{2-}	25	15.90	16.06	0.34	15.2	16.3	2.15
^{18}O-SO_4^{2-}	25	13.30	13.4	0.31	12.8	14.0	2.33
^{15}N-NO_3^{-}	25	10.10	8.0	3.64	6.4	17.9	36.07
^{18}O-NO_3^{-}	25	7.20	4.8	4.09	2.4	15.0	57.11

*See Tables A6 and A7 for detailed hydrogeochemical and dual (stable) isotope data

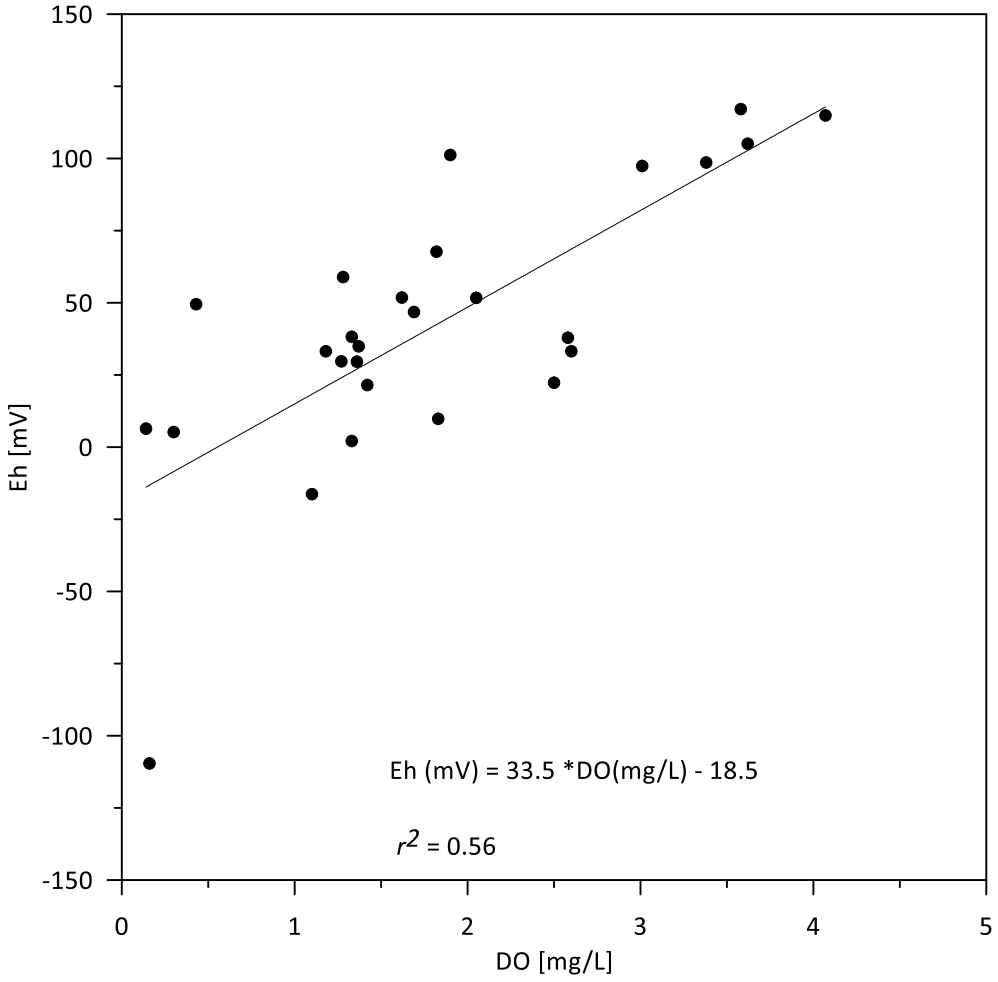

Figure 4.4. Relationship between redox potential (Eh) and dissolved oxygen (DO) concentrations.

To distinguish relevant hydrogeochemical processes under varying influencing conditions (natural and anthropogenic), I evaluated the relationships between some hydrogeochemical variables. In the first instance, this study shows that Ca^{2+} (M=569.60, MD=571, SD=38.1, CV=6.69 %), Mg^{2+} (M = 71.2, MD=66.3, SD = 11.2, CV = 15.71 %), Na^{+} (M = 10.80, MD=11, SD = 0.80, CV = 7.29 %), K^{+} (M = 7.90, MD=8.3, SD = 3.20, CV = 40.02 %), SO_4^{2-} (M = 1333.60, MD=1317, SD = 64.20, CV = 4.81 %), HCO_3^{-} (M = 404.06, MD=408.21, SD = 15.67, CV = 3.88 %), NO_3^{-} (M = 19.90, MD=16.9, SD = 9.50, CV = 47.45 %), Cl^{-} (M = 20.20, MD=18.8, SD = 4.50, CV = 22.09 %) are the principal dissolved constituents, and constitute up to 80 % of the groundwater total dissolved solids, TDS (mg/L) ≈ 0.7 groundwater EC (µS/cm) (Walton, 1989). Using the Gibbs diagram/scheme (Figure 4.5; Gibbs, 1970), I identified the processes controlling the geochemical evolution of the groundwater. The scheme, which illustrates three natural mechanisms: water-rock interactions, evaporation, and atmospheric precipitation plots the ratios of $Na^{+}/(Na^{+} + Ca^{2+})$ and $Cl^{-}/(Cl^{-} + HCO_3^{-})$ against TDS. Based on the scheme, I found that all the groundwater samples fell in a clustered form near the rock dominance area, but not without some evaporative effects, indicating that the shallow groundwater chemistry comprises waters having as their dominant source of dissolved solids, the rocks of the area.

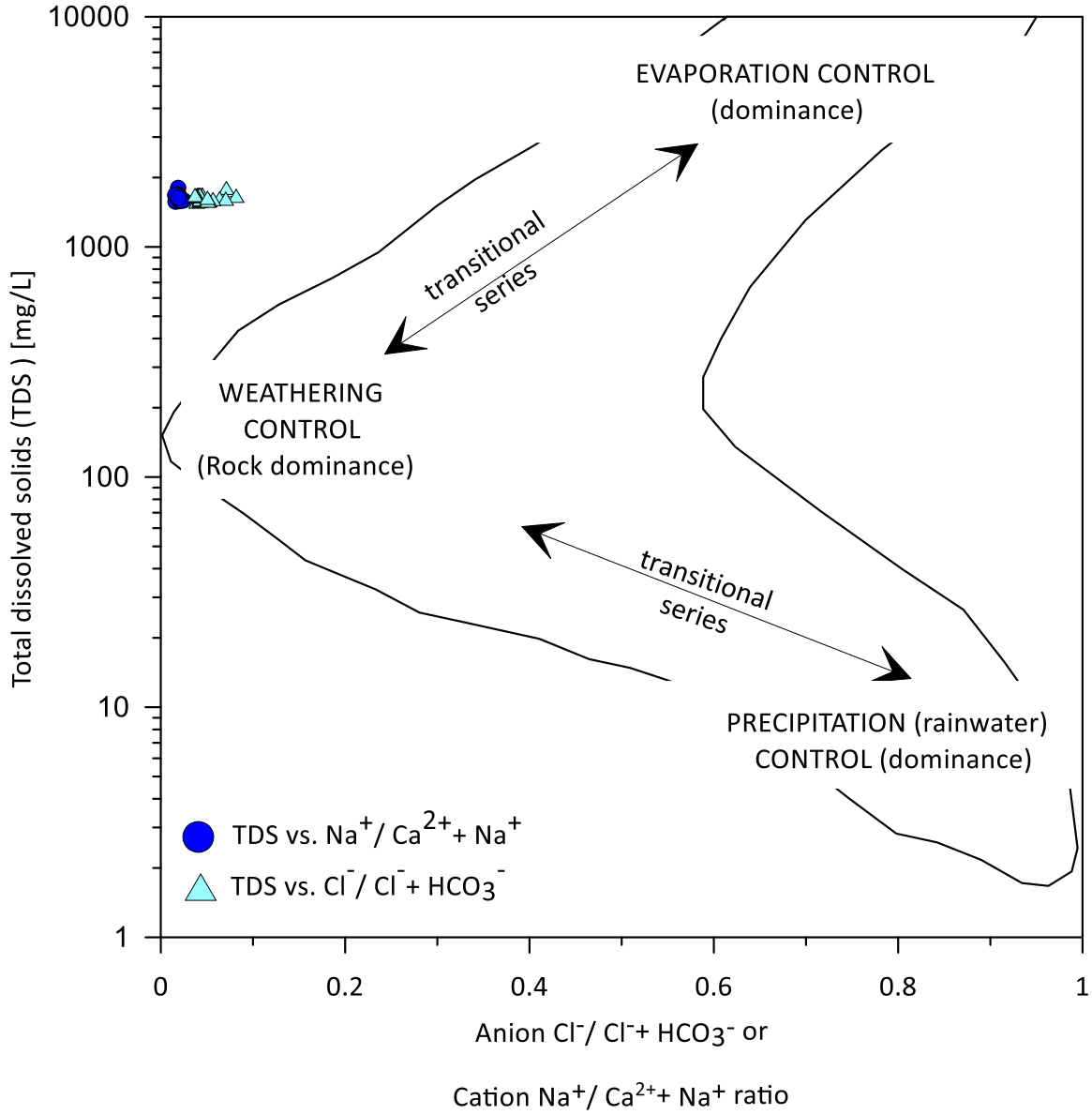

Figure 4.5. Gibbs diagram plot of the total dissolved solids (TDS) as a function of the ratio of anion $Cl^-/Cl^- + HCO_3^-$ and cation $Na^+/Ca^{2+} + Na^+$. It shows the processes controlling the chemistry of the groundwater samples (After Gibbs, 1970).

Examining the mixing model (Figure 4.6) as proposed by Gaillardet et al. (1999), I also found that carbonate rock weathering contributed majorly to the groundwater chemical composition. However, the anion sequence: $SO_4^{2-} > HCO_3^- > NO_3^- > Cl^-$ and the tendency for adsorption amongst the major cations: (strongly adsorbed) $Ca^{2+} > Mg^{2+} > Na^+ > K^+$ (weakly adsorbed) resulted in a calcium sulfate ($CaSO_4$) water type, typical of gypsum-rich groundwater (classification based on the Piper (1944) trilinear diagram plot (Figure 4.7), Morris et al., 1983). It is possible that the gypsum formed on the carbonate, just as the Ca^{2+} required to form the gypsum may have originated from the carbonate. In other words, the $CaSO_4$ water type would have evolved from the calcium bicarbonate ($CaHCO_3$) water type. Therefore, the dissolution of the carbonate and the gypsum characterized the chemical composition of the groundwater.

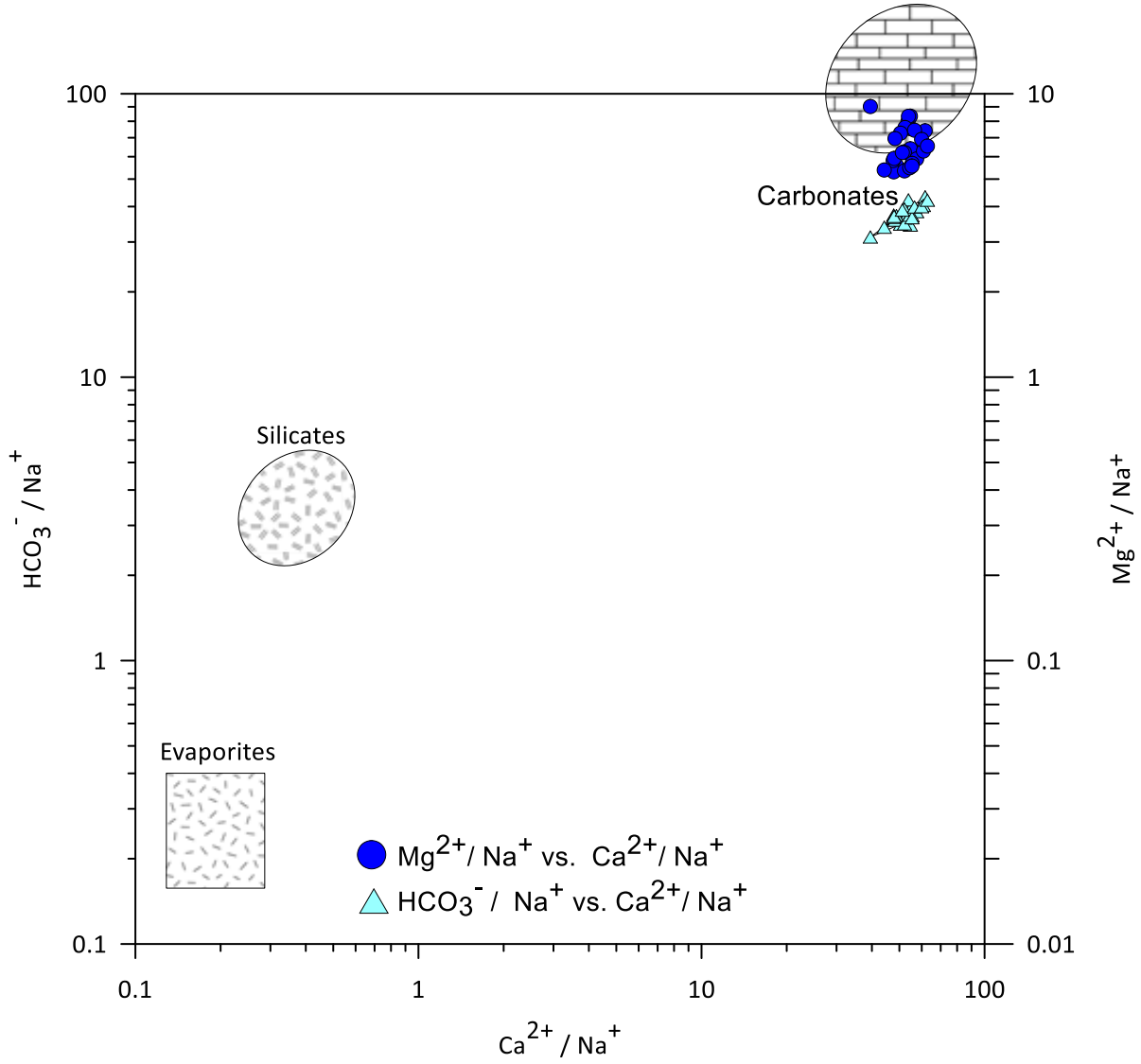

Figure 4.6. HCO_3^-/Na^+ versus Ca^{2+}/Na^+. End members of carbonates, silicates and evaporates are from Gaillardet et al. (1999).

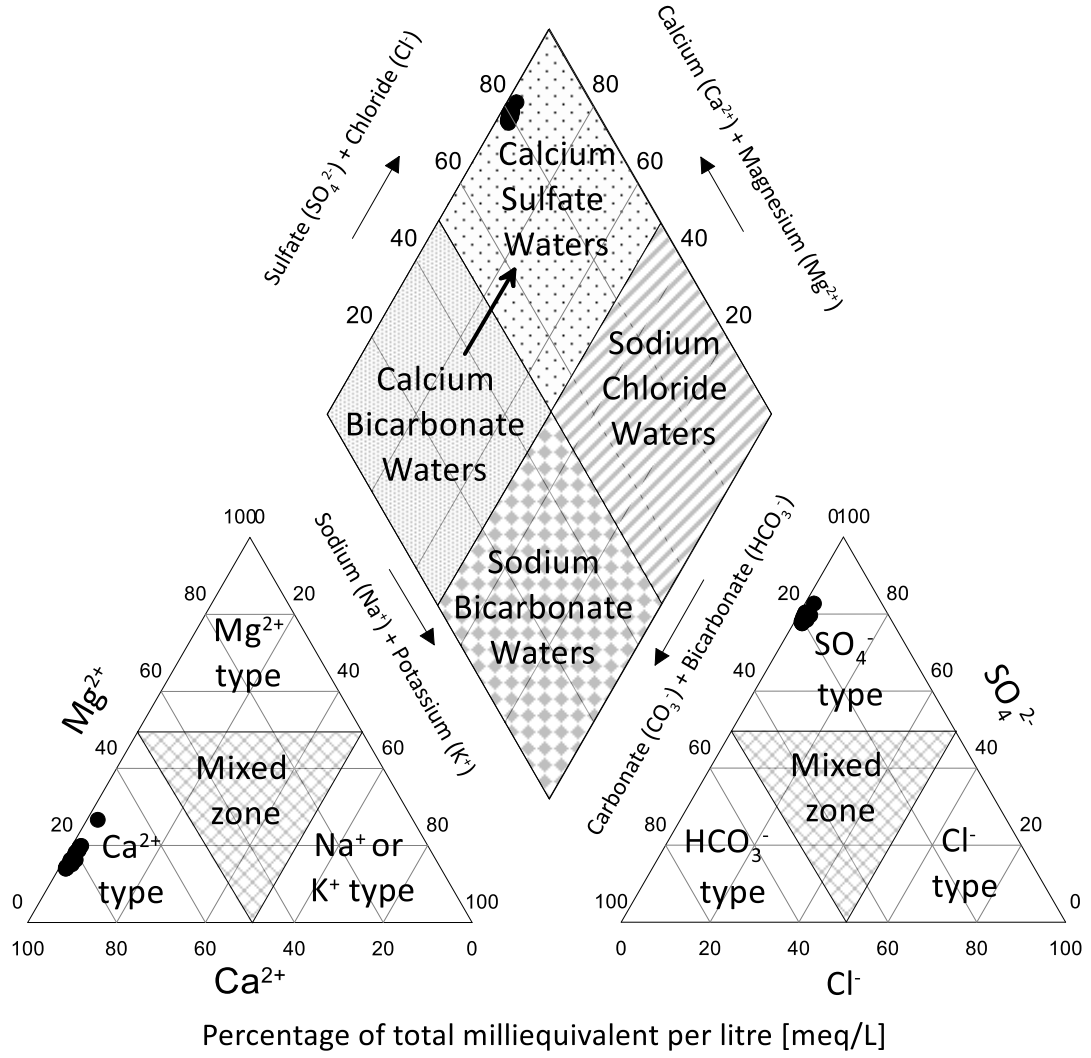

Figure 4.7. Piper trilinear diagram showing the hydrogeochemical facies for the groundwater of the study area.

Moreover, the near-equal distribution of the groundwater samples on both sides of the 1:1 correlation line between HCO_3^- + SO_4^{2-} and Ca^{2+} + Mg^{2+} ($r^2 = 0.16$; Figure 4.8) indicate that both reverse and ion exchange processes dominated the reaction. The shifting of the data points to the right (excess HCO_3^- + SO_4^{2-}) and to the left (excess Ca^{2+} + Mg^{2+}) indicates ionic and reverse exchange processes, respectively. As a result of these reactions, Ca^{2+} resulting from the dissolution of the carbonate matrix of the host aquifer would have entered the groundwater and may be subsequently exchanged for Mg^{2+} from post-depositional replacement of calcite by dolomite ($CaMg(CO_3)_2$) (that is, Mg^{2+} for Ca^{2+} exchange by Mg-rich pore waters).

To understand the extent of Mg^{2+} and Ca^{2+} substitutions in the reaction, I made a scatter plot (Figure 4.9) of Ca^{2+} against SO_4^{2-} ($r^2 = 0.19$), Mg^{2+} against SO_4^{2-} ($r^2 = 0.05$), Ca^{2+} against HCO_3^- ($r^2 = 0.09$), Mg^{2+} against HCO_3^- ($r^2 = 0.23$), which indicates a weak association between the cations (Ca^{2+}, Mg^{2+}) and anions (SO_4^{2-}, HCO_3^-). The lack of significant correlation between Na^+, and the major ions (not shown except with NO_3^-, which is discussed further below) could mean that most of the Na^+ may have been depleted from the mainly gypsiferous carbonate aquifer. Na^+,

which in natural waters originates from the dissolution of feldspathic minerals, is not only one of the most mobile of the common cations but also has low affinity for soil exchange sites (Weil and Brady, 2017). Unlike Na^+, K^+ is relatively resistant to weathering. Illustrating the uptake and release of K^+, a moderately positive correlation ($r^2 = 0.53$) was observed between Ca^{2+} and K^+ while a weakly negative correlation ($r^2 = 0.11$) was observed between Mg^{2+} and K^+ (Figure 4.10).

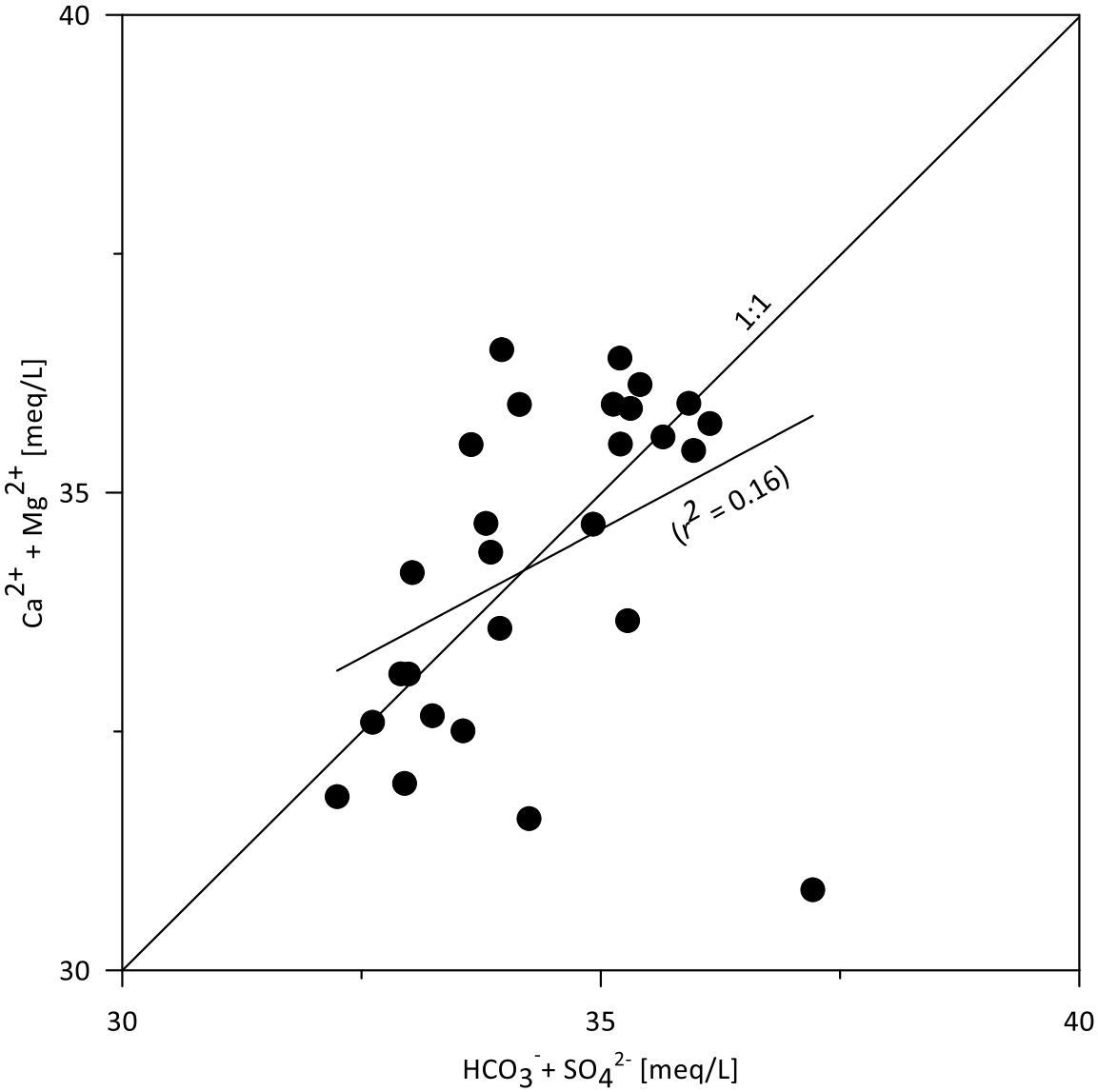

Figure 4.8. Plot of the relation between Ca^{2+} + Mg^{2+} and HCO_3^- + SO_4^{2-}. (e) Plots of HCO_3^- and SO_4^{2-} versus Ca^{2+} and Mg^{2+}.

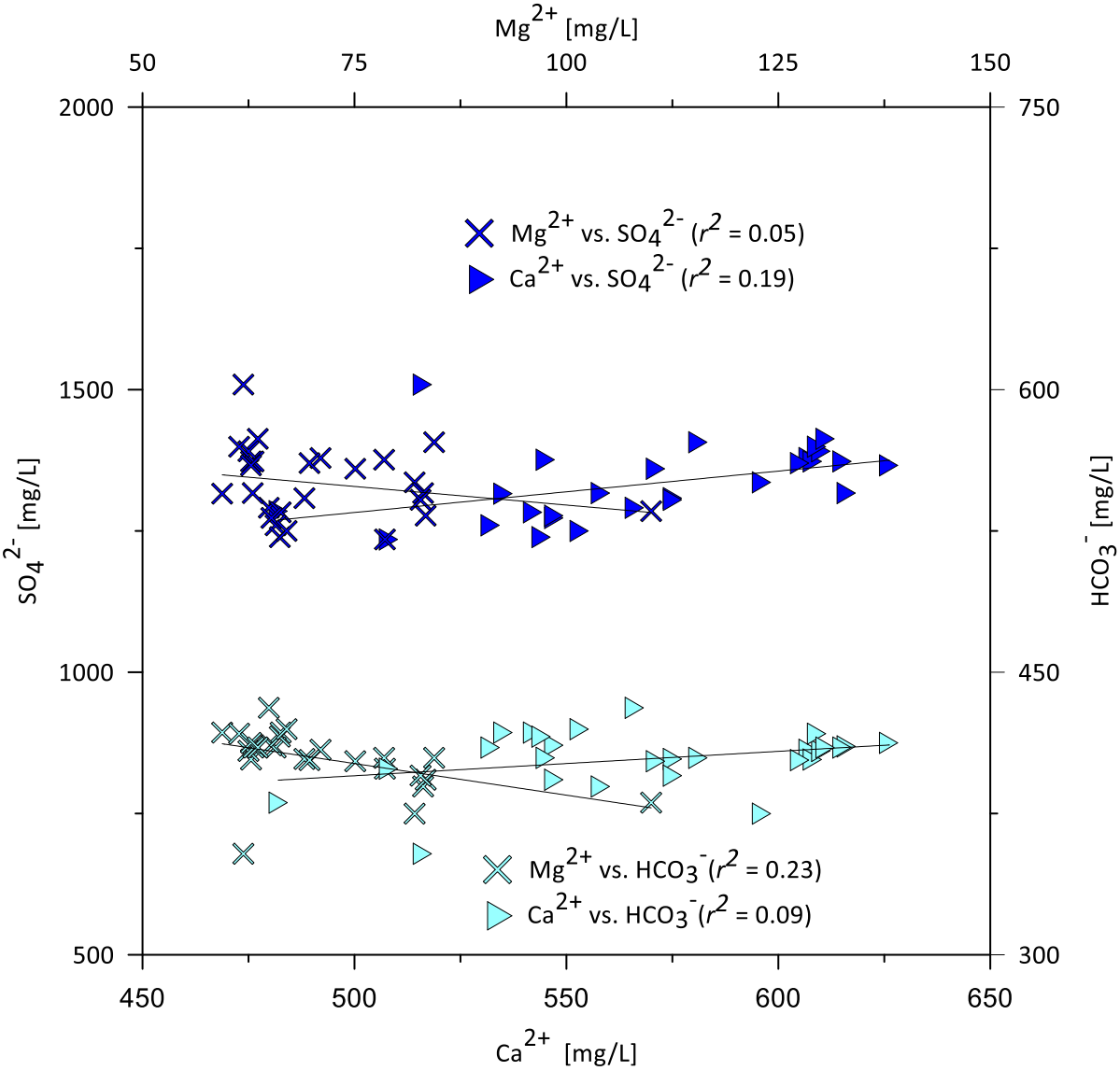

Figure 4.9. Plots of HCO_3^- and SO_4^{2-} versus Ca^{2+} and Mg^{2+}.

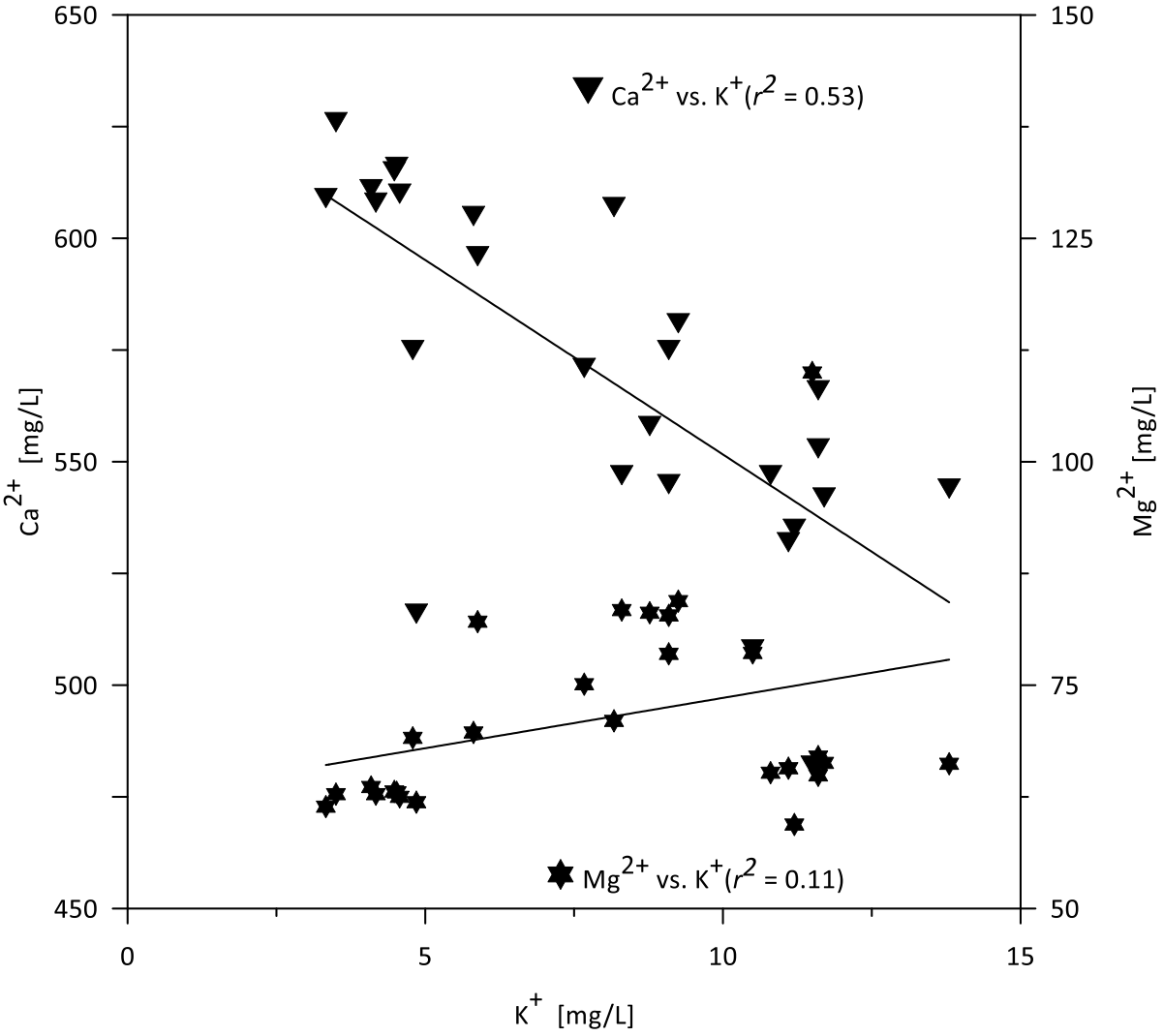

Figure 4.10. Plots of K^+ versus Ca^{2+} and Mg^{2+}.

Presently measured groundwater NO_3^- concentrations were below the EU Drinking Water Directives guide level of 50 mg/L as NO_3^- with respect to the quality of water intended for human consumption (OJEC, 2015). Although having NO_3^- concentrations below or at set maximum contaminant level is not generally an adult public-health threat, NO_3^- in drinking water can cause low oxygen levels in the blood, which is a potentially fatal condition for infants (Spalding and Exner, 1993; Gasperikova et al., 2012). In pristine aquifers, Cl^- concentrations are usually lower than 10 mg/L and sometimes less than 2 mg/L (Chapman, 1992). However, this study shows higher Cl^- concentrations.

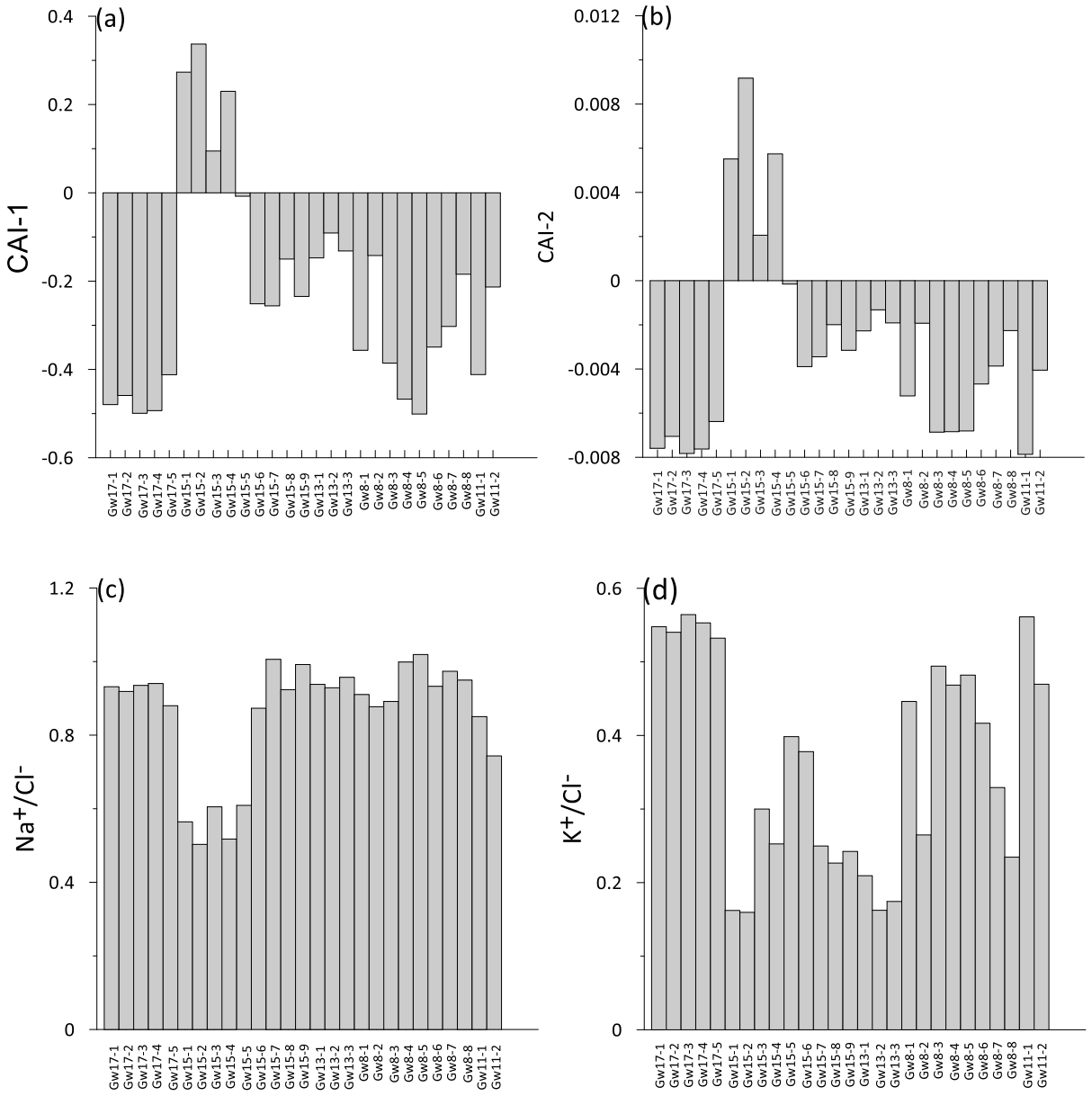

Figure 4.11. (a) and (b) Distribution of the chloro-alkaline indices (CAI-1 and CAI-2) (After Schoeller, 1967). (c) Na^+/Cl^- and (d) K^+/Cl^- ratios within the aquifer.

To further constrain the processes of water-rock interactions from the geochemical indicators point of view, I examined the degree of ion exchange (a geochemical modifier associated with transport and reactivity of solute process) that also depends on various lithological contents (e.g., clay content), and environmental (e.g., pH, solute composition) factors (Vengosh, 2003)). In this sense, I quantified the chloro-alkaline indices according to Schoeller (1967): (a) CAI-1= $[Cl^- - (Na^+ + K^+)]/Cl^-$ and (b) CAI-2 = $[Cl^- - (Na^+ + K^+)]/(SO_4^{2-} + HCO_3^- + CO_3^{2-} + NO_3^-)$. All values used in the computation of the chloro-alkaline indices are expressed in meq/L. As shown in Figure 4.11 (a and b), I found the range of values of -0.5 – 0.34 and -0.007 – 0.009 for CAI-1 and CAI-2, respectively. A negative CAI-1 or CAI-2 signifies that ion exchange takes place between Ca^{2+} or Mg^{2+} in the groundwater and Na^+ or K^+ adsorbed in the aquifer medium, while a positive CAI-1 or CAI-2 indicates that ion-exchange takes place between Na^+ or K^+ in the groundwater and Ca^{2+} or Mg^{2+} adsorbed in the aquifer medium. I also used the Na^+/Cl^- ratio (Figure 4.11c) to indicate the efficacy of the base-exchange reactions (Vengosh and Keren, 1996). As most soils have limited

anion exchange capacity and given that Cl^- is usually considered conservative in the environment (Neal and Kirschner, 2000), major changes in the Na^+/Cl^- ratios can be linked to cation-exchange reactions. Basically, the trend in the Na^+/Cl^- ratios is conceptualized as follows. Initially, as the dissolved Na^+ is sequestered at the exchange site, the resulting Na^+/Cl^- ratios is less than 1. The continued increase in the concentration of dissolved Na^+ implies exceedance of the cation-exchange capacity such that little or no Na^+ removal by adsorption takes place and the ratios approaches a value of 1 (Long et al., 2015). Also, the ratios often increase to levels well above one as Na^+ is released from the exchange sites due to flushing. Werner and diPretoro (2006) observe that as Na^+ is depleted from the exchange sites, the ratios return to 1 with the soil approaching equilibrium with literally no more Na^+-containing water. The consequence of the highlighted scenarios is that the Na^+/Cl^- ratios could mirror the solute concentration histories and response to supplying sources, environmental conditions, and nature of flow pathways and storage capacity of the containing-media. Similarly in Figure 4.11d, the K^+/Cl^- ratios was used to indicate the ability of the clay minerals to absorb K^+. Böhlke (2002) noted that low K^+/Cl^- ratios less than unity potentially indicate the absorption of K^+ onto clay minerals. Overall reduction in the groundwater K^+/Cl^- ratios may be caused by sorption by clays (Oren et al., 2004).

From Figure 4.12, it is shown that two groups of groundwater samples (A and B) exist. Group A samples are mostly associated with higher NO_3^- concentrations (range: 29.1 – 49.8 mg/L), whereas group B samples are associated lower NO_3^- concentrations (range: 12 – 19.2 mg/L). The existence of these groups may be reflective of the effect of two distinct biogeochemical heterogeneities influencing groundwater NO_3^- in the sampled aquifer zones. From the lower NO_3^- concentrations of group B samples, some within the range of 10 – 15 mg/L, it might be suggested that the groundwater NO_3^- is of natural/geogenic origin. Heaton (1986) noted that groundwater NO_3^- concentrations > 5 mg/L generally show contamination by animal wastes, fertilizers and/or effluents. Kohn et al. (2016) also presumed the impact of agricultural activities on high concentrations of NO_3^- (i.e., > 13 mg/L) and/or Cl- (i.e., > 20 mg/L). Moreover, because Cl^- is also not considered a major component of the area's environmental geochemistry, the relationship between NO_3^- and Cl^- concentrations exhibiting a good and positive correlation (Figure 4.12a, $r^2 = 0.84$), suggests that much of the NO_3^- and Cl^- are probably transported from a common anthropogenic source/activities (e.g., Murgulet and Tick, 2013), rather than originating from the dissolution of the gypsiferous carbonate rock of the area (e.g., Wendland et al., 2005; Wendland et al., 2008). Cl^- can be used as a natural tracer of manure in agricultural settings. Unlike manure nutrients, Cl^- is neither consumed by plants nor impacted by physical, chemical and microbiological reactions. Thus, tracking the relationship between Cl^- and NO_3^- seems to be an interesting approach to assessing whether NO_3^- was anthropogenically introduced into the groundwater. Numerous studies have also suggested that such a strong positive correlation between NO_3^- and Cl^- could be an evidence of predominantly faecal- and/or waste water-derived NO_3^- influence (e.g., Chapman, 1992; Barrett and Howard, 2002; Murgulet and Tick, 2013; Dzakpasu et al., 2014). Previously in the study area (Schollenberger, 1998), it was assumed that 80 - 95 % of the plume of NO_3^- in the groundwater can be linked to N fertilizer application in the form of NH_4^+ (diffuse N source). There is also an assumption that a hypothetical landfill site (potential point source; see Figure 4.1) would have contributed to the investigated groundwater NO_3^- plume.

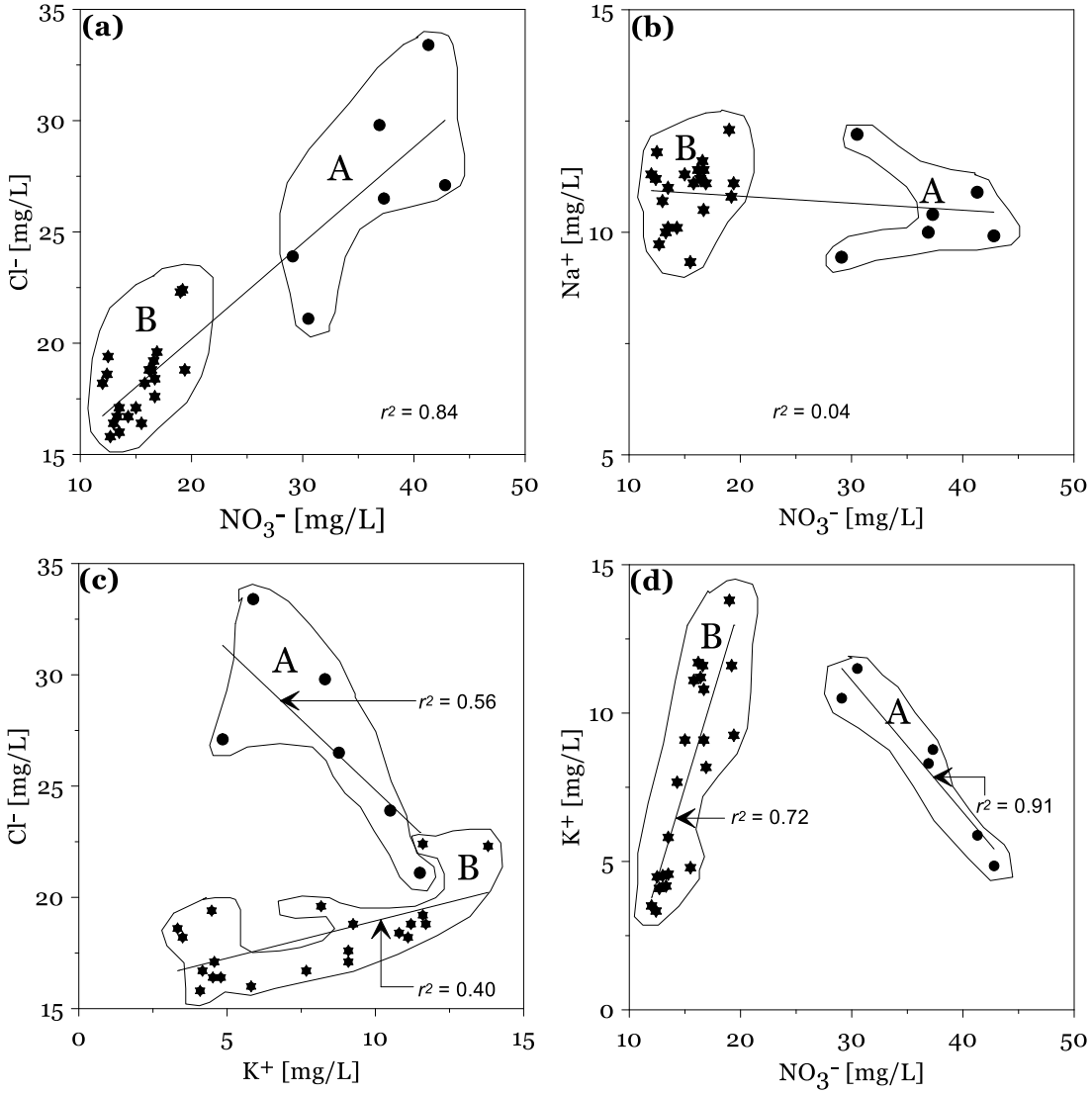

Figure 4.12. (a) Relationship between NO_3^- and Cl^- concentrations. (b) Plot of Na^+ versus NO_3^-. (c) Plot of Cl^- versus K^+. (d) Plot of K^+ versus NO_3^-. Groups A and B groundwater samples are shown to be associated with NO_3^- end-member groups.

In an aquifer impacted by a landfill, typical major cations may include Ca^{2+} , Mg^{2+}, Na^+ and K^+) (Deutsch and Siegel, 1997; Christensen et al., 2001). However, as previously explained, it is obvious in this study that concentration values of Ca^{2+}, Mg^{2+} are most representative of the area's natural environmental geochemistry (that is, gypsiferous carbonate rock system). Ranjbar and Jalali (2012) reported that farm animal wastes and septic tank effluents for instance are typically enriched in Cl^-, Na^+, and K^+ among many other contaminants which are released by decomposing organic matter (Minet et al., 2017). Even though Na^+ is not as mobile as NO_3^-, Minet et al. (2017) demonstrated that as one of the most mobile of the common cations, Na^+ adsorption should be further reduced as the sorption sites within the plumes of contamination become saturated. Consequently, it is expected that Na^+ concentrations should be elevated (in particular, in the deeper parts of the aquifer – mostly group A samples) and deemed indicative of point source of N-rich organic effluents relative to the shallower parts of the aquifer – mostly group B samples. Na^+ concentrations did not vary widely across the aquifer (Table 4.2). The weak correlation observed between Na^+ and NO_3^- (Figure 4.12b) points to little or no impact of point sources associated with NO_3^- groundwater loading. Nonetheless, it is worth noting that for the Na^+ concentration values

to be used as an indicator of contamination by organic wastes, it behooves investigators to determine if the wastes (in septic tanks and landfills) contain Na^+-enriched components (e.g., human salty diets, water softeners and certain detergents, etc).

Although K^+ can be contained in diffusely applied synthetic N-P-K, KNO_3 and/or non-N fertilizers (e.g., potash (KCl)) as well as animal/human wastes (Maule and Fonstad, 2000), the relationships between Cl^- and K^+ and NO_3^- and K^+ (Figure 4.12 (c and d)) for the two groups of groundwater samples distinctly varied. The nature of the observed correlation between Cl^- and K^+ and NO_3^- and K^+ (Figure 4.12(c and d)) suggest that the dynamics of groundwater in the aquifer can be relatively deciphered. In the sedimentary environments, K^+ can also be released predominantly from the chemical weathering of K^+-containing primary minerals. These minerals weather more slowly than those containing Ca^{2+}, Mg^{2+}, Na^+ during water-rock interaction (Berner and Berner, 1996). In this regard also, K^+ has been considered one of the hydrogeochemical indicators to estimate groundwater residence time in carbonate aquifers (Lalbat et al., 2007). Thus, it is anticipated that K^+ concentrations would increase as the residence time increases and vice-versa. Based on this, it is provisionally interpreted that in group A groundwater samples wherein K^+ decreased with increase in NO_3^- could be related to zones of shorter groundwater residence times whereas in group B groundwater samples wherein K^+ increased with increase in NO_3^- (however, less than the NO_3^- concentration levels of group A groundwater samples) were associated with zones of longer groundwater residence times. In tandem with this interpretation, some investigators (e.g., Zarnetske et al., 2011; Briggs et al., 2013) have demonstrated that a net nitrification environment would have short residence times while a net denitrification environment would have long residence times. This may be the reason why the Group A samples appear to have higher NO_3^- concentrations than Group B samples. Perhaps the channelized aquifer structure from which the Group A samples were collected, played a crucial role in the distribution of the NO_3^- concentration levels. Although these inferences imply that the shallower group B groundwater samples would be more associated with denitrified groundwaters compared to the group A samples from within the channelized deeper parts of the aquifer, the effect of groundwater residence times on the groundwater NO_3^- at the study site needs further investigations. These attempts to identify specific contributory source of the groundwater NO_3^- are useful, however, they are not definitive enough with the present set of hydrogeochemical data. Thus, as discussed in the subsequent sections, further efforts were made to reduce uncertainties over source apportionment and fate of NO_3^- using complementary studies.

4.4.2 Sulfate sources using $\delta^{34}S\text{-}SO_4^{2-}$ and $\delta^{18}O\text{-}SO_4^{2-}$

I used the dual isotopic composition of SO_4^{2-} ($\delta^{18}O$ and $\delta^{34}S$) to distinguish groundwater SO_4^{2-} sources and to ascertain the contributory cause of these sources in the groundwater. This is based on the concept that the SO_4^{2-}-derived from different sources usually has distinct $\delta^{18}O$ and $\delta^{34}S$ values (e.g., Onac et al., 2011). This approach has been also applied in inferring processes (e.g., mixing or bacteria SO_4^{2-} reduction) that affect the concentrations and/or isotopic compositions of SO_4^{2-} (e.g., Miao et al., 2013). The studied groundwater samples (Table 4.2 and Table A7) have $\delta^{34}S\text{-}SO_4^{2-}$ values ranging from 15.2 to 16.3 ‰ (M = 15.9, MD=16.06, SD = 0.342, CV = 2.15 %) and $\delta^{18}O\text{-}SO_4^{2-}$ values ranging from 12.8 to 14.0 ‰ (M = 13.3, MD=13.40, SD = 0.310, CV = 2.33 %).

The cross plot of the $\delta^{34}S\text{-}SO_4^{2-}$ and $\delta^{18}O\text{-}SO_4^{2-}$ values (Figure 4.13) shows isotopic composition values clustered in one region, indicating that the groundwater SO_4^{2-} emanated from a common source. I used a three end-member mixing model defined by Samborska et al. (2013) to interpret the isotopic measurements of SO_4^{2-} dissolved in the groundwater (Graf et al., 1994; Phillips and Gregg, 2003; Moore and Semmens, 2008; Samborska and Halas, 2010). The model is based on estimates of average, lower and upper confidence interval for the fraction of each source of SO_4^{2-} ion in the groundwater on the recharge areas of the Triassic carbonate formation. The considered sources of SO_4^{2-} characterized by its own range and distribution of $\delta^{34}S\text{-}SO_4^{2-}$ and $\delta^{18}O\text{-}SO_4^{2-}$ are as follows: (1) sulfide(S) as a result of sulfide mineral oxidation; (2) SO_4^{2-} originating from atmospheric precipitation/recharge water, and (3) SO_4^{2-} from the dissolution of gypsum. Figure 4.13 shows that the groundwater samples are mainly plotted toward the vertexes corresponding to the mean isotopic composition influenced by the gypsum source. The enrichment in the measured $\delta^{34}S\text{-}SO_4^{2-}$ and $\delta^{18}O\text{-}SO_4^{2-}$ did not reflect fractionation due to bacterial SO_4^{2-} reduction or signatures of isotopic sources influenced by precipitation/recharge water (Mongelli et al., 2013).

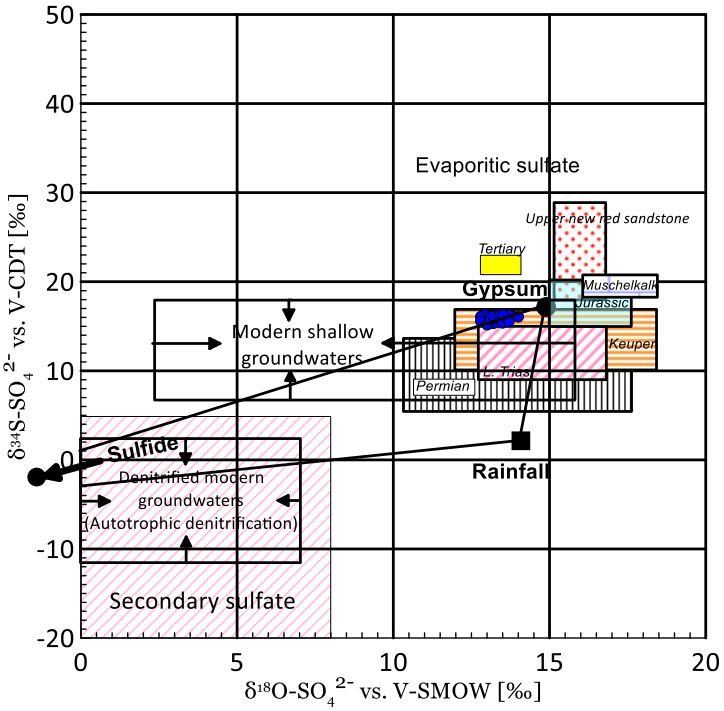

Figure 4.13. Plot of $\delta^{34}S\text{-}SO_4^{2-}$ and $\delta^{18}O\text{-}SO_4^{2-}$ (closely clustered blue circles). Typical ranges of $\delta^{34}S\text{-}SO_4^{2-}$ versus $\delta^{18}O\text{-}SO_4^{2-}$ values for different sources of SO_4^{2-} are taken from Graf et al. (1994), Pauwels et al. (2010), Samborska et al. (2013) and Miao et al. (2013).

Overall, the groundwater samples plotted in the evaporitic sulfate field as shown in Clark and Fritz (1997). In this field, the sampled groundwater is characterized by isotope values consistent with the Keuper (e.g., Krouse and Grinenko, 1991). Prior investigations also have reported a similar range of $\delta^{34}S\text{-}SO_4^{2-}$ and $\delta^{18}O\text{-}SO_4^{2-}$ values for the SO_4^{2-} evaporites such as gypsum (e.g., Krouse and Mayer, 2000; Knöller et al., 2005; Samborska et al., 2013). Based on an interpretation framework provided by Pauwels et al. (2010), the groundwater samples are mainly classified into the domain of modern shallow groundwaters, particularly NO_3^--contaminated groundwater (that is, NO_3^- > 5mg/L) with $\delta^{34}S\text{-}SO_4^{2-}$ values ranging from +8 to +16 ‰ and not in the denitrified modern

groundwaters domain, where autotrophic denitrification is assumed (that is, in groundwaters influenced by S dissolution with lower isotopic ratios down to – 10 ‰ for $\delta^{34}SSO_4^{2-}$ (Aquilina et al., 2015). Further evaluations in the next sections are expected to inject a new perspective into this observation with regards to the fate of NO_3^-.

4.4.3 Refined understanding of the NO_3^- sources

Based on the plot of the N and O isotopes of NO_3^- (Figure 4.14), the dual isotopic composition of NO_3^- ($\delta^{18}O$, $\delta^{15}N$) shows that 64 % of the 25 groundwater samples considered (Table 4.2 and Table A7) with $\delta^{15}N$-NO_3^- values ranging from +6.7 to 8.1 ‰ and $\delta^{18}O$-NO_3^- values ranging from +3.4 to 4.6 ‰ plotted in the area of overlap between soil organic N and animal waste (manure) and sewage plus septic waste, respectively. The groundwater samples were mainly collected from the shallower compartment of the aquifer. Given the presented values of $\delta^{15}N$-NO_3^- and $\delta^{18}O$-NO_3^-, it can be assumed that this signature was most representative of NO_3^- derived from organic N in the soil (Silva et al., 2000; Kendall et al., 2007). However, Fang et al. (2015) noted that $\delta^{15}N$ of soil-extracted NO_3^- was generally negative in surface soils, being much lower (by 6 to 13.4 ‰) than the $\delta^{15}N$ of soil organic N, which ranged from 0 to 7.5 ‰. Böhlke et al. (2002) and Böhlke (2002) observed that anomalously low $\delta^{15}N$ values of around 0±1 ‰ in groundwater NO_3^- from some agricultural sites in the US have been interpreted as a result of mineralization, nitrification, and recharge. If true, this would imply that denitrification could be responsible for the recorded $\delta^{15}N$-NO_3^- values ranging from +6.7 to 8.1 ‰. However, animal manure have commonly exhibited $\delta^{15}N$ values of + 6 ‰ on the land surface.

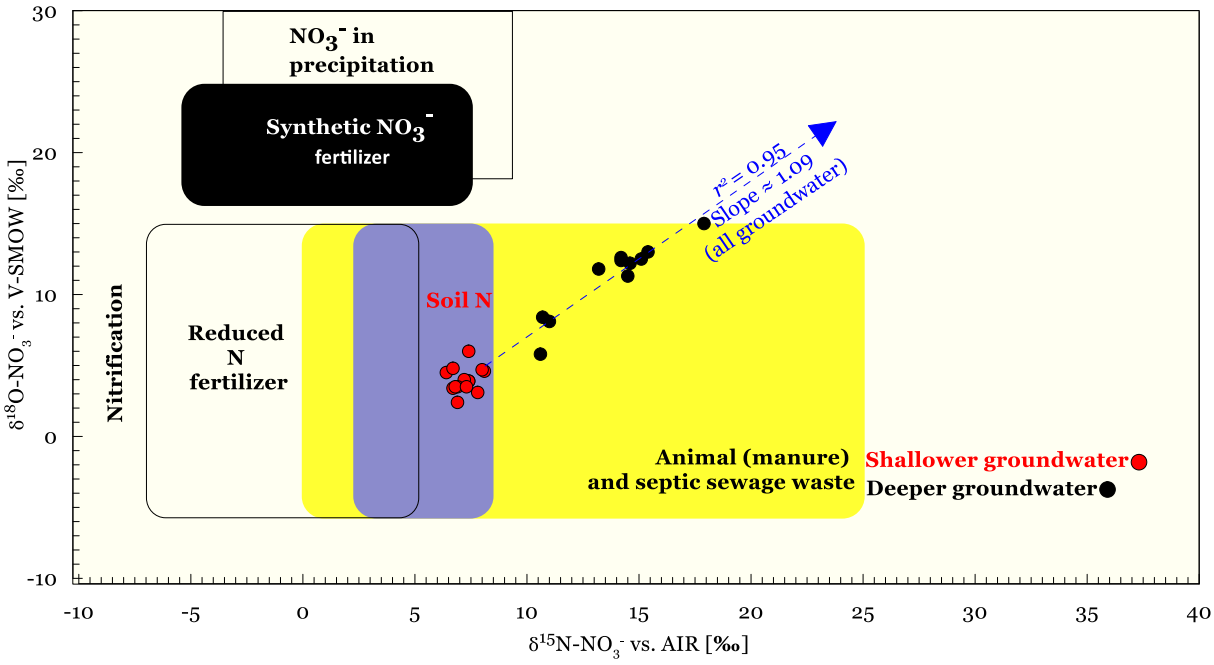

Figure 4.14. Dual NO_3^- isotope plot showing ranges of $\delta^{15}N$-NO_3^- and $\delta^{18}O$-NO_3^- values in permil (‰) characteristic with NO_3^- from soil organic N and animal (manure)/septic sewage sources (after Kendall, 1998).

The remaining 36 % of the groundwater samples from the deeper section of the aquifer was characterized by values ranging from +10.6 to +17.9 ‰ and from + 5.8 to + 15.0 ‰ for δ^{15}N-NO_3^- and δ^{18}O-NO_3^-, respectively. The elevated δ^{15}N-NO_3^- and δ^{18}O-NO_3^- values compared to those of the shallower groundwater samples are consistent with signatures of NO_3^- likely derived from animal waste (manure) and sewage plus septic waste (Canter, 1997; Kendall et al., 2007). However, the overlapping dual NO_3^- isotope signature range for animal waste (manure) and sewage plus septic waste does not permit precise quantification of the contribution of these sources to NO_3^- in the groundwater (Burns et al., 2009). Also, this could probably result from wide variations in the isotopic composition of sources, mixing and biological cycling. Studies have reported that the average δ^{15}N-NO_3^- value from landfill leachates would fall between the average for animal-septic wastes and the average from natural soil NO_3^- (Wolterink et al., 1979; Cravotta, 1995). Taking together with the consideration that the major ion geochemical data did not indicate clear evidence that the NO_3^- emanated from a landfill in a point source form, establishing the existence of the proposed hypothetical landfill site is difficult.

Specifically, the nature of landfill leachates depends on the type of waste deposed of at the site, landfilling technique used, the waste degradability and their stage of degradation (Maximova and Koumanova, 2006) as well as of environment geochemistry and climate. Presently, there is no information that directly probes the content of the feature suspected to be a landfill site. In other words, discerning the content of the suspected landfill feature would be a topic of great research concern. During one of the conducted field campaigns however, I witnessed the fertigation of the agricultural soil with liquid manure. Based on the results presented in section 4.4.2, the infiltrating rainwater would have facilitated the leaching of the produced NO_3^- into the Quaternary aquifer system. Under this scenario, it could be that the most likely NO_3^- source in the groundwater is the liquid manure, but the dilemma admittedly faced is distinguishing between animal manure and septic wastes in the deeper compartment of the aquifer. Obviously, given the characteristics of septic and animal manure wastes (Fleming and Ford, 2002) in terms of potentially being a point source (e.g., septic systems) or diffuse source (animal manure) and their microbiological characteristics, there is no scientific basis for classifying them into the same category as displayed in Figure 4.14.

Where a point source of NO_3^-, for example the hypothetical landfill site occurs in a heterogeneous aquifer environment with a transmissive preferential flow path as it is being considered in this present study; it is hardly distinguished from a diffuse source as in the case of the application liquid animal manure. This is because the existence of such a flow path would mean that all infiltrating fluids and solutes (irrespective of point or diffuse source) can be entrained into the deeper aquifer compartment, making it difficult to discriminate between a point and a diffuse N-source. Nevertheless, as higlighligted in this study's outlook in Chapter five, an approach for distinguishing between landfill, sewage, animal manure using a variety of other chemical, microbiology and stable isotope indicators is recommended combined with probing the content of the study site environment where the hypothetical landfill site is suspected.

From the distribution of the plotted data, I found no readily available hint for direct input of synthetic NO_3^- fertilizer or NO_3^- from atmospheric deposition (Kendall and Aravena, 2000; Vitòria et al., 2004). This is due to the fact that synthetic fertilizer applied as NO_3^- and NO_3^- from atmospheric deposition would typically have a higher δ^{18}O values of 19 to 25 ‰ and more than 30 ‰, respectively (Mayer et al., 2001; Mengis et al., 2001). However, observation of the impact of the greater δ^{18}O values from the synthetic NO_3^- in the groundwater would normally not be expected

due to immobilization-mineralization cycles in the soil. This is also because during immobilization processes, the three O atoms of the NO_3^- are removed and hence, NO_3^- from atmospheric deposition or synthetic NO_3^- fertilizers loses its original $\delta^{18}O$ signature. Fertilizer applied as NO_3^- would be taken up by plants or microbes (assimilation), transformed to organic N (immobilization), then returned to the soil followed by eventual reoxidization to NO_3^-(nitrification). With these processes, the resulting $\delta^{18}O$ values would be different from those of the initial applied NO_3^- and could have $\delta^{18}O$ values close to those of the applied reduced N that were nitrified in the soil zone (that is, through oxidation of the mineralized organic N). In effect, the residence time of the applied synthetic NO_3^- fertilizer in the soil-plant zone are always helpful in explaining the difference in the isotopic signatures of NO_3^- fertilizer which leached soon after application from that taken up by the plant and later returned to the soil (Panno et al. 2006). The lithological characters of the unsaturated zone and operating environmental factors in such an agricultural setting as illustrated in this study could also to act as a buffer with various N transformation processes modifying the original chemical composition of infiltrating organic wastes, be it animal manure, wastewater or landfill leachates (Krapac et al., 2002; Hao and Chang, 2003). Overall, considering the range of the $\delta^{15}N\text{-}NO_3^-$ isotopic values (that is, relatively higher than those of the reduced N fertilizer), Aravena et al. (1993) and Mengis et al. (2001) suggested that the shallower groundwater samples may have been so affected by the above-mentioned processes.

The slope of 1.09 obtained for the denitrification trend line exceeded those often reported for groundwater between 0.5 and 0.8 (Granger and Wankel, 2016). This shows that the partitioning of the groundwater NO_3^- sources into the two aquifer compartments results from complex processes that cannot just be explained by denitrification processes alone. As explained in section 4.4.7, mixing can be a counfounding factor in the observed slope of the denitrification trend line. Because mixing of NO_3^- sources alone cannot account for the range of isotopic values, it appears that denitrification has played an important role. Tracing the denitrification line (Figure 4.14) back to its interception as suggested by Panno et al. (2006). shows that the two distinct groundwater NO_3^- sources partitioned into the shallower and deeper aquifer compartments originated from the same reduced nitrogen fertilizer. The following sections further highlight the various mechanisms responsible for the partitioning of the NO_3^- sources in the shallower and deeper aquifer compartments.

4.4.4 Groundwater recharge origin based on $\delta^2H\text{-}H_2O$ and $\delta^{18}O\text{-}H_2O$

Isotopic enrichments of $\delta^{18}O$ and δ^2H in groundwater relative to the mean ocean water are determined and correlated with natural meteoric water derived from precipitation (Epstein and Mayeda, 1953; Craig, 1961; Kendall and Caldwell, 1998). This is essentially true, if the stable isotope ratios ($^{18}O/^{16}O$ and $^2H/^1H$) are considered homogeneous on a regional and time scale provided evaporation- and condensation-influencing processes are kept to a minimum (Clark and Fritz, 1997). As constituents of a water molecule, $\delta^2H\text{-}H_2O$ and $\delta^{18}O\text{-}H_2O$ can serve specifically, as natural and environmental tracers for tracking the sources of groundwater recharge (Guay and Eastoe, 2007). Because the relationship between $\delta^2H\text{-}H_2O$ and $\delta^{18}O\text{-}H_2O$ arises from fractionation during condensation from the vapor mass and the evolution of the $\delta^{18}O$ and δ^2H composition of meteoric waters begins with evaporation from the oceans, the plotting of $\delta^2H\text{-}H_2O$ against $\delta^{18}O$-

H_2O also opens up the possibility to visualize important groundwater recharge processes (Souchez and Lorrain, 2006).

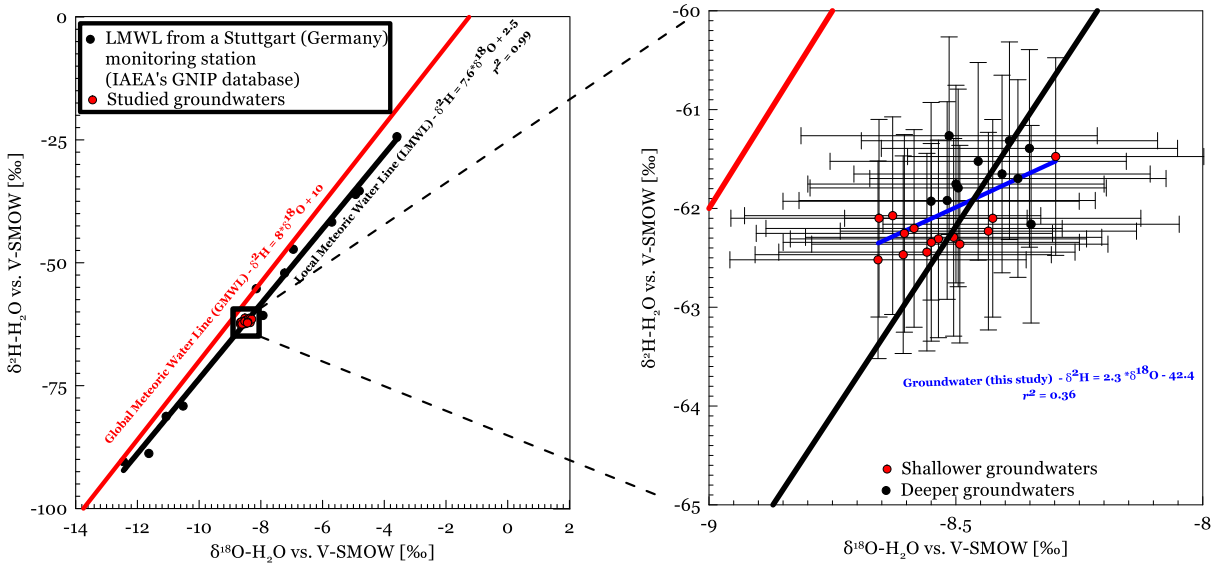

Figure 4.15. Representative δ^2H - $\delta^{18}O$ pairs from studied aquifer groundwater showing their relation to the global and local meteoric water lines. The vertical and horizontal error bars represent the measurement uncertainties of δ^2H (1.0 ‰) and $\delta^{18}O$ (0.3 ‰), respectively.

As shown in Table 4.2 and Table A7, the isotopic ratios in the groundwater of the investigated aquifer system ranges from – 8.7 to – 8.3 ‰ (M = -8.5, MD=-8.50, SD = 0.10, CV = - 1.18 %) for $\delta^{18}O$-H_2O and from – 62.5 to – 61.3 ‰ (M = -62.0, MD=-62.1, SD = 0.38, CV = - 0.62 %) for δ^2H-H_2O. As shown in Figure 4.15, the fact that the groundwater δ^2H-H_2O and $\delta^{18}O$-H_2O values did not vary widely and clustered on the local meteoric water line (LMWL): $\delta^2H = 7.6*\delta^{18}O + 2.5$ (r^2 = 0.99; n = 12) indicates that the groundwater recharge originates from local modern meteoric water source. The LMWL data represents water isotopic compositions of mean monthly precipitation (data acquired between January and December 2012) from an IAEA's Global Network of Isotopes in Precipitation (GNIP) monitoring station at Stuttgart (Germany) (Stumpp et al., 2014). The reason for the strong linear correlation in the LMWL data is due to the fractionation of isotopes during evaporation-condensation processes resulting in differential increase in δ^2H-H_2O and $\delta^{18}O$-H_2O values (Gourcy et al., 2005). Contrarily, a noticeable positive but weak correlation (Figure 4.15b) between the groundwater δ^2H-H_2O and $\delta^{18}O$-H_2O values: $\delta^2H = 2.3*\delta^{18}O - 42.4$ (r^2 = 0.36; n = 25) was observed. The weak correlation is also reflected in the large spread and variability of the measurement precision from the groundwater δ^2H-H_2O and $\delta^{18}O$-H_2O values, which however does not invalidate the data. Although identification of the uncertainty source is beyond the scope of the present study, the observed trend of δ^2H-H_2O and $\delta^{18}O$-H_2O signatures would not exclude the impact of transport processes created by the aquifer heterogeneity (e.g., Hendry et al., 2016) or water-rock interactions (Savard et al., 2010). More importantly, apart from the unexplainable groundwater sample Gw8-6 with the δ^2H-H_2O and $\delta^{18}O$-H_2O of -61.5 ‰ and -8.3 ‰, we observe systematic distinction in the stable water isotopes with relation to the identified shallower and deeper groundwater samples (based on the dual-NO_3^- isotope approach, see Figure 4.14).

The groundwater samples plot below the global meteoric water line (GMWL): $\delta^2H = 8*\delta^{18}O + 10$ (Craig, 1961), suggesting a more humid moisture source. The slope of the LMWL is 7.6, which is close to that of the GMWL with a slope of 8. First, this shows that the LWML data set may be considered representative of the mesoscale processes and combined effects of relative humidity, evaporation, storm source and enrichment or depletion on originating precipitation and averages inter-annual and intra-annual variability between δ^2H-H_2O and $\delta^{18}O$-H_2O values within the region (Ingraham, 1998; Rugel et al., 2016). Second, the slope of the LMWL shifting away a bit from that of the GMWL is an indication that the LMWL sample was affected by evaporation that occurred after condensation. Similarly, the much lower slope and intercept of the groundwater δ^2H-H_2O and $\delta^{18}O$-H_2O regression line indicate the effects of evaporative enrichment on the groundwaters as a whole.

The deuterium excess (d-excess) information, calculated after (Dansgaard, 1964) with d-excess = $\delta^2H - 8*\delta^{18}O$ was examined as an indirect measure of the extent of the evaporation impact (Gonfiantini, 1986) influenced mainly by relative humidity (Jouzel et al., 1982) and temperature (Johnsen et al., 1989) in the moisture's source area. Lower values support the assumption of increasing evaporation (Liotta et al., 2006; Murad and Mirghni, 2012). The calculated mean d-excess values averaged 6.0 ‰ (ranging from 4.6 ‰ and 7.0 ‰) and 5.6 ‰ (ranging from 2.72 ‰ and 9.93 ‰) for the groundwater and the LMWL data, respectively, lower than that of the global precipitation (+10 ‰), further indicate that partial evaporation of the recharging groundwater occurred. In general, the shallow aquifer groundwater NO_3^- is most likely a result of infiltrating rainwater, that is, evaporation of rain water prior to recharge (Clark and Fritz, 1997,Petrides et al., 2006; Guay et al., 2006; Pastén-Zapata et al., 2014).

Although there was no supporting age measurement data and water isotopes do not provide age information of the sampled groundwater, $\delta^{18}O$ abundances have been used to distinguish between Holocene and Pleistocene ground waters (Deak and Coplen, 1996). On this note, I show that the $\delta^{18}O$ values of the sampled groundwater are all more positive than - 9.9 ‰ indicating that the infiltrating rainwater represents a modern recharge after the late Pleistocene (Skelton et al., 2014).

4.4.5 NO_3^- dynamics in relation to aquifer heterogeneity, conservative and redox-sensitive constituents

The complexity of the groundwater NO_3^- fate and transport reflects the variability of the prevailing geologic conditions, subsurface hydrologic regimes and biogeochemical processes (Denver et al., 2014), which ultimately combine to control NO_3^- attenuation in the saturated zone (Rivett et al., 2008). The fate of groundwater NO_3^- is intimately linked to the redox conditions (Aravena and Mayer, 2010). According to Barlow and Kröger (2014), flowpaths drive chemical transport. The assumption that NO_3^- reduction does not occur often in the oxic zone between the bottom of the root zone and the redox interface and that all NO_3^- passing below this interface is immediately reduced, makes NO_3^- reduction in the subsurface only dependent on the flowpaths and the location of the redox interface (Refsgaard et al., 2014). However, this assumption of redox stratification in terms of anoxic denitrification is only basic, simplistic, and relatively well-understood and may not hold sway in capturing complex network of redox dependent metabolic

pathways and factors that potentially define the spatial and temporal variability of the NO_3^- sources and frequent mixing of groundwater of different origins (Vrzel et al., 2016; Briand et al., 2017). This is because when driven by diffusion of solutes (Canfield et al., 2005; Kessler et al., 2013), the interpretation of redox processes can become more complicated. The absence or presence of the groundwater EC, DO, NO_3^-/Cl^-, NO_3^-, Mn^{2+}, Fe^{2+}, SO_4^{2-}, NH_4^+, and HCO_3^- was used to characterize the heterogeneity of the aquifer system, redox conditions and demonstrate NO_3^- attenuation capacity.

I observed that the vertical profiles of the groundwater EC and SO_4^{2-}concentrations show near uniform distribution (Figure 4.16 (a and b)). Even though groundwater EC can be a natural tracer of pathways of physical mechanisms and biogeochemical fluxes (Garner and Mahler, 2007), from the homogeneous distribution of the groundwater EC and SO_4^{2-} concentrations across the entire depth intervals, it seems likely that the delineated channelized low resistivity feature was unconnected to a zone of higher groundwater EC sensitive to the SO_4^{2-} as initially hypothesized in Chapter three. Hence, the groundwater EC differences were not a good candidate for explaining the development of the observed low resistivity zone. This also indicates the DP EC logs (see Chapter three – Sections 3.7.4, 3.7.5, and 3.7.6) within the aquifer are reflective of conductivity differences produced by the aquifer lithologic variations. Furthermore, I observed steep vertical gradients for the DO and NO_3^- concentrations (Figure 4.16c) noticeably, for the deeper wells at sites Gw8 and Gw15. I found that the low DO values appear to correlate the high NO_3^- values in most cases. Such steep geochemical gradients indicate the existence of aerobic-anaerobic transition interface as mixing-controlled biogeochemical hotspots for enhanced microbial activities. The observed presence of steep geochemical gradients and correlations also re-emphasize the need for multilevel groundwater sampling and monitoring on a vertical axis in order to properly identify chemical heterogeneities, and microbiological processes.

Quantifying the relationships between the nature of flow and the heterogeneities in the different parts of the aquifer with physical methods can be challenging (Macpherson and Townsend, 2002), given the invisible nature of subsurface flow patterns. However, it has been demonstrated that one can track water movement and solute mixing patterns from the chemical and isotopic tracer that they carry (Kirchner et al., 2000). In this regard, the patterns and extent of vertical variations recognized in the water chemistry (Figure 4.16) within the aquifer may have been informed by the varying degrees of heterogeneity in the aquifer matrix composition, mineral dissolution/precipitation, ion exchange, sorption, and flow dynamics, which invariably influence redox adjustments. For instance, because within the redox ladder, the consumption or respiration of the NO_3^- oxygen or NO_3^- reduction by microbial populations enhanced by organic loading would proceed that of the SO_4^{2-}, it is most likely that the presence of NO_3^- inhibited the activities of the SO_4^{2-}-reducing bacteria, particularly in the deeper parts of the aquifer leading to a homogeneous SO_4^{2-} concentration levels (Churchill and Elmer, 1999). One would have also expected a correlation of low DO with low NO_3^- to indicate the presence of canonical denitrification. However, the reverse was the case in this study wherein the NO_3^- dynamics show an inverse relation with the DO concentrations (Figure 4.16c), re-affirming complex nitrogen turnover.

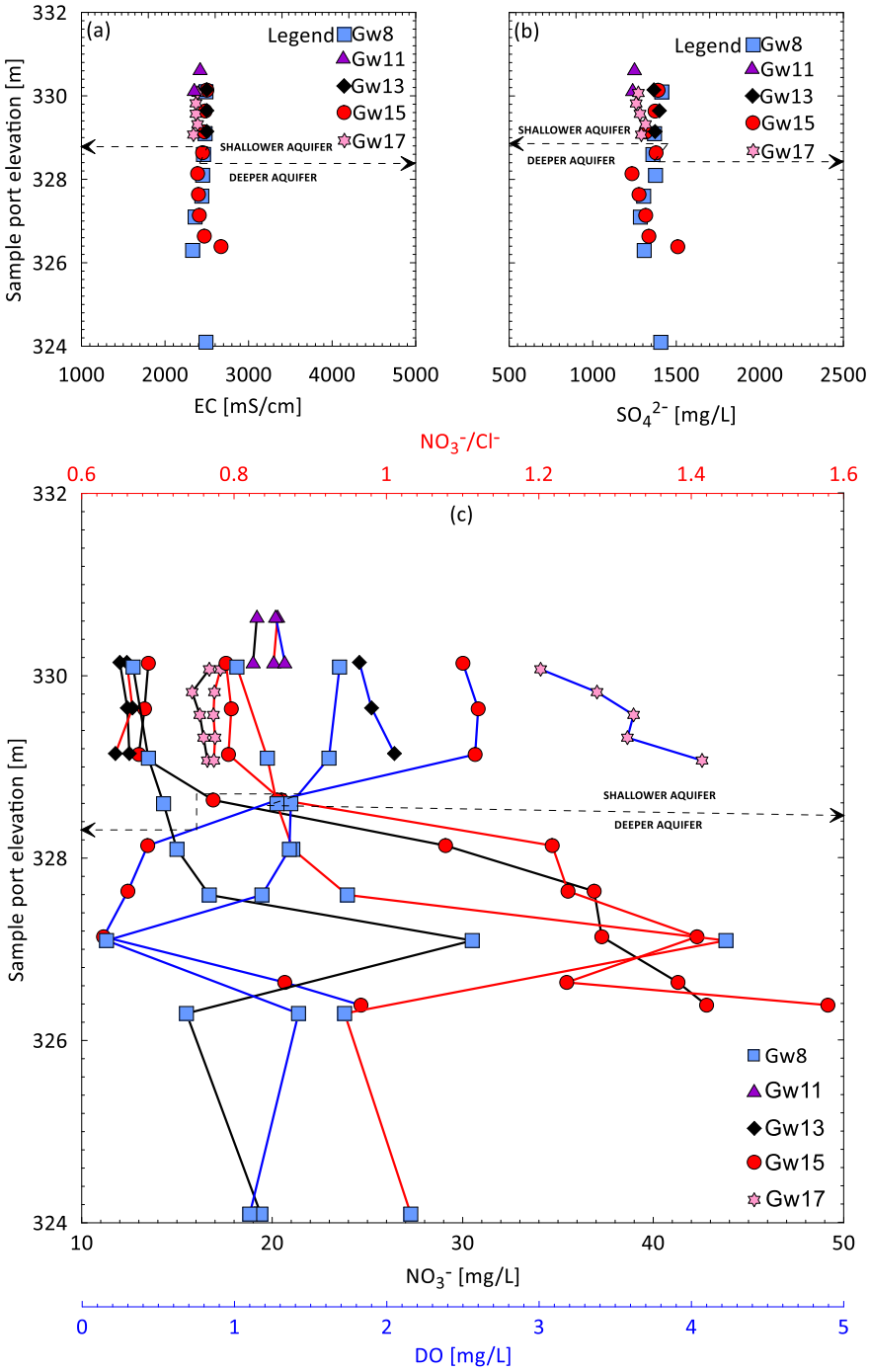

Figure 4.16. Vertical profiles of groundwater EC values (a), and SO_4^{2-} concentration levels (b). (c) Vertical profiles of dissolved oxygen, nitrate and nitrate-to-chloride ratios. The shallower and deeper aquifer groundwater samples are separated by the dashed line based on dual isotopic ratios of nitrate presented in Figure 4.14.

Based on the threshold given by Burow et al. (2010), a reducing condition with DO concentrations less than 0.5 mg/L can be expected to favor denitrification mechanisms. Against this threshold/scheme, some other studies (Barkle et al. 2007; Stenger et al., 2008; Weymann et al., 2008; Burbery et al., 2013; Clague et al., 2013) considered DO concentrations below 2 mg/L to be conducive for redox-related processes such as complete denitrification. Although these schemes agree that DO must be closer to zero before denitrification can be effective, up till now, the level of DO at which denitrification begins remains elusive. Also, given that NO_3^- is plainly not a useful

indicator of reducing groundwaters, the role of traditional denitrification should be reconsidered. Considering the distribution of the DO and NO_3^- in relation to the channelized deeper parts of the aquifer, this work suggests that the pattern of groundwater flow may provide answers as to why there was no significant NO_3^- removal in the low DO environment. The vertical concentration profiles of the solutes in the aquifer indicate that hydrologic processes in the shallower compartments of the aquifer may be different from those in the deeper compartments of the aquifer. This further confirms the the critical role of complex biogeochemical processes in shaping the observed uniform vertical profiles of the groundwater EC and SO_4^{2-} concentrations and steep concentration gradients in DO and NO_3^-.

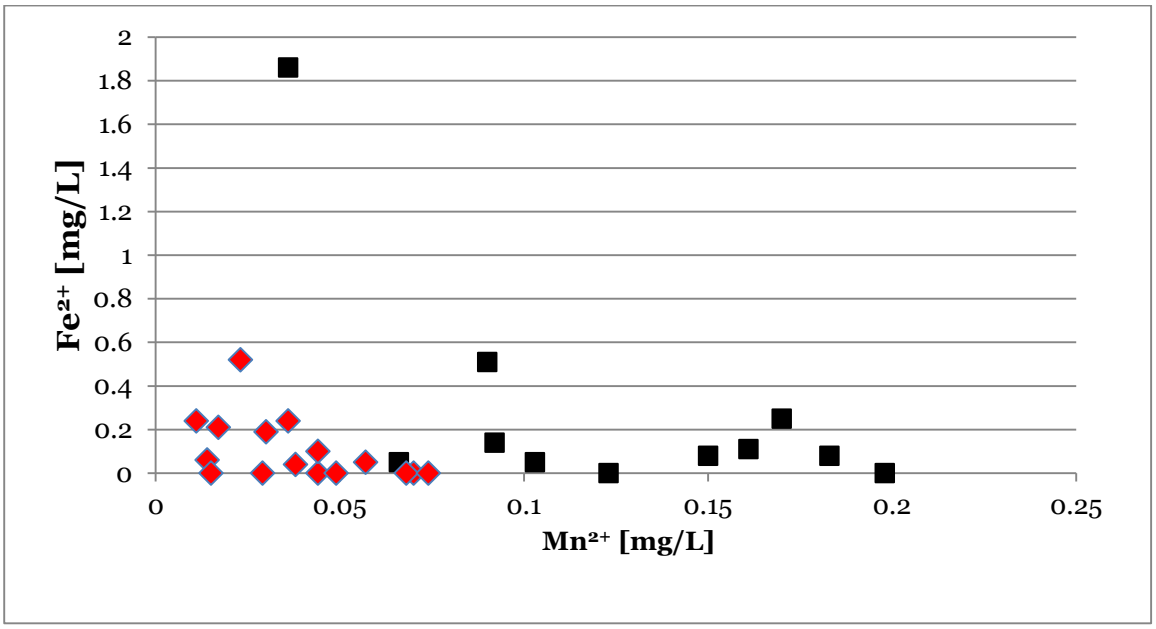

Figure 4.17. A plot of Fe^{2+} versus Mn^{2+} concentrations. Red and black notations indicate shallower and deeper groundwater samples, respectively.

A methodology for identifying the processes controlling the concentrations of the NO_3^- in the investigated aquifer can be based on the NO_3^-/Cl^- levels (Figure 4.16c). Altman and Parizek (1995) and Koba et al. (1997) noted that the ratio of NO_3^- to Cl^- can be effective in separating the effects of mixing and chemical processes. The rationale behind the application of the NO_3^- to Cl^- ratio method stems from the fact that Cl^- is a conservative/passive/nonreactive element, largely indifferent to physical, chemical and microbial mechanisms occurring in the groundwater (Altman and Parizek, 1995; Kirchner, 2003; Dzakpasu et al., 2014). Although NO_3^- is also a chemically conservative tracer, unlike Cl^-, NO_3^- can be microbially degraded (Hill et al., 1998; Curie et al., 2009; Kirchner et al., 2010). Therefore, considering that Cl^- is not a significant component of the surrounding geologic formation and may have been introduced to the aquifer system from the same land surface as NO_3^-, a change of Cl^- relative to the NO_3^- can be used to indicate NO_3^- addition or removal in the aquifer system. The increasing NO_3^-/Cl^- ratios with NO_3^- concentrations (Figure 4.16c) in the deeper compartment of the aquifer indicates the addition and mixing of the NO_3^- species in the groundwater along the flow path relative to the low NO_3^-/Cl^- ratios which support that NO_3^--consuming process was probably occurring in the shallower parts of the aquifer (Schilling et al., 2006; Fenton et al., 2009). Low concentration values of NH_4^+ sometimes below the detection

limit (Table A6), however, does not indicate dissimilatory NO_3^- reduction either.

Apart from N losses through ammonia volatilization from agricultural lands, it is possible that most of the NH_4^+ would have been oxidized to NO_3^- (mostly at soil-plant system) which eventually leached into the aquifer. Datry et al. (2004) explained that nitrification and subsequently denitrification as illustrated in a number of infiltration basins may have influenced the low values of NH_4^+ through the oxidation of the NH_4^+ produced from the microbial degradation of organic matter. NH_4^+ in an anaerobic aquifer system is more difficult to remove than the metals, because it strongly hold onto clay mineral exchange sites (Deutsch and Siegel, 1997). However, considering the environmental geochemistry of the study site, it would not be surprising to expect increased efficiency in the removal of NH_4^+, given the competition for the exchange sites from a divalent cation such as Ca^{2+} and/or Mg^{2+}.

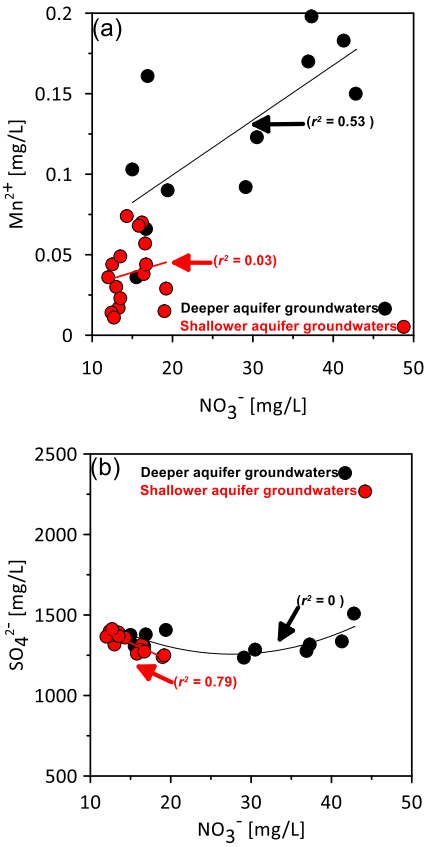

Figure 4.18. Relationship between NO_3^- and (a) Mn^{2+}, (b) SO_4^{2-}.

Mn^{2+} and Fe^{2+}concentrations were generally low (Figure 4.17, Table A6) with Mn^{2+} concentrations (Table 4.2) ranging from 0.011 to 0.198 mg/L and Fe^{2+}concentrations ranging from < 0.04 (below detection limit) to 1.86 mg/L. However, unlike the Fe^{2+}concentrations, there is a remarkable separation of the Mn^{2+}concentrations in the shallower and deeper aquifer compartments. While it is understandable that the high and near-uniform groundwater SO_4^{2-} concentrations (Figure 4.16b) is primarily due to the presence of gypsum in the area's environmental geochemistry, the observed concentrations of the Mn^{2+}, Fe^{2+} and SO_4^{2-}constituents may not be unconnected to the critical influence of the redox reactions in the aquifer system invariably controlled by the pattern of fluid flow/solute transport, motivating further assessment of the NO_3^- concentration trends in relation to the Mn^{2+}, Fe^{2+} and SO_4^{2-}constituents.

I evaluated the relationship between Mn^{2+} and NO_3^- concentrations to evaluate the evidence of potential anoxic nitrification by reduction of Mn-oxide that results from the oxidation of ammonia by Mn-oxide (e.g., Aller et al., 1998; Hulth et al., 1999; Mortimer et al., 2004). This belief goes against the conventional association of Mn-oxide reduction with the zone of NO_3^- reduction under anoxbic conditions. That is, when conditions are anoxic, Mn^{2+} is formed and released according to the standard view (Sarmiento and Gruber, 2006). These conditions and viewpoint, as noted by Stumm and Morgan (1996), Carlson et al. (1997), Bratina et al. (1998), and Homoncik et al. (2010), tend to follow denitrification in the sequence of redox reactions. Although Mn^{2+} concentrations were generally low in this study (Table 1), Figure 4.18a shows the strong positive correlation between NO_3^- and Mn^{2+} in the deeper compartment of the aquifer. This correlation simply indicates that where NO_3^- and Mn^{2+} concentrations are correspondingly high, the redox conditions are not favorable to denitrification (Kingsbury, 2003). Such correlations suggesting anoxic NO_3^- production during Mn-oxide reduction were also emphasized by Hulth et al. (1999) as an indication of simultaneous occurrences of nitrification and denitrification at the expense of NH_4^+. Taken in conjunction with previous explanations, anoxic nitrification may also explain why I observed depleted NH_4^+ concentrations. An insignificant correlation between NO_3^- and Mn^{2+} was also observed in the shallower compartment of the aquifer (Figure 4.18a). This further shows that even if traditional microbial denitrification played a critical role, the occurrence of the process in the presence of oxygen probably provided evidence for aerobic denitrification.

Three possible explanations for the observed low Fe^{2+} concentrations (especially for the aquifer zones with below detection limit Fe^{2+} concentrations) are: (1) Fe-bearing minerals was less abundant in the gypsiferous carbonate alluvial aquifer (e.g., Kunkel et al., 2004), (2) groundwater NO_3^- acted as a redox buffer, preventing the reduction of Fe-oxides, if present in the aquifer (Smolders et al., 2010), and (3) because microbial ferric iron (Fe(III)) reduction depends upon the groundwater pH, it is possible that the Fe-reducing bacteria respired SO_4^{2-} as an alternative electron acceptor in the studied near-neutral pH groundwater. Particularly in the case of more acidic groundwater and presence of electron donor, Fe (and Mn)-oxides will dissolve more readily. In this regard, even though limestone, dolomite, and Mn-carbonate are notable Mn sources and by implication, Mn would have resulted from the studied gypsiferous carbonate rock system, the near-neutral pH of the sampled groundwater may have also been responsible for the observed low Mn^{2+} concentrations. With respect to the the third possible explanation, Flynn et al. (2014) show how Fe-reducing bacteria can switch to sulfur reduction as their main energy source in an alkaline environment (Friedrich and Finster, 2014). According to Ledin and Pedersen (1996), microbial SO_4^{2-} reduction, a process that is affected little by changes in pH (Flynn et al., 2014) is the main source of dissolved sulfide in the subsurface. Jakobsen and Postma (1999) also indicate that Fe(III) reduction and SO_4^{2-} reduction co-occur frequently in the subsurface (Flynn et al., 2014). At such recorded low concentration levels of Fe^{2+} and under the groundwater pH range of 6.72 to 7.2 (especially in a situation where DOC does not seem to be labile as an electron donor – see section 4.48, Figure 4.23), it is possible that Fe-reducing bacteria would depend on the activity of SO_4^{2-}-reducing bacteria (Flynn et al., 2013). That being noted, evaluation of sulfur-driven chemoautotrophic denitrification, wherein for instance NO_3^- reduction is coupled to SO_4^{2-} production is also necessary. The correlation between NO_3^- and SO_4^{2-} for the deeper aquifer compartment groundwater samples portrayed insignificant relationships (Figure 4.18b). Given the clear evidence of NO_3^- production in the deeper aquifer compartment and that NO_3^- reduction is thermodynamically and energetically more favorable than SO_4^{2-} reduction (Whitmire and Hamilton,

2005), I explain that the reason for the observed relation in the deeper aquifer compartment is simply because the oxygen atoms of the NO_3^- were yet to be depleted to a level that permits SO_4^{2-} reduction. Conversely, a strong inverse relation was observed between SO_4^{2-} and NO_3^- concentrations in the shallower aquifer compartment (Figure 4.18b), wherein NO_3^- concentrations decreased with increase in SO_4^{2-} concentrations. Such a relation is commonly taken as evidence that reduced sulfur supports denitrification (i.e., autotrophic denitrification) (e.g., Hayakawa et al., 2013). Nevertheless, it has been demonstrated by several studies that nitrite (an intermediate during NO_3^- reduction) can be toxic/inhibitory to microbial SO_4^{2-} reduction (e.g., Schramm et al., 1999; Callbeck et al., 2013; Wu et al., 2018). The underlying chemolithotrophic metabolism supposes that the addition of NO_3^- can stimulate heterotrophic denitrifiers that outcompetes SO_4^{2-}-reducing bacteria for energy sources (Hubert and Voordouw, 2007) such that NO_3^--reducing, sulfide oxidizing bacteria is coupled to the oxidation of sulfide supplied by SO_4^{2-}-reducing bacteria, resulting in the production of intermediate elemental sulfur or certain amount of SO_4^{2-} relative to the NO_3^- removal (Schulz and Jorgensen, 2001; Burgin et al., 2007). Greene et al. (2003) also observed that inhibition of SO_4^{2-}-reducing bacteria by NO_3^--reducing, sulfide oxidizing bacteria is caused by 60 % of nitrite produced per NO_3^- reduced. Hence, measurements of nitrite concentrations and its isotopic composition would be an important activity in further studies. Overall, considering the little or no major changes in the SO_4^{2-} concentration, I cannot confidently argue for the dominance of autotrophic denitrification over heterotrophic denitrification until further data such as that in section 4.4.6 are evaluated. Also, given such inference as simultaneous occurrence of heterotrophic and autotrophic denitrification (Kadlec and Wallace, 2008), an interesting question begging for answers would therefore be, can aerobic denitrifiers proposed overall in this study as heterotrophic denitrifiers function as both heterotrophic and autotrophic denitrifers, and if not, how can the major pathway be identified?

4.4.6 Distinguishing between autotrophic and heterotrophic denitrification

Because solute concentration data alone as presented here is limited to decipher the underlying mechanisms for the occurrence of oxic lower NO_3^- and anoxic higher NO_3^- in the shallower and deeper parts of the aquifer, respectively, use was made of the stable isotope methods. I applied the isotopic signature of NO_3^- ($\delta^{15}N$) and SO_4^{2-} ($\delta^{34}S$) to understand if the metabolic pathways have been partitioned into autotrophic or heterotrophic denitrification. The fitted trend lines (see Aravena and Robertson, 1998; Hosono et al., 2014; Abbott et al., 2016) in the plot of $\delta^{15}N\text{-}NO_3^-$ against $\delta^{34}S\text{-}SO_4^{2-}$ (Figure 4.19) agrees to the fact that heterotrophic denitrification occurs in the aquifer system. If autotrophic denitrification were to be dominant, then $\delta^{34}S\text{-}SO_4^{2-}$ would have declined with increasing $\delta^{15}N\text{-}NO_3^-$. This also confirms the discussion throughout the previous sections that autotrophic denitrification may be unlikely or at least not dominating. Bacterial SO_4^{2-} and NO_3^- removal would preferentially utilize the lighter isotopes of sulfur and nitrogen resulting in the observed enrichment of the heavier isotopes in the shallower compartment. The recorded isotope signatures and associated fractionations are nonetheless dependent on the extent of the reduction/removal, and prevailing conditions. The significance of this line of evidence is that instead of wasting effort hypothetically modeling a system as being either autotrophic or heterotrophic and both, one can confidently rule out and ignore the occurrence of autotrophic denitrification. Apart from saving time in the modeling process, this

would allow focused and more reliable simulation of N biogeochemical processes.

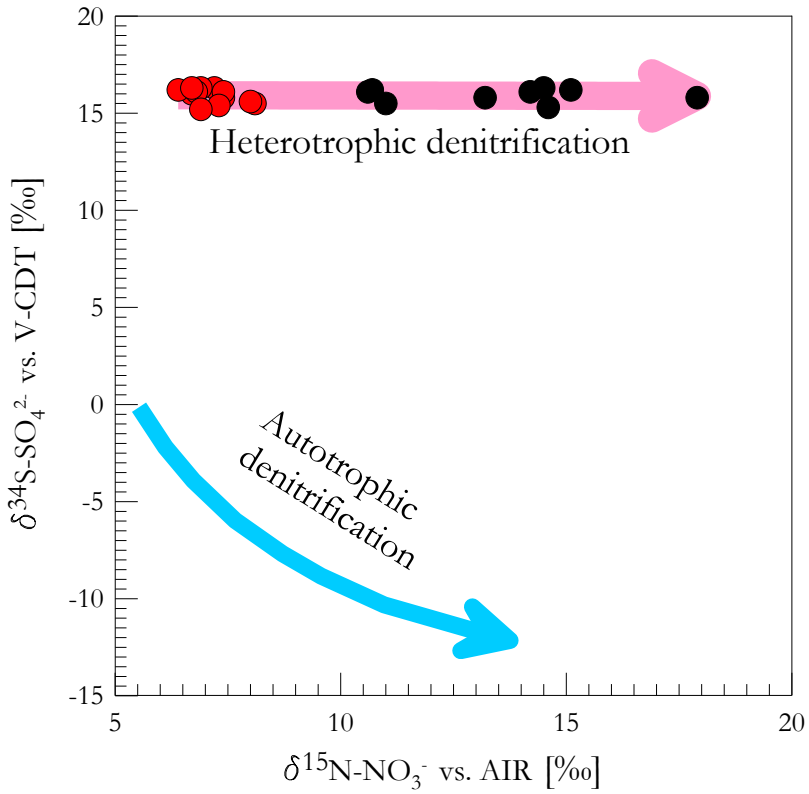

Figure 4.19. Relationship between δ^{15}N-NO_3^- and δ^{34}S-SO_4^{2-} in the groundwater samples from the study area.

4.4.7 Biogeochemical processes controlling NO_3^- fate by paired δ^{15}N-NO_3^- and δ^{18}O-NO_3^-

The analysis of the paired stable isotopes of NO_3^- and the slopes of the dual NO_3^- isotope plot can be used to quantify reaction processes and mechanisms (e.g., Böttcher et al., 1990; Einsiedl and Mayer, 2006; Wassenaar et al., 2006; Sacchi et al., 2013) responsible for the observed distribution of NO_3^- in the aerobic shallower and anaerobic deeper aquifer compartments

Unitless kinetic fractionation factor $\alpha_{p/s}$ that describes the extent of unidirectional isotopic fractionation and reaction between the substrate (reactant), S (heavier) and biologically mediated product, P (lighter) (that is, the fractionation of the product relative to the substrate) can be represented as

$$\alpha_{p/s} = \frac{R_{pi}}{R_s} = \frac{\delta_{pi}+1}{\delta_s+1} \quad (4.3)$$

where R_{pi} and R_s are the $^{15}N/^{14}N$ ratios of the instantaneous product which appears in an infinitely short time and substrate at the same time. The equation on the extreme right shows the expression of the fractionation factor in terms of isotope ratios in the δ notation on a logarithmic scale.

$\alpha_{p/s}$ relates to the isotope enrichment factor, $\varepsilon_{p/s}$ on the ‰ scale (as the fractionation factor generally differs by less than 5 % from unity (Mariotti et al., 1981) by:

$$\alpha_{p/s} = 1 + 10^{-3}\varepsilon_{p/s} \quad (4.4)$$

$\varepsilon_{p/s}$ can also be represented as:

$$\varepsilon_{p/s} = 10^{3}\left(\frac{1-\beta}{\beta}\right) \quad (4.5)$$

where $\beta = \alpha_{s/p} = 1/\alpha_{s/p}$, the kinetic isotope effect (inverse of fractionation factor) is the ratio of the rate constants of the light isotope to the heavy isotope representing the fractionation of the substrate relative to the product.

If $\alpha_{p/s} < 1$, then $\varepsilon_{p/s}$ will be negative and the product will be isotopically depleted relative to the substrate and vice-versa. The more negative the $\varepsilon_{p/s}$, the larger the isotopic fractionation. Basically, if $\varepsilon_{p/s}$ is small relative to 1000 (i.e., $\varepsilon_{p/s} \ll 1000$ ‰), Mariotti et al. (1981) also approximated $\varepsilon_{p/s}$ by the difference between the isotopic composition of the reactant and its instantaneous product ($\varepsilon_{p/s} \cong \delta_{pi} - \delta_s$). So, an instantaneous product with a particular amount of enrichment will be approximately that amount of enrichment lower than that of the reactant.

Initially, the concentration and isotopic composition of the substrate is almost constant as shown by:

$$\varepsilon_{p/s} \cong \delta_{pi} - \delta_s \ (t = 0) \quad (4.6)$$

Eqn (4.6), however, does not hold when substantial amount of substrate is consumed during the reaction. After more rigorous derivation and integration, Mariotti et al. (1981) clearly linked concentration to the isotopic ratios in the unreacted residual solute, classically termed "Rayleigh" equation (Rayleigh distillation model), which can be used to quantitatively describe the isotope effects (that is, the extent of deviation from perfect chemical equivalence) imparted on the solute during microbial solute concentrations reduction/transformations:

$$(\alpha_{p/s} - 1)\ln\left[\frac{C_o}{C_o}\right] = \ln\left[\frac{10^{-3}\delta_t + 1}{10^{-3}\delta_o + 1}\right] \quad (4.7)$$

and/or as its linear approximation:

$$\delta_t \sim \delta_o + \varepsilon \times \ln f, \quad (4.8)$$

where δ_t and δ_o are the total measured and initial relative δ units in the investigated substrate (that is, NO_3^-), C_t and C_o are the total measured and initial substrate concentration. f equals C_t/C_o denotes the fraction of unreacted/remaining residual substrate (e.g., NO_3^-).

The simplified form of the classical Rayleigh equation (Mariotti et al., 1981; Kendall, 1998) for independent O and N system of the residual NO_3^- can be expressed as follows:

$$\delta_t^{15}N = \delta_o^{15}N + {}^{15}\varepsilon_N \ln\left[\frac{NO_3^-{}_t}{NO_3^-{}_i}\right] \quad (4.9)$$

$$\delta_t^{18}O = \delta_o^{18}O + {}^{18}\varepsilon_O \ln\left[\frac{NO_3^-{}_t}{NO_3^-{}_i}\right] \quad (4.10)$$

$^{15}\varepsilon_N$ and $^{18}\varepsilon_O$ for N and O isotopes in NO_3^- are respectively expressed as:

$$^{15}\varepsilon_N = 10^3\left(\frac{1-\beta_N}{\beta_N}\right) \text{ and } ^{18}\varepsilon_O = 10^3\left(\frac{1-\beta_O}{\beta_O}\right) \quad (4.11)$$

$\beta_N = k^{14}/k^{15}$ and $\beta_O = k^{16}/k^{18}$ values of ~1.030 and 1.015 have been reported in laboratory column experiments using isolated NO_3^- reductases (Olleros, 1983 and Amberger and Schmidt 1987 as cited in Chen and MacQuarrie, 2005). Using Eqn (4.11), enrichment factors of $^{15}\varepsilon_N = -29.13$ ‰ and $^{18}\varepsilon_O = -14.78$ ‰ can be calculated k^{14} and k^{15} are rate constants of the reaction for $^{14}N-$ and $^{15}N-$containing reactants, repectively.k^{16} and k^{18} are rate constants of the reaction for $^{16}O-$ and $^{18}O-$containing reactants, repectively.

By solving for $(NO_3^-{}_t/NO_3^-{}_i)$, Eqns (4.9) and (4.10) can be distilled into the following analytical relationships between $\delta^{15}N$ and $\delta^{18}O$ of the residual NO_3^-:

$$\delta_t^{18}O = a + b\delta_t^{15}N \quad (4.12)$$

where a and b are

$$a = \delta_o^{18}O - \frac{^{18}\varepsilon_O}{^{15}\varepsilon_N}\delta_o^{15}N \quad (4.13)$$

$$b = \frac{^{18}\varepsilon_O}{^{15}\varepsilon_N} \quad (4.14)$$

The straight line relationship between $\delta^{15}N$ and $\delta^{18}O$ (Eqn (4.12)) has been observed in the laboratory and field investigations as an indication of denitrification processes. The slope b (Eqn (4.14)) referred to as the fractionation ratio (Böttcher et al., 1990) is dependent on the enrichment factors, $^{15}\varepsilon_N$ and $^{18}\varepsilon_O$ for N and O isotopes in NO_3^-, respectively; meaning that the slope b is controlled by the denitrification reaction rate constants k^{14}, k^{15}, k^{16}, and k^{18}. Unlike well-defined laboratory column experiments that can provide a constant initial substrate concentration (C_o), the problem in evaluating the classical Rayleigh equation with respect to field data lies in determining actual specific initial concentration values. Fukada et al. (2003) however, demonstrate that $\delta^{15}N$ and $\delta^{18}O$ values of the residual NO_3^- plotted against $\ln([NO_3^-])$ can approximate the linear derivation of the Rayleigh equation with slopes of $^{15}\varepsilon_N$ and $^{18}\varepsilon_O$, respectively.

Traditionally, the identical enrichment, progressive increase and close coupling of $\delta^{15}N$-NO_3^- and $\delta^{18}O$-NO_3^- values (Figure 4.14) are expected to show the occurrence of microbial denitrification. However, a closer examination of the relationship between the $\delta^{15}N$-NO_3^- values and NO_3^- concentrations (Figure 4.20a) reveals a trend of hyperbolic increase in $\delta^{15}N$-NO_3^- with decreasing NO_3^- concentration values. This pattern does not support the presence of the conventional denitrification process, wherein the $\delta^{15}N$-NO_3^- values should increase exponentially with decreasing NO_3^- concentrations under anaerobic conditions. In this scenario, the microbial denitrification reaction alone cannot clearly explain the partitioning of the NO_3^- sources in the two identified compartments of the aquifer. Following Mayer et al. (2002), such a 2nd degree polynomial relation (r^2=0.81) showing increase in the $\delta^{15}N$-NO_3^- values with increase in the NO_3^-

concentrations is indicative of N cycling processes associated with admixtures of NO_3^- of sewage or manure sources. Because denitrification can significantly complicate the interpretation of two NO_3^- sources using $\delta^{15}N\text{-}NO_3^-$ signatures and based on the Rayleigh fractionation model (Mariotti et al., 1981; Mariotti et al., 1988) can also display similar curvilinear relationship between $\delta^{15}N\text{-}NO_3^-$ and NO_3^- concentration values as mixing (Figure 4.20b), exercise of caution is often advised when interpreting mixing lines (Kendall et al., 2007). A diagnostic test of whether the $\delta^{15}N\text{-}NO_3^-$ values can be explained by mixing can be made by plots of $\delta^{15}N\text{-}NO_3^-$ against the natural log of concentration ($\ln NO_3^-$) and against the inverse of concentration ($1/NO_3^-$). As illustrated in this study, the curve and not the straight lines (Figure 4.20c), and the straight line and the not curves (Figure 4.20d) for the described data confirms that the curves on the plot of $\delta^{15}N\text{-}NO_3^-$ against NO_3^- results from mixing-controlled N cycling processes. Nevertheless, however indicative the plots may be, the uniqueness of the presented information lies in the overall positive correlations between $\delta^{15}N\text{-}NO_3^-$ and NO_3^-/or $\ln NO_3^-$ in contrast to the negative correlation trends commonly expected for anoxic denitrification. This observation of mixing-controlled N turnover is a complete opposite of conventional denitrification-controlled N turnover presented in Mariotti et al. (1988). Because the locations of the sampling ports within the aquifer are known, it seems reasonable to suggest that the shallower groundwaters descended into the deeper compartments of the aquifer via vertical migration and that the deeper aquifer structures potentially channeled lateral fluid flow and solute transport. Rafter et al. (2013) noted that if mixing is the dominant process, the $\delta^{15}N$ values of the sinking N should reflect the original sources of the N. In this sense, even though the contribution of the soil organic N resulting either from plant root decomposition or from direct uptake in the soil microbial community cannot be dismissed entirely, the deeper groundwater with increasing $\delta^{15}N\text{-}NO_3^-$ values from +10.6 to +17.9 ‰ that reflect animal manure/septic sewage sources is more likely to have been significantly transformed during recharge, leaving the shallower groundwater with $\delta^{15}N\text{-}NO_3^-$ values that reflect soil organic N sources. This result also suggests that although the shallower and deeper aquifer compartments seem connected by diffusion-controlled mixing, they are also hydrobiogeochemically distinct. This also means that distinct redox condition-controlling geohydrology and niches for a wider variety of microbial communities and their functional diversity variously accounted for the observed solute concentration trends and N stable isotope systematics in the two aquifer compartments. Although the role of diffusion-related isotope fractionation as a potential confounder in field-scale applications of N stable isotopes is obvious from the above discussion and across the reviewed literature, it is not yet clear how the introduction of low NO_3^- and low dual-NO_3^- isotopes from the higher-DO-concentration shallower aquifer compartment into the lower-DO-concentration deeper aquifer compartment would suddenly result in a progressive increase in NO_3^- concentrations and dual-NO_3^- isotope signatures. In the following section, I further explore the use of NO_3^- dual isotope analysis for estimating the extent of N isotopic fractionation and the possible reasons for the observed NO_3^- concentrations and dual-NO_3^- isotope signatures in the shallower and deeper aquifer compartments.

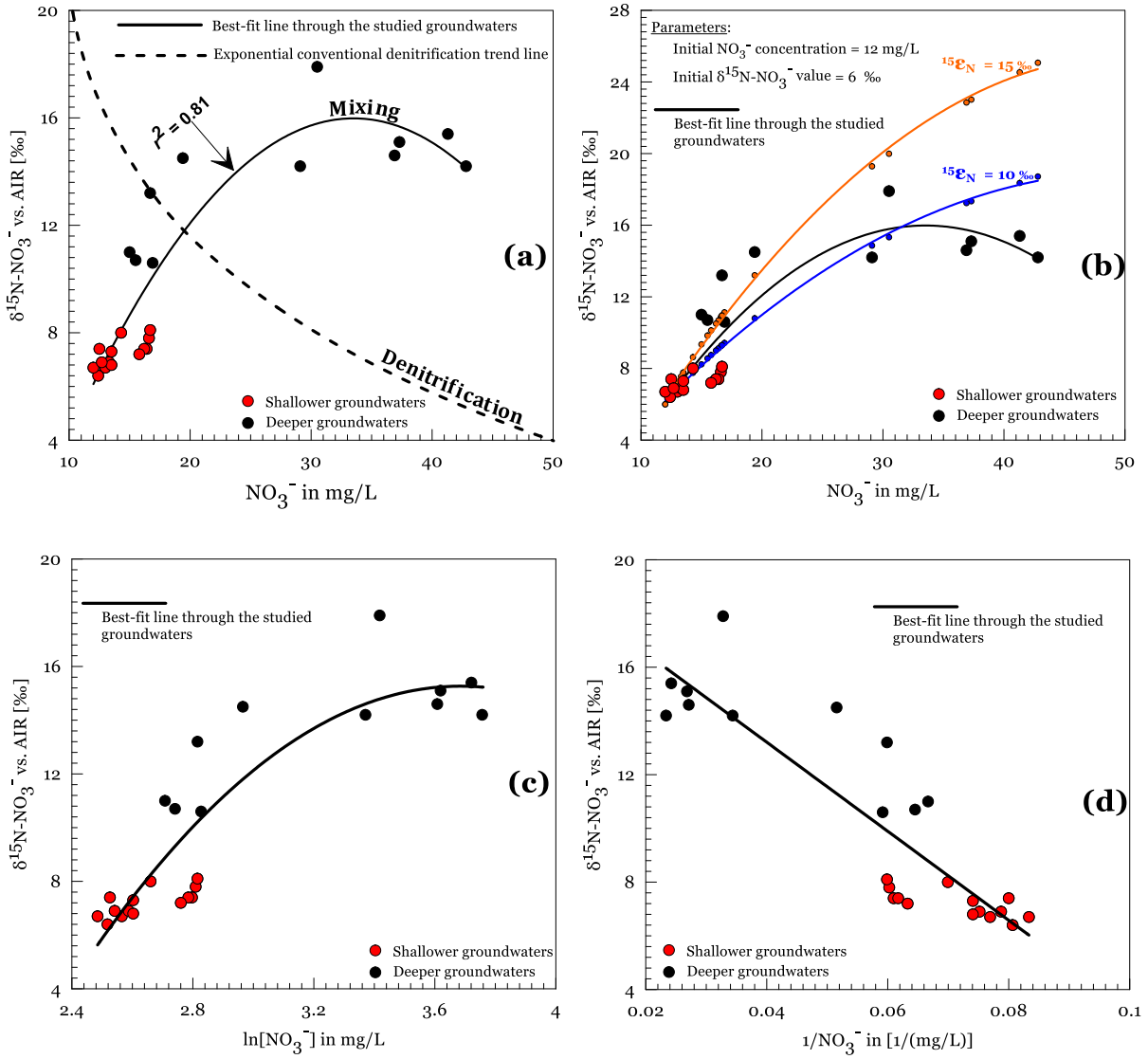

Figure 4.20. (a) Curves on a plot δ^{15}N-NO_3^- against NO_3^- exhibiting best-fit polynomial regression trend (r^2 = 0.81) of increasing δ^{15}N-NO_3^- with increasing NO_3^- concentrations, suggesting a scenario of admixture of two NO_3^- sources (Mayer et al., 2002) and a typical conventional denitrification trend of increasing δ^{15}N-NO_3^- with decreasing NO_3^- concentrations in a system with a single source of NO_3^-. (b) Curves on a plot of δ^{15}N-NO_3^- against NO_3^- showing curvilinear relationships for the data understudy and Rayleigh-based model of denitrification with two enrichment factors indicating denitrification (exponential) can be confused with mixing (hyperbolic), if the distinction between the two processes was to be based simply on the face value of curves. (c) Plot of δ^{15}N-NO_3^- against ln NO_3^-, where mixing yields a curve and different denitrification enrichment factors yield straight lines. (d) Plot of δ^{15}N-NO_3^- against 1/NO_3^-, where mixing yields a straight line and different denitrification enrichment factors yield curves.

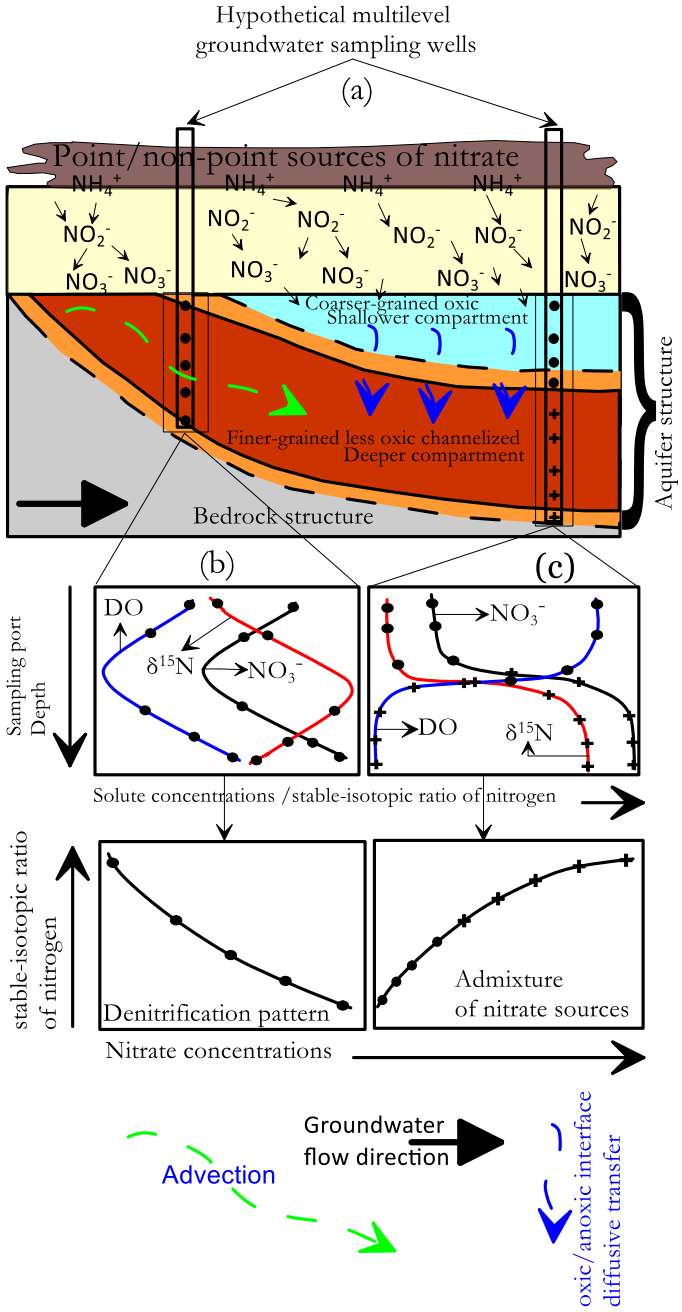

Figure 4.21. (a) Conceptual model of the subsurface showing how the aquifer geometry/heterogeneity and conditions influences nitrogen cycling pathway on physical (hydrological) transport. (b) The Shark Fin pattern of the NO_3^- concentrations and $\delta^{15}N$ of the residual NO_3^- composition shows typical gradients within an anoxic environment wherein conventional denitrification occurs without the dominance of diffusion-limited transfer of NO_3^- across such interface explain in (c). (c) Increase of NO_3^- concentrations and $\delta^{15}N$ of the residual NO_3^- composition with depth (and occurrence of steep biogeochemical gradient), indicating masking of the denitrification signal due to diffusion-controlled transport/admixture of NO_3^- sources from the oxic shallower compartment across a transition interface into the less oxic deeper compartment. It is noteworthy to acknowledge that the strengths of the developed gradient in the anoxic zone would also be dependent on the advective flow velocity.

In the conceptual model showing aquifer interfaces (Figure 4.21a), it is explained that the evidence for conventional denitrification indicating a decrease in NO_3^- with an increase in $\delta^{15}N$ of residual NO_3^- would have been supported if the system is not diffusion-limiting (Figure 4.21b). In

this study however, it is interpreted that the two distinct aquifer compartments: coarser-grained shallower and finer-grained deeper compartments created the distinct geohydrology that resulted in the observed steep geochemical gradients (Figure 4.16c) and possibly drove diffusion-controlled transport and admixture of solutes from the aerobic shallower to the anaerobic deeper compartment leading to the interpreted higher $\delta^{15}N$ of residual NO_3^- signatures accompanied by higher NO_3^- concentrations in the lower DO zone (Figure 4.21a). This is because denitrification occurs within the same phase wherein NO_3^- is present (Figure 4.21b) unlike in the diffusion-controlled transport/mixing scenario between two compartments of the aquifer system separated by a transition interface (Figure 4.21c).

The question however is how diffusion limitation on simultaneous admixture effect would result in the occurrence of higher NO_3^- in the anaerobic deeper compartments of the aquifer and lower NO_3^- in the aerobic shallower compartments of the aquifer. To provide complementary and more convincing evidence for the occurrence of N biogeochemical processes, I estimated the fractionation ratios of O to N in NO_3^- ($^{18}\varepsilon_O : {}^{15}\varepsilon_N$) (see Eqn (4.3) – (4.12) and Figure 4.22) (dual nitrate isotopic approach).

Figure 4.22 indicates enrichment factors of 3.02 ‰ and -1.09 ‰ for the N and O isotopes, respectively in the shallower compartment whereas enrichment factors of 3.90 ‰ and 4.64 ‰ for N and O isotopes, respectively were obtained for groundwater samples from the deeper compartment. These calculated enrichment factors are not within the range for N and O isotopes reported for conventional/riparian denitrification, when it implies reduction of NO_3^- during convective transfer through reducing environments: $^{15}\varepsilon_N$ = -40 to -5 ‰ (Kendall, 1998; Sebilo et al., 2003) and $^{18}\varepsilon_O$ =-18.3 to -8.0 ‰ (Böttcher et al., 1990; Fukada et al., 2003). This study's enrichment factors re-affirm that NO_3^- diffusion through the aerobic shallower-anaerobic deeper transition interface limited the rate of complex biogeochemical processes (e.g., Semaoune et al., 2012). The established concentration gradient is interpreted to cause molecular diffusion of NO_3^- from the coarser-grained shallower aquifer compartment towards finer-grained deeper aquifer compartment which act as a NO_3^- sink. According to Mariotti et al. (1988), this molecular diffusion process can explain why the recorded enrichment factors is lower than the magnitude of isotopic effect/apparent isotopic fractionation associated with conventional denitrification. Mariotti et al. (1988) further noted the possibility that both diffusion and denitrification acting simultaneously could lower isotope effect associated denitrification and diffusion of NO_3^- toward the sink also left with small (null) isotope effect.

For the shallower aquifer groundwater samples (Figure 4.22 (a and b)), the O:N ratio for isotopic discrimination ($^{18}\varepsilon_O : {}^{15}\varepsilon_N$) of 0.36 estimated indicates the potentials of NO_3^- consumption by denitrification and coupling of N and O isotopic fractionation. This estimated $^{18}\varepsilon_O : {}^{15}\varepsilon_N$ value is within the $^{18}\varepsilon_O : {}^{15}\varepsilon_N$ range of 0.33 obtained during laboratory experiments (Knöller et al., 2011) to 0.47 (Böttcher et al., 1990; Wexler et al., 2014) and 0.72 (Fukada et al., 2003; Wexler et al., 2014) in field studies for denitrification processes in terrestrial environments. Given that anammox has similar kinetic stable isotope fractionation pattern as denitrification, Granger and Wankel (2016) have also suggested that anammox may emerge as a compelling candidate to explain the $^{18}\varepsilon_O : {}^{15}\varepsilon_N$ trend (< 1) in freshwater systems. This is also due to the potential co-occurrence of anammox with denitrification of NO_3^- produced by nitrite oxidizing bacteria. In this present study however, whether anammox bacteria exist and has a role in N cycling is unknown and remains speculative. Overall, for higher DO/lower NO_3^- to have existed in the

shallower compartment, it means that there is a favorable anaerobic microsite of an otherwise aerobic media for the microbial degradation of the leached NO_3^-. Also, the recorded depleted $\delta^{15}N$ and $\delta^{18}O$ of the residual NO_3^- signatures suggest this extent of isotopic fractionation and the possibility that NO_3^- removal may not have proceeded to completion.

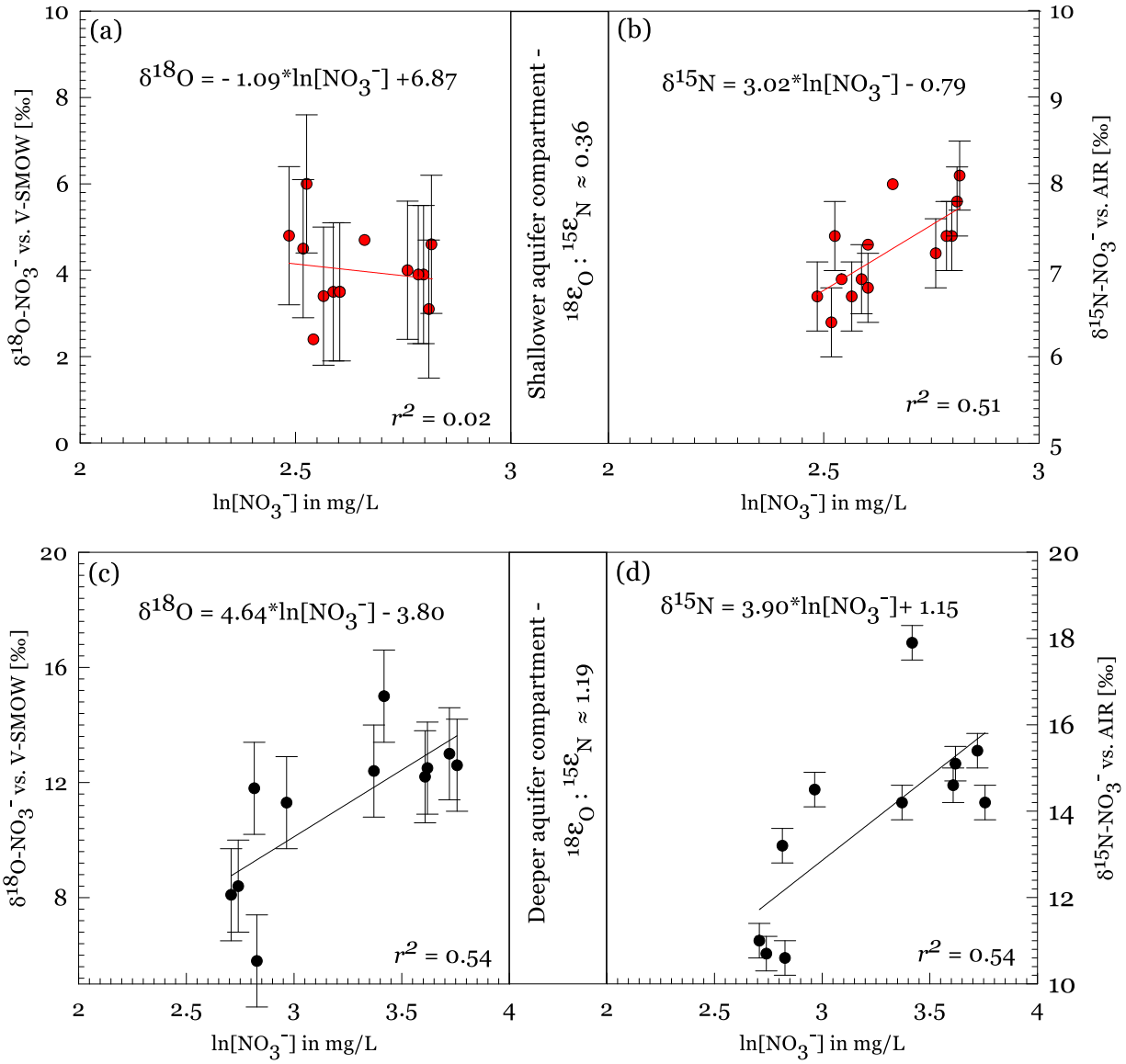

Figure 4.22. (a) and (b) Cross-plots of $\delta^{15}N\text{-}NO_3^-$ and $\delta^{18}O\text{-}NO_3^-$ values, respectively, versus the natural log of the NO_3^- concentrations (in mg/L) for the shallower groundwater samples, resulting in a $^{18}\varepsilon_O : {}^{15}\varepsilon_N$ ratio of 0.36. (c) and (d) Cross-plots of the $\delta^{15}N\text{-}NO_3^-$ and $\delta^{18}O\text{-}NO_3^-$ values, respectively, versus the natural log of the NO_3^- concentrations (in mg/L) for the deeper groundwater samples, resulting in a $^{18}\varepsilon_O : {}^{15}\varepsilon_N$ ratio of 1.19. The term ε, which approximates the slopes in the various plots, represents the enrichment factors (positive or negative) for N and O in NO_3^-. The spread of the analytical precision (vertical error bars) is noticeably larger for $\delta^{18}O$ (1.6 ‰) than for $\delta^{15}N$ (0.4 ‰), especially in shallower aquifer groundwater. The analytical uncertainties were predefined; duplicate measurements were repeated when their standard deviation exceeded the quality control precision, so the error bars' greater variability for $\delta^{18}O$ than for $\delta^{15}N$ could have arisen from the complexity of the biological and abiotic processes in the aquifer compartments and their potential effect on recorded isotope signatures in the two aquifer compartments.

For the deeper aquifer groundwaters (Figure 4.22 (c and d)), the $^{18}\varepsilon_O : {}^{15}\varepsilon_N$ of 1.19 was obtained. A theoretical constant $^{18}\varepsilon_O : {}^{15}\varepsilon_N$ of 0.5 (Lehmann et al., 2003) and 1 (Casciotti et al., 2002; Granger et al., 2008) indicating coupling of O and N in residual NO_3^- are well-validated in the literature as a diagnostic tool to identify denitrification processes in groundwater and marine systems, respectively. A high fractionation ratio of not just close to 1 but more than 1, has been suggested as a yardstick for measuring the likelihood of emergence of N biogeochemical processes in marine and freshwater systems. Granger and Wankel (2016) suggest that $^{18}\varepsilon_O : {}^{15}\varepsilon_N$ trends above the nominal value of 1 have an intrinsically greater likelihood of emerging in marine systems, whereas $^{18}\varepsilon_O : {}^{15}\varepsilon_N$ trends below 1 are more likely for freshwater systems. The authors were however unable to reconcile the divergent interpretations of NO_3^- isotope systematics between marine and freshwater ecosystems and suggested the need to bridge the gap in both systems. In other words, together with gypsiferous carbonate environment geochemistry, the investigated Wurmlingen field site aquifer with $^{18}\varepsilon_O : {}^{15}\varepsilon_N$ ratio of 0.36 and 1.19 in the shallower and deeper compartments, respectively might provide a useful atural laboratory for refining N cycling understanding in groundwater and other ecosystems. Contrary to freshwater environments (in particular, aquifer systems), marine systems are relatively well characterized with respect to the dual-NO_3^- isotope systematics. For instance, deviation in the $^{18}\varepsilon_O : {}^{15}\varepsilon_N$ trends above 1 in marine ecosystem have been associated with partial association of NO_3^-, remineralization or un-modeled biogeochemical processes. Although $^{18}\varepsilon_O : {}^{15}\varepsilon_N$ varies between less 0.5 and 1 (and commonly between 0.96 and 1.09) as reported for laboratory experiments with pure denitrifying cultures (Karsh et al., 2012; Wunderlich et al., 2013), the reason for a $^{18}\varepsilon_O : {}^{15}\varepsilon_N$ trend that reaches or exceeds 1 between cultures and aquifer (field) conditions remains poorly understood and has been referred to as the freshwater conundrum (Granger et al., 2008; Dähnke and Thamdrup, 2013; Granger and Wankel, 2016). Discussed further below, I tie findings of different studies to the probable reason why the $^{18}\varepsilon_O : {}^{15}\varepsilon_N$ of 1.19 observed in the deeper compartment of the investigated aquifer system would have deviated from the widely described $^{18}\varepsilon_O : {}^{15}\varepsilon_N$ of 0.5 for denitrification in terrestrial field studies.

Granger et al. (2004) and Wankel et al. (2007) hypothesized that if NO_3^- is being regenerated within the mixed layer, then there should be a manifestation of a deviation from the expected $^{18}\varepsilon_O : {}^{15}\varepsilon_N$ of 1 for NO_3^- reduction in marine environments. On inferring riverine N processing, Cohen et al. (2012) suggest that $^{18}\varepsilon_O : {}^{15}\varepsilon_N$ of more than 1 or indistinguishable from 1 that do not conform to the predicted 1:2 relationship should be plausibly explained as an evidence of decoupling between $\delta^{18}O$ and $\delta^{15}N$ of the residual NO_3^-. Gaye et al. (2013) explained that remineralization and nitrification of nitrite in low-oxygen zones can lead to the decoupling of $\delta^{18}O$ and $\delta^{15}N$ of the residual NO_3^- resulting in $^{18}\varepsilon_O : {}^{15}\varepsilon_N$ trend exceeding 1. Rohde et al. (2015) also demonstrated that a decoupling of the $\delta^{18}O$ and $\delta^{15}N$ of the residual NO_3^- relationship is expected if nitrification occur concomitantly with NO_3^- reduction. Frey et al. (2014) observed that a slope factor higher than that of denitrification (~0.5 – for freshwater or 1 – for marine) might reflect the impact of simultaneous nitrification and denitrification of NO_3^-. At best, the lack of such decoupling should indicate the absence of significant nitrification. These previous observations mirror the results of this present study. Model exercise by Granger and Wankel (2016) demonstrates that anoxic NO_3^- production by anammox also cannot, by itself, explain the $^{18}\varepsilon_O : {}^{15}\varepsilon_N$ trajectories exceeding 1, not only in marine systems but also in freshwater systems,

where this tenet has been largely overlooked. The reason given is that nitrite reoxidation to the NO_3^- pool would far exceed stoichiometric and biochemical limitations of anammox even if anammox is assumed to account for 100% of N_2 production. Based on these reviews, we believe the groundwater samples collected from the deeper aquifer compartment have undergone an anoxic nitrification process. Considering also that a negative correlation between groundwater NH_4^+ and NO_3^- under anoxic conditions has been linked to the occurrence of DNRA (Jahangir et al., 2012), the low measured NH_4^+ concentrations may suggest that N as NH_4^+ was not conserved. Nevertheless, apart from N losses through ammonia volatilization from agricultural land such as the one at the Wurmlingen study site and possible oxidation of most of the NH_4^+ to NO_3^- (which eventually leached into the aquifer) at the soil-plant zone and the expectation of increased efficiency in the removal of NH_4^+ given the competition for the exchange sites from divalent cations such as Ca^{2+} and/or Mg^{2+} in the gypsiferous carbonate environmental geochemistry of the study site, it might also be possible that any conserved N was oxidized back to NO_3^-; thus, further studies on the occurrence DNRA bacteria are warranted. Additionally, for now, I will stick with the term 'anoxic nitrification' until proven otherwise.

4.4.8 Hypothesis and explanation of aerobic denitrification

Contrary to conventional observations that denitrification requires completely anoxic conditions because the presence of oxygen as an energetically favorable terminal electron acceptor inhibits the activities of NO_3^--reducing enzymes, findings from a number of studies now show that denitrification can also occur in anaerobic microsites within aerated sediments (frequently termed "aerobic denitrification") (Robertson and Kuenen, 1984). The explanation for this hypothesis is that even though the microenvironment of the denitrifiers is depleted of oxygen, resulting in NO_3^- utilization by the cells, considerable amounts of oxygen in the medium remain measurable. It is now also clear that there are widespread microorganisms that vary in their sensitivities to oxygen (Lloyd, 1993). Some denitrifiers contain a specific periplasmatic nitrate reductase that is seemingly tolerant to high oxygen concentrations (see Rivett et al., 2008 and references within) – these organisms are true 'aerobic denitrifiers'. Granger et al. (2008) also determined the N- and O-isotope fractionation of NO_3^- reduction by an organism that contained a periplasmatic nitrate reductase (*R. sphaeroides*). As noted by Bernat and Wojnowska-Baryla (2007), most aerobic denitrifiers are heterotrophic organisms and are widespread in the environment. This also means that carbon supply is a major parameter limiting NO_3^- removal. However, even though a greater number of the groundwater samples contained relatively high dissolved organic carbon (DOC) (range: <1 – 12.43 mg/L, Table A6), the statistically insignificant random relationships between the DOC content and DO concentrations (see section 4.4.9, Figure 4.23), implies that much of the measured DOC in the aquifer is less bioavailable and likely to be the remnant of substantial microbial cycling (Chapelle et al., 2012) or the capacity of silicate minerals (if applicable) present in aquifer materials to adsorb absorb DOC, removing it from the dissolved phase (Jardine et al., 2006). Bernat and Wojnowska-Baryla (2007) demonstrated that intracellular accumulated bacterial storage compounds expressed as poly (-β-hydroxybutyrate) PHB can be used as electron donors, such that aerobic denitrification may still proceed where fluctuating oxygen concentrations and reduced carbon (or 'no external carbon source') occur (Ji et al., 2015). Brigham et al. (2012) mostly noted that periplasmic nitrate reductase is among a group of genes induced during PHB production that remained induced during

PHB utilization. However, more insights into the kinetics and stoichiometry of such bacterial storage compound production and consumption is required. Thus, I suggest that the observed evidence of denitrification in the presence of oxygen within the shallower aquifer compartment may result from the adaptation of the denitrifiers to periodic hydrologically induced redox alternations. Using the relative changes in $\delta^{15}N$, NO_3^- concentration, and water chemistry, Koba et al. (1997), as cited in Kendall (1998), conclude that intermittent denitrification can occur in anaerobic microsites in otherwise aerobic soils as the water table fluctuates in response to storm events and as pores become temporarily waterlogged. Under such a condition, residence times could also prove a useful indicator of denitrification extent. For instance, long residence times could indicate that denitrifiers had enough time to perform their catalytic activities.

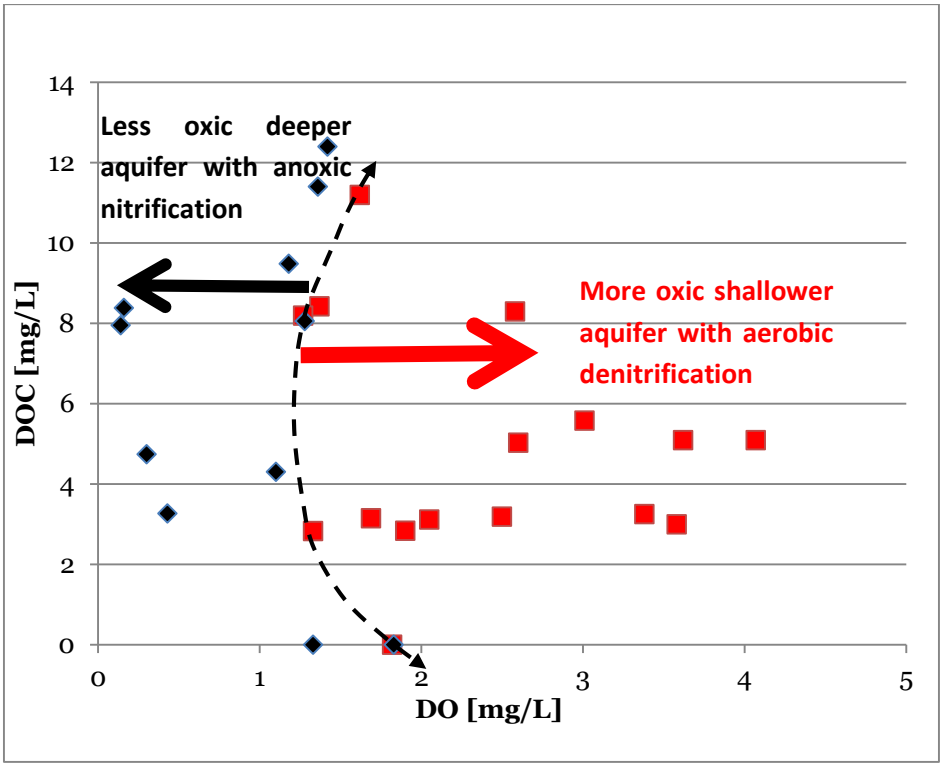

Figure 4.23. A plot of DO versus DOC concentrations. Red and black notations indicate shallower and deeper groundwater samples, respectively.

Overall, together with the steep gradient in the groundwater chemical and N stable isotope stratification of the aquifer, it is difficult to distinguish the influence of the microsites on the distribution of the groundwater chemistry and N stable isotopes without accounting for the diffusion-controlled mechanism. For instance, the observed higher concentrations of DO in the shallower compartment indicate that an oxygen supply (via diffusion) that was slower than its consumption (via microbial aerobic respiration) may have given rise to the relatively oxygen-depleted deeper aquifer compartment. Conventional microbial denitrification of NO_3^- to N_2 (and also in the case of anammox) carries a high ^{15}N-enrichment of > 10 ‰ (Godfrey and Glass, 2011) and large N isotope effects. My N isotope fractionation data, which appear to show much lower enrichment factors than that commonly predicted from conventional microbial denitrification, was quite important in the evaluation of the aerobic denitrification hypothesis. Therefore, we explain that the lower ^{15}N-enrichment of 6.7 - 8.1 ‰ and the small isotopic fractionation attributed to

aerobic denitrification is due to oxidative processes involving both oxygen and NO_3^- (Brandes and Devol, 1997) in the shallower aquifer compartment.

4.4.9 Bioavailability of dissolved organic carbon as a function of dissolved oxygen

Dissolved organic carbon (DOC) can be used as carbon substrate for microbial metabolism and for assessing the quality of chemical affinity in groundwater (Chapelle et al., 2012). In heterotrophic denitrification, for instance, the most important factor limiting NO_3^- removal is the carbon supply (Rivett et al., 2008; Jahangir et al., 2012). DOC can be delivered to the groundwater environment from a wide range of different sources such as surface soils presumably derived from decaying plants (Lundquist et al., 1999), remnants of microbial cell material (Birdwell and Engle, 2009) and mobilization/sequestration from aquifer sedimentary organic carbon (Chapelle et al., 2012). Due to the complex mixture of organic materials from different sources and the role played by available micronutrients (Repert et al., 2006), changes in carbon bioavailability and chemical properties are not clear, however are necessary to provide greater insights into denitrification activity. DO, on the other hand, tend to be uniformly labile to microbes. Consequently, in Chapelle et al. (2012), it was demonstrated that DO versus DOC relationships may indicate bioavailability or non-bioavailability of the DOC. Whereas a statistically significant hyperbolic relationship with increasing DO as DOC decreases may suggest greater extent of reaction and high bioavailability of the DOC, a random scatter may imply relatively small reaction force and less bioavailable DOC. In this study (Figure 4.23), I show that the DO-DOC relationship for the groundwater samples from the shallower and deeper aquifer compartment is random and statistically insignificant, indicating the measured DOC was probably less bioavailable.

4.4.10 Explanation of anoxic NO_3^- production based on NO_2^- data

Incubation experiments with anoxic denitrifying aquatic sediments by Wunderlich et al. (2013) and lake research studies by Wenk et al. (2014) were performed in an attempt to provide a mechanistic explanation for the anoxic production of NO_3^- and the freshwater conundrum phenomenon. Wunderlich et al. (2013) demonstrated that NO_2^--oxidizing microorganisms catalyzed the incorporation of oxygen atoms from ambient water into NO_3^- under anoxic conditions. The authors suggested that this process may distort the observed increase in the $\delta^{18}O$-NO_3^- values and likely explains the deviation of the observed $^{18}\varepsilon_O : {}^{15}\varepsilon_N$ values associated with denitrification in terrestrial field studies from the values commonly observed in laboratory experiments using pure cultures. The inferred oxic denitrification in the shallower aquifer compartment is suggested to lead to an accumulation of NO_2^- I suggest that the possible reoxidation of accumulated, diffusively transported nitrite occurs in the anoxic deeper aquifer compartment. This hypothesis was corroborated by the general consistency of the NO_2^- maxima (Figure 4.24) over which NO_3^- concentrations (Figure 4.16c) (which also positively correlate $\delta^{15}N$-NO_3^- signatures) showed corresponding increases and DO concentrations (Figure 4.16c) showed marked declines. Because NO_2^- is unstable, its concentrations are usually much lower than NO_3^-

concentrations. The presented data suggest that NO_2^- functioned as an intermediate product of the oxidation pathways in the deeper aquifer compartment. Nevertheless, the oxidation of NO_2^- to NO_3^- tended to decrease and increase the $\delta^{15}N$ values of residual NO_3^- and NO_2^-, respectively. Additionally, according to Buchwald et al. (2012), the incorporation of oxygen atoms from water during NO_2^--water exchange is expected to further lower the $\delta^{18}O$ value of the final NO_3^-. Since the oxidation of NO_2^- is a reversible process, the NO_2^- oxidoreductase can be expected to reduce NO_3^- to NO_2^- in the absence of oxygen (Sundermeyer-Klinger et al., 1984; Bock and Wagner, 2013). Consequently, denitrifiers in the deeper compartment are likely simultaneously taking up regenerated NO_3^-, resulting in the observed increases in $\delta^{15}N\text{-}NO_3^-$ and $\delta^{18}O\text{-}NO_3^-$ values. Thus, the relatively lower DO concentrations, higher NO_3^- concentrations and higher $\delta^{15}N\text{-}NO_3^-$ and $\delta^{18}O\text{-}NO_3^-$ values do not exclude the co-occurrence of nitrification and denitrification in the deeper aquifer compartment. In line with the conclusions by Semaoune et al. (2012) that the isotopic fractionation affecting the isotopic signature of NO_3^- is not affected by diffusive transport through soils and sediments or that diffusion-limited microbial denitrification below the well-mixed aerobic water-anaerobic sediment does not discriminate isotopically (Mayer et al., 2002; Sebilo et al., 2003), we report in this field-scale study that the role of diffusion is clear, from the potential transport of NO_2^- from the oxic shallower aquifer compartment to the microbes that biologically turn it over (by reoxidation) in the anoxic deeper aquifer compartment, without which the positive correlation between $\delta^{15}N\text{-}NO_3^-$ and NO_3^-, low enrichment factors (i.e., minimal N and O fractionation), and positive deviations in the $^{18}\varepsilon_O : {}^{15}\varepsilon_N$ trends above 1 would be inconceivable. Mayer et al. (2002) further highlighted that such relations are expected of in-stream denitrification, which is not a single source closed system process wherein partially denitrified NO_3^- enter rivers from soils, aquifers, riparian and hyporheic zones. This is true also for the conceptual model of Wurmlingen the study site, wherein the deeper aquifer compartment function as a former stream channel receives partially denitrified N from the shallower and surrounding aquifer compartments. To the best of my knowledge, this is the first study to demonstrate the occurrence of anoxic nitrification in the groundwater system. Accordingly, the Wurmlingen study site may represent an interesting natural laboratory for probing and clarifying the understanding of discrepancies in N isotope biogeochemistry between freshwater and marine environments. Overall, under the investigated field (aquifer) conditions, the activities of physical transport and biogeochemical drivers in explaining the observed solute concentration and stable isotope distribution trends may not be mutually exclusive.

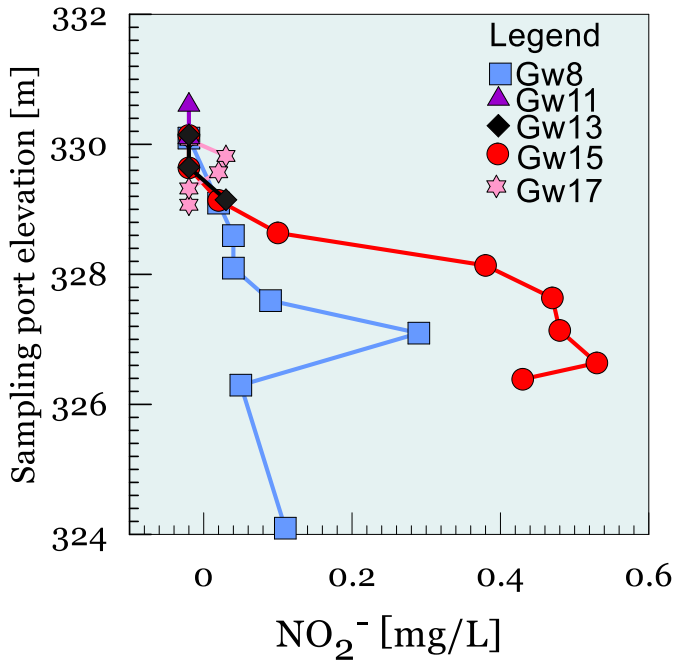

Figure 4.24. Vertical profile of NO_2^- concentrations.

4.4.11 Alternative explanations

Based upon knowledge of the fractional isotopic contributions, $\delta^{18}O$ of NO_3^- during complete nitrification is widely accepted to be derived from one-third of atmospheric oxygen (Kroopnick and Craig, 1972) and two-third of water oxygen (measured). As a result, it is expected that $\delta^{18}O$ of water and $\delta^{18}O$ of NO_3^- should portray a positive correlations. The relationship between $\delta^{18}O$ of NO_3^- and $\delta^{18}O$ of water was however generally weakly correlated (Figure 4.24a), which might suggest that there is a weak link to water as the potential source of oxygen in the NO_3^- : - negative relations in the shallower and positive relations in the deeper compartments of the aquifer however, express and re-affirm distinct occurrence of processes. Snider et al. (2010) concluded that the varying amount of abiotic exchange between nitrite and water is the reason why the $\delta^{18}O$ of microbial NO_3^- cannot be successfully predicted. Furthermore, going by the results of earlier experiments, ammonia oxidizing microbial communities (Hollocher et al., 1981; Andersson and Hooper, 1983) and nitrite-oxidizing microbial communities (DiSpirito and Hooper, 1986) can grow separately while utilizing the first and second oxygen contributed by water under conditions wherein NO_3^- is produced. Most recently, however, complete ammonia oxidizers (comammox) have been discovered in nitrite-oxidizing bacteria genus *Nitrospira* to singly convert ammonia to NO_3^-. (Daims, et al., 2015; van Kessel et al., 2015; Kits et al., 2017; Wang et al., 2017). Altogether, it is suggested here that the extent to which variations in $\delta^{18}O$ of atmospheric oxygen and $\delta^{18}O$ of water would affect the $\delta^{18}O$ of NO_3^- can be deciphered appropriately through the understanding of microbial community levels and should not be easily observable per se from the mere relation between $\delta^{18}O$ of NO_3^- and $\delta^{18}O$ of water.

Alternatively, the kinetics of oxygen incorporation suggests that HCO_3^- would have played an inevitable role in water splitting reactions and as a chemical intermediate in oxygen evolution (for a historical survey, readers are referred to Stemler (2002) and reference therein for details on

this assertion). This concept originated from Metzner (1979) who reasoned that if oxygen developed directly from water, $\delta^{18}O$ of the evolved oxygen could under no circumstances, be minutely greater than that of water in the medium. As a step to producing either oxygen or hydrogen peroxide, a single electron is extracted from water. However, a single electron could easily be extracted from HCO_3^- to produce carbonic acid peroxide intermediate than from water molecules wherein a far more energy than is contained in a low energy photon (such as red light) would be required. A good correlation between HCO_3^- and $\delta^{18}O$ of the residual NO_3^- (Figure 4.24b) confirm the role that the HCO_3^- would have played in coupling oxic denitrification to anoxic nitrification from the shallower to the deeper compartments of the aquifer system. The partitioning role of HCO_3^- (HCO_3^- effect) in isotopic equilibrium with water is expected when $\delta^{18}O$ of HCO_3^- (not measured in this study, however, measurement is highly recommended) is slightly higher than that of water. A good positive correlation between $\delta^{18}O$ of HCO_3^- and $\delta^{18}O$ of the residual NO_3^- should be able to validate the described role of HCO_3^-. Although this partitioning effect is well demonstrated in photosynthetic evolution of oxygen, so far, little to no attention has been paid to this area under N isotope biogeochemistry.

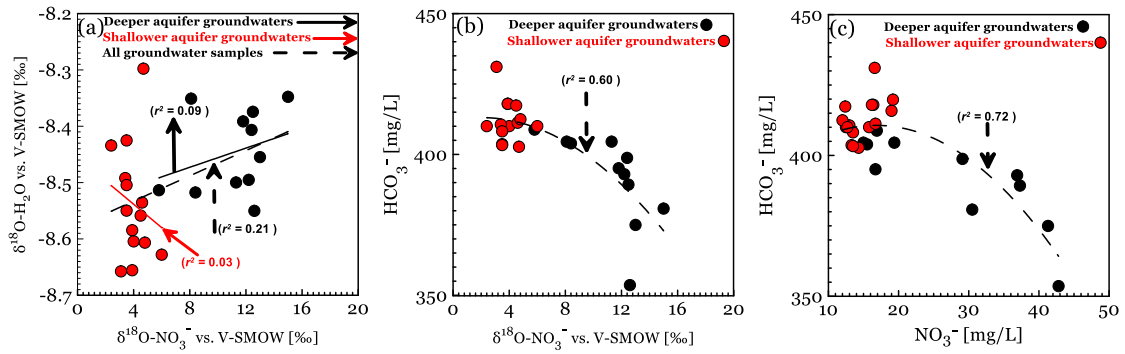

Figure 4.25. Relation between: (a) δ^2H-H_2O and $\delta^{18}O$-NO_3^- , (b) HCO_3^- and $\delta^{18}O$-NO_3^-, and HCO_3^- and NO_3^-.

Contrary to the explanation by Wunderlich et al. (2013) that incorporation of the oxygen-atoms stemming from ambient water into NO_3^- can occur even in the absence of external electron acceptors; it is observed in this study that HCO_3^- would have provided the necessary structural and reproduction source for chemolithotrophic nitrifying bacteria. As an indicator of microbial metabolic pathways, how HCO_3^- relates to nitrification and denitrification is well-established. Whereas nitrification consumes HCO_3^- alkalinity due to the production of hydrogen ions (that is, acidity) and uptake by nitrifiers (Belser, 1984), denitrification produces HCO_3^- alkalinity. The production rate and magnitude, however, depend on the electron donor. Based on a model developed by Gujer and Jenkins (1975), about 8.64 mg/L of HCO_3^- will be utilized for each mg/L of ammonia-nitrogen (NH_3-N) oxidized. In juxtaposition to nitrification, denitrification has been shown to produce alkalinity to the theoretical ratio of 3.57 g $CaCO_3$ per g of nitrate-nitrogen (NO_3-N) reduced to N_2 (van Rijn et al., 2006). The observed decrease in HCO_3^- concentrations with increase in NO_3^- from the shallower to the deeper compartments of the aquifer (Figure 4.24c) support these previous studies and this study's conclusion that denitrification predominates in the shallower compartment while nitrification predominates in the deeper compartment. Moreover, for such an aquifer system with closely located compartments, it is possible that HCO_3^- alkalinity production during denitrification in the shallower compartment can be partly compensated by the consumption of the HCO_3^- alkalinity during nitrification in the deeper compartment resulting in

the observed relatively stable pH (Shao et al., 2016). The combined results of this study also agree with those of Marchant et al. (2016) that nitrification would have fueled denitrification by providing an additional source of NO_3^- and vice-versa and as such masks true N turnover in the aquifer system.

4.5 Summary and conclusions

Based on the combined evaluation of hydrogeochemical and multi-isotopic approach with an understanding of the subsurface flow system in an effort to enhance conceptual understanding of the hydrogeochemical evolution and processes that control groundwater recharge, SO_4^{2-} and NO_3^- within the aquifer, the following summarizes results from this study:

1 Natural groundwater chemistry controlled by the gypsiferous carbonate rock environment interact with and responds to the anthropogenic N loading in the alluvial aquifer;
2 Water isotopic composition (δ^2H, $\delta^{18}O$) measured from the collected groundwater indicate that the NO_3^- was transported from an anthropogenic source on the land surface through infiltrating rainwater with secondary effect of evaporation;
3 Uniform distribution of the SO_4^{2-} concentrations and the clustered isotopic composition of SO_4^{2-} ($\delta^{34}S$, $\delta^{18}O$) confirm that the groundwater SO_4^{2-} is mainly derived from a gypsum source;
4 Observations based on $\delta^{18}O$-NO_3^- and $\delta^{15}N$-NO_3^- suggest that the shallower aquifer is dominated by groundwater NO_3^- of soil organic N while the deeper aquifer groundwater NO_3^- is reflective of animal manure/septic waste sources . Analysis of the two sources of NO_3^- is an indication that one source (probably animal manure) was biogeochemically transformed and partitioned into the two compartments of the aquifer;
5 Apart from source identification of the groundwater recharge, SO_4^{2-} and NO_3^-, the dual isotopic and the chemical data and ratios highlighted the potential linkage between the NO_3^- variability and N transformation processes. I document that the dominance of diffusion-controlled admixture of NO_3^- to the deeper compartment of the aquifer system and NO_3^- removal in the shallower compartment of the aquifer masked the conventional denitrification signal expected using chemical and isotope data. The existence of a transport limiting channel structure in the deeper compartment created a localized flow system, mixing interface and ultimately the geochemically and isotopically distinct conditions used to explain the occurrence of NO_3^- removal in the anaerobic microsite of otherwise aerobic shallower compartment of the aquifer and anoxic nitrification in the deeper compartment. Nevertheless, the role of microbes is not to be dismissed in the explanation of the alternative nitrogen cycling pathways.

In conclusion, the procedure involving the combined use of dual isotopic and chemical data provided elucidations on the origin of the groundwater solutes and susceptibility of the shallow groundwater flow system to the transformation of the NO_3^-. Some uncertainties however remains that require attention to foster interpretation accuracy. For one, the flow and transport-limited interactions between the oxic low NO_3^- shallower and anoxic high NO_3^- deeper pore water did not conform to the basic assumptions of oxic nitrification and anoxic denitrification due to a complex subsurface hydrologic systems and biogeochemical exchanges. Although the emphasis of diffusion limitation mechanisms on N cycling and isotope fractionation (that is, shallower to deeper exchange

is controlled by diffusion) are major findings of this study, the observed indicators of coupled NO_3^- removal and addition processes which relate closely to ecosystems (e.g., marine) other than terrestrial freshwater systems show the need for further scrutiny in the investigated aquifer systems and the other settings. Accordingly, to fully understand the factors governing the variability (spatiotemporal) in the geochemical and isotope trends and reveal the root cause of the differences between freshwater and laboratory/marine, more multidisciplinary environmental research on the potential role of subsurface hydrologic and biogeochemical drivers should also be explored. The studied Wurmlingen site would provide a characterized natural system for such a project. Overall, the conclusions reached here have implications on the effectiveness of processes that add or remove NO_3^- along flow systems and how to manage nitrogen responsibly, especially those emanating from agricultural activities.

Chapter 5

General discussion, conclusions and outlook

Chapter summary

This chapter summarizes the findings of this dissertation. The main contributions of the dissertation are as follows:

1) The development of an observation-based conceptual site model (CSM) framework for improved and reliable understanding of subsurface structural controls on physical (hydrological) and biogeochemical processes influencing the behavior of N turnover in an alluvial aquifer was largely successful. The approach of the framework includes iteratively combining multidisciplinary field site characterization and laboratory analytical tools consisting of: (a) surface geophysical and direct push-based delineation of subsurface features and (b) the use of depth-specific chemical and multi('dual')-stable isotope analyses to constrain the fate of the groundwater nitrate;
2) Hypotheses on the origin of the groundwater NO_3^- were evaluated. Deeper insight into the connectivity of identified shallower and deeper aquifer compartments proved helpful in understanding how the aquifer's physical and biogeochemical parameterization partitioned NO_3^- sources into the aquifer compartments. Such knowledge is critical to improving the management practices associated with efficient water resource protection.

The summary of findings presented in this chapter is organized as follows: (i) General assessment of the applicability of the developed observation-based CSM framework, (ii) 3-D alluvial architecture – Implications for the study site's geohydrology and N biogeochemistry, (iii) Synthesis of the NO_3^- source hypotheses, (iv) Summary of the conclusions, (v) Scientific significance and impact, and (vi) Outlook.

5.1 Applicability of the developed observation-based CSM framework

I proposed and developed an observation-based CSM framework for the large-scale investigation of groundwater contaminant plumes. The hallmarks of the framework include: formulation of clear and interesting questions regarding the contaminant plume in relation to the plume size and boundary, variability in the contaminant sources and heterogeneities in the physical and biogeochemical pathways and processes; collection of facts regarding the problems based on historical and current reconnaissance surveys; advancement of uncertain but testable hypotheses/possible explanations regarding the questions; and an adaptive experimentation procedure to test the hypotheses.

The large-scale study arises in a successful site characterization using iterative combination of such multidisciplinary tools as surface geophysics, direct push technologies, hydrogeochemistry and stable isotope geochemistry. Such framework and approaches help to provide reliable subsurface CSM information, leading to improved mathematical model predictions for a contaminant plume source-pathway-receptor scenario.

Specific results of a case study and application of the CSM framework are generally discussed in the following sections.

5.2 3-D alluvial architecture – Implications for the study site's geohydrology and N biogeochemistry

Because of the potential development of a groundwater NO_3^- plume in the investigated alluvial aquifer at the Wurmlingen study site, it was essential to define the groundwater flow and solute pathways by means of a 3-D arrangement of the alluvial deposits and the aquifer. This is justified by agricultural activities and the advanced existence of a hypothetical landfill site uphill of the study site as potential sources of the NO_3^- plume observed in the groundwater by the previous study (Schollenberger, 1998). Figure 5.1 shows a simplified subsurface conceptual model of the study site representing the interpretation of crucial subsurface geological structures, aquifer connectivity and key hydrological and biogeochemical interfaces. The model was constructed using surface geophysical data, direct push (DP) investigations, and groundwater chemistry and stable isotope analysis discussed in chapters three and four. The developed conceptual, 3-D alluvial architecture model (Figure 5.1a) identified two forms of unconfined shallow aquifer systems: (1) one that occupies the first half of the study site up Northwest/toward the hillslope environment (up North), and (2) the other occupies the second half on the floodplain area. This distinction is very much visible from the area's subsurface resistivity variations, particularly as shown in Figure 3.8b

The unconsolidated sediments that make up the aquifer system (up North) are interpreted to consist of interbedded clayey and silty sediments deposited on the bedrock. Coarsening upward

sediments comprising the water-yielding parts of the aquifer system with two compartments on the floodplain are also shown to overlie the bedrock. The shallower aquifer compartment on the floodplain consists of homogeneous coarser-grained sediments, whereas the deeper aquifer compartment is dominated by heterogeneous finer-grained sediments (Figure 5.1b). Overlaying the aquifer is an unsaturated sand with a gravel layer covered by alluvial silty clay sediments. The interpretation given here is that the accumulated alluvium sediments would have resulted largely from debris erosion and transport from parent rock materials, such as Schilfsandstein, Bunte Mergel and Stubensandstein Formations as the hillslope up North typifies, as well as the widespread Gipskeuper. I also reveal that the geometry and the 3-D arrangement of the alluvial stratigraphy can give information about the nature of the sediment supply, processes of deposition and hydrologic regimes (that is, the sediment-transport processes) leading to the interpretation of the site history. It is reasonable to expect that the coarser-grained sediments, for instance, in the shallower aquifer compartment, would have been deposited in a high-energy environment because fast-flowing and agitated water (and possibly glacial meltwater) is able to carry large grain sizes. In a low-energy depositional environment, the converse would be the case, particularly for the finer-grained sediments deposited in the deeper compartment within the channel structure. In Figure 5.1a, I also show that the up Northwest/hillslope aquifer system is connected to the deeper aquifer compartment in the floodplain aquifer system by the indicated channel feature. Given the interpretation that the channel feature might represent a buried stream channel, it is also possible that the channel may trace the entrance into the apex of the debris-flow fan (see the geologic map in Figure 3.1). It is also not clear how the channel bedrock may be related to the inferred border zone between the Lettenkeuper and Gipskeuper Formations. Further studies beyond the present study site boundary can be elucidatory to this question. In this study, I demonstrated that the channel structure preferentially controlled the orientation of the groundwater NO_3^- plume previously identified by Schollenberger (1998). There is an existing understanding that the high sulfate concentrations in the aquifer may have resulted from a fractured bedrock in relation to the Gipskeuper origin. Nevertheless, I speculate that the dissolution of gypsum in Keuper potentially deposited during the formation of the alluvial sediment cannot be totally ruled out in providing answers to the origin of the sulfate-saturated aquifer. Over a long-term period, agricultural management practices in conjunction with changing environmental and climatic conditions, as well as the residence time of fertilizer-derived nitrogen in agricultural soils leading to various nitrogen mineralization-immobilization cycles, can result in the uptake of approximately one-third of the nitrogen pool by the crops, with one-third leaching toward the hydrosphere and the remainder likely lost via gaseous emissions (Sebilo et al., 2013). However, there is also a 2-D cross-sectional numerical analysis of an Ammer valley-Wurmlinger Kapelle-Neckar valley water divide hypothesis, which advanced that, because both the Ammer and Neckar floodplains contain Holocene sediments that are relatively high in organic carbon, agricultural NO_3^- is reduced therein and does not reach the groundwater (Kortunov et al., 2016), predicting that NO_3^- in the Neckar valley aquifer may have largely emanated from NO_3^- applied to the hillslopes underlain by fractured oxidized mudrock transported to an unknown extent by groundwater recharge in the Ammer valley. How the water divide hypothesis and the delineated groundwater NO_3^- plume-controlling channel structure are connected remains to be further investigated.

Going by the results of this study, it may be tempting to assert that the deeper parts of the aquifer, dominated by finer-grained sediments, lack the capacity to transmit fluid compared to the nearly homogeneous coarse-grained sediments at the shallower parts immediately below the water

table. Although there are presently no data regarding the permeability of the aquifer, high transmissivity of the heterogeneous finer-grained sediments within the channelized structure can be expected because of the apparently higher saturated thickness. Moreover, considering the geometry of the quantified subsurface structure, Rosenshein (1988) explained that, the more steeply sloping the channel side, the less likely it is that the permeability of that part of the channel will be decreased by fine-grained deposits. Additionally, from the elevation of the bedrock from the floodplain area toward the Wurmlingen settlement in the Northwest, I suggest that the bedrock channel plays a critical role in preferentially guiding deep groundwater flow from the hillslope environment to the wells sited deeper in the floodplain area. The groundwater table elevation measured in some DP wells tends to show that the advective fluid transport through the channelized feature could follow the local hydraulic gradient. The channel may also function as a zone for both convergent and divergent flows depending on how flows encounter the channel and the flow periods. Worthy of note, however, is that the distribution of the groundwater table may not be the best indicator of groundwater flow direction, especially in the case of vertical solute transport. Certainly, the directional orientation of the detected channel structure and internal subsurface architecture (especially the presence of a two-compartment aquifer on the floodplain) hold implications and promise for understanding a complex two-domain macropore/matrix model (e.g., Beven and Germann, 1982; Beven and Germann, 2013). In this context, the macropore indicates the depression within the bedrock that forms a preferential channel controlling flow through the deep groundwater system, whereas the matrix model represents the shallower compartment of the aquifer as demarcated on the floodplain area. Apart from the aquifer recharge via infiltration from the hillslope environment and potentially from the Ammer valley as hypothesized (Kortunov et al., 2016), the entire ground surface in the Neckar valley is available for the recharge of the aquifer in relation to the direct infiltration of rainwater. Here, it is hypothesized that water infiltrating through the channel entrance (from the hillslope environment) or simultaneously into the matrix and macropores within the floodplain area would, at later stages, all converge into the profile along the macropore system.

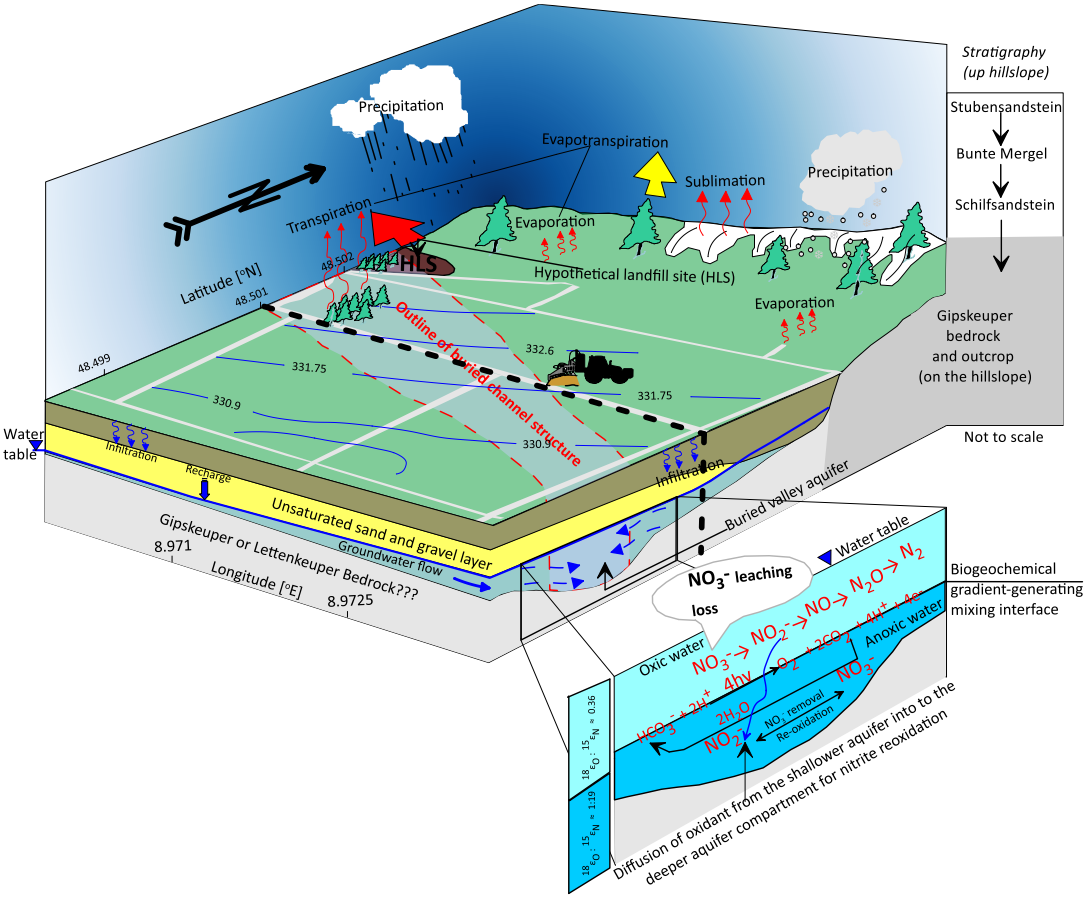

Figure 5.1. (a) Conceptual model of the Wurmlingen study site (Neckar valley) showing subsurface interfaces/connecting features and geohydrologic zones. The red arrow points northwest in the direction of the Wurmlingen settlement whereas the yellow arrow points in the direction of the Ammer valley. Broken black line metaphorically divides the study site's aquifer into two halves (based on the isoresistivity map in Figure 3.8 b): (1) first Northwest/toward the hillslope environment (up North), and (2) floodplain area. The outline of a linearized buried channel structure (the dashed red line) at the base of the aquifer delineated by combined interpretation of surface geophysical and direct push-based results is also shown. The channelized aquifer bedrock configuration is interpreted to follow the hydraulic head distribution (that is, the water table contours in meters, the blue line with elevation numbers) from the northwestern to the southeastern part of the study site. The channel structure also has the capability to function as both flow divergence and convergence zone. This study proposes that the channel feature traces a transmissive preferential flow pathway that is capable of inducing exchange of materials in the aquifer. The channelized aquifer is interpreted to entrain infiltrating fluids/solutes from point and nonpoint sources, and it connects the aquifer system towards the hillslope and northwest part of the area to that in the floodplain area. As shown in (b), however, on the floodplain area, a two-compartment aquifer system (coarser-grained aerobic shallower and finer-grained anaerobic deeper zones) provides an avenue for the interaction of microbial communities and rapid change in solute concentrations and stable-isotope compositions. Biogeochemical hotspots are commonly located in this unique environment. Driven by steep biogeochemical gradients, distinct geohydrologic and redox conditions promote diffusion-limited transport of oxygen/solute from the shallower to the deeper compartment. This study noted that oxic denitrification characterized the shallower aquifer compartment with an oxygen (O):nitrogen (N) fractionation ratio of 0.36. Nitrite inferred to have emanated from a coupled sulfate-reducing, nitrate-reducing, sulfide-oxidizing process is shown to have diffused into and reoxidized in an anoxic deeper compartment, resulting in an O:N fractionation ratio of 1.19. Although water is the conclusive source of O in the production of nitrate, this study hypothesizes the role of bicarbonate as a chemical intermediate for oxygen evolution (see Stemler, 2002).

I also predict that performing hydraulic calculations in the understudied aquifer system would be complex due to the described level of geologic heterogeneities. For instance, it might be possible and easy to perform Darcian-based estimation of hydraulic functions in the more homogeneous coarser-grained shallower matrix flow system. However, incorporating the concept of preferential channeling as illustrated in this study means that an integrated strategy would be required to adequately describe variations in water flux and solute transport in the combined matrix-macropore-system. Also problematic is the doubt that may arise regarding the representativeness of hydraulic conductivity values in the macropore system dominated by heterogeneous finer-grained sediments. Due to the shortcomings associated with hydraulic estimations in fine-grained sediments, common scale-dependent hydraulic conductivity measurements using permeameter tests on small cores or even with double-ring infiltrometers may produce hydraulic conductivity estimates that do not match the exact flow behavior in the macropore system. In situ field tests involving classical aquifer testing (via pumping) and 'slug' tests of a reasonable duration are often recommended for extracting the average hydraulic conductivity used to make flow and transport predictions or build a model. However, these evaluations of the hydraulic conductivity values without recognizing the overall subsurface structural control on the spatial distribution of the hydraulic conductivities could lead to divergent and contradictory interpretations of transport processes acting at different scales (see de Marsily et al., 2005). This is often the reason why the use of transmissivity fields rather than permeability is preferred when describing the hydraulic functions around a macropore structure. Hence, there is no way to skip the necessity of mapping the aquifer structure and heterogeneities as a foundation for understanding contaminant transport and distribution patterns (Payne et al., 2008). In recognition of the fact that the concept of a homogeneous aquifer commonly applied in the water supply would not work for groundwater and solute transport problems, Charles V. Theis wrote in 1967 that: "*I consider it certain that we need a new conceptual model, containing the known heterogeneities of natural aquifers, to explain the phenomenon of transport in groundwater.*" Tracer studies have become very successful in visualizing preferential pathways of infiltrating water through hydraulically transmissive zones and have provided some of the most convincing evidence of connectivity of a matrix-macropore system. However, all of these physical methods provide information most often in small scale, whereas hydrologists are mostly concerned about the hydrological importance of macropores in channeling aquifer water flows and pollutants at not just profile and plot scale but also hillslope and catchment scale. Moreover, attempts to upscale small-scale measurements could lead to the neglect of relevant large-scale local variabilities. This situation reemphasizes the necessity for matching the results of modeling studies with such field-scale observations as demonstrated in this report. In particular, the delineation of large-scale subsurface features can represent an important prerequisite for efficient tracer testing.

The capability to relate changes in the depositional architecture to coupled geohydrology and aquifer N biogeochemical cycling is the hallmark of developing the 3-D alluvial architecture model shown in Figure 5.1. This is because N cycling processes, for instance, are strongly dependent on hydrological fluctuations and aerobic-anaerobic saturation conditions within the floodplain (e.g., Burt and Pinay, 2005; Claxton et al., 2003). Despite studies suggesting enzymatic irreversibility of NO_3^- reduction in pure cultures of denitrifiers (Knöller et al., 2011; Dähnke and Thamdrup, 2016), one of the most interesting questions posed by this study is how the reversibility of reactions against the canonical assumption of anoxic nitrification and oxic denitrification in the aquifer could have maintained higher NO_3^- in the anoxic deeper compartments and lower NO_3^- in

the oxic shallower compartments as observed from depth-specific groundwater chemical and dual-NO_3^- isotope data (Figure 5.1b). A proposed answer was found rooted in the distinct solute transport regimes between the delineated shallower and deeper compartments of the aquifer in the floodplain area, which received leached NO_3^- through infiltrating/recharging rainwater. The major differences in the two compartments would result primarily from the changes in the rates of concentration and adjustments due to competing redox reactions. Given the geometry of the investigated aquifer system, the transport of fluid and solute through the macropore domain from the hillslope environment can occur by convection that influences the advective (average linear) flow velocity in direct proportion to the local solute concentration. Nevertheless, chemical and stable isotope results also show that the steep solute concentration gradients due to the presence of the deeper 'channelized' aquifer drove downward diffusion-controlled admixture and invariably solute fluxes across the transition interface between the high-oxygen, high-energy depositional environment consisting of coarser-grained sediments in the shallower compartment of the aquifer and the low-oxygen, low-energy depositional environments consisting of fine-grained sediments within the channelized/deeper compartment of the aquifer system. Although diffusion can occur in the absence of groundwater flow velocities, any advective push within the channel structure may further determine how great and sharpened the concentration gradients become.

Also aligned with other studies (Haggerty et al., 2004; Zhang et al., 2007; LaBolle et al., 2008) regarding diffusion rate-limited mass transfer between the channelized principal flowpaths and juxtaposed slow-velocity regions, a process that is ubiquitous in groundwater systems and would have induced complex isotopic fractionations, this study also interprets that the higher isotopic enrichments and NO_3^- concentrations in the anoxic deeper compartment of the aquifer were resultant effects of diffusive fractionation of solutes balanced by isotopic depletion and lower NO_3^- concentrations in the anaerobic microsites of the aerobic shallower compartment of the aquifer contrasting isotopic enrichments conventionally associated with traditional biodegradation. Observed higher concentrations of DO in the shallower compartment relative to the deeper compartment indicate that slower oxygen supply into the deeper aquifer (via diffusion) than its consumption (via microbial aerobic respiration) gave rise to the relatively oxygen-depleted deeper aquifer compartment. The lower NO_3^- concentration levels in the more oxic shallower compartment, relative to the higher NO_3^- in the less oxic deeper compartment, means that anaerobic microsites in a supposedly better-aerated shallower media favored NO_3^- removal, and the recorded dual-NO_3^- isotope signature is a consequence of the rate of removal and prevailing hydrologic and biogeochemical conditions. Although it is widely recognized that slower flow processes and invariably longer residence times of water lend support for slow reaction and transformation processes carried out by facultative anaerobes, such as denitrifying bacteria and other strict anaerobes in contrast to faster flow processes with shorter residence time of water, this present study did not definitively evaluate the effect of residence times of water on the N biogeochemical dynamics, which however is an interesting topic for further investigations.

Based on my observations, I also hypothesized that flow through the preferential flow structures that connect the up Northwest/up North hillslope aquifer system to the deeper aquifer compartment on the floodplain area would commonly favor denitrification due to the occurrence of reduction conditions. However, the diffusion-controlled mixing of NO_3^- solute sources would result in the observed masked canonical denitrification in the compartments of the floodplain aquifer, whereby $\delta^{15}N$ of the residual NO_3^- showed a polynomial increase with NO_3^- concentrations rather than increasing $\delta^{15}N$ with decreasing NO_3^-. The estimation of a small N isotope effect in the

shallower and deeper aquifer compartments compared to the large N isotope effect commonly associated with denitrification further buttresses the role played by diffusion transport processes in the investigated aquifer. Moreover, because denitrification occurs continuously in advection-dominated systems in a single phase/homogeneous medium, the recognition that vertical mixing from the shallower to the deeper aquifer compartment has occurred provides an additional hint that advection (although present) would not be a dominant process. In this study, I also highlighted that the diffusion-controlled mixing promoted the occurrence of alternate N-cycling processes, such as oxic denitrification in the shallower aquifer closely coupled to and compensated by anoxic nitrification in the deeper aquifer. Oxic denitrification and anoxic nitrification as observed in the shallower and deeper compartments of the aquifer, respectively, are incomplete processes wherein nitrification fuels denitrification and vice versa. Thus, for the hint of denitrification to have existed in the oxic shallower compartment, it means that there exist certain species of denitrifiers that do not possess a complete pathway. Such denitrifiers would have produced the nitrite that was subsequently transported by diffusion into the deeper aquifer compartment for anoxic reoxidation to NO_3^-. Incomplete nitrification in the anoxic deeper compartment would also mean that the regeneration of NO_3^- was not efficient because of the slow response of nitrite-oxidizing bacteria to periodic aerobic/anoxic operation (Kornaros et al., 2010). Consistency in the increasing trend of nitrite, NO_3^- and $\delta^{15}N$ of the residual NO_3^- from the shallower to deeper aquifer compartment support the interpretation of anoxic nitrification in the deeper aquifer compartment. Plainly, this study posits that the occurrence of oxic denitrification and anoxic nitrification in the shallower and deeper compartments, respectively, may simply be a consequence of oxygen sensitivity of the nitrite-reducing and –oxidizing bacteria. Thus, the nature and roles of microbes should be seriously taken into account to adequately understand the complexity of the nitrogen-cycling pathways. Acting as a chemical intermediate in the oxygen evolution process, I also inferred that HCO_3^- would have played a vital role in the water splitting reaction, providing an alternative explanation to the proposed nitrite-water abiotic exchange reaction that impacted the $\delta^{18}O$ of the residual NO_3^- during the NO_3^- regeneration process.

Insightful information provided by this study on the floodplain area is that there exists a distinct hydrobiogeochemical interface that created a boundary between the aerobic shallower and anaerobic deeper aquifer compartments. The evidence for this is reflected in the observed steep chemical and isotopic gradients. Although interfaces: vadose zone/saturated zones, surface water/groundwater (hyporheic zone), and surface water/underlying sediment are often considered when evaluating dynamic zones of nutrient/oxygen fluxes that can drive biodegradation processes, the detected transition in redox conditions between the aerobic shallower and anaerobic deeper aquifer compartments have been interpreted to represent important biogeochemical hotspot for N processing. Certainly, without a realistic understanding of the implication of the subsurface conditions and their hydrologic system, such coupled N turnover as reported in this study would not have been known. In a nutshell, particularly in the floodplain part of the study site, even though I propose a dual-domain type of mass transfer between the shallower and deeper aquifer compartments, I also propose that the subsurface aquifer model conceptualized in this study (in the floodplain) be treated as an advection-diffusion-reaction system side-by-side with the dual-domain transport behavior and metagenomics of microbes playing useful roles in the inferred alternative N cycling routes.

5.3 Synthesis of the NO_3^- source hypotheses

In dealing with the hypotheses on the proposed two sources of NO_3^- at the study site, I have systematically analyzed the different lines of hints emanating from the employed testing methodologies and multimethod approach. Within the framework of the presented observation-based conceptualization process, key questions that significantly influence the N origin, the form through which they influence the groundwater quality and are introduced into the environment, were addressed. Based on the accumulated hints, the diagnosis of the nitrate source origin hypotheses in relation to their support or rebuttal was synthesized. At the agriculturally impacted Wurmlingen study site, an NO_3^- plume potentially following the area's local hydraulic gradient in the NW – SE direction was thought to emanate from either a hypothetical landfill site, HLS (point source) or the application of reduced N (RN) fertilizer in the form of NH_4^+ (diffuse source). Landfills as a common point source of N compounds would have potentially resulted in the formation of a plume and would be the case if the diffusely applied N fertilizer moved into a heterogeneous sand and gravel aquifer system. However, after evaluation of the subsurface conditions using surface geophysical and direct push investigations, a steep solute concentration distribution-influencing channelized aquifer structure was detected. Such a channelized bedrock structure would have entrained all infiltrating fluid (and solute) irrespective of its point or diffuse source origin. This first hint ruled out the possibility that the HLS alone would have formed the investigated NO_3^- plume, emphasizing the importance of adequately mapping subsurface structural controls on groundwater flow and solute transport. Of course, there is a hypothesis that the NO_3^- in the Neckar valley aquifer largely comes from fertilizer applied on the hillslopes underlain by fractured oxidized mudrock. As highlighted earlier, how the fractured oxidized mudrock is related to the channel structure inferred to be preferentially controlling the NO_3^- plume will be a critical further investigation.

Despite the fact that NH_4^+ would remain an issue even after the organic strength of a landfill leachate has been significantly reduced by methanogenic bacteria because there is no degradation pathway for NH_4^+ in anaerobic systems, the observation of low NH_4^+ (sometimes below the detection limit) did not support the concept that a landfill would have impacted the groundwater both in the oxic shallower and less-oxic deeper aquifer compartment. Given the gypsiferous carbonate rock environment, it is anticipated that the abundance of the divalent cations (Ca^{2+} and/or Mg^{2+}) and their competition for the exchange sites with NH_4^+ would have increased efficiency in the removal of NH_4^+; hence, the observed low NH_4^+ concentration values. Although the circumstances that promote NO_3^- biogeochemical processes may have been predicted for the investigated aquifer system in the floodplain area of the study site, there is presently limited groundwater biogeochemical data (in particular, groundwater NH_4^+ concentration and DO conditions, which are critical for maintaining N turnover processes) near the assumed location of the HLS (that is, toward the up Northwest/up North hillslope environment).

Complications arising from biogeochemical and mixing processes may blur effective identification of the NO_3^- sources. To reduce the uncertainties over NO_3^- source apportionment and fate within the aquifer, I made use of the dual-NO_3^- isotope data. The shallower aquifer compartment was characterized by soil organic N, whereas the deeper aquifer compartment was characterized by the animal (manure) and septic system waste. Further evaluation of the

fractionation between the N and O isotopes of the residual NO_3^-, and in relation to the mode of solute transport, indicate that, despite the partitioning of the NO_3^- source into shallower and deeper compartments of the aquifer by distinct and complex hydrologic and biogeochemical processes, $\delta^{15}N$ of the remineralized NO_3^- in the deeper aquifer compartment reflected the animal (manure)/septic system waste NO_3^- source. Tracing the denitrification line (Figure 4.14) backward also led to the interpretation that the soil organic N and the animal/septic waste would have originated from one source (RN fertilizer). It is possible that the RN may have resulted from liquid manure fertigation on the agricultural soil as observed during one of my field campaigns. However, that is not to say that the RN source of the groundwater NO_3^- is a very recent occurrence. I consider the investigated NO_3^- as a legacy resulting from decades of recharge of high NO_3^-. Again, I am aware of an existing hypothesis (Kortunov et al., 2016) that, since both floodplains in the Ammer and Neckar valley contain Holocene sediments relatively high in organic carbon, agricultural NO_3^- is reduced therein and does not reach the groundwater. Nevertheless, considering the residence and lag times of the fertilizer when applied and various impacting biogeochemical processes/mineralization and immobilization turnover of nitrogen at the soil-plant system, as well as varying environment/climatic conditions, leaching of produced NO_3^- cannot be completely dismissed. The positive correlation between NO_3^- and Cl^- concentrations further indicates that the groundwater NO_3^- was predominantly fecal- and/or wastewater-derived. Although the dual-NO_3^- isotope and chemical analyses proved their mettle in N source apportionment, there was not enough clarity given that the average $\delta^{15}N$ of the residual NO_3^- from the landfill leachates falls between the average for animal-septic wastes and the average from natural soil NO_3^-.

It is worth noting also that both landfill leachates and septic wastes can be classified into the N point source category, whereas the animal (manure) wastes are commonly diffuse in nature. Attempt to use the Na^+ indicator to segregate between point and nonpoint sources of decomposing organic matter was also not very helpful. In this study, there was no significant relation between Na^+ and NO_3^- (see Figure 4.12b), which, according to Minet et al. (2017), could be due to there being minimal or no impact of point sources (that is, animal/human waste influence) on NO_3^- groundwater loading. The rationale behind the use of the Na^+ indicator as a chemical tracer of an organic matter-derived contaminant plume of the point source stems from the understanding that it is one of the most mobile of the common cations whose adsorption should be further reduced as the sorption sites within plumes of contamination become saturated. Nonetheless, proper use of Na^+ as an indicator of the point source of organic matter relies on the enrichment of the decomposing organic matter in compounds that contain Na^+. Because the nature and content of the suspected landfill whose leachate would depend on the type of waste disposed of and the waste degradability among other factors was not directly probed, this present study cannot definitively associate the groundwater NO_3^- to a landfill site. In conjunction with the fact that there is no scientific basis for classifying both animal and septic system wastes into the same category as portrayed in Figure 4.14, a major conclusion reached is that fingerprinting of the groundwater NO_3^- sources in terms of their landfill, septic system and animal manure origins will be an interesting topic for further research, as highlighted in section 5.6: "*Enhanced understanding of the nitrate sources*." Studies including but not limited to the following have demonstrated such future research needs: Widory et al., 2005; Xue et al., 2009; Kaushal et al., 2011; Fenech et al., 2012; Toledo-Hernandez et al., 2013; Vrzel et al., 2016; Briand et al., 2017. Most importantly, performing groundwater sampling from the upper half of the study site toward the hillslope environment (up North)/ Wurmlingen settlement (NW) would greatly enhance the prospect of determining the groundwater

NO_3^- sources through the comparison of results from the two geohydrologically distinct regions of the study site.

5.4 Summary of conclusions

From the examined data, the following conclusions were reached in line with the questions highlighted in the introductory part of this work (see Chapter one).

- **Through which hydrologic pathway is the nitrogen nutrient physically transported?** This study identified a channelized subsurface hydrologic/preferential flow pathway, which connects the two regions of the study site: (1) up Northwest/hillslope environment (up North), and (2) down South on the floodplain area. This identification was made possible by the wider coverage of the preliminary Schlumberger-based depth sounding surveys, which provided a rough screening and estimation of the subsurface structural conditions in terms of the resistivity variations. Isoresistivity maps, specifically at a depth level or electrode spacing of 60 m, showed a linearized low-apparent-resistivity feature aligned in the NW-SE direction of the investigated groundwater plume of nitrate. The existence of the low-apparent-resistivity feature was later confirmed by the 2-D electrical resistivity imaging results. The low-resistivity feature also correlated a trough-like low P-wave velocity structure delineated from refraction seismic (with DP-based reversed vertical seismic profile travel time) tomography. Corroboration of the trough-like low-resistivity and low-velocity feature/anomaly by the DP soil EC and lithologic logging (that is, geostratigraphic profiling) indicated that the channelized feature marked the alluvium-bedrock interface. Further assessment of the feature and the heterogeneity of the aquifer using a chemical and stable isotope data set indicated that the aquifer system on the floodplain area is partitioned into two compartments. The shallower aquifer compartment (matrix structure) and deeper channelized compartment (macropore) displayed different hydrologic regimes characterized by distinct groundwater concentrations and dual-NO_3^- isotope signatures. It was interpreted that the channelized hydrologic pathway could preferentially entrain fluid/solutes infiltrating into the aquifer and govern the mechanisms of the biogeochemical processes. The occurrence of steep biogeochemical gradients shows that the interface between the shallower and deeper compartments of the aquifer could represent a local hot spot where there are preferential exchange fluxes and biogeochemical cycling.

- **What is the origin of the nitrogen nutrient, and where at the site are its source areas?** Comparatively, the oxidized form of N (that is, NO_3^-) dominated the reduced form (that is, NH_4^+) as measured in the aquifer groundwater. Using the dual-NO_3^- isotope data, two sources of NO_3^- are distinguishable in the shallower (that is, soil organic nitrogen source) and deeper (that is, animal manure and/or septic waste source) compartments of the aquifer on the floodplain area. However, following the denitrification trend line (Figure 4.14) back to its interception as suggested by Panno et al. (2006) shows that the two distinct groundwater NO_3^- sources partitioned into the shallower and deeper aquifer compartments originated from the reduced nitrogen fertilizer. Attribution of the groundwater NO_3^- to the

animal manure and/or septic waste sources was relatively concretized on the observation of liquid manure fertigation on the agricultural soil during one of my field campaigns. The perfect positive correlation between NO_3^- and Cl^- suggested that the NO_3^- was fecal- and wastewater-derived. Groundwater isotope data showed minimal or no variation across the two compartments, indicating that the groundwater originated from the same source (infiltrating rainwater), which carried the anthropogenic NO_3^- into the aquifer from the land surface. Controversy, however, ensued in the apportionment of N in relation to animal manure and septic system wastes given that there was no scientific basis for classifying them together as indicated by the form of chemical and stable isotopic indicators presented in this study. Apart from the fact that animal manure and septic wastes can be discriminated by different biogeochemical indicators, septic wastes are often termed point sources, whereas animal manure wastes are termed nonpoint sources. Distinguishing the sources as point or nonpoint was difficult in light of the presence of a channelized aquifer bedrock structure that is capable of channeling both point and nonpoint sources of NO_3^- in infiltration. This present study could not associate the groundwater NO_3^- with the hypothetical landfill site because there is presently no information regarding the content of wastes in the suspected landfill site (if such a site does exist at all). As noted earlier, separating animal manure, septic waste and landfill leachate in relation to the source of groundwater NO_3^- would constitute an important research effort.

- **What is the effect of the parent materials and development of the hydrologic pathways on the N cycling, and what biogeochemical processes are likely to occur?** Complex transport and fate mechanisms of coupled oxic NO_3^- removal and anoxic nitrification characterize N biogeochemical transformation pathways in the alluvial aquifer system. This conclusion was reached based on the following observations. Lower NO_3^--to-Cl^- ratios pointing to NO_3^--removing processes in the aerobic shallower compartment of the aquifer relative to the higher NO_3^--to-Cl^- ratios pointing to mixing processes in the anaerobic deeper compartment contradicts the basic assumption of nitrification and denitrification reaction pathways and demonstrates the complexity of processes in the system. The positive correlation between Mn^{2+} and NO_3^- inferred that it is possible for anoxic nitrification to occur in the deeper compartment of the aquifer. Additionally, the weakness in this relationship in the shallower compartment of the aquifer indicates that NO_3^- removal may have taken place, but not completely. The strong negative correlation between SO_4^{2-} and NO_3^- in the shallower compartments suggests possible inhibition of the activities of sulfate-reducing bacteria through symbiotic oxidation of the resulting sulfide by nitrate-reducing, sulfide-oxidizing bacteria, leading to the production of a slightly elevated SO_4^{2-} relative to the reduced NO_3^-. This process has been observed to produce some amount of nitrite if there is no resistance from the nitrite reductase that is widely distributed in the sulfate-reducing bacteria (Greene et al., 2003).

In the deeper aquifer compartment, there was no significant relationship between SO_4^{2-} and NO_3^- simply because the regenerated NO_3^- is energetically a more favorable electron acceptor than SO_4^{2-}. Although biological denitrification is commonly indicated by a progressive enrichment and coupled increase in $\delta^{18}O$ and $\delta^{15}N$ of the residual NO_3^- with a decline in NO_3^- concentration, the observed 2nd-degree polynomial increase in the $\delta^{15}N$ of the residual NO_3^- with NO_3^- concentration

suggests the admixture of groundwater NO_3^- from the shallower compartment into the deeper compartment. Further discrimination of the N-processing pathways was based on the slope of the association between the $\delta^{18}O$ and $\delta^{15}N$ of the residual NO_3^-. Whereas the $\delta^{18}O$ vs. $\delta^{15}N$ trajectory of 0.36 estimated from the shallower groundwater samples fell within the range of fractionation ratios reported for groundwater denitrification due to the coupling of the $\delta^{15}N$ and $\delta^{18}O$ of residual NO_3^-, the trajectory of 1.19 estimated for the deeper groundwater samples is interpreted as evidence of anoxic nitrification processes due to the decoupling of the $\delta^{15}N$ and $\delta^{18}O$ of residual NO_3^-. It is most likely that, as an incomplete process, denitrification in the anaerobic microsite of an aerobic shallower media produced the nitrite that diffused into the deeper aquifer compartment. Alternatively, this nitrite in question may to have emanated from the shallower aquifer compartment, wherein there is possible stimulation of nitrate-reducing, sulfide-oxidizing and heterotrophic denitrifying bacteria. Although this present study explained the dominance of heterotrophic pathway over autotrophic pathway, the true nature of the microbial communities remains to be investigated. The anoxic nitrification processes in the deeper aquifer compartment is also considered to be incomplete. This is because the elevation of the $\delta^{15}N$ of residual NO_3^- would have only occurred in the presence of denitrification, meaning that the nitrite-oxidizing bacteria would have responded to a periodic anaerobic/aerobic operation. The observation of NO_2^- in the deeper aquifer compartment corroborate this hypothesis. Therefore, this study also suggests that nitrification and denitrification are tightly coupled in the aquifer system. The observation of a decrease in HCO_3^- concentration with an increase in NO_3^- further affirms the higher potential for NO_3^- removal in the shallower compartment relative to nitrification in the deeper compartment. The evaluation of the relation between HCO_3^- and the $\delta^{18}O$ of residual NO_3^- also shows that the incorporation of oxygen from water would not have merely occurred without something such as the HCO_3^- effect besides water as the chemical intermediate source of evolved oxygen (see Metzner, 1979; Stemler, 2002). The summary of the investigation on N turnover in the alluvial aquifer is that both physical (hydrology) and the nature of microbes and their ability to cycle N nutrient transferred to them variably distinctly in the shallower and deeper aquifer compartments.

5.5 Scientific significance and impact

The observation-based CSM framework approach developed demonstrates how to recognize complexities associated with a natural aquifer system riddled with uncertainties to foster effective groundwater flow, solute fate and transport modeling. The defined architecture and configuration of the investigated aquifer system made it possible to develop key understanding of the hydrologic flow system and biogeochemical processes. In general, evaluation of preferential flow pathways aids in the understanding of migration pathways of recalcitrant chemical constituents for efficient remediation processes. By analyzing the geologic history (e.g., stratigraphy, structures, and water-rock interactions), I was able to catch a glimpse of how the distribution of flow paths, electron donor availability or diffusion control the extent of N processes in an alluvial aquifer. Interpretation of the processes impacting the distribution of NO_3^- concentrations would have been wrong and complicated had groundwater sampling been performed only from within the shallower compartment of the aquifer without the acknowledgement of the steep solute concentration and stable isotope gradient created due to the presence of a channelized deeper aquifer compartment.

I have also demonstrated in this study that it would have been difficult to determine the boundary and dominating processes around the investigated NO_3^- plume by the traditional approach to site characterization alone. The channelized deeper flow system identified by employing the observation-based CSM framework resulted in the knowledge of the steep biogeochemical gradients that drove diffusive transport of solute and oxygen from the shallower into the deeper aquifer compartment. This made it possible to distinguish hydrobiogeochemical interactions and processes that may be taking place in the deeper compartment from those that are controlled instead by processes within the shallower aquifer compartment, as well as how the processes are connected to each other. Based on the study results, it was possible to infer how these processes impacted the original source of the N nutrient loaded into aquifer groundwater. The unraveling of the channel structure provided a new concept in the understanding of the N hydrobiogeochemical processes. In particular, the presence of the channelized aquifer structure provided opportunity for me to interprete in-stream denitrification (e.g., Mayer et al., 2002) hidden in the aquifer, wherein diffusion-controlled transport mechanism and admixture of NO_3^- sources plays crucial role in determining the distribution of the NO_3^- concentrations.

This foundational information is useful for addressing one of the pressing water resource and environmental challenges, particularly in agricultural settings. In a bid to feed the burgeoning world population, agricultural activities have become the major sources of anthropogenic reactive N. However, rather than purely contributing to food production, deficient understanding of the N turnover has resulted in the loss of almost three quarters of agricultural N to water bodies and the atmosphere (Oita et al., 2016). Consequently, it has become increasingly imperative to manage and remove N input into the environment. Removal of a large chunk of N entering aquatic environments has been primarily attributed to a respiratory denitrification mechanism. However, alternative, microbially mediated N transformation processes have altered this basic assumption that oxic nitrification precedes anoxic denitrification. Most of what is known about these alternative NO_3^- removal pathways is based on laboratory cultures, lakes, rivers, and coastal estuaries studies, with far less attention being paid to such pathways in the terrestrial subsurface below the water table. This has been primarily attributed to the lack of ease of access into complex subsurface systems and inadequate understanding of the systems' physical and biogeochemical processes. It is even suggested that N transformation pathways operative in freshwater and marine ecosystems are fundamentally different. By developing a deeper understanding of N nutrient processing in the alluvial aquifer setting, this research work provides new knowledge and tools required to predict complex biogeochemical cycling, such as aerobic denitrification and anaerobic nitrification as observed in the shallower and deeper aquifer compartments, respectively.

The recognition of NO_3^- regeneration processes as reported for the anaerobic deeper compartment of the aquifer is crucial for reliable prediction of the long-term development of the NO_3^- load of water resources. Aerobic denitrification as an incomplete NO_3^- reduction process may result in the emission of undesirable nitrous oxide (a greenhouse gas that is over 300 times more potent than carbon dioxide). Moreover, anaerobic nitrification and aerobic denitrification are coupled nitrification-denitrification processes. The observation-based conceptual site model framework demonstrated in this study proved helpful because the identification of the degree to which nitrification and denitrification are coupled also influences how denitrification is modeled in natural and agricultural systems (Boyer et al., 2006). According to Seitzinger et al. (2006), "one might expect that models of systems with tightly coupled nitrification and denitrification would be strongly influenced by diffusive processes, whereas models of more loosely coupled systems would

be influenced primarily by advective (or other ecosystem or climatic) processes." With these insights, the N budget from the mostly inaccessible and highly heterogeneous aquifer system can be accounted for as an aid to the development of strategies for effective management and control of N added via synthetic fertilizers, manures and slurries, while ensuring that complete NO_3^- utilization is accomplished through the production of dinitrogen gas. The complexity of the N-cycling pathways identified in this study reinforce the message that anaerobic denitrification alone should not be thought of as the primary mechanism responsible for NO_3^- disappearance in aquifer systems (Lloyd, 1993). The results from this study suggest that the understanding of N biogeochemical processes is far from complete, a problem that is, as of now, unresolved and still largely open to discussion. Whereas N serves as a representative use case, the systematic CSM approach adopted in this study can be extended to bridge the mechanistic knowledge gap on the complex fate and transport of other chemical constituents of concern between experimentation and corresponding modeling studies, as well as their impact on human and environmental health.

5.6 Outlook

Although this study has evaluated a CSM by delineating the variability of the subsurface structures, vertical distribution of groundwater solutes, inferred potential hotspot and sources of a nitrate plume origin as well as identified N transformation pathways, key data gaps and uncertainties still remain, but they also open up some questions that point to new research directions. These knowledge gaps include but are not limited to the following.

Expanded search for biogeochemical hotspots within the floodplain aquifer

- I showed that the channelized part of the investigated aquifer system could represent a potential zone within the NO_3^- plume where reaction rates of biogeochemical activity are disproportionately higher (that is, a hotspot) than those in the surrounding/upgradient aquifer matrix. However, there is still limited knowledge of the extent to which the NO_3^- plume migrates laterally beyond the selected and studied section of the study site. Mapping biogeochemical hotspot zones in an ecosystem is not only important for contaminant management and remediation but also necessary as a fruitful direction of floodplain management research, especially for processes, such as denitrification, that rely simplistically on anoxic microsites and evaluation of multiple substrates, such as nitrate and bioavailable carbon. Developing an understanding of these zones can be quite challenging due to the spatiotemporal variability of complex linkages between hydrological dynamics and biogeochemical processes that govern flow and transport within a naturally heterogeneous environment. Advancing the developed CSM approach, which logically combines multidisciplinary geoscience tools, is one promising move toward better quantification of hotspot zones and associated hydrobiogeochemical exchanges.

Enhanced understanding of the nitrate sources

- Present data have increased the understanding of nitrogen nutrient sources and have

provided indications of their potential transformations in the aquifer on the floodplain part of the site. However, expanding the evaluated chemical and isotopic data beyond the present variables could improve the ability to substantiate a proposition of a potential landfill contributory source of the NO_3^-. For example, iodine, the boron isotope ratio and Cl^-/bromide ratios could be a useful proxy for the identification of NO_3^- sources. Additionally, microbiological markers could be combined with the chemical and isotopic data to reveal major differences in organic contaminations between human and animal wastes. Certainly, such research effort should also include groundwater sampling on both the floodplain aquifer and the aquifer system towards the hypothetical landfill site (that is, up Northwest/hillslope environment). This will help in making adequate comparisons of how N processing in the inferred geohydrologically distinct aquifer influences the N source(s).

Geophysical monitoring of the dynamics of aquifer groundwater mixing zones

- I reported that the inferred subsurface preferential flow zone encourages the channelization of flow and physical mixing of water, solute reactions and mobilization processes. It was also highlighted that the development of higher solute fluxes associated with the channelized part of the aquifer could be water volume-dependent, given the configuration and geometry of the aquifer bedrock. Similar to many other ecohydrological interfaces, the identified mixing-controlling aerobic/anaerobic transition zone may provide information regarding transient/seasonal storage within the channelized aquifer. In particular, this encourages consideration of the channel water balance (e.g., Payn et al., 2009) when analyzing the dependence of the solute dynamics (that is, the addition and removal of channel solute loads) on the geochemical fate and transport or biological processes. Such a zone is critical for biogeochemical processing in terrestrial/aquatic ecosystems, and understanding it is fundamental to elucidating complex subsurface geohydrology. Additional studies using time-lapse monitoring for the detection of variations in fluid flow-dependent geophysical attributes should be carried out to elucidate the intra-seasonal controls on the dynamics of the mixing zone.

Coupled hydrological and biogeochemical processes controlling the nitrogen nutrient cycling

- Although I identified that the aquifer is partitioned into two zones of distinct biogeochemical processing, understanding the link and interaction patterns of hydrological and biogeochemical processes controlling nitrogen nutrient cycling merits further scrutiny. To gain considerable insight into these processes, closely spaced multilevel monitoring wells should be strategically installed within these identified aquifer compartments for temporal and systematic analysis of N-cycling responses to precipitation patterns, water table dynamics, and isotopic and site-specific geochemical indicators. These measurements could reveal how the largely overlooked mechanisms of N removal and production are coupled to hydrological processes at event, seasonal, and inter-annual scales. Ultimately, such a work could enhance the development of a watershed-scale model of coupled hydrological and biogeochemical responses.

Microbial diversity within the alluvial aquifer system

- Linking N dynamics with bacterial community levels has proved largely unsuccessful due to such reasons as the following: (1) the facultative nature of NO_3^- reduction, which means that genes responsible for NO_3^- reduction processes play only a minor role in determining the location of the bacteria that carries them, and (2) complexity of the media, so links between bacterial communities and environmental factors are not clearly defined. Although the aquifer system under study is now relatively well characterized, the existence of complex N-cycling pathways, such as coupled oxic nitrification-anoxic denitrification, as well as the speculation that an anammox and DNRA would have occurred or co-occurred with denitrification, allude to the fact that the understanding of N biogeochemical processes is far from complete. Because of the pivotal roles played by microbial activities in biogeochemical cycling of nutrients, additional studies involving the correlation of the diversity and abundance patterns of the microbial communities, as well as gene expression assays with the conservative and reactive chemical and isotopic tracers at spatiotemporal scales, would be of particular interest in confirming the existence of the pathways of NO_3^- conversion interpreted in this study.

Role of the HCO_3^- effect in the evolution of the oxygen isotope abiotically exchanged between nitrite and water

- Studies have suggested that the oxidation of ammonium/nitrification would result in a large amount of oxygen isotope exchange between nitrite and water (Buchwald et al., 2012). A large range of $\delta^{18}O$ of the residual NO_3^- predicted in the process has been attributed to the variations in the amount of exchange and kinetic isotopic fractionation expressed during ammonia oxidation and nitrite oxidation among the different bacterial communities (Buchwald and Casciotti, 2010). Although determining the oxygen isotopic exchange and fractionation during nitrification under natural environmental conditions is crucial to predicting the source of $\delta^{18}O$ in NO_3^- and its variation with water and atmospheric oxygen, it has been noted that this range of values lacks the predictive power required for the interpretation and modeling of NO_3^- isotope distribution (Snider et al., 2010; Buchwald et al., 2012). Clearly, in this study, there is a weak relation between $\delta^{18}O$ of water that is expected to contribute two-thirds of the required oxygen to the produced NO_3^- and $\delta^{18}O$ of the residual NO_3^-. Apart from being a microbial indicator of N biogeochemical processes and considering the carbonate rock environment of the investigated site, this present study appears to show that, besides water (a well-known and conclusive source of oxygen), HCO_3^- would have been an immediate source of the evolved oxygen by participating in the water-splitting reaction. This phenomenon, known as the HCO_3^- partitioning effect, results in oxygen evolution but has not been investigated in N isotope biogeochemical studies. On thermodynamic grounds, Metzner (1978) proposed that water entered the splitting reaction that would have carbon dioxide product continuously rehydrated in the form of HCO_3^-, from which it is much easier to extract electrons than from water itself. Unlike the results presented in this study wherein the values of $\delta^{18}O$ of water were far below those of the residual NO_3^-, the argument put forward by Metzner et al. (1979) is that, if oxygen was developed directly from water, the $\delta^{18}O$ of evolved oxygen could, under no circumstance,

be even minutely greater than that of the water in the medium (see Stemler, 2002). Put together with the significant relation observed between HCO_3^- and (NO_3^- and $\delta^{18}O$ of NO_3^-), this study proposes to test whether the ^{18}O enrichment is due to the HCO_3^- or to isotopic exchange between the HCO_3^- and water. Such information is essential for interpreting the factors impacting the $\delta^{18}O$ of the regenerated NO_3^- in the anaerobic deeper compartment of the alluvial aquifer.

Aerobic denitrification and anaerobic nitrification as a function of residence time across a critical biogeochemical hotspot in a channelized floodplain aquifer

- The classical description of nitrification and denitrification holds that the presence of oxygen is inhibitory. Although the use of NO_3^- when oxygen is present is of no known advantage, simultaneous use of oxygen and NO_3^- as terminal electron acceptors has now been found not to be precluded in many bacteria (Lloyd, 1993). Thus, the notion that denitrification is singularly an anaerobic process has been debunked in both theory and practice. Similarly, it has been found that nitrite-oxidizing bacteria are capable of promoting the incorporation of oxygen atoms from ambient water into dissolved NO_3^- under anoxic conditions (Wunderlich et al., 2013), resulting in NO_3^- regeneration. My hypothesis is that aerobic denitrification and anaerobic nitrification are incomplete processes that account for the reversibility of NO_3^- consumption and production reaction in a complex natural setting, such as that identified in this study's shallower and deeper compartments of the channelized floodplain aquifer. Although I used the chemical and dual stable isotope of NO_3^- to advance the mechanistic process understanding of the N biogeochemical turnover, the fundamental open question is how the exchange between the shallower and deeper compartments through a transition interface that represents potential biogeochemical hotspots and hot moments is organized. Indeed, this is a valid question given that oxygen sensitivity of the microbial nitrification and denitrification depends on hydrologic forcing, which determines how the fluctuations in oxygen supply may occur on timescales. The impact of flow-dependent residence time distributions on the dynamics of biogeochemical fluxes across ecohydrological interfaces has been identified by several studies (e.g., Zarnetske et al., 2011). It is therefore considered important to test the hypothesis that complex biogeochemical reactions associated with N cycling, such as aerobic denitrification and anaerobic nitrification, are controlled by water residence times in the distinct compartments of the channelized floodplain aquifer.

Modeling the relation between nitrate and seasonal redox dynamics

- Following the identification of coupled oxic denitrification and anoxic nitrification processes in the shallower and deeper compartments of the aquifer, respectively, as alternatives to the traditional nitrification-denitrification process, the aquifer was adjudged to be a complex one. It is hypothesized that the complex distribution of the N-cycling pathways results from diffusion-controlled redox processes, which are controlled by the subsurface hydrologic conditions. In both oxic denitrification and anoxic denitrification processes, HCO_3^- alkalinity appears to have a played vital role such that its accumulation during denitrification in the shallower compartment of the aquifer was probably

compensated by its consumption during nitrification in the deeper compartment of the aquifer. In particular, HCO_3^- is a reliable indicator of microbial activities. Mn-oxide also appears to be coupled to anoxic nitrification. In this regard, it could be necessary to consider a reactive multicomponent transport modeling of the redox dynamics wherein the fate and mobility of NO_3^- is simulated with Mn^{2+} and HCO_3^- alkalinity as major uncertainty coupling and decoupling variables. Additionally, SO_4^{2-} was found to have also played a role in the aquifer N-cycling processes. It would also be worthwhile to model the impact of anthropogenic NO_3^- on S cycling and SO_4^{2-} reactive transport.

References

Abbott, B.W., Baranov, V., Mendoza-Lera, C., Nikolakopoulou, M., Harjung, A., Kolbe, T., Balasubramanian, M.N., Vaessen, T.N., Ciocca, F., Campeau, A., Wallin, M.B., Romeijn, P., Antonelli, M., Gonçalves, J., Datry, T., Laverman, A.M., de Dreuzy, J.-R., Hannah, D.M., Krause, S., Oldham, C., Pinay, G., 2016. Using multi-tracer inference to move beyond single-catchment ecohydrology. Earth-Sci. Rev. 160, 19 – 42. http://dx.doi.org/10.1016/j.earscirev.2016.06.014.

Akber Hassan, W. A., Jiang, X., 2012. Upscaling and its application in numerical simulation of long-term CO2 storage. Greenhouse Gas Sci. Technol., 2(6), 408 – 418. http://dx.doi.org/10.1002/ghg.1306.

Alexander, R.B., Böhlke, J.K., Boyer, E.W., Davide, M.B., Harvey, J.W., Mulholland, P.J., Seitzinger, S.P., Tobias, C.R., Tonito, C., Wollheim, W.M., 2009. Dynamic modeling of nitrogen losses in river network unravels the coupled effects of hydrological and biogeochemical biogeochemical processes. Biogeochem. 93, 91 – 116. http://dx.doi.org/10.1007/s10533-008-9274-8.

Aller, R. C., Hall, P.O.J., Rude, P.D., Aller, J.Y., 1998. Biogeochemical heterogeneity and suboxic diagenesis in hemipelagic sediments of the Panama Basin. Deep Sea Res. Part I: Oceanographic Res. Papers. 45(1), 133-165. http://dx.doi.org/10.1016/S0967-0637(97)00049-6.

Almasri, M.N., 2007. Nitrate contamination of groundwater: A conceptual management framework. Environ. Impact Assess. Rev. 27(3), 220–242. http://dx.doi.org/10.1016/j.eiar.2006.11.002.

Altman, S.J., Parizek, R.R., 1995. Dilution of nonpoint-source nitrate in groundwater. J. Environ. Qual. 24, 707 - 718. http://dx.doi.org/10.2134/jeq1995.00472425002400040023x.

Amberger, A., Schmidt, H.-L., 1987. Natürliche isotopengehalte von nitrate als indikatoren für dessen Herkunft. Geochim. Cosmochim. Acta. 51(10), 2699–2705. http://dx.doi.org/10.1016/0016-7037(87)90150-5.

Amos, R.T., Blowes, D.W., 2008. Versatile direct push profiler for the investigation of volatile compounds near the water table. Water Resour. Res. 44, W00D17. http://dx. doi.org/10.1029/2008WR006936.

Anderson, M.P., McCray, J., 2011. Foreword: Lessons learned about contaminant hydrogeology from legacy research sites. Ground Water. 49, 617–619. http://dx.doi.org/10.1111/j.1745-6584.2011.00842.x.

Anderson, M.P., 2007. Introducing groundwater physics. Phys. Today. 60(5), 42–47. http://dx.doi.org/10.1063/1.2743123.

Andersson, K.K., Hooper, A.B., 1983. O_2 and H_2O are each the source the source of one O in NO_2^- produced from NH_3 by Nitrosomonas: ^{15}N-NMR evidence. FEBS Lett. 64, 236 – 240. http://dx.doi.org/10.1016/0014-5793(83)80292-0.

Andriashek, L.D., Atkinson, N., 2007. Buried channels and glacial-drift aquifers in the Fort McMurray region, Northeast Alberta. Alberta Geol. Surv. Earth Sciences Report 2007-01. http://ags.aer.ca/document/ESR/ESR_2007_01.pdf.

Anneser, B., Einsiedl, F., Meckenstock, R.U., Richters, L., Wisotzky, F., Griebler, C., 2008. High-resolution monitoring of biogeochemical gradients in a tar oil-contaminated aquifer. Appl. Geochem. 23 (6), 1715 – 1730. https://doi.org/10.1016/j.apgeochem.2008.02.003.

Apparao, A., Rao, T.G., 1974. Depth of investigation in resistivity methods using linear electrodes. Geophys. Prospect. 22, 211 – 223. https://doi.org/10.1111/j.1365-2478.1974.tb00080.x.

Aquilina, L., Vergnaud-Ayraud, V., Armandine Les Landes, A., Pauwels, H., Davy, P., Petelet-Giraud, E.T., Roques, C., Chatton, E., Bour, O., Maamar, S.B., Dufresne, A., Khaska, M., Le Gal La Salle, C., Barbecot,

References

F., 2015. Impact of climate changes during the last 5 million years on groundwater in basement aquifers. Sci. Rep. 5, 14132. http://dx.doi.org/10.1038/srep1432.

Aravena, R., Evans, M. L., Cherry, J. A., 1993. Stable isotopes of oxygen and nitrogen in source identification of nitrate from septic systems. Ground Water. 31(2), 180–186. http://dx.doi.org/ 10.1111/j.1745-6584.1993.tb01809.x.

Aravena, R., Mayer, B., 2010. Isotopes and processes in the nitrogen and sulfur cycles, in: Aelion, C.M., Höhener, P., Hunkeler, D., Aravena, R. (Eds.), Environmental Isotopes in Biodegradation and Bioremediation. CRC Press, Inc, New York, pp. 203–246. http://dx. doi.org/10.1201/9781420012613.ch7.

Aravena, R., Robertson, W. D., 1998. Use of multiple isotope tracers to evaluate denitrification in ground water: Study of nitrate from a large-flux septic system plume. Ground Water. 36, 975–982. http://dx. doi.org/10.1111/j.1745-6584.1998.tb02104.x.

Archie, G.E., 1942. The electrical resistivity log as an aid in determining some reservoir characteristics. Pet. Trans. AIME. 146 (1), 54 - 62. http://dx.doi.org/10.2118/942054-G.

ASTM Standard E1689-95, 2014. Standard Guide for Developing Conceptual Site Models for Contaminated Sites. ASTM International, USA http://dx.doi.org/10.1520/E1689-95R08 (www.astm.org).

Atekwana, E.A., Atekwana, E.A., 2010. Geophysical signatures of microbial activity at hydrocarbon contaminated sites: A review. Surv. Geophys. 31(2), 247 – 283. http://dx.doi.org/10.1007/s10712-009-9089-8.

Atkins, P.W., Jones, L., 2010. Chemical Principles: The Quest for Insight. W.H. Freeman, New York, 787p.

Baillieux, A., Campisi, D., Jammet, N., Bucher, S., Hunkeler, D., 2014. Regional water quality patterns in an alluvial aquifer: Direct and indirect influences of rivers. J. Contam. Hydrol. 169, 123-131. http://dx.doi.org/10.1016/j.jconhyd.2014.09.002.

Bain, J.G., Blowes, D.W., Robertson, W.D., Frind, E.O., 2000. Modelling of sulfide oxidation with reactive transport at a mine drainage site. J. Contam. Hydrol. 41(1-2), 23 – 47. http://dx.doi.org/10.1016/S0169-7722(99)00069-8.

Balia, R., Gavaudo, E., Ardau, F., Ghiglieri, G., 2003. Geophysical approach to the environmental study of a coastal plain. Geophys. 68(5),1446–1459. http://dx.doi.org/ 10.1190/1.1620618.

Barazzuoli, P., Nocchi, M., Rigati, R., Salleolini, M., 2008. A conceptual and numerical model for groundwater management: A case study on coastal aquifer in southern Tuscany, Italy. Hydrogeol. J. 16 (8), 1557 – 1576. http://dx.doi.org/10.1007/s10040-008-0324-z.

Barcelona, M.J., Gibb, J.P., Helfrich, J.A., Garske, E.E., 1985. Practical guide for ground-water sampling. Illinois State Water Surv. SWS Contract Report 374. http://www.isws.illinois.edu/pubdoc/CR/ISWSCR-374.pdf.

Barkle, G., Clough, T., Stenger, R., 2007. Denitrification capacity in the vadose zone at three sites in the Lake Taupo catchment, New Zealand. Australian J. Soil Res. 45, 91-99. http://dx. doi.org/10.1071/SR06141.

Barlow, J.R.B., Kröger, R., 2014. Nitrogen transport within an agricultural landscape: insights on how hydrology, biogeochemistry, and the landscape intersect to control the fate and transport of nitrogen in the Mississippi Delta. J. Soil Water Conserv. 69,11A−16A. http://dx.doi.org/10.2489/jswc.69.1.11A.

Barnes, R.T., Raymond, P.A., 2010. Land-use controls on sources and processing of nitrate in small watersheds: insights from dual isotopic analysis. Ecol. Appl. 20, 1961 - 1978. http://dx.doi.org/10.1890/08-1328.1.

Barrett, M.H., Howard, A.G., 2002. Urban groundwater and sanitation - developed and developing countries, in: Howard, K.W.F., Israfilov, R.G. (Eds.), Current Problems of Hydrogeology in Urban Areas,

References

Urban Agglomerated and Industrial Centres. Kluwer Academic Publishers, The Netherlands, p. 39 - 56. http://dx.doi.org/10.1007/978-94-010-0409-1_3.

Barry, K.M., 1967. Delay time and its application to refraction profile interpretation, in: Musgrave, A.W. (Ed.), Seismic Refraction Prospecting. SEG, Tulsa, OK, pp. 348 – 361.

Barth, J.A.C., Kappler, A., Piepenbrink, M., Werth, C., Regenspurg, S., Semprini, L., Slater, G. F., Schüth, C., Grathwohl, P., 2005. New challenges in biogeochemical gradient research. Eos Trans. AGU. 86(44), 432–432. http://dx.doi.org/10.1029/2005EO440008.

Bauer, K., Moeck, I., Norden, B., Schulze, A., Weber, M., Wirth, H., 2010. Tomographic P wave velocity and vertical velocity gradient structure across the geothermal site Groß Schönebeck (NE German Basin): Relationship to lithology, salt tectonics, and thermal regime. J. Geophys. Res. 115, B08312, http://dx.doi.org/ 10.1029/2009JB006895.

Beck, F.P., Clark, P.J., Puls, R.W., 2000. Location and characterization of subsurface anomalies using a soil conductivity probe. Ground Water Monitoring & Remediation. 20, 55–59. http://dx.doi.org/10.1111/j.1745-6592.2000.tb00265.x.

Belser, L.W., 1984. Bicarbonate uptake by nitrifiers: effects of growth rate, pH, substrate concentration, and metabolic inhibitors. Appl. Environ. Microbiol. 48, 1100–1104.

Benning, J.L., Barnes, D.L., Burger, J., Kelley, J.J., 2009. Amchitka Island, Alaska: moving towards long term stewardship. Polar Record. 45(233), 133 - 146. http://dx.doi.org/10.1017/S003224740800795X.
Benson, A.K., Payne, K.L., Stubben, M.A., 1997. Mapping groundwater contamination using DC resistivity and VLF geophysical methods – a case study. Geophys. 62(1), 80–86. http://dx.doi.org/10.1190/1.1444148.

Berg, S.J., Illman, W.A., 2013. Field study of subsurface heterogeneity with steady-state hydraulic tomography. Ground Water. 51(1), 29 – 40. http://dx.doi.org/10.1111/j.1745-6584.2012.00914.x.

Berner, E.K.; Berner, R.A., 1996. Global Environment: Water, Air, and Geochemical Cycles. Prentice Hall.

Bermejo, J.L., Sauck, W.A., Atekwana, E.A., 1997. Geophysical discovery of a new LNAPL plume at the former Wurtsmith AFB, Oscoda, Michigan. Groundwater Monitoring & Remediation. 17 (4), 131 – 137. http://dx.doi.org/10.1111/j.1745-6592.1997.tb01273.x.

Bernat, K., Wojnowska-Baryla, I., 2007. Carbon source in aerobic denitrification. Biochemical Eng. J. 36(2), 116 – 122. http://dx.doi.org/10.1016/j.bej.2007.02.007.

Bock, E., Wagner, M., 2013. Oxidation of Inorganic Nitrogen Compounds as an Energy Source, in: The Prokaryotes. Springer Berlin Heidelberg, Berlin, Heidelberg, pp. 83– 118.

Bethune, J., Randell, J., Runkel, R.L., Singha, K., 2015. Non-invasive flow path characterization in a mining-impacted wetland. J. Contam. Hydrol. 183, 29-39. http://dx.doi.org/10.1016/j.jconhyd.2015.10.002.

Beven, K., Germann, P., 1982. Macropores and water flow in soils. Water Resour. Res.18(5), 1311 – 1325. http://dx.doi.org/10.1029/WR018i005p01311.

Beven, K., Germann, P., 2013. Macropores and water flow in soils revisited. Water Resour. Res. 49(6), 3071 – 3092. http://dx.doi.org/10.1002/wrcr.20156.

Beven, K., 2009. Environmental Modelling: An Uncertain Future? An Introduction to Techniques for Uncertainty Estimation in Environmental Prediction. Routledge, UK.

Beyer, D., 2015. Evolution of reservoir properties in the Lower Triassic aquifer sandstones of the Thuringian Syncline in Central Germany, PhD dissertation, FAC. Chem. and Earth Sci., Friedrich-Schiller-Universität, Jena, Germany.

References

Binley, A., Ramirez, A., Daily, W., 1995. Regularized image reconstruction of noisy electrical resistance tomography data, in: Process Tomography. 401 – 410.

Binley, A., Hubbard, S.S., Huisman, J.A., Revil, A., Robinson, D.A., Singha, K., Slater, L.D., 2015. The emergence of hydrogeophysics for improved understanding of subsurface processes over multiple scales. Water Resour. Res. 51, 3837 - 3866. http//dx.doi.org/10.1002/2015WR17016.

Biondi, B.L., 2007. Concepts and Applications in 3D Seismic Imaging. Soc. of Explor. Geophys, Tulsa, OK. http://dx.doi.org/10.1190/1.9781560801665.

Birdwell, J.E., Engel, A.S., 2009. Variability in terrestrial and microbial contributions to dissolved organic matter fluorescence in the Edwards Aquifer, central Texas. J. Cave and Karst Studies. 71(2), 144 – 156.

Blasch, K.W., Bryson, J.R., 2007. Distinguishing Sources of Ground Water Recharge by Using δ^2H and $\delta^{18}O$. Ground Water. 45, 294–308. http://dx.doi.org/10.1111/j.1745-6584.2006.00289.x.

Böhlke, J.K., 2002. Groundwater recharge and agricultural contamination. Hydrogeol. J. 10(1), 153 - 179. http://dx.doi.org/10.1007/s10040-001-0183-3.

Böhlke, J. K., Smith, R. L., Miller, D. N., 2006. Ammonium transport and reaction in contaminated groundwater: Application of isotope tracers and isotope fractionation studies. Water Resour. Res. 42, W05411. http://dx.doi.org/ 10.1029/2005WR004349.

Böhlke, J.K., Wanty, R., Tuttle, M., Delin, G., Landon, M., 2002. Denitrification in the recharge area and discharge area of a transient agricultural nitrate plume in a glacial outwash sand aquifer, Minnesota. Water Resour. Res. 38 (7), 1105. http://dx.doi.org/ 10.1029/2001WR000663.

Böttcher, J., Strebel, O., Voerkelius, S., Schmidt, H.-L., 1990. Using isotope fractionation of nitrate-nitrogen and nitrate-oxygen for evaluation of microbial denitrification in a sandy aquifer. J. Hydrol. 114, 413 - 424. http://dx.doi.org/10.1016/0022-1694(90)90068-9.

Bond, C.E., Lunn, R.J., Shipton, Z.K., Lunn, A.D., 2012. What makes an expert effective in interpreting seismic images? Geol. 40 (1), 75 - 78. http://dx.doi.org/10.1130/G32375.1.

Bosma, T.N.P, Middeldorp, P.J.M., Schraa, G., Zehnder, A.J.B., 1997. Mass transfer limitation of biotransformation: Quantifying bioavailability. Environ. Sci. Technol. 31(1), 248–252. 10.1021/es960383u.

Bowling, J.C., Rodriguez, A.B., Harry, D.L., Zheng, C., 2005. Delineating alluvial aquifer heterogeneity using resistivity and GPR Data. Ground Water. 43, 890–903. http://dx.doi.org/10.1111/j.1745-6584.2005.00103.x.

Boyer, E.W., Alexander, R.B., Parton, W.J., Li, C., Butterbach-Bahl, K., Donner, S.D., Skaggs, R.W., Del Grosso, S. J., 2006. Modeling denitrification in terrestrial and aquatic ecosystems at regional scales. Ecol. Appl. 16 (6), 2123-2142. http://dx.doi.org/10.1890/1051-0761(2006)016[2123:MDITAA]2.0.CO;2.

Brandes, J.A., Devol, A.H., 1997. Isotopic fractionation of oxygen and nitrogen in coastal marine sediments. Geochim. Cosmochim. Acta. 61(9), 1793 - 1801. http://dx.doi.org/10.1016/S0016-7037(97)00041-0.

Bratina, B.J., Stevenson, B.S., Green, W.J., Schmidt, T.M., 1998. Manganese reduction by microbes from oxic regions of the lake vanda (Antarctica) water column. Appl. Environ. Microbiol. 64, 3791 - 3797.

Bredehoeft, J., 2005. The conceptualization model problem – surprise. Hydrogeol. J. 13(1), 37 - 46. http://dx.doi.org/10.1007/s10040-004-0430-5.

Briand, C., Sebilo, M., Louvat, P., Chesnot, T., Vaury, V., Schneider, M., Plagnes, V., 2017. Legacy of contaminant N sources to the NO_3^- signature in rivers: a combined isotopic ($\delta^{15}N$-NO_3^-, $\delta^{18}O$-NO_3^-, $\delta^{11}B$) and microbiological investigation. Sci. Rep. 7, 41703. http://dx.doi.org/10.1038/srep41703.

References

Briggs, M.A., Lautz, L.K., Hare, D.H., González-Pinzón, R., 2013. Relating hyporheic fluxes, residence times and redox-sensitive biogeochemical processes upstream of beaver dams. Freshwater Sci. **32**(2), 622–641. http://dx.doi.org/10.1899/12-110.1.

Brigham, C.J., Speth, D.R., Rha, C., Sinskey, A.J., 2012. Whole-genome microarray and gene deletion studies reveal regulation of the polyhydroxyalkanoate production cycle by the stringent response in Ralstonia eutropha H16. Appl. Environ. Microbiol. 78, 8033–8044. http://dx.doi.org/10.1128/AEM.01693-12.

Brody, A.G., Pluhar, C.J., Stock, G.M., Greenwood, W.J., 2015. Near-surface geophysical imaging of a talus deposit in Yosemite Valley, California. Environ. Eng. Geosci. 21(2), 111–127. http://dx.doi.org/10.2113/gseegeosci.21.2.111.

Buchwald, C., Casciotti, K.L., 2010. Oxygen isotopic fractionation and exchange during bacterial nitrite oxidation. Limnol. Oceanogr. 55(3), 1064 - 1074. http://dx.doi.org/10.4319/lo.2010.55.3.1064.

Buchwald, C., Santoro, A.E., McIlvin, M.R., Casciotti, K.L., 2012. Oxygen isotopic composition of nitrate and nitrite produced by nitrifying cocultures and natural marine assemblages. Limnol. Oceanogr. 57, 1361 – 1375. http://dx.doi.org/10.4319/Io.2012.57.5.1361.

Burbery, L.F., Flintoft, M.J., Close, M.E., 2013. Application of the re-circulating tracer well test method to determine nitrate reaction rates in shallow unconfined aquifers. J. Contam. Hydrol. 145,1-9. http://dx.doi.org/10.1016/j.jconhyd.2012.11.006.

Burger, H.R., Sheehan, A.F., Jones, C.H., 2006. Introduction to Applied Geophysics: Exploring the Shallow Subsurface. W.W. Norton, New York.

Burger, J., Mayer, H.J., Greenberg, M., Powers, C.W., Volz, C.D., Gochfeld, M. 2006. Conceptual site models as a tool in evaluating ecological health: The case of the department of energy's Amchitka Island nuclear test site. J. Toxicol. Environ. Health. 69, 1217-1238. http://dx.doi.org/10.1080/15287390500360232.

Burgin, A.J., Hamilton, S.K., 2007. Have we overemphasized the role of denitrification in aquatic ecosystems? A review of nitrate removal pathways. Front. Ecol. Environ. 5(2), 89 – 96. http://dx.doi.org/10.1890/1540-9295(2007)5[89:HWOTRO]2.0.CO;2.

Burkholder, B. K., Grant, G. E., Haggerty, R., Khangaonkar, T., Wampler, P. J., 2008. Influence of hyporheic flow and geomorphology on temperature of a large, gravel-bed river, Clackamas River, Oregon, USA. Hydrol. Process. 22, 941–953 http://dx.doi.org/10.1002/hyp.6984.

Burns, D. A., Boyer, E. W. , Elliott, E. M., Kendall, C., 2009. Sources and transformations of nitrate from streams draining varying land uses: Evidence from dual Isotope analysis. J. Environ. Qual. 38,1149–1159. http://dx.doi.org/10.2134/jeq2008.0371.

Burow, K. R., Nolan, B.T., Rupert, M.G., Dubrovsky, N.M., 2010. Nitrate in groundwater of the United States, 1991 - 2003. Environ. Sci. Technol. 44, 4988–4997. http://dx.doi.org/10.1021/es100546y.

Burt, T.P., Pinay, G., 2005. Linking hydrology and biogeochemistry in complex landscapes. Progress in Physical Geography. 29, 297 – 316. http://dx.doi.org/10.1191/0309133305pp450ra.

Butler, D. K. (Ed.), 2005. Near-Surface Geophysics (Invest. Geophys., no. 13). Soc. of Explor. Geophys., Tulsa, OK.

Cadini, F., Bertoli, I., De Sanctis, J., Zio, E., 2012. A novel particle tracking scheme for modeling contaminant transport in a dual-continua fracture medium. Water Resour. Res. 48, W10517. http://dx.doi.org/10.1029/2011WR011694.

References

Caldwell, T.G., Bibby, H.M., 1998. The instantaneous apparent resistivity tensor: a visualization scheme for LOTEM electric field measurements. Geophys. J. International, 135 (3), 817 – 834. http://dx.doi.org/10.1046/j.1365-246X.1998.00668.x.

Callbeck, C.M., Agrawal, A., Voordouw, G., 2013. Acetate production from oil under sulfate-reducing conditions in bioreactor injected with sulfate and nitrate. Appl. Environ. Microbiol. 79, 5059 – 5068. https://doi.org/10.1128/AEM.01251-13.

Canfield, D.E., Thamdrup, B., Kristensen, E., 2005. Aquatic Geomicrobiology, 1st ed., Elsevier, New York, vol. 48.

Canter, L.W., 1997. Nitrates in Groundwater. CRC Press, Boca Raton, FL.

Canter, L.W., 2008. Conceptual models, matrices, networks, and adaptive management – emerging methods for CEA (ext. abs.). Proceedings of the 28th Annual Conference of the International Association for Impact Assessment, Calgary, Canada, November 6 – 9, 2008, 46 p.

Carlson, K.H., Knocke, W.R., Gertig, K.R., 1997. Optimizing treatment through Fe and Mn fractionation. J. AWWA. 84, 162 - 171.

Carrera, J., 1992. Methodological conceptualization of mathematical modelling, Mathematical and Computer Modelling. 16 (12), 19-28. http://dx.doi.org/10.1016/0895-7177(92)90015-D.

Casciotti, K.L., Sigman, D.M., Hastings, M.G., Bohlke, J. K., Hilkert, A., 2002. Measurement of the oxygen isotopic composition of nitrate in seawater and freshwater using the denitrifier method. Anal. Chem. 74, 4905–4912. http://dx.doi.org/10.1021/ac020113w.

Chandra, P.C., 2015. Groundwater Geophysics in Hard Rock. CRC Press, Inc, New York

Chapelle, F.H., 1993. Ground-Water Microbiology and Geochemistry. Wiley, New York, 424p.

Chapelle, F.H., Bradley, P.M., McMahon, P.B., Kaiser, K., Benner, R., 2012. Dissolved oxygen as an indicator of bioavailable dissolved organic carbon in groundwater. Ground Water. 50, 230 – 241. http://dx.doi.org/10.1111/j.1745-6584.2011.00835.x.

Chapman, D., 1992. Water Quality Assessments: A Guide to the Use of Biota, Sediments and Water in Environmental Monitoring. Chapman & Hall, London.

Chen, D.J.Z., MacQuarrie, K.T.B., 2005. Correlation of $\delta^{15}N$ and $\delta^{18}O$ in NO_3^- during denitrification in groundwater. J. Environ. Eng. Sci. 4(3), 221-226. http://dx.doi.org/10.1139/s05-002.

Chen, S.T., Zimmerman, L.J., Tugnait, J.K., 1990. Subsurface imaging using reversed vertical seismic profiling and crosshole tomographic methods. Geophys. 55(11), 1478-1487. http://dx.doi.org/10.1190/1.1442795.

Chen, J., Hubbard, S.S., Gaines, D., Korneev, V., Baker, G., Watson, D., 2010. Stochastic estimation of aquifer geometry using seismic refraction data with borehole depth constraints. Water Resour. Res. 46, W11539, http://dx.doi.org/10.1029/2009WR008715.

Chien, H., Mackay, D.S., 2013. How much complexity is needed to simulate watershed streamflow and water quality? A test combining time series and hydrological model. Hydrol. Process. 28, 5624 - 5636. http://dx.doi.org/10.1002/hyp.10066.

Christakos, G., Hristopulos, D.T., 1996. Stochastic indicators for waste site characterization, Water Resour. Res. 32(8), 2563 - 2578. http://dx.doi.org/10.1029/96WR01393.

Christensen, N.B., Sorensen, K.I., 1998. Surface and borehole electric and electromagnetic methods for hydro-geophysical Investigations. European J. Environ. Eng. Geophys. 3, 75-90.

References

Christensen, T.H., Kjeldsen, P., Bjerg, P.L., Jensen, D.L., Christensen, J.B., Baun, A., Albrechtsen, H.-J., Heron, G., 2001. Biogeochemistry of landfill leachate plumes. Appl. Geochem. 16 (7–8), 659 – 718. http://dx.doi.org/10.1016/S0883-2927(00)00082-2.

Churchill, P., Elmer, D., 1999. Hydrogen sulfide odor control in wastewater collection systems. NEWEA J. 33(1), 57 - 63.

Cirpka, O.A., Dietrich, P., Leven, C., 2017. Floodplain hydrology - P3 Structural controls of the hydrological functioning of a floodplain, in: CAMPOS - Catchment as Reactors. http://www.uni-tuebingen.de/forschung/forschungsschwerpunkte/sonderforschungsbereiche/sfb-1253/projects/p3-floodplain-hydrology.html.

Cirpka, O.A., Frind, E.O., Helmig, R., 1999. Numerical simulation of biodegradation controlled by transverse mixing. J.Contam. Hydrol. 40(2), 159-182. http://dx.doi.org/10.1016/S0169-7722(99)00044-3.

Cirpka, O.A., Valocchi, A.J., 2007. Two-dimensional concentration distribution for mixing-controlled bioreactive transport in steady state. Adv. Water Resour. 30 (6 -7), 1668 – 1679. http://dx.doi.org/10.1016/j.advwatres.2006.05.022.

Clague, J.C., Stenger, R., Clough, T., 2013. The impact of relict organic materials on the denitrification capacity in the unsaturated-saturated zone continuum of three volcanic profiles. J. Environ. Qual. 42,145-154. http://dx.doi.org/ 10.2134/jeq2012.0239.

Clark, I.D., Fritz, P., 1997. Environmental Isotopes in Hydrogeology. CRC Press, Inc., New York.

Claxton, A.J., Bates, P.D., Cloke, H. L., 2003. Mixing of hillslope, river and alluvial groundwaters in lowland floodplains. Groundwater. 41, 926 – 936. http://dx.doi.org/0.1111/j.1745-6584.2003.tb02435.x.

Clement, W.P., Liberty, L.M., Knoll, M.D., 1999. Reverse VSPs and crosshole seismic tomography while coring. 12th EEGS Symposium on the Application of Geophysics to Engineering and Environmental Problems, March 14, 1999, pp. 713-722.

Cohen, M.J., Heffernan, J.B., Albertin, A., Martin, J.B., 2012. Inference of riverine nitrogen processing from longitudinal and diel variation in dual nitrate isotopes. J. Geophys. Res. 117, G01021. http://dx.doi.org/10.1029/2011JG001715.

Corwin, D. L., Letey, J., Carrillo, M. L. K., 1999. Modeling non-point source pollutants in the vadose zone: back to the basics, in assessment of non-point source pollution in the vadose Zone, in: Corwin, D. L., Loague, K., Ellsworth, T. R. (Eds.). American Geophysical Union, Washington, DC. http://dx.doi.org/10.1029/GM108p0323.

Cozzarelli, I.M., Herman, J.S., Baedecker, M.J., Fischer, J.M., 1999. Geochemical heterogeneity of a gasoline-contaminated aquifer. J. Contam. Hydrol. 40, 261 - 284. http://dx.doi.org/10.1016/S0169-7722(99)00050-9.

Craig, H., 1961. Isotopic variations in meteoric waters. Science.133, 1702-1703. http://dx.doi.org/ 10.1126/science.133.3465.1702.

Cravotta, C.A., 1995. Use of stable isotopes of carbon, nitrogen, and sulfur to identify sources of nitrogen in surface waters in the lower susquehanna river basin, Pennsylvania. US Geological Survey Open-File Report 94-510. Washinghton (DC). US Geogical Survey. Demer, CO, USA (https://pubs.usgs.gov/of/1994/0510/report.pdf).

Crook, N., Binley, A., Knight, R., Robinson, D.A., Zarnetske, J., Haggerty, R., 2008. Electrical resistivity imaging of the architecture of substream sediments. Water Resour. Res. 44, W00D13. http://dx.doi.org/10.1029/2008WR006968.

References

Crumbling, D.M., 2004. The Triad approach to managing environmental data. Proceedings of the 20th Annual National Environmental Monitoring Conference, Washington DC, July 19 – 23, 2004, pp. 307 – 317.

Crumbling, D.M., Griffith, J., Powell, D.M., 2003. Improving decision quality: Making the case for adopting next generation site characterization practices. Remediation J. 13(2), 91-111. http://dx.doi.org/10.1002/rem.10066.

Crumbling, D.M., Groenjes, C., Lesnik, B., Lynch, K., Shockley, J., van Ee, J., Howe, R.A., Keith, L.H., McKenna, J., 2001. Managing uncertainty in environmental decisions: Applying the concept of effective data at contaminated sites could reduce costs and improve cleanups. Environ. Sci. Technol. 35, 404A-409A. http://dx.doi.org/10.1021/es012490g.

Crumbling, D. M., Hayworth, J. S., Johnson, R. L. Moore, M., 2004a. The Triad approach: A catalyst for maturing remediation practice. Remediation J. 15, 3–19. http://dx.doi.org/10.1002/rem.20029.

Crumbling, D. M., Hayworth, J. S., Call, B. A., Davis, W. M., Howe, R., Miller, D. S., Johnson, R., 2004b. The maturing of the Triad approach: Avoiding misconceptions. Remediation J. 14, 81–96. http://dx.doi.org/10.1002/rem.20023.

Curie, F., Ducharne, A., Sebilo, M., Bendjoudi, H., 2009. Denitrification in a hyporheic riparian zone controlled by river regulation in the Seine river basin (France). Hydrol. Process. 23, 655–664. http://dx.doi.org/10.1002/hyp.7161.

Cypher, J.A., Lemke, L.D., 2009. Multiple working transport hypotheses in heterogeneous glacial aquifer system. Ground Water Monitoring & Remediation. 29 (3), 105 – 119. http://dx.doi.org/10.1111/j.1745-6592.2009.01245.x.

Dähnke, K., Thamdrup, B., 2016. Isotope fractionation and isotope decoupling during anammox and denitrification in marine sediments. Limnol. Oceanogr. 61, 610–624. http://dx.doi.org/10.1002/lno.10237.

Dagan, G., 1989. Flow and Transport in Porous Formations. Springer Verlag, Heidelberg.

Daily, W., Ramirez, A., Binley, A., LaBrecque, D., 2004. Electrical resistance tomography. Leading Edge. 23(5), 438 – 442. http://dx.doi.org/10.1190/1.1729225.

Daims, H., Lebedeva, E.L., Pjevac, P., Han, P., Herbold, C., Albertsen, M., Jehmlich, N., Palatinszky, M., Vierheilig, J., Bulaev, A., Kirkegaard, R.H., von Bergen, M., Rattei, T., Bendinger, B., Nielsen, P.H. and Wagner, M., 2015. Complete Nitrification by Nitrospira Bacteria. Nature. 528, 504-509. http://dx.doi.org/10.1038/nature16461.

Dansgaard, W., 1964. Stable isotopes in precipitation. Tellus. 16, 436–468. http://dx.doi.org/10.1111/j.2153-3490.1964.tb00181.x.

Datry, T., Malard, F., Gibert, J., 2004. Dynamics of solutes and dissolved oxygen in shallow urban groundwater below a stormwater infiltration basin. Sci. Total Environ. 329(1–3), 215-229. http://dx.doi.org/10.1016/j.scitotenv.2004.02.022.

Davies, J.A., Yabusaki, S.B., Carl, I.S., Zachaora, J.M., Curtis, G.P., Redden, G.D., Criscenti, L.J., Honeyman, B.D., 2004. Assessing conceptual models for subsurface reactive transport of inorganic contaminants. Eos Trans. AGU. 85 (44), 449 – 455. http://dx.doi.org/10.1029/2004EO440002.

Deak, J., Coplen, T., 1996. Identification of Holocene and Pleistocene groundwaters in Hungary using oxygen and hydrogen isotopic ratios. Isotopes in Water Resources Management (International Atomic Energy Agency, Vienna, Austria, IAEA-SM-336/25P). 1, 438. http://www.iaea.org/inis/collection/NCLCollectionStore/_Public/27/061/27061798.pdf.

Dehnert, J., Leven, C., Trabitzsch, R., Weiss, H., 2010. Determination of high-resolution concentration profiles of nitrate in groundwater by means of direct push soundings (in German). Grundwasser. 15, 221-230. http://dx.doi.org/10.1007/s00767-010-0150-9.

References

de Marsily, G., Delay, F., Goncalves, J., Renard, Ph., Teles, V., Violette, S., 2005. Dealing with spatial heterogeneity. Hydrogeol. J. 13,161–183. http://dx.doi.org/10.1007/s10040-004-0432-3.

Dentith, M., Mudge, S.T., 2014. Geophysics for Mineral Exploration Geoscientist. Cambride University Press, UK.

Denver, J.M., Ator, S.W., Lang, M.W., Fisher, T.R., Gustafson, A.B., Fox, R., Clune, J.W., McCarty, G.W., 2014. Nitrate fate and transport through current and former depressional wetlands in an agricultural landscape, Choptank Watershed, Maryland, United States. J. Soil Water Conserv. 69, 1−16. http://dx.doi.org/10.2489/jswc.69.1.1.

Deutsch, W.J., Siegel, R., 1997. Groundwater Geochemistry: Foundamentals and Applications to Contamination. CRC Press, Inc, New York.

Devic, G., Djordjevic, D., Sakan, S., 2014. Natural and anthropogenic factors affecting the groundwater quality in Serbia, Sci. Total Environ. 468–469, 933-942. http://dx.doi.org/10.1016/j.scitotenv.2013.09.011.

Diaz, R.J., Rosenberg, R., 2008. Spreading dead zones and consequences for marine ecosystems. Science. 321 (5891), 926–929. http://dx.doi.org/10.1126/science.1156401.

Dietrich, P., Leven, C., 2009. Direct push-technologies, in: Kirsch, R. (Ed.), Groundwater Geophysics: A Tool for Hydrogeology. Springer, Berlin, pp. 347 – 366. http://dx.doi.org/ 10.1007/978-3-540-88405-7_12.

Dietrich, P., Tronicke, J., 2009. Integrated analysis and interpretation of crosshole P- and S-wave tomograms: A case study. Near Surface Geophys. 7, 101–109. http://dx.doi.org/10.3997/1873-0604.2008041.

DiSpirito, A.A., Hooper, A.B., 1986.Oxygen exchange between nitrate molecules during nitrite oxidation by *Nitrobacter*. J. Biol. Chem. 261, 10534–10537.

Dogan, M., Remke, L.V.D., Bohling, G.C., Butler Jr., J.J., Hyndman, D.W., 2011. Hydrostratigraphic analysis of the MADE site with full-resolution GPR and direct-push hydraulic profiling. Geophys. Res. Lett. 38, L06405. http://dx.doi.org/10.1029/2010GL046439.

Dogramaci, S., Skrzypek, G., Dodson, W., Grierson, P.F., 2012. Stable isotope and hydrochemical evolution of groundwater in the semi-arid Hamersley Basin of subtropical northwest Australia. J. Hydrol. 475, 281-293. http://dx.doi.org/10.1016/j.jhydrol.2012.10.004.

Ducommun, P., Boutsiadou, X., Hunkeler, D., 2013. Direct-push multilevel sampling system for unconsolidated aquifers. Hydrogeol. J. 21, 1901 - 1908. http://dx.doi.org/10.1007/s10040-013-1035-7.

Duff, J.H., Tesoriero, A.J., Richardson, W.B., Strauss, E.A., Munn, M.D., 2008. Whole-Stream response to nitrate loading in three streams draining agricultural landscapes. J. Environ. Qual. 37, 1133-1144. http://dx.doi.org/10.2134/jeq2007.0187.

Dzakpasu, M., Scholz, M., Harrington, R., McCarthy, V., Jordan, S., 2014. Groundwater quality impacts from a full-scale integrated constructed wetland. Groundwater Monitoring & Remediation. 34, 51–64. http://dx.doi.org/10.1111/gwmr.12059.

Eberts, S.M., Thomas, M.A., Jagucki, M.L., 2013. The quality of our Nation's waters – Factors affecting public-supply-well vulnerability to contamination – Understanding observed water quality and anticipating future water quality. U.S. Geological Supply Circular 1385, U.S. Geol. Surv., Reston, VA (http://pubs.usgs.gov/circ/1385/pdf/Cir1385.pdf).
Einarson, M.D. 2006. Multi-Level ground water monitoring, in: Nielsen, D. M. (Ed.), Practical Handbook of Environmental Site Characterization and Ground-Water Monitoring, CRC Press, pp. 807-848.

Einarson, M.D., Cherry, J.A., 2002. A new multilevel ground water monitoring system using multichannel tubing. Groundwater Monitoring & Remediation. 22, 52–65. http://dx.doi.org/10.1111/j.1745-6592.2002.tb00771.x.

Einsiedl, F., Mayer, B., 2006. Hydrodynamic and microbial processes controlling nitrate in a fissured-porous karst aquifer of the Franconian Alb, Southern Germany. Environ. Sci. Technol. 40, 6697–702. http://dx.doi.org/10.1021/es061129x.

Ehlers, L.J., Luthy, R.G., 2003. Contaminant bioavailability in soil and sediment. Environ. Sci. Technol. 37(15), 295A – 302A. http://dx.doi.org/10.1021/es032524f.

Elango, L., Kannan, R., 2007. Rock–water interaction and its control on chemical composition of groundwater, in: Sarkar, D., Datta, R., Hannigan, R. (Eds.), Developments in Environmental Science - Concepts and Applications in Environmental Geochemistry, Elsevier, Amsterdam, vol. 5, chapter 11, pp. 229-243.

Elliott, E.M., Kendall, C., Boyer, E.W., Burns, D.A., Lear, G.G., Golden, H.E., Harlin, K., Bytnerowicz, A., Butler, T.J., Glatz, R., 2009. Dual nitrate isotopes in dry deposition: Utility for partitioning NO_x source contributions to landscape nitrogen deposition. J. Geophys. Res. 114, G04020. http://dx.doi.org/10.1029/2008JG000889.

Ellsworth, T.R., 1996. Influence of transport variability structure on parameter estimation and model discrimination, in: Corwin D.L., Loague, K. (Eds.), Application of GIS to the Modeling of Non-Point Source Pollution in the Vadoze Zone, SSSA Special Publication No. 48, Soil Science Society of America, Madison, WI, pp. 101 - 130.

Ehrlich, A., 1988. Risk Assessment Guidelines Update. EPA 600/D-88/264. Environmental Protection Agency, Washington, D.C., U.S.

Elsner, M., 2010. Stable isotope fractionation to investigate natural transformation mechanisms of organic contaminants: principles, prospects and limitations. J. Environ. Monit. 12, 2005 – 2031. http://dx.doi.org/10.1039/C0EM00277A.

Engdahl, N.B., Weissmann, G.S., Bonal, N.D., 2010. An integrated approach to shallow aquifer characterization: combining geophysics and geostatistics. Comput. Geosci. 14(2), 217 – 229. http://dx.doi.org/10.1007/s10596-009-9145-y.

Epstein, S., Mayeda, T., 1953. Variation of O^{18} content of waters from natural sources. Geochim. Cosmochim. Ac. 4, 213-224. http://dx.doi.org/10.1016/0016-7037(53)90051-9.

Falgàs, E., Ledo, J., Benjumea, B., Queralt, P., Marcuello, A., Teixidó, T., Martí, A, 2011. Integrating hydrogeological and geophysical methods for the characterization of a deltaic aquifer system. Surv. Geophys. 32(6), 857 - 873. http://dx.doi.org/10.1007/s10712-011-9126-2.

Fang, Y., Koba, K., Makabe, A., Takahashi, C., Zhu, W., Hayashi, T., Hokari, A.A., Urakawa, R., Bai, E., Houlton, B.Z., 2015. Microbial denitrification dominates nitrate losses from forest ecosystems. Proc. Natl. Acad. Sci. U. S. A. 112, 1470e1474.

Fenech, C., Rock, L., Nolan, K., Tobin, J., Morrissey, A., 2012. The potential for a suite of isotope and chemical markers to differentiate sources of nitrate contamination: A review. Water Res. 46(7), 2023-2041. ISSN 0043-1354, http://dx.doi.org/10.1016/j.watres.2012.01.044.

Fenton, O., Richards, K.G., Kirwan, L., Khalil, M.I., Healy, M.G., 2009. Factors affecting nitrate distribution in shallow groundwater under a beef farm in South Eastern Ireland, J. Environ. Manage. 90(10), 3135-3146, http://dx.doi.org/10.1016/j.jenvman.2009.05.024.

Filippini, M., Stumpp, C., Nijenhuis, I., Richnow, H.H., Gargini, A., 2015. Evaluation of aquifer recharge and vulnerability in an alluvial lowland using environmental tracers. J. Hydrol. 529 (Part 3), 1657-1668. http://dx.doi.org/10.1016/j.jhydrol.2015.07.055.

References

Fleming, R., Ford,M., 2002. Comparison of storage,treatment, utilization and disposal systems for human and livestock wastes. http://agrienvarchive.ca/res_papers/download/fleming_wastes.pdf.

Flynn, T.M., Sanford, R.A., Ryu, H., Bethke, C.M., Levine, A. D., Ashbolt, N.J., Santo Domingo, J.W., 2013. Functional microbial diversity explains groundwater chemistry in a pristine aquifer. BMC Microbiol. 13, 146. http://dx.doi.org/10.1186/1471-2180-13-146.

Flynn, T.M., O'Loughlin, E.J., Mishra, B., DiChristina, T.J., Kemner, K.M., 2014. Sulfur-mediated electron shuttling during bacteria iron reduction. Sci. 344 (6187), 1039 – 42. http://dx.doi.org/10.1126/science.1252066.

Freeze, R.A., Cherry, J.A., 1979. Groundwater, 1st ed. Prentice-Hall, Englewood Cliffs, New Jersey.

French, H.K., Kästner, M., van der Zee, S.E.A.T.M., 2014. New approaches for low-invasive contaminated site characterization, monitoring and modeling. Environ. Sci. Pollut. Res. 21(15), 8893 - 8896. http://dx.doi.org/10.1007/s11356-014-2840-9.

Frey, C., Dippner, J. W., Voss, M., 2014. Close coupling of N-cycling processes expressed in stable isotope data at the redoxcline of the Baltic Sea. Global Biogeochem. Cycles. 28, 974–991. http://dx.doi.org/10.1002/2013GB004642.

Friedrich, M.W., Finster, K.W., 2014. Geochemistry - How sulfur beats iron. Sci. 344, 974-975. http://dx.doi.org/10.1126/science.1255442.

Foster, A.R., Veatch, M.D., Baird, S.L., 1987. Hazardous waste geophysics. The Leading Edge. 6(8), 8–13. http://dx.doi.org/10.1190/1.1439424.

Fukada, T., Hiscock, K. M., Dennis, P. F., Grischek, T., 2003. A dual isotope approach to identify denitrification in groundwater at a river-bank infiltration site. Water Res. 37(13), 3070-3078. http://dx.doi.org/10.1016/S0043-1354(03)00176-3.

Gabàs, A., Macau, A., Benjumea, B., Bellmunt, F., Figueras, S., Vilà, M., 2014. Combination of geophysical methods to support urban geophysical mapping. Surv. Geophys. 35 (4), 983 - 1002. http://dx.doi.org/10.1007/s10712-013-9248-9.

Gaillardet, J., Dupre, B., Louvat, P., Allegre, C. J., 1999. Global silicate weathering and CO_2 consumption rates deduced from the chemistry of large rivers. Chem. Geol. 159, 3–30. http://dx.doi.org/10.1016/S0009-2541(99)00031-5.

Gallardo, L.A., Meju, M.A., 2003. Characterization of heterogeneous near-surface materials by joint 2D inversion of dc resistivity and seismic data. Geophys. Res. Lett., 30, 1658, http://dx.doi.org/10.1029/2003GL017370.

Galloway, J.N., Townsend, A.R., Erisman, J.W., Bekunda, M., Cai, Z., Freney, J.R., Martinelli, L.A., Seitzinger, S.P., Sutton, M.A., 2008. Transformation of the nitrogen cycle: recent trends, questions, and potential solutions. Science. 320 (5878), 889 – 92. http://dx.doi.org/10.1126/science.1136674.

Garner, B.D., Mahler, B.J., 2007. Relation of specific conductance in ground water to intersection of flow paths by wells, and associated major ion and nitrate geochemistry, Barton Springs segment of the Edwards aquifer, Austin, Texas, 1978 - 2000, Rep. 2007-5002. U.S. Geol. Surv., Austin, TX (https://pubs.usgs.gov/sir/2007/5002/pdf/sir07-5002_508.pdf).

Gasperikova, E., Hubbard, S.S., Watson, D. B., Baker, G.S., Peterson, J.E., Kowalsky, M. B., Smith, M., Brooks, S., 2012. Long-term electrical resistivity monitoring of recharge-induced contaminant plume behavior. J. Contam. Hydrol. 142–143, 33-49. http://dx.doi.org/10.1016/j.jconhyd.2012.09.007.

References

Gaye, B., Nagel, B. Dähnke, K., Rixen, T., Emeis, K.-C., 2013. Evidence of parallel denitrification and nitrite oxidation in the ODZ of the Arabian Sea from paired stable isotopes of nitrate and nitrite. Global Biogeochem. Cycles. 27, 1059–1071. http://dx.doi.org/10.1002/2011GB004115.

Gazoty, A., Fiandaca, G., Pedersen, J., Auken, E., Christiansen, A.V., Pedersen, J.K., 2012. Application of time domain induced polarization to mapping of lithotypes in a landfill site. Hydro. Earth Syst. Sci. 16, 1793 – 1804. http://dx.doi.org/10.5194/hess-16-1793-2012.

Gentine, P., Troy, T.J., Lintner, B.R., Findell, K.L., 2012. Scaling in surface hydrology: Progress and challenges. J. Contemporary Water Res. Educ. 147(1), 28 – 40. http://dx.doi.org/10.1111/j.1936-704X.2012.03105.X.

Gerhard, J.I., Keuper, B.H., Sleep, B.E., 2014. Modeling source zone remediation, in: Keuper, B.H., Stroo, H.F., Vogel, C.M., Ward, C.H. (Eds.), Chlorinated Source Zone Remediation. Springer-Verlag, New York, pp. 113 – 144.

Ghiorse, W.C., Wilson, J.T., 1988. Microbial ecology of the terrestrial subsurface. Adv. Appl. Microbiol. 33, 107–172. http://dx.doi.org/10.1016/S0065-2164(08)70206-5.

Gibbs, R. J., 1970. Mechanisms controlling world water chemistry. Science. 170, 1088-1090. http://dx.doi.org/10.1126/science.170.3962.1088.b

Gish, T.J., Dulaney, W.P., Kung, K-J.S., Daughtry, C.S.T., Doolittle, J.A., Miller P.T., 2002. Evaluating use of ground penetrating radar for identifying subsurface flow pathways. Soil Sci. Soc. Am. J. 66, 1620 - 1629.

Godfrey, L.V., Glass, J.B., 2011. The geochemical record of the ancient nitrogen cycle, nitrogen isotopes, and metal cofactors. Methods Enzymol. 486, 483–506. http://dx.doi.org/10.1016/B978-0-12-381294-0.00022-5.

Gonfiantini, R., 1986. Environmental Isotopes in Lake Studies, in: Fritz, P., Fontes, J.C., (Eds.), Handbook of Environmental Isotope Geochemistry. Elsevier, Amsterdam, pp. 113 - 168.

Gourcy, L.L., Groening, M., Aggarwal, P.K., 2005. Stable oxygen and hydrogen isotopes in precipitation. In: Aggarwal, P.K., Gat, J.R., Froehlich, K.F. (eds.) Isotopes in the Water Cycle. Springer, Dordrecht.

Graf, W., Trimborn, P., Ufrecht, W., 1994. Isotope geochemical and characterization of karst groundwaters and mineral waters in the Upper Muschelkalk from the Stuttgart area under the special consideration of Oxygen-18 and Sulfur-34 (in German). Schriftenreihe des Amtes für Umweltschutz. 2, 75–115.

Granger, J., Sigman, D.M., Needoba, J.A., Harrison, P.J., 2004. Coupled nitrogen and oxygen and isotope fractionation of nitrate during assimilation by cultures of marine phytoplankton. Limnol. Oceanogr. 49, 1763 – 1773. http://dx.doi.org/10.2008.53.6.2533.

Granger J., Wankel S. D., 2016. Isotopic overprinting of nitrification on denitrification as a ubiquitous and unifying feature of environmental nitrogen cycling. Proc. Natl. Acad. Sci. U.S.A. 113, E6391–E6400. http://dx.doi.org/10.1073/pnas.1601383113.

Granger, J., Sigman, D.M., Lehmann, M.F., Tortell, P.D., 2008. Nitrogen and oxygen isotope fractionation during dissimilatory nitrate reduction by denitrifying bacteria. Limnol. Oceanogr. 53, 2533–2545. http://dx.doi.org/10.4319/lo.2008.53.6.2533.

Grapes, T.R., Bradley, C., Petts, G.E., 2006. Hydrodynamics of floodplain wetlands in a chalk catchment: the River Lambourn, UK. J. Hydrol. 320 (3-4), 324-341. http://dx.doi.org/10.1016/j.jhydrol.2005.07.028.

Greenberg, M.S., Chapman, P.M., Allan, I.J., Anderson, K.A., Apitz, S.E., Beegan, C., Bridges, T.S., Brown, S.S., Cargill, J.G., McCulloch, M.C., Menzie, C.A., Shine, J.P., Parkerton, T.F., 2014. Passive sampling methods for contaminated sediments: Risk assessment and management. Integr. Environ. Assess. Manag. 10, 224–236. http://dx.doi.org/10.1002/ieam.1511.

References

Greene, E.A., Hubert, C., Nemati, M., Jenneman, G.E., Voordouw, G., 2003. Nitrite reductase activity of sulphate-reducing bacteria prevents their inhibition by nitrate-reducing, sulphide-oxidizing bacteria. Environ. Microbiol. 5, 607–617. http://dx.doi.org/10.1046/j.1462-2920.2003.00446.x.

Greer, B.M., Burbey, T.J., Zipper, C.E., Hester, E.T., 2017. Electrical resistivity imaging of hydraulic flow through surface coal mine valleys with comparison to other landforms. Hydrol. Process. 31(12), 2244 – 2260. http://dx.doi.org/10.1002/hyp.11180.

Griesemer, J., 2001. Diving plumes: The development and investigation of dissolved contaminant plumes that migrate vertically downward to depths below the water table. Site Remediation News. 13 (1), 7 – 10. http://www.nj.gov/dep/srp/news/2001/0105_04.htm.

Griffiths, N. A., Jackson, C. R., McDonnell, J. J., Klaus, J., Du, E., Bitew, M.M., 2016. Dual nitrate isotopes clarify the role of biological processing and hydrologic flow paths on nitrogen cycling in subtropical low-gradient watersheds. J. Geophys. Res. Biogeosci. 121,422–437. http://dx.doi.org/10.1002/2015JG003189.

Guay, B., Eastoe, C., 2007. Tracking groundwater sources with environmental isotopes, Southwest Hydrol. 6, 18 - 19. http://www.swhydro.arizona.edu/archive/V6_N4/feature2.pdf.

Guay, B., Eastoe, C., Bassett, R., Long, A., 2006. Identifying sources of groundwater in the lower Colorado River valley, USA, with $\delta^{18}O$, δD and ^{3}H: Implications for river accounting. Hydrogeol. J. 14(1), 146-158. http://dx.doi.org/10.1007/s10040-004-0334-4.

Günther, T., Rücker, C., Spitzer, K., 2006. Three-dimensional modelling and inversion of dc resistivity data incorporating topography – II. Inversion. Geophys. J. Int. 166, 506–517. http://dx.doi.org/10.1111/j.1365-246X.2006.03011.x.

Gujer, W., Jenkins, D., 1975. A nitrification model for the contact stabilization activated sludge process. Water Res. 9 (5 - 6), 561 - 566. http://dx.doi.org/10.1016/0043-1354(75)90082-2.

Gupta, H.V., Clark, M.P., Vrugt, J.A., Abramowitz, G., Ye, M., 2012. Towards a comprehensive assessment of model structural adequacy. Water Resour. Res. 48, W08301. http://dx.doi.org/10.1029/2011WR011044.

Gurumurthy, G.P., Balakrishna, K., Tripti, M., Riotte, J., Audry, S., Braun, J.-J., Lambs, L., Udaya Shankar, H. N., 2015. Sources of major ions and processes affecting the geochemical and isotopic signatures of subsurface waters along a tropical river, Southwestern India. Environ. Earth Sci., 73, 333 - 346. http://dx.doi.org/10.1007/s12665-014-3428-x.

Habberjam, G.M., 1979. Apparent resistivity observations and use of the square array technique, in: Saxov, S., Flathe, H. (Eds.), Geoexploration Monographs series 1, no. 9, pp. 1 - 52.

Haeni, F.P., 1988. Application of seismic-refraction techniques to hydrologic studies. Technical Report TWRI — 02-D2. United States Geological Survey.

Händel, F., Dietrich, P., 2012. Relevance of deterministic structures for modeling of transport: the Lauswiesen case study. Ground Water, 50(6), 935-942. http://dx.doi.org/10.1111/j.1745-6584.2012.00948.x.

Hahn, W., Schädel, K., 1973. Explanations of the geological map of Tübingen and its surroundings 1:50000 (in German). Editor: Landesamt, Baden-Württemberg, Freiberg, 66pp; 15 Figures.

Haggerty, R., Harvey, C. F., Freiherr von Schwerin, C., Meigs, L. C., 2004. What controls the apparent timescale of solute mass transfer in aquifers and soils? A comparison of experimental results. Water Resour. Res. 40, W01510. http://dx.doi.org/ 10.1029/2002WR001716.

Hall, R.O., Baker, M. A., Arp, C. D., Koch, B. J., 2009. Hydrologic control of nitrogen removal, storage, and export in a mountain stream. Limnol. Oceanogr. 54(6), 2128-2142. http://dx.doi.org/10.4319/lo.2009.54.6.2128.

References

Halm, D., Grathwohl, P., 2005. Integrated soil and water protection against diffuse pollution SOWA. Proceedings of European Geosciences Union General Assembly, Vienna, Austria, April 24 – 29, 2005, Geophysical Research Abstracts 7 (05086) SRef-ID: 1607-7962/gra/EGU05-A-05086.

Han, W.S., Kim, K.Y., Choung, S., Jeong, J., Jung, N.H., Park, E., 2014. Non-parametric simulations-based conditional stochastic predictions of geologic heterogeneities and leakage potentials for hypothetical CO_2 sequestration sites. Environ. Earth Sci. 71(6), 2739 – 2752. http://dx.doi.org/10.1007/s12655-013-2653-z.

Hao, X., Chang, C., 2003. Does long-term heavy cattle manure application increase salinity of a clay loam soil in semi-arid southern Alberta? Agric. Ecosyst. Environ. 94 (1), 89-103. http://dx.doi.org/10.1016/S0167-8809(02)00008-7.

Hassan, A., Pohlmann, K., Champan, J., 2002. Modeling groundwater flow and transport of radionuclides at Amchitka Island's underground nuclear tests: Milrow, Long Shot, and Cannikin (DOE/NV/11508-51 - Publication No. 45172). Desert Research Institute, Desert Research Institute, Las Vegas, NV.

Hassan, A., Chapman , J., 2006. Verification and uncertainty reduction of Amchitka underground nuclear testing models (DOE/NV/13609-46 - Publication No. 45216). Desert Research Institute, Las Vegas, NV.

Hassan, A.E., 2004. Validation of numerical ground water models used to guide decision making. Ground Water. 42(2), 277–290. http://dx.doi.org/10.1111/j.1745-6584.2004.tb02674.x.

Hauck, C., Vieira, G., Gruber, S., Blanco, J., Ramos, M., 2007. Geophysical identification of permafrost in Livingston Island, maritime Antarctica. J. Geophys. Res. 112, F02S19, http://dx.doi.org/10.1029/2006JF000544.

Hausmann, J., Steinel, H., Kreck, M., Werban, U., Vienken, T., Dietrich, P., 2013. Two-dimensional geomorphological characterization of a filled abandoned meander using geophysical methods and soil sampling. Geomorphol. 201(1), 335 – 343. http://dx.doi.org/10.1016/j.geomorph.2013.07.009.

Hayakawa, A., Hatakeyama, M., Asano, R., Ishikawa, Y., Hidaka, S., 2013. Nitrate reduction coupled with pyrite oxidation in the surface sediments of a sulfide-rich ecosystem. J. Geophys. Res. Biogeosci.118, 639–649. http://dx.doi.org/10.1002/jgrg.20060.

He, Q., He, Z., Joyner, D.C., Joachimiak, M., Price, M.N., Yang, Z.K., Yen, H.B., Hemme, C.L., Chen, W., Fields, M.M., Stahl, D.A., Keasling, J.D., Keller, M., Arkin, A.P., Hazen, T.C, Wall, J.D., Zhou, J., 2010. Impact of elevated nitrate on sulfate-reducing bacteria: a comparative study of Desulfovibrio vulgaris. ISME J. 4,1386–1397. http://dx.doi.org/ 10.1038/ismej.2010.59.

Heaton, T.H.E., 1986. Isotopic studies of nitrogen pollution in the hydrosphere and atmosphere: A review. Chem. Geol.: Isotope Geoscience section. 59, 87 – 102. http://dx.doi.org/10.1016/0168-9622(86)90059-X.

Heffernan, J. B., Cohen, M. J., Frazer, T. K., Thomas, R. G., Rayfield, T. J., Gulley, J., Martin, J. B., Delfino, J. J., Graham, W. D., 2010. Hydrologic and biotic influences on nitrate removal in a subtropical spring-fed river. Limnol. Oceanogr. 55, 249–263. http://dx.doi.org/10.4319/lo.2010.55.1.0249.

Hendry, M.J., Barbour, S.L., Schmeling, E.E., 2016. Defining near-surface groundwater flow regimes in the semi-arid glaciated plains of North America. Isotopes Environ. Health Stud. 2016. 52(3), 1 - 11. http://dx.doi.org/10.1080/10256016.2016.1092966.

Hermana, R., 2001. An introduction to electrical resistivity in geophysics. Am. J. Phys. 69 (9), 943 – 952. http://dx.doi.org/10.1119/1.1378013.

Hill, A.R., Labadia, C.F., Sanmugadas, K., 1998. Hyporheic zone hydrology and nitrogen dynamics in relation to the streambed topography of a N-rich stream. Biogeochem. 42, 285–310. http://dx.doi.org/10.1023/A:1005932528748.

References

Hinkle, S.R., Böhlke, J.K., Duff, J.K., Morgan, D.S., Weick, R.J., 2007. Aquifer-scale controls on the distribution of nitrate and ammonium in ground water near La Pine, Oregon, U.S.A. J. Hydrol. 333, 486–503. http://dx.doi.org/10.1016/j.jhydrol.2006.09.013.

Hirsch, M., Bentley, L.R., Dietrich, P., 2008. A comparison of electrical resistivity, ground penetrating radar and seismic refraction results at a river terrace site. J. Environ. Eng. Geophys. 13(4), 325–333.

Hodlur, G.K., Dhakate, R., 2010. Correlation of vertical electrical sounding and electrical borehole log data for groundwater exploration. Geophys. Prospect. 58, 485 - 503. http://dx.doi.org/10.1111/j.1365-2478.2009.00831.x.

Hoffmann, R., Dietrich, P., 2004. An approach to determine equivalent solutions to the geoelectrical 2D inversion problem. J. Appl. Geophys. 56(2), 79-91. http://dx.doi.org/10.1016/j.jappgeo.2004.03.005.

Holbrook, W.S., Riebe, C.S., Elwaseif, M., Hayes, J.L., Basler-Reeder, K., Harry, D.L., Malazian, A., Dosseto, A., Hartsough, P.C., Hopmans, J.W., 2014. Geophysical constraints on deep weathering and water storage potential in the Southern Sierra Critical Zone Observatory. Earth Surf. Proc. Land. 39, 366–380. http://dx.doi.org/ 10.1002/esp.3502.

Hollocher, T.C., Tate, M.E., Nicholas, D.J.D., 1981. Oxidation of ammonia by Nitrosomonas europaea. J. Biol. Chem. 256,10834– 10836.

Holloway, J.M., Dahlgren, R.A., Hansen, B., Casey, W.H., 1998. Concentration of bedrock nitrogen to high nitrate concentrations in stream water. Nature. 395, 785 – 788. http://dx.doi.org/10.1038/27410.

Homoncik, S.C., MacDonald, A.M., Heal, K.V., Dochartaigh, B.É.Ó., Ngwenya, B.T., 2010. Manganese concentrations in Scottish groundwater. Sci. Total Environ. 408 (12), 2467-2473. http://dx.doi.org/10.1016/j.scitotenv.2010.02.017.

Hosono, T., Tokunaga, T., Kagabu, M., Nakata, H., Orishikida, T., Lin, I.-T., Shimada, J., 2013. The use of $\delta^{15}N$ and $\delta^{18}O$ tracers with an understanding of groundwater flow dynamics for evaluating the origins and attenuation mechanisms of nitrate pollution. Water Res. 47, 2661 - 2675. http://dx.doi.org/10.1016/j.watres.2013.02.020.

Hosono, T., Tokunaga, T., Tsushima, A., Shimada, J., 2014. Combined use of $\delta^{13}C$, $\delta^{15}N$, and $\delta^{34}S$ tracers to study anaerobic bacterial processes in groundwater flow systems. Water Res. 54, 284-296. http://dx.doi.org/10.1016/j.watres.2014.02.005.

Hou, B., Mauger, A., 2005. How well does remote sensing aid paleochannel identification? - An example from the Harris Greenstone Belt, MESA Journal, 38, 46 - 52.

Hounslow, A., 1995. Water Quality Data: Analysis and Interpretation. CRC Press, Inc., New York.

Hubbard, S.S., Chen, J., Peterson, J., Majer, E., Williams, K., Swift, D.J., Mailloux, B., Rubin, Y., 2001. Hydrogeological characterization of the South Oyster bacterial transport site using geophysical data. Water Resour. Res. **37**(10), 2431–2456. http://dx.doi.org/10.1029/2001WR000279.

Hubert, C., and Voordouw, G., 2007. Oil field souring control by nitrate-reducing *Sulfurospirillum* spp. that outcompete sulfate-reducing bacteria for organic electron donors. Appl. Environ. Microbiol. 73(8), 2644–2652. http://dx.doi.org/10.1128/AEM.02332-06.

Hulth, S., Aller, R.C., Glibert, F., 1999. Coupled anoxic nitrification/manganese reduction in marine sediments. Geochim. Cosmochim. Acta. 63, 49–66. http://dx.doi.org/10.1016/S0016-7037(98)00285-3.

Hsu, H.L., Yanites, B.J., Chen, C.C., Chen, Y.G., 2010. Bedrock detection using 2D electrical resistivity imaging along the Peikang River, central Taiwan. Geomorphol. 114, 406–414. http://dx.doi.org/10.1016/j.geomorph.2009.08.004.

References

Ibrahim, T.G., Thornton, S.F., Wainwright, J. 2010. Interplay of geomorphic and hydrogeologic features at reach- and channel unit-scales on riverbed hydrology and hydrochemistry: a conceptual model in the Lower Coal Measures, South Yorkshire, UK. Hydrogeol. J. 18(6), 1391-1411. http://dx.doi.org/10.1007/s10040-010-0623-z.

Ingraham, N. L., 1998. Isotopic variation in precipitation, in: Kendall, C., McDonnell, J.J. (Eds.), Isotope Tracers in Catchment Hydrology. Elsevier, New York, pp. 87 – 118.

Interstate Technology and Regulatory Council (ITRC), 2003. Technical and regulatory guidance for the Triad approach: A new paradigm for environmental project management (SCM-1). Prepared by the ITRC Sampling, Characterization and Monitoring Team. http://www.itrcweb.org/SCM-1.pdf (accessed 20.10.16).

Jackson, P., 2004. Determination of inorganic anions in drinking water by ion chromatography. Application Note 133. https://tools.thermofisher.com/content/sfs/brochures/AN-133-IC-Inorganic-Anions-Drinking-Water-AN71691-EN.pdf (accessed March 12, 2018).

Jahangir, M.M.R., Johnston, P., Khalil, M.I., Richards, K.G., 2012. Linking hydrogeochemistry to nitrate abundance in groundwater in agricultural settings in Ireland. J. Hydrol. 448 - 449, 212 - 222. http://dx.doi.org/10.1016/j.jhydrol.2012.04.054.

Jakobsen, R., Postma, D., 1999. Redox zoning, rates of sulfate reduction and interactions with Fe-reduction and methanogenesis in a shallow sandy aquifer, Rømø, Denmark. Geochim. Cosmochim. Acta 63, 137–151 (1999). http://dx.doi.org/10.1016/S0016-7037(98)00272-5.

Jakubick, A.T., Kahnt, R., 2002. Remediation oriented use of conceptual site models at WISMUT GmbH: Remediation of the Trünzig tailings management area, in: Merkel, B.J., Planer-Friedrich, B., Wolkersdorfer, C. (Eds.),. Uranium in the Aquatic Environment. Springer, Berlin, pp. 9 - 24.

Jankovic, I., Fiori, A., Dagan, G., 2006. Modelling flow and transport in highly heterogeneous three-dimensional aquifers: Ergodicity, Gaussianity and anomalous behavior – 1. Conceptual issues and numerical simulations. Water Resour. Res. 42, W06D12. http://dx.doi.org/10.1029/2005/WR004734.

Jarvis, M., Larsson, M., 2001. Modeling macropore flow in soils: Field validation and use for management purposes, in: National Research Council (Ed.), Conceptual Models of Flow and Transport in the Fractured Vadose Zone. National Academy Press, Washington, DC, pp. 189 - 215.

Jiang, X.-W., Wan, L., Wang, J.-Z., Yin, B.-X., Fu, W.-X., Lin, C.-H., 2014. Field identification of groundwater flow systems and hydraulic traps in drainage basins using a geophysical method. Geophys. Res. Lett. 41(8), 2812–2819. http://dx.doi.org/10.1002/2014GL059579.

Jiang, Y., Wu, Y., Groves, C., Yuan, D., Kambesis, P., 2009. Natural and anthropogenic factors affecting the groundwater quality in the Nandong karst underground river system in Yunan, China. J. Contam. Hydrol. 109(1–4), 49-61. http://dx.doi.org/10.1016/j.jconhyd.2009.08.001.

Ji, B., Yang, K., Zhu, L., Jiang, Y., Wang, H., Zhou, J., Zhang, H., 2015. Aerobic denitrification: A review of important advances of the last 30 years. Biotechnol. Bioprocess Eng. 20, 643 – 651. http://dx.doi.org/10.1007/s12257-015-0009-0.

Johnsen, S. J., Dansgaard, W., White, J. W. C., 1989. The origin of Arctic precipitation under present and glacial conditions. Tellus B. 41B, 452–468. http://dx.doi.org/10.1111/j.1600-0889.1989.tb00321.x.
Johnson, T.C., Slater, L.D., Ntarlagiannis, D., Day-Lewis, D., Elwaseif, M., 2012. Monitoring groundwater surface water interaction using time-series and time-frequency analysis of transient three-dimensional electrical resistivity changes. Water Resour. Res. 48, W07506. http://dx.doi.org/10.1029/2012WR011893.

Jorgensen, S.E., Fath, B.D., 2011. Fundamentals of Ecological Modelling: Applications in Environmental Management and Research, fourth ed. Elsevier, Amsterdam.

References

Jouzel, J., Merlivat, L., Lorius, C., 1982. Deuterium excess in an East Antarctic ice core suggests higher relative humidity at the oceanic surface during the last glacial maximum. Nature. 299(5885), 688–691. http://dx.doi.org/10.1038/299688a0.

Kadlec, R.H., Wallace, S., 2008. Treatment Wetlands, 2nd edition. CRC Press, Inc., New York.

Käser, D., Hunkeler, D., 2016. Contribution of alluvial groundwater to the outflow of mountainous catchments. Water Resour. Res. 52, 680–697. http://dx.doi.org/10.1002/2014WR016730.

Kästner, M., Cassiani, G., 2009. ModelPROBE: model driven soil probing, site assessment and evaluation. Rev. Environ. Sci. Biotechnol. 8(2), 131 - 136. http://dx.doi.org/10.1007/s11157-009-9157-z.

Kalbus, E., Schmidt, C., Molson, J. W., Reinstorf, F., Schirmer, M., 2009. Influence of aquifer and streambed heterogeneity on the distribution of groundwater discharge. Hydrol. Earth Syst. Sci. 13, 69–77. http://www.hydrol-earth-syst-sci.net/13/69/2009/.

Kanz, W.,1977. Impacts of agricultural fertilization on groundwater (in German). Geologische Rundschau. 66 (1), 877 – 890. http://dx.doi.org/10.1007/BF01989615.

Kapur, J.N., 2015. Mathematical Modelling, second ed. New Age International, New Delhi.

Karsh, K.L., Granger, J., Kritee, K., 2012. Eukaryotic assimilatory nitrate reductase fractionates N and O isotopes with a ratio near unity. Environ. Sci. Technol. 46(11), 5727–5735. http://dx.doi.org/10.1021/es204593q.

Kaushal, S.S., McCutchan Jr., Lewis, J.W.M., McCutchan, James H., 2006. Land use change and nitrogen enrichment of a rocky mountain watershed. Ecol. Appl. 16 (1), 299 - 312. http://dx.doi.org/10.1890/05-0134.

Kearey, P., Brooks, M., Hill, I., 2002. An Introduction to Geophysical Exploration, 3rd ed. Wiley-Blackwell, Hoboken.

Keller, G.V., Frischknecht, F.C., 1966. Electrical Methods in Geophysical Prospecting. Pergamon Press, Oxford.

Kendall, C., 1998. Tracing nitrogen sources and cycling in catchments, in: Kendall, C., McDonnell, J.J. (Eds.), Isotope Tracers in Catchment Hydrology. Elsevier, Amsterdam, pp. 519 – 576.

Kendall, C., Aravena, R., 2000. Nitrate isotopes in groundwater systems, in: Cook, P., Herczeg, A. (Eds.), Environmental Tracers in Subsurface Hydrology. Kluwer Academic Publishers, Boston, MA, pp. 261–297.

Kendall, C., Caldwell, E.A., 1998. Fundamentals of isotope geochemistry, in: Kendall, C., Mcdonnell, J.J. (Eds.), Isotope Tracers in Catchment Hydrology. Elsevier, Amsterdam, pp. 51 - 86.

Kendall, C., Elliott, E. M., Wankel, S. D., 2007. Tracing Anthropogenic Inputs of Nitrogen to Ecosystems, in Stable Isotopes in Ecology and Environmental Science, Second Edition (eds R. Michener and K. Lajtha), Blackwell Publishing Ltd, Oxford, UK. http://dx.doi.org/10.1002/9780470691854.ch12.

Kessler, A.J., Glud, R. N., Cardenas, M. B., Cook, P. L. M., 2013. Transport zonation limits coupled nitrification-denitrification in permeable sediments. Environ. Sci. Technol. 47, 13404−13411. http://dx.doi.org/10.1021/es403318x.

Keys, W. S., 1989. Borehole Geophysics Applied to Ground-Water Investigation. National Water Association. Dublin, Ohio.

Khalil, M.A., Santos, F.A., 2013. 2D and 3D resistivity inversion of Schlumberger vertical electrical soundings in Wadi El Natrun, Egypt: A case study. J. Appl. Geophy. 89, 116-124. http://dx.doi.org/10.1016/j.jappgeo.2012.11.014.

References

Kim, K.-Ho., Yun, S.-T., Mayer, B., Lee, J.-H., Kim, T.-S., Kim, H.-K., 2014. Quantification of nitrate sources in groundwater using hydrochemical and dual isotopic data combined with a Bayesian mixing model. Agric. Ecosyst. Environ. 199, 369-381. http://dx.doi.org/10.1016/j.agee.2014.10.014.

Kirchner, J.W., 2003. A double paradox in catchment hydrology and geochemistry. Hydrol. Process. 17, 871–874. http://dx.doi.org/10.1002/hyp.5108.

Kirchner, J.W., Feng, X., Neal, C., 2000. Fractal stream chemistry and its implications for contaminant transport in catchments. Letter to Nature. 403, 524 - 527. http://dx.doi.org/10.1038/35000537.

Kirchner, J. W., Tetzlaff, D., Soulsby, C., 2010. Comparing chloride and water isotopes as hydrological tracers in two Scottish catchments. Hydrol. Process. 24, 1631–1645. http://dx.doi.org/10.1002/hyp.7676.

Kingsbury, J.A., 2003. Shallow ground-water quality in agricultural areas of Northern Alabama and Middle Tennessee, 2000-2001. U.S. Geol. Surv. Water- Resources Investigations Report 03-4181. https://pubs.er.usgs.gov/publication/wri034181.

Kirsch, R., Rumpel, H.-M., Scheer, W., Wiederhold, H.(Eds.), 2006. Groundwater Resources in Buried Valleys. Leibniz Institute for Applied Geosciences (GGA-Institut).

Kits, K.D., Sedlacek, C.J., Lebedeva, E.V., Han, P., Bulaev, A., Pjevac, P., Daebeler, A., Romano, S., Albertsen, M., Stein, L.Y., Daims, H., Wagner, M., 2017. Kinetic analysis of a complete nitrifier reveals an oligotrophic lifestyle. Nature. 549, 269 – 272. http://dx.doi.org/10.1038/nature23679.

Kleinert, K.,1976. The groundwater in gravel aquifer of the Upper Neckar Valley between Rottenburg and Tübingen (in German), PhD dissertation, Inst. of Geosci., Univ. of Tübingen, Germany.

Knight, R. J., Endres, A. L., 2005. An introduction to rock physics principles for near-surface geophysics, in: Butler, D. K. (Ed.), Near-Surface Geophysics (Invest. Geophys., no. 13), chap. 3, pp. 31–70. Soc. of Explor. Geophys., Tulsa, OK.

Knight, R., Grunewald, E., Irons, T., Dlubac, K., Song, Y., Bachman, H. N., Grau, B., Walsh, D., Abraham, J. D., Cannia, J., 2012. Field experiment provides ground truth for surface nuclear magnetic resonance measurement. Geophys. Res. Lett., 39, L03304. http://dx.doi.org/10.1029/2011GL050167.

Knödel, K., 2007. Environmental Geology – Handbook of Field Methods and Case Studies. Springer, Berlin Heidelberg.

Knöller, K., Vogt, C., Haupt, M., Feisthauer, S., Richnow, H.-H., 2011. Experimental investigation of nitrogen and oxygen isotope fractionation in nitrate and nitrite during denitrification. Biogeochem. 103 (1), 371−384. http://dx.doi.org/10.1007/s10533-010-9483-9.

Knöller, K., Trettin, R., Strauch, G., 2005. Sulphur cycling in the drinking water catchment area of Torgau-Mockritz (Germany): insights from hydrochemical and stable isotope investigations. Hydrol. Process. 19, 3445-3465. http://dx.doi.org/10.1002/hyp.5980.

Koba, K., Tokuchi, N., Wada, E., Nakajima, T., Iwatsubo, G., 1997. Intermittent denitrification: The application of a ^{15}N natural abundance method to a forested ecosystem. Geochim. Cosmochim. Acta. 61, 5043-5050. http://dx.doi.org/10.1016/S0016-7037(97)00284-6.

Koch, K., Wenninger, J., Uhlenbrook, S., Bonell, M., 2009. Joint interpretation of hydrological and geophysical data: electrical resistivity tomography results from a process hydrological research site in the Black Forest Mountains, Germany. Hydrol. Process. 23, 1501–1513. http://dx.doi.org/10.1002/hyp.7275.

Kohn, J., Soto, D.X., Iwanyshyn, M., Olson, B., Kalischuk, A., Lorenz, K., Hendry, M.J., 2016. Groundwater nitrate and chloride trends in an agriculture intensive area in southern Alberta, Canada. Water Qual. Res. J. 51(1), 47–59. http://dx.doi.org/10.2166/wqrjc.2015.132.

References

Komor, S.C., Anderson, H.W., 1993. Nitrogen isotopes as indicators of nitrate sources in Minnesota sand-plain aquifers. Ground Water. 31, 260 - 270. http://dx.doi.org/doi:10.1111/j.1745-6584.1993.tb01818.x.

Konikow, L. F., Bredehoeft, J. D., 1992. Groundwater models cannot be validated? Adv. Water Resour. 15, 75-83. http://dx.doi.org/10.1016/0309-1708(92)90033-X.

Kornaros, M., Dokianakis, S.N., Lyberatos, G., 2010. Partial nitrification/denitrification can be attributed to the slow response of nitrite oxidizing bacteria to periodic anoxic disturbances. Environ. Sci. Technol. 44 (19), 7245 - 7253. http://dx.doi.org/10.1021/es100564j.

Kosso, P., 2010. Super-rotation of Earth's inner core and the structure of scientific reasoning. GSA Today, 20 (7), 52 - 53. http://dx.doi.org/10.1130/GSATG90GW.1.

Kostic, B., Aigner, T., 2007. Sedimentary architecture and 3D ground-penetrating radar analysis of gravelly meandering river deposits (Neckar Valley, SW Germany). Sedimentology. 54(4), 789 – 808. http://dx.doi.org/10.1111/j.1365-3091.2007.00860.x.

Kozur, H.W., Bachmann, G.H., 2005. Correlation of the Germanic Triassic with the international scale, Albertiana, 32, 21 - 35.

Krásný, J., 2002. Quantitative hardrock hydrogeology in a regional scale. Norges geologiske underøkelse Bulletin. 439, 7 - 14.

Krapac, I.G., Dey, W.S., Roy, W.R., Smyth, C.A., Storment, E., Sargent, S.L., Steele, J.D., 2002. Impacts of swine manure pits on groundwater quality. Environ. Pollut. 120 (2), 475-492. http://dx.doi.org/10.1016/S0269-7491(02)00115-X.

Krasovec, M.L., 2001. Subsurface imaging with reverse vertical seismic profiles, Ph.D. dissertation, Massachusetts Inst. Technol.

Krause, S.; Lewandowski, J.; Grimm, N.B.; Hannah, D.M.; Pinay, G.; McDonald, K.; Martí, E.; Argerich, A.; Pfister, L.; Klaus, J., Battin, T., Larned, S.T., Schelker, J., Fleckenstein, J., Schmidt, C., Rivett, M.O., Watts, G., Sabater, F., Sorolla, A., Turk, V., 2017. Ecohydrological interfaces as hot spots of ecosystem processes. Water Resour. Res. 53, 6359–6376, http://dx.doi.org/10.1002/2016WR019516.

Krautblatter, M., Draebing, D., 2014. Pseudo 3D - P-wave refraction seismic monitoring of permafrost in steep unstable bedrock. J. Geophys. Res.: Earth Surf. 119, 287–299. http://dx.doi.org/10.1002/2012JF002638.

Kroopnick, P.M., Craig, H., 1972. Atmospheric oxygen: isotopic composition and solubility fractionation. Science . 175, 54–5. http://dx.doi.org/10.1126/science.175.4017.54.

Krouse, H.R., Mayer, B., 2000. Sulfur and oxygen isotopes in sulphate, in: Cook, P.G., Herczeg, A.L. (Eds.), Environmental Tracers in Subsurface Hydrology. Kluwer Academic Press, Boston, pp. 195–231.

Krouse, H.R., Grinenko, V.A., 1991. Stable Isotopes: Natural and Anthropogenic Sulphur in the Environment, SCOPE 43. John Wiley and Sons, Chichester.

Krueger, C. J., Radakovich, K. M., Sawyer, T.E., Barber, L.B., Smith, R.L., Field, J.A., 1998. Biodegradation of the surfactant linear alkylbenzenesulfonate in sewage-contaminated groundwater: a comparison of column experiments and field tracer tests. Environ Sci Technol. 32, 3954 – 3961. http://dx.doi.org/10.1021/es9803456.

Krzeminska, D., Bogaard, T., Debieche, T., Cervi, F., Marc, V., Malet, J., 2014. Field investigation of preferential fissure flow paths with hydrochemical analysis of small-scale sprinkling experiments. Earth Surf. Dyn. 2 (1), 181 – 195. http://dx.doi.org/10.5194/esurf-2-181-2014.

Kunkel, R., Bach, M., Behrendt, H., Wendland, F., 2004. Groundwater-borne nitrate intakes into surface waters in Germany. Water Sci. Technol. 49(3), 11 – 9.

References

Kortunov, E., Luc, C., Amos, R., Grathwohl, P., 2016. Large scale reactive transport of nitrate across the surface water divide. Abstract #H33F-1597 presented at 2016 Fall Meeting, AGU, San Francisco, Calif., 12 - 16 Dec.

LaBolle, E.M., Fogg, G.E., Eweis, J.B., Gravner, J., Leaist, D.G., 2008. Isotopic fractionation by diffusion in groundwater, Water Resour. Res. 44, W07405. http://dx.doi.org/10.1029/2006WR005264.

Lagmanson, M., 2005. Electrical resistivity imaging. Advanced Geosciences, San Antonio, TX.

Lalbat, F., Blavoux, B., Banton, O., 2007. Description of a simple hydrochemical indicator to estimate groundwater residence time in carbonate aquifers. Geophys. Res. Lett. 34, L19403. http://dx.doi.org/10.1029/2007GL031390.

Lamontagne, S., Taylor, A. R., Batlle-Aguilar, J., Suckow, A., Cook, P. G., Smith, S. D., Morgenstern, U., Stewart, M. K., 2015. River infiltration to a subtropical alluvial aquifer inferred using multiple environmental tracers. Water Resour. Res. 51, 4532–4549. http://dx.doi.org/10.1002/2014WR015663.

Lane, T., 2012. Multilevel groundwater monitoring provides clearer picture of contaminated sites. Environ. Sci. Eng. Magazine. 25 (2), 66 -68. http://ese.dgtlpub.com/2012/2012-04-30/pdf/Multilevel_groundwater_monitoring_provides_clearer_picture_of_contaminated_sites.pdf.

Lansdown, K., Trimmer, M., Heppell, C. M., Sgouridis, F., Ullah, S., Heathwaite A. L., Binley, A., Zhang, H., 2012. Characterization of the key pathways of dissimilatory nitrate reduction and their response to complex organic substrates in hyporheic sediments. Limnol. Oceanogr. 57. http://dx.doi.org/10.4319/lo.2012.57.2.0387.

Lanz, E., Maurer, H., Green, A. G., 1998. Refraction tomography over a buried waste disposal site. Geophys. 63(4), 1414–1433. http://dx.doi.org/10.1190/1.1444443.

Lawton, D.C., 1989. Computation of refraction static corrections using first-break traveltime differences. Geophys. 54, 1289 – 1296. http://dx.doi.org/10.1190/1.1442588.

Ledin, M., Pedersen, K., 1996. The environment impact of mine wastes - Roles of microorganisms and their significance in treatment of mine waters. Earth Sci. Rev. 41, 67 - 108. http://dx.doi.org/10.1016/0012-8252(96)00016-5.

Lehmann, M.F., Reichert, P., Bernasconi, S.M., Barbieri, A., McKenzie, J.A., 2003. Modelling nitrogen and oxygen isotope fractionation during denitrification in a lacustrine redox-transition zone. Geochim. Cosmochim. Acta. 67(14), 2529–2542. http://dx.doi.org/10.1016/S0016-7037(03)00085-1.

Leibundgut, C., Seibert, J., 2011. Tracer hydrology. In: Wilderer, P. (Ed.), Treatise on Water Science, Elsevier, Amsterdam, pp 215–234. http://dx.doi.org/10.1016/B978-0-444-53199-5.00036-1.

Lendvay, J.M., Dean, S.M., Adriaens, P., 1998. Temporal and spatial trends in biogeochemical conditions at a groundwater-surface water interface: Implications for natural bioattenuation. Environ. Sci. Technol. 32(22), 3472 – 3478. http://dx.doi.org/10.1021/es980049t.

Leube, P.C., Geiges, A., Nowak, W., 2012. Bayesian assessment of the expected data impact on prediction confidence in optimal sampling design. Water Resour. Res. 48, W02501. http://dx.doi.org/10.1029/2010WR010137.

Leven, C., Weiss, H., Vienken, T., Dietrich, P., 2011. Direct Push technologies – An efficient investigation method for subsurface characterization. Grundwasser. 16(4), 221-234. http://dx.doi.org/10.1007/s00767-011-0175-8.

Li, S, Zhang, Y., Zhang, X. 2011. A study of conceptual model uncertainty in large-scale CO_2 storage simulation. Water Resour. Res. 47, W05534. http://dx.doi.org/10.1029/2010WR009707.

References

Li, X.B., Tsai, F.T.C., 2009. Bayesian model averaging for groundwater head prediction and uncertainty analysis using multimodel and multimethod. Water Resour. Res. 45 (9), W09403. http://dx.doi.org/10.1029/2008WR007488.

Liotta, M., Favara, R., Valenza, M., 2006. Isotopic composition of the precipitations in the central Mediterranean: Origin marks and orographic precipitation effects. J. Geophys. Res. 111, D19302. http://dx.doi.org/10.1029/2005JD006818.

Liu, Y., Yamanaka, T., 2012. Tracing groundwater recharge sources in a mountain–plain transitional area using stable isotopes and hydrochemistry. J. Hydrol. 464–465,116-126. http://dx.doi.org/10.1016/j.jhydrol.2012.06.053.

Livingston, R.J., 2000. Eutrophication Processes in Coastal Systems: Origin and Succession of Plankton Blooms and Effects on Secondary Production in Gulf Coast Estuaries, sixth ed. CRC Press, Boca Raton.

Lizarralde, D., Swift, S., 1999. Smooth inversion of VSP traveltime data. Geophys. 64(3), 659–661. http://dx.doi.org/10.1190/1.1444574.

Lloyd, D., 1993. Aerobic denitrification in soils and sediments: from Fallacies to facts. Trends in Ecol. Evol. 8, 352 – 356. http://dx.doi.org/10.1016/0169-5347(93)90218-E.

Loke, M.H., 2001. Electrical Imaging Surveys for Environmental and Engineering Studies: A Practical Guide to 2D and 3D Surveys. www.geoelectrical.com.

Loke, M.H., Chambers, J.E., Rucker, D.F., Kuras, O., Wilkinson, P.B., 2013. Recent developments in the direct-current geoelectrical imaging method. J. Appl. Geophys. 95, 135-156, http://dx.doi.org/10.1016/j.jappgeo.2013.02.017.

Lohse, K.A., Brooks, P.D., McIntosh, J.C., Meixner, T., Huxman, T.E., 2009. Interactions between biogeochemistry and hydrologic systems, Ann. Rev. Environ. Resour. 34(1), 65–96. http://dx.doi.org/10.1146/annurev.environ.33.031207.111141.

López Loera, H., Ramos Leal, J.A., Dávila Harris, P., Torres Gaytan, D. E., Martinez Ruiz, V. J., Gogichaishvili, A., 2014. Geophysical exploration of fractured-media aquifers at the Mexican Mesa Central: Satellite City, San Luis Potosí, Mexico. Surv. Geophys. 36(1), 167–184. http://dx.doi.org/10.1007/s10712-014-9302-2.

Long, D.T., Voice, T.C., Chen, A., Xing, F., Li, S.-G., 2015. Temporal and spatial patterns of Cl^- and Na^+ concentrations and Cl/Na ratios in salted urban watersheds. Elem Sci. Anth. 3, 49. http://dx.doi.org/10.12952/journal.elementa.000049.

Lovley, D. R., Chapelle, F. H., 1995. Deep subsurface microbial processes, Rev. Geophys. 33(3), 365–381. http://dx.doi.org/10.1029/95RG01305.

Lowe, M., Wallace, J., 2001. Evaluation of potential sources of nitrate contamination in groundwater, Cedar valley, Iron County, Utah with emphasis on the Enoch area. Utah Geological Survey (a division of Utah Department of Natural Resources), 51p.

Lundquist, E.J., Jackson, L.E., Scow, K.M., 1999. Wet-dry cycles affect dissolved organic carbon in two California agricultural soils. Soil Biol. Biogeochem. 31(7), 1031 – 1038. http://dx.doi.org/10.1016/S0038-0717(99)00017-6.

LUBW (Landesanstalt für Umwelt, Messungen und Naturschutz Baden-Württemberg), 2015. Groundwater monitoring programme: results of sampling 2015 – short report (in German). http://www4.lubw.baden-wuerttemberg.de/servlet/is/261999/grundwasserueberwachung_ergebnisse_2015_kurz.pdf?command=downloadContent&filename=grundwasserueberwachung_ergebnisse_2015_kurz.pdf.

References

Ma, R., Shi, J.S., Liu, J.C., Gui, C.L., 2014. Combined use of multivariate statistical analysis and hydrochemical analysis for groundwater quality evolution: a case study in north chain plain. J. Earth Sci.-China. 25, 587–597. http://dx.doi.org/10.1007/s12583-014-0446-2.

Ma, R., Wang, Y., Sun, Z., Zheng, C., Ma, T., Prommer, H., 2011. Geochemical evolution of groundwater in carbonate aquifers in Taiyuan, northern China. Appl. Geochem. 26, 884 - 897. http://dx.doi.org/10.1016/j.apgeochem.2011.02.008.

Mackay, R., Cooper, T.A., Metcalfe, A.V., O'Connell, P.E. 1996. Contaminant transport in heterogeneous porous media: a case study. 2. Stochastic modelling. J. Hydrol. 175 (1-4), 429-452. http://dx.doi.org/10.1016/S0022-1694(96)80019-9.

Macpherson, G.L., Townsend, M.A., 1998. Water chemistry and sustainable yield; In: M. Sophocleous (Ed.), Perspectives on Sustainable Development of Water Resources in Kansas. Kansas Geological Survey, Bulletin 239 (http://www.kgs.ku.edu/Publications/Bulletins/239/Macpherson/).

Maier, R.N., 2000. Bioavailability and its importance to bioremediation, In Valdes, J. J., (Ed.), Bioremediation (pp. 59–78). Massachusetts: Kluwer Academic Publishers. https://doi.org/10.1007/978-94-015-9425-7_4.

Maier, U., Flegr, M., Rügner, H., Grathwohl, P., 2013. Long-term solute transport and geochemical equilibria in seepage water and groundwater in a catchment cross section. Environ. Earth Sci. 69 (2), 429 – 441. http://dx.doi.org/10.1007/s12665-013-2393-0.

Maliva, R.G., 2016. Aquifer Characterization Techniques – Schlumberger Methods in Water Resources Evaluation Series No.4. Springer, Switzerland.

Marchant, H. K., Holtappels, M., Lavik, G., Ahmerkamp, S., Winter, C., Kuypers, M. M. M., 2016. Coupled nitrification–denitrification leads to extensive N loss in subtidal permeable sediments. Limnol. Oceanogr. 61, 1033–1048. http://dx.doi.org/10.1002/lno.10271.

Marion, D., Nur, A., Yin, H., Han, D., 1992. Compressional velocity and porosity in sand-clay mixtures. Geophys. 57, 554–563. http://dx.doi.org/10.1190/1.1443269.

Mariotti, A., Germon, J. C., Hubert, P., Kaiser, P., Letolle, R., Tardieux, A., Tardieux, P., 1981. Experimental determination of nitrogen kinetic isotope fractionation: Some principles; illustration for the denitrification and nitrification processes. Plant and Soil. 62(3), 413 – 430. http://dx.doi.org/10.1007/BF02374138.

Mariotti, A., Landreau, A., Simon, B., 1988. ^{15}N isotope biogeochemistry and natural denitrification process in groundwater: application to the chalk aquifer of northern France. Geochim. Cosmochim. Acta. 52, 1869 – 1878. http://dx.doi.org/10.1016/0016-7037(88)90010-5.

Marker, B. R., 2007. Contaminants in the subsurface: source zone assessment and remediation, National Research Council. The National Academies Press, Washington, D.C., 2005. ISBN 0 309 09447 X, xii + 358 pp. Land Degrad. Dev. 18, 471–472. http://dx.doi.org/10.1002/ldr.788.

Martin, T.D., Brockhoff, C.A., Creed, J.T., 1994. Method 200.7, Revision 4.4: Determination of Metals and Trace Elements in Water and Wastes by Inductively Coupled Plasma-Atomic Emission Spectrometry. U.S. EPA National Exposure Research Laboratory, Cincinnati, OH. https://www.epa.gov/sites/production/files/2015-08/documents/method_200-7_rev_4-4_1994.pdf (accessed March 12, 2018).

Matott, L.S., Babendreier, J.E., Purucker, S.T., 2009. Evaluating uncertainty in integrated environmental models: A review of concepts and tools. Water Resour. Res. 45, W06421. http://dx.doi.org/10.1029/2008WR007301.

References

Mattern, S., Sebilo, M., Vanclooster, M., 2011. Identification of the nitrate contamination sources of the Brusselian sands groundwater body (Belgium) using a dual-isotope approach. Isotopes Environ. Health Stud. 47, 297-315. http://dx.doi.org/10.1080/10256016.2011.604127.

Maule, C.P., Fonstad, T.A., 2000. Impacts of cattle penning on groundwater quality beneath feedlots. Can. Agric. Eng. 42, 87-93.

Maximova, A., Koumanova, B., 2006. Study on the content of chemicals in landfill leachate, in: Simeonov, L., Chirila, E. (Eds.), Chemicals as Intentional and Accidental Global Environmental Threats. NATO Security through Science Series. Springer, Dordrecht. http://dx.doi.org/10.1007/978-1-4020-5098-5_27.

Mayer, B., Bollwerk, S. M., Mansfeldt, T., Hütter, B., Veizer, J., 2001. The oxygen isotope composition of nitrate generated by nitrification in acid forest floors. Geochim. et Cosmochim. Acta. 65 (16), 2743-2756. http://dx.doi.org/10.1016/S0016-7037(01)00612-3.

Mayer, B., Boyer, E.W., Goodale, C., 2002. Sources of nitrate in rivers draining sixteen watersheds in the northeastern US: Isotopic constraints. Biogeochem. 57, 171–197. http://dx.doi.org/10.1023/A:1015744002496.

Mazac, O., Cislerova, M., Vogel, T., 1988. Application of geophysical methods in describing spatial variability of saturated hydraulic conductivity in the zone of aeration. J. Hydrol. 103, 117–126. http://dx.doi.org/10.1016/0022-1694(88)90009-1.

McLachlan, P.J., Chambers, J.E., Uhlemann, S.S., Binley, A., 2017. Geophysical characterisation of the groundwater–surface water interface. Adv. Water Resour. 109, 302-319. https://doi.org/10.1016/j.advwatres.2017.09.016.

McMahon, P.B., 2001. Aquifer/aquitard interfaces—Mixing zones that enhance biogeochemical reactions. Hydrogeol. J. 9 (1), 34–43. http://dx.doi.org/10.1007/s100400000109.

Meju, M. A., Gallardo, L. A., Mohamed, A. K., 2003. Evidence for correlation of electrical resistivity and seismic velocity in heterogeneous near-surface materials. Geophys. Res. Lett. 30, 1373. http://dx.doi.org/10.1029/2002GL016048, 7.

Mendes, M., Mari, J.-L, Hayet, M., 2014. Imaging geological structures up to the acquisition Surface using a hybrid refraction-reflection seismic method. Oil & Gas Science and Technology - Revue d'IFP Energies nouvelles, Institut Fran¸cais du P´etrole. 69 (2), 351-361.

Mengis, M., Schiff, S.L., Harris, M., English, M.C., Aravena, R., Elgood, R.J., MacLean, A., 1999. Multiple geochemical and isotopic approaches for assessing ground water NO_3^- elimination in a riparian zone. Ground Water. 37, 448–457. http://dx.doi.org/10.1111/j.1745-6584.1999.tb01124.x.

Mengis, M., Walther, U., Bernasconi, S.M., Wehrli, B., 2001. Limitations of using $\delta^{18}O$ for the source identification of nitrate in agricultural soils. Environ. Sci. Technol. 39 (9), 1840 - 1844. http://dx.doi.org/10.1021/es0001815.

Metzner, H., 1978. Oxygen evolution as energetic problem. In: Metzner, H. (Ed.), Photosynthetic Oxygen Evolution, Academic Press, London, pp 59–76.

Metzner, H., Fischer, K., Bazlen, O., 1979. Isotope ratios in photosynthetic oxygen. Biochim. Biophys. Acta. 548, 287–295. http://dx.doi.org/10.1016/0005-2728(79)90136-1.

Miao, Z., Carroll, K. C., Brusseau, M. L., 2013. Characterization and quantification of groundwater sulfate sources at a mining site in an arid climate: The Monument Valley site in Arizona, USA. J. Hydrol. 504, 207-215. http://dx.doi.org/10.1016/j.jhydrol.2013.09.030.

References

Miles, B., 2007. Practical approaches to modelling natural attenuation processes at LNAPL contaminated sites. PhD Dissertation, University of Tübingen 127p.

Milsom, J., Eriksen, A., 2011. Field Geophysics. Wiley-Blackwell, Hoboken, NJ.

Minet, E.P., Goodhue, R., Meier-Augenstein, W., Kalin, R.M., Fenton, O., Richards, K.G., Coxon, C.E., 2017. Combining stable isotopes with contamination indicators: A method for improved investigation of nitrate sources and dynamics in aquifers with mixed nitrogen inputs. In Water Res. 124, 85-96. http://dx.doi.org/10.1016/j.watres.2017.07.041.

Mohamed, L., Sultan, M., Ahmed, M., Zaki, A., Sauck, W., Soliman, F., Yan, E., Elkadiri, R., Abouelmaged, A., 2015. Structural controls on groundwater flow in basement terrains: geophysical, remote sensing, and field investigations in Sinai. Surv. Geophys. 36(5), 717 - 742. http://dx.dor.org/10.1007/s10712-015-9331-5.

Mongelli, G., Monni, S., Oggiano, G., Paternoster, M., Sinisi, R., 2013. Tracing groundwater salinization processes in coastal aquifers: A hydrogeochemical and isotopic approach in Na-Cl brackish waters of north-western Sardinia, Italy. Hydrol. Earth Syst. Sci. 17, 2917-2928. http://dx.doi.org/10.5194/hess-17-2917-2013.

Moore, J.W., Semmens, B.X., 2008. Incorporating uncertainty and prior information into stable isotope mixing models. Ecol. Lett. 11, 470–480. http://dx.doi.org/10.1111/j.1461-0248.2008.01163.x.

Moorkamp M., Roberts, A. W., Jegen, M., Heincke, B., Hobbs, R. W., 2013.Verification of velocity-resistivity relationships derived from structural joint inversion with borehole data. Geophys. Res. Lett. 40, 3596–3601. http://dx.doi.org/10.1002/grl.50696.

Moradkhani, H., Hsu, K.-L., Gupta, H., Sorooshian, S., 2005. Uncertainty assessment of hydrologic model states and parameters: Sequential data assimilation using the particle filter. Water Resour. Res. 41, W05012. http://dx.doi.org/10.1029/2004WR003604.

Moret, G.J.M., Clement, W.P., Knoll, M.D., Barrash, W., 2004. VSP traveltime inversion: Near-surface issues. Geophys. 69, 345–351. http://dx.doi.org/10.1190/1.1707053.

Morris, M.D., Berk, J.A., Krulik, J.W., Eckstein, Y., 1983. A computer program for a trilinear diagram plot and analysis of water mixing systems. Ground Water. 21, 67–74. http://dx.doi.org/10.1111/j.1745-6584.1983.tb00706.x.

Morse, J.L., Werner, S.F., Gillin, C.P., Goodale, C.L., Bailey, S.W., McGuire, K.J., Groffman, P.M., 2014. Searching for biogeochemical hot spots in three dimensions: Soil C and N cycling in hydropedologic settings in a northern hardwood forest. J. Geophys. Res. Biogeosci. 119, 1596–1607. http://dx.doi.org/10.1002/2013JG002589.

Mortimer, R.J.G., Harris, S. J., Krom, M. D., Freitag, T. E., Prosser, J. I., Barnes, J., Anschutz, P., Hayes, P. J., Davies, I.M., 2004. Anoxic nitrification in marine sediments Mar. Ecol. Prog. Ser. 276, 37–52.

Moysey, S.M., Oware, E.K., Khan, T., 2012. Picture-based physics: Using POD derived process constraints to enhance imaging of groundwater systems. Abstract #H33A-1281 presented at 2012 Fall Meeting, AGU, San Francisco, Calif., 3-7 Dec.

Murad, A.A., Mirghni, F.M., 2012. Isotopic variations of oxygen and hydrogen in groundwater of carbonate aquifer in an arid environment. Arab J. Geosci. 5, 1459 - 1468. http://dx.doi.org/10.1007/s12517-011-0325-4.

Murdoch, P.S., Stoddard, J.L., 1992. The role of nitrate in the acidification of streams in the Catskill Mountains of New York. Water Resour. Res. 28 (10), 2707 – 2720. http://dx.doi.org/10.1029/92WR00953.

References

Murgulet, D., Tick, G.R., 2013. Understanding the sources and fate of nitrate in a highly developed aquifer system. J. Contam Hydrol. 155, 69 - 81. http://dx.doi.org/10.1016/j.jconhyd.2013.09.004.

Naidu, R., Wong, M.H., Nathanail, P., 2015. Bioavailability - the underlying basis for the risk-based land management. Environ. Sci. Pollut. Res. 22(12), 8775 - 8778. http://dx.doi.org/10.1007/s11356-015-4295-z.

Nakaya, S., Uesugi, K., Motodate, Y., Ohmiya, I., Komiya, H., Masuda, H., Kusakabe, M., 2007. Spatial separation of groundwater flow paths from a multi-flow system by a simple mixing model using stable isotopes of oxygen and hydrogen as natural tracers. Water Resour. Res. 43, W09404. http://dx.doi.org/10.1029/2006WR005059.

National Research Council (NRC), 2003. Bioavailability of Contaminants in Soils and Sediments: Processes, Tools and Applications. Committee on Bioavailability of Contaminants in Soils and Sediments. National Academies Press, Washington, D.C.

National Research Council (NRC), 2001. Conceptual Models of Flow and Transport in the Fractured Vadose Zone. National Academy Press, Washington, DC (https://www.nap.edu/download/10102#).

Neal, C., Kirchner, J.W., 2000. Na^+ and Cl^- levels in rainfall, mist, streamwater and groundwater at the Plynlimon catchments, mid-Wales: inferences on hydrological and chemical controls. Hydrol. Earth Syst. Sci. 4(2), 295–310.

Neuman, S. P., 2003. Maximum likelihood Bayesian averaging of uncertain model predictions. Stochastic Environ. Res. Risk Assess. 17(5), 291–305. http://dx.doi.org/10.1007/s00477-003-0151-7.

Neumann, S. P., 2005. Trends, prospects and challenges in quantifying flow and transport through fractured rock. Hydrogeol. J. 13, 124–147. http://dx.doi.org/10.1007/s10040-004-0397-2.

Neuman, S.P., Wierenga, P.J., 2003. A Comparative Strategy of Hydrogeologic Modeling and Uncertainty Analysis for Nuclear Facilities and Sites, University of Arizona, Tucson, Arizona, United States, Rep. NUREG/CR-6805 (http://www.nrc.gov/docs/ML0324/ML032470827.pdf).

Nikolaidis, N.P., Shen, H., 2000. Conceptual site model for evaluating contaminant mobility and pump- and –treat remediation. Global Nest: the Int. J., 2(1), 67 – 76.

Nordstrom, D.K., 2012. Models, validation, and applied geochemistry: Issues in sciences, communication and philosophy. Appl. Geochem. 27, 1899 – 1919. http://dx.doi.org/10.1016/j.apgeochem.2012.07.007.

Nyquist, J. E., Freyer, P. A., Toran, L., 2008. Stream bottom resistivity tomography to map ground water discharge. Ground Water. 46, 561–569. http://dx.doi.org/10.1111/j.1745-6584.2008.00432.x.

Official Journal of the European Community (OJEC), 2015. Commission Directive (EU) 2015/1787 of 6 October 2015 amending Annexes II and III to Council Directive 98/83/EC on the quality of water intended for human consumption. Official Journal of the European Communities. L 260, 6 - 17. http://eur-lex.europa.eu/legal-content/EN/TXT/?uri=uriserv%3AOJ.L_.2015.260.01.0006.01.ENG.

Ofterdinger, U.S., Balderer, W., Loew, S., Renard, P., 2004. Environmental isotopes as indicators for ground water recharge to fractured granite. Ground Water. 42, 868–879. http://dx.doi.org/10.1111/j.1745-6584.2004.t01-5-.x.

Ohte, N., Sebestyen, S. D., Shanley, J. B., Doctor, D. H., Kendall, C., Wankel, S. D., Boyer, E. W., 2004. Tracing sources of nitrate in snowmelt runoff using a high-resolution isotopic technique. Geophys. Res. Lett. 31, L21506. http://dx.doi.org/10.1029/2004GL020908.

Oita, A., Malik, A., Kanemoto, K., Geschke, A., Nishijima, S., Lenzen, M., 2016. Substantial nitrogen pollution embedded in international trade. Nat. Geosci. 9, 111-115. http://dx.doi.org/10.1038/ngeo2635.

References

Olleros, T., 1983. Kinetische Isotopeneffekte der Arginase-und Nitratreduktase-Reaktion; ein Beitrag zur Aufklä rung der entsprechenden Reaktionschanismen. Diss. Techn. Univ. MünchenWeihenstephan.

Olsson, A.H., Grathwohl, P., 2007. Transverse dispersion of non-reactive tracers in porous media: a new nonlinear relationship to predict dispersion coefficient. J. Contam. Hydrol. 92, 149 – 161.

Onac, B.P., Wynn, J.G., Sumrall, J.B., 2011. Tracing the sources of cave sulfates: a unique case from Cerna Valley, Romania. Chem. Geol. 288,105-114. http://dx.doi.org/10.1016/j.chemgeo.2011.07.006.

Oren, O., Yechieli, Y., Böhlke, J.K., Dody, A., 2004. Contamination of groundwater under cultivated fields in an arid environment, central Arava Valley, Israel. J. Hydrol. 290(3–4), 312-328. http://dx.doi.org/10.1016/j.jhydrol.2003.12.016.

Oreskes, N., Shrader-Frechette, K., Belitz, K., 1994. Verification, validation, and confirmation of numerical models in the earth sciences. Science. 263 (5147), 641 - 646, http://dx.doi.org/10.1126/science.263.5147.641.

Oreskes, N., Belitz, K., 2001. Philosophical issues in model assessment, in: Anderson, M.G., Bates, P.D. (Eds.), Model Validation: Perspectives in Hydrological Science. John Wiley & Sons, New York, pp. 23 – 41.

Ortega-Calvo, J.-J., Harmsen, J., Parsons, J.R., Semple, K.T., Aitken, M.D., Ajao, C., Eadsforth, C., Galay-Burgos, M., Naidu, R., Oliver, R., Peijnenburg, W.J.G.M., Rombke, J., Streck, G., Versonnen, B., 2015. From bioavailability science to regulation of organic chemicals. Environ. Sci. Technol. 49(17), 10255 - 10264. http://dx.doi.org/10.1021/acs.est.5b02412.

Ouellon, T., Lefebvre, R., Marcotte, D., Boutin, A., Blais, V., Parent, M., 2008. Hydraulic conductivity heterogeneity of a local deltaic aquifer system from the kriged 3D distribution of hydrofacies from borehole logs, Valcartier, Canada. J. Hydrol. 351(1-2), 71 - 86. http://dx.doi.org/10.1016/j.jhydrol.2007.11.040.

Paasche, H., Wendrich, A., Tronicke, J., Trela, C., 2008. Detecting voids in masonry by cooperatively inverting P-wave and georadar traveltimes. J. Geophys. Eng. 5, 256 - 267. http://dx.doi.org/10.1088/1742-2132/5/3/002.

Paasche, H., Werban, U., Dietrich, P., 2009. Near-surface seismic traveltime tomography using a direct-push source and surface-planted geophones. Geophysics 74(4), G17–G25. http://dx.doi.org/10.1190/1.3131612.

Pakiser, L.C., Black, R.A., 1957. Exploring for ancient channels with the refraction seismic seismograph. Geophys. 22(1), 32 – 47. http://dx.doi.org/10.1190/1.1438336.

Palermo, D., Aigner, T., Nardon, S., Blendinger, W., 2010. Three-dimensional facies modeling of carbonate sand bodies: Outcrop analog study in an epicontinental basin (Triassic, southwest Germany). AAPG Bulletin. 94(4), 475–512. http://dx.doi.org/10.1306/08180908168.

Palmer, D., 1981. An Introduction to the generalized reciprocal method of seismic refraction interpretation. Geophys. 46(11), 1508-1518. http://dx.doi.org/10.1190/1.1441157.

Panno, S.V., Hackley, K.C., Kelly, W.R., Hwang, H.H., 2006. Isotopic evidence of nitrate sources and denitrification in the Mississippi River, Illinois. J. Environ. Qual. 35(2), 495 - 504. http://dx.doi.org/10.2134/jeg2005.0012.

Parfitt, R.L., Schipper, L.A., Baisden, W.T., Elliott, A.H., 2006. Nitrogen inputs and outputs for New Zealand in 2001 at national and regional scales. Biogeochem. 80(1), 71 - 88. http://dx.doi.org/10.1007/s10533-006-0002-y.

Park, J., Morgan, J.K., Zelt, C.A., Okubo, P.G., Peters, L., Benesh, N., 2007. Comparative velocity structure of active Hawaiian volcanoes from 3-D onshore–offshore seismic tomography. Earth and Planetary Sci. Lett. 259 (3–4), 500-516. http://dx.doi.org/10.1016/j.epsl.2007.05.008.

References

Parry, D., Lawton, D. C., 1994. Near-surface velocity structure from borehole and refraction seismic surveys. SEG Technical Program Expanded Abstracts 1994, pp. 602-604. http://dx.doi.org/10.1190/1.1932189.

Parsekian, A. D., Singha, K., Minsley, B. J., Holbrook, W. S., Slater, L., 2015. Multiscale geophysical imaging of the critical zone. Rev. Geophys. 53, 1–26. http://dx.doi.org/10.1002/2014RG000465.

Pastén-Zapata, E., Ledesma-Ruiz, R., Harter, T., Ramírez, A.I., Mahlknecht, J., 2014. Assessment of sources and fate of nitrate in shallow groundwater of an agricultural area by using a multi-tracer approach. Sci. Total Environ. 470–471, 855 - 864. http://dx.doi.org/10.1016/j.scitotenv.2013.10.043.

Pathak, C., Teegavarapu, R., Olson, C., Singh, A., Lal, A., Polatel, C., Zahraeifard, V., Senarath, S., 2015. Uncertainty analysis in hydrologic/hydraulic modeling: Challenges and proposed resolutions. J. Hydro. Eng. http://dx.doi.org/10.1061/(ASCE)HE.1943-5584.0001231.

Pauwels, H., Ayraud-Vergnaud, V., Aquilina, L., Molénat, J., 2010. The fate of nitrogen and sulfur in hard-rock aquifers as shown by sulfate-isotope tracing. Appl. Geochem. 25, 105-115. http://dx.doi.org/10.1016/j.apgeochem.2009.11.001.

Payne, F.C., Quinnan, J.A., Potter, S.T., 2008. Remediation Hydraulics. CRC Press. Boca Raton, FL.

Payn, R. A., Gooseff, M. N., McGlynn, B. L., Bencala, K. E., Wondzell, S. M., 2009. Channel water balance and exchange with subsurface flow along a mountain headwater stream in Montana, United States. Water Resour. Res. 45, W11427. http://dx.doi.org/10.1029/2008WR007644.

Peters, N.E., 1994. Hydrologic studies, In: Moldan, B., and J. Cerny (Eds.), Biogeochemistry of Small Catchments: A Tool for Environmental Research, SCOPE Report 51, Ch. 9, pp. 207 – 228.

Petrides, B., Cartwright, I., Weaver, T., 2006. The evolution of groundwater in the Tyrrell catchment, south-central Murray Basin, Victoria, Australia. Hydrogeol. J. 14, 1522–1543. http://dx.doi.org/10.1007/s10040-006-0057-9.

Phillips, D.L., Gregg, J.W., 2003. Source partitioning using stable isotopes: coping with too many sources. Oecologia. 136, 261–269. http://dx.doi.org/10.1007/s00442-003-1218-3.

Philips, F.M., 2001. Investigating flow and transport in the fractured vadose zone using environmental tracers, in: National Research Council (Ed.), Conceptual Models of Flow and Transport in the Fractured Vadose Zone. National Academy Press, Washington, DC, pp. 271 - 294.

Piper, A. M., 1944. A graphic procedure in the geochemical interpretation of water-analyses. Eos Trans. AGU. 25, 914–928. http://dx.doi.org/10.1029/TR025i006p00914.

Polson, D., Curtis, A., 2010. Dynamics of uncertainty in geological interpretation. J. Geol. Soc. London. 167, 5 - 10. http://dx.doi.org/10.1144/0016-76492009-055.

Power, C., 2014. Electrical resistivity tomography for mapping subsurface remediation, PhD Dissertation, Graduate Program in Civil Environ. Eng., The University of Western Ontario, Canada.

Prommer, H., Tuxen, N., Bjerg, P.L., 2006. Fringe-controlled natural attenuation of phenoxy acids in a landfill plume: Integration of field-scale processes by reactive transport. Environ. Sci. Technol. 40(15), 4732–4738. http://dx.doi.org/10.1021/es0603002.

Rabbel, W., 2010. Seismic methods, in: Kirsch, R. (Ed.), Groundwater Geophysics: A Tool for Hydrogeology. Springer, Berlin, pp. 23–84. http://dx.doi.org/10.1007/978-3-540-88405-7.

Rafter, P. A., DiFiore, P. J., Sigman, D. M., 2013. Coupled nitrate nitrogen and oxygen isotopes and organic matter remineralization in the Southern and Pacific Oceans. J. Geophys. Res. Oceans. 118, 4781–4794. http://dx.doi.org/10.1002/jgrc.20316.

References

Ranjbar, F., Jalali, M., 2012. Calcium, magnesium, sodium and potassium release during decomposition of some organic residues. Commun. Soil Sci. Plant Anal. 43(4), 645 – 659. http://dx.doi.org/10.1080/00103624.2012.644005.

Rastetter, M., Gawler, J. Kiviluoma, M., Suoniemi-Kähärä, A., 2015. Determination of water pollutants using photometric analysis. Application Note 71728. https://tools.thermofisher.com/content/sfs/brochures/AN-71728-DA-ISO-Water-Pollutants-AN71728-EN.pdf (accessed March 12, 2018).

Rayner, S., Rosenthal, S., 2008. Buried Bedrock Channels in the Athabasca Oil Sands Region Conceptual Understanding and Implications to Water Supply. Proceedings of WaterTech 2008 Conference, Environmental Services Association of Alberta, Lake Louise Alberta, April 16-18. http://www.esaa.org/wp-content/uploads/2015/01/WaterTech2008-Paper03.pdf.

Redpath, B.B., 1973. Seismic Refraction Exploration for Engineering Site Investigation. National Technical Information Service, U.S. Dept. of Commerce. http://www.wgeosoft.ch/Document/redpath.pdf.

Refsgaard, J.C., Auken, E., Bamberg, C.A., Christensen, B.S.B., Clausen. T., Dalgaard, E., Effersø, F., Ernstsen, V., Gertz, F., Hansen, A.L., He, X., Jacobsen, B.H., Jensen, K.H., Jørgensen, F., Jørgensen, L.F., Koch, J., Nilsson, B., Petersen, C., De Schepper, G., Schamper, C., Sørensen, K.I., Therrien, R., Thirup, C., Viezzoli, A., 2014. Nitrate reduction in geologically heterogeneous catchments—A framework for assessing the scale of predictive capability of hydrological models. Sci. Total Environ. 468–469, 1278–1288. http://dx.doi.org/10.1016/j.scitotenv.2013.07.042.

Refsgaard, J. C., Hansen, J. R., 2010. A good-looking catchment can turn into a modeller's nightmare. Hydrol. Sci. J., 55, 899–912. http://dx.doi.org/10.1080/02626667.2010.505571.

Repert, D.A., Barber, L.B., Hess, K.M., Keefe, S.H., Kent, D.B., LeBlanc, D.R., and Smith, R.L., 2006. Long-term natural attenuation of carbon and nitrogen within a groundwater plume after removal of the treated wastewater source. Environ. Sci. Technol. 40(4), 1154 – 1162. http://dx.doi.org/10.1021/es051442j.

Revil, A., Cary, L., Fan, Q., Finizola, A., Trolard, F., 2005. Self-potential signals associated with preferential ground water flow pathways in a buried paleo-channel. Geophys. Res. Lett. 32, L07401. http://dx.doi.org/10.1029/2004GL022124.

Reynolds, J.M., 2011. An Introduction to Applied and Environmental Geophysics. Wiley-Blackwell, Hoboken, NJ:

Rice, E.W., Baird, R.B., Eaton, A.D., Clesceri, L.S. (Eds.), 2012. Standard Methods for the Examination of Water and Wastewater, 22nd ed. APHA-AWWA, WEF, Washington, D.C.

Ritzi, R.W. Jr, Dai, Z., Rubin, Y.N., 2004. Review of permeability in buried-valley aquifers: centimetre to kilometre scales: Calibration and reliability in groundwater modelling; a few steps closer to reality. Proceedings of the ModelCARE 2002 Conference, Prague, Czech Republic, June 17–20, 2002, 409–418.

Rivett, M.O., Buss, S.R., Morgan, P., Smith, J.W.N., Bemment, C.D., 2008. Nitrate attenuation in groundwater: A review of biogeochemical controlling processes. Water Res. 42, 4215-4232. http://dx.doi.org/10.1016/j.watres.2008.07.020.

Robertson, L.A., Kuenen, J.G., 1984. Aerobic denitrification: a controversy revived. Arch. Microbiol. 139, 351 - 354. http://dx.doi.org/10.1007/BF00408378.

Robinson, C., Brovelli, A., Barry, D.A., Li, L., 2009. Tidal influence on BTEX biodegradation in sandy coastal aquifers. Adv. Water Resour. 32 (1), 16-28. http://dx.doi.org/10.1016/j.advwatres.2008.09.008.

References

Robson, A., Beven, K., Neal, C., 1992. Towards identifying sources of subsurface flow: A comparison of components identified by a physically based runoff model and those determined by chemical mixing techniques. Hydrol. Process. 6, 199–214. http://dx.doi.org/10.1002/hyp.3360060208.

Rohde, M.M., Granger, J., Sigman, D.M., Lehman, M.F., 2015. Coupled nitrate N and O stable isotope fractionation by a natural marine plankton consortium. Front. Mar. Sci. 2(28). http://dx.doi.org/10.3389/fmars.2015.00028.

Rojas, R., Feyen, L., Dassargues, A., 2008. Conceptual model uncertainty in groundwater modeling: Combining generalized likelihood uncertainty estimation and Bayesian model averaging. Water Resour. Res. 44, W12418. http://dx.doi.org/10.1029/2008WR006908.

Rolle, M., Maier, U., Grathwohl, P., 2011. Contaminant fate and reactive transport in groundwater, in: Swartjes, F.A. (Ed.), Dealing with Contaminated Sites - From Theory towards Practical Application. Springer, The Netherlands, pp. 851 - 885.

Ronayne, M.J., Gorelick, S.M., Caers, J., 2008. Identifying discrete geologic structures that produce anomalous hydraulic response: an inverse modeling approach. Water Resour. Res. 44, W08426. http://dx.doi.org/10.1029/ 2007WR006635.

Rosenshein, J. S., 1988. Region 18, Alluvial Valleys. In Hydrogeology, in: Back, W., Rosenshein, J. S., Seaber, P. R. (Eds.), The Geology of North America, Vol. O-2. The Geological Society of America: Boulder, CO.

Rose, S., Long, A., 1988. Monitoring dissolved oxygen in ground water: Some basic considerations. Groundwater Monitoring & Remediation. 8, 93–97. http://dx.doi.org/10.1111/j.1745-6592.1988.tb00981.x.

Roy, A., Apparao, A., 1971. Depth of investigation in direct current methods. Geophys. 36(5), 943 – 959. http://dx.doi.org/10.1190/1.1440226.

Rubin, Y., Hubbard, S., 2005. Hydrogeophysics. Springer, Netherlands.

Rugel, K., Golladay, S.W., Jackson, C.R., Rasmussen, T.C., 2016. Delineating groundwater / surface water interaction in a karst watershed: Lower Flint River Basin, southwestern Georgia, USA. J. Hydrol.: Regional Studies. 5, 1-19 . http://dx.doi.org/10.1016/j.ejrh.2015.11.011.

Ryan, G. A., Peacock, J. R., Shalev, E., Rugis, J., 2013. Montserrat geothermal system: A 3D conceptual model. Geophys. Res. Lett. 40, 2038–2043. http://dx.doi.org/10.1002/grl.50489.

Sacchi, E., Acutis, M., Bartoli, M., Brenna, S., Delconte, C.A., Laini, A., Pennisi, M., 2013. Origin and fate of nitrates in groundwater from the central Po plain: insights from isotopic investigations. Appl. Geochem. 34, 164–80. http://dx.doi.org/10.1016/j.apgeochem.2013.03.008.

Sain, K., Kaila, K.L., 1996. Interpretation of first arrival travel times in seismic refraction work. Pure Appl. Geophys. 147, 181–194. http://dx.doi.org/10.1007/BF00876443.

Samborska, K., Halas, S., 2010. ^{34}S and ^{18}O in dissolved sulfate as tracers of hydrogeochemical evolution of the Triassic carbonate aquifer exposed to intense groundwater exploitation (Olkusz–Zawiercie region, southern Poland). Appl. Geochem. 25, 1397-1414. http://dx.doi.org/10.1016/j.apgeochem.2010.06.010.

Samborska, K., Halas, S., Bottrell, S. H., 2013. Sources and impact of sulphate on groundwaters of Triassic carbonate aquifers, Upper Silesia, Poland. J. Hydrol. 486, 136 - 150. http://dx.doi.org/10.1016/j.jhydrol.2013.01.017.

Sandmeier, K., 2012. Reflexw manual version 8.0. Sandmeier Scientific Software, Karlsruhe.

Sarmiento, J.L., Gruber, N., 2006. Ocean biogeochemical dynamics. Princeton University Press, Princeton, New Jersey.

Savard, M., Somers, G., Smirnoff, A., Paradis, D., van Bochove, E., Liao, S., 2010. Nitrate isotopes unveil distinct seasonal N-sources and the critical role of crop residues in groundwater contamination. J. Hydrol. 381 (1-2), 134 - 141. http://dx.doi.org/10.1016/j.jhydrol.2009.11.033.

Schilling, K.E., Li, Z., Zhang, Y.-K., 2006. Groundwater– surface water interaction in the riparian zone of an incised channel, Walnut Creek, Iowa. J. Hydrol. 327, 140–150, http://dx.doi.org/10.1016/j.jhydrol.2005.11.014.

Schoeller H., 1967. Qualitative evaluation of groundwater resources (in methods and techniques of groundwater investigation and development). UNESCO Water Resources Series #33, pp. 54–83.

Schollenberger, U., 1998. Chemical composition and dynamics of the groundwater in the Neckar valley in the area of Tübingen (in German). PhD dissertation. Inst. of Geosci., Univ. of Tübingen, Germany.

Schramm, A., de Beer D., Heuvel, J.C., Ottengraf, S., Amann, R., 1999. Microscale distribution of populations and activities of Nitrosospira and Nitrospira spp. along a macroscale gradient in nitrifying bioreactor: quantification by in situ hybridization and the use of microsensors. Appl. Environ. Microbiol. 65(5), 3690 - 3696.

Schütze, C., Vienken, T., Werban, U., Dietrich, P., Finizola, A., Leven, C., 2012. Joint application of geophysical methods and Direct Push-soil gas surveys for the improved delineation of buried fault zones. J. Appl. Geophys. 82, 129-136. http://dx.doi.org/10.1016/j.jappgeo.2012.03.002.

Schulmeister, M.K., Butler, J.J., Healey, J.M., Zheng, L., Wysocki, D.A., McCall, G.W., 2003. Direct-Push electrical conductivity logging for high-resolution hydrostratigraphic characterization. Groundwater Monitoring & Remediation. 23, 52–62. http://dx.doi.org/10.1111/j.1745-6592.2003.tb00683.x.

Schulmeister, M.K., Healey, J.M., Butler Jr., J.J., McCall, G.W., 2004. Direct-push geochemical profiling for assessment of inorganic chemical heterogeneity in aquifers. J. Contam. Hydrol. 69 (3–4), 215–232. http://dx.doi.org/10.1016/j.jconhyd.2003.08.002.

Schulz, H.N., Jorgensen, B.B., 2001. Big bacteria. Annu. Rev. Microbiol. 55, 105 – 137. http://dx.doi.org/10.1146/annurev.micro.55.1.105.

Schuster, G. T., 1988. An analytic generalized inverse for common depth-point and vertical seismic profile traveltime equations. Geophys. 53, 314–325. http://dx.doi.org/10.1190/1.1442465.

Schwartz, F.W., Zhang, H., 2003. Fundamentals of Ground Water. Wiley, New York.

Sebilo, M., Billen, G., Grably, M., Mariotti, A., 2003. Isotopic composition of nitrate-nitrogen as a marker of riparian and benthic denitrification at the scale of the Seine River system. Biogeochem. 63, 35 - 51. http://dx.doi.org/10.1023/A:1023362923881.

Sebilo, M., Mayer, B., Nicolardot, B., Pinay, G., Mariotti, A., 2013. Long-term fate of nitrate fertilizer in agricultural soils. PNAS. 110(45), 18185 - 9. http://dx.doi.org/10.1073/pnas.1305372110.

Seitzinger, S., Harrison, J.A., Böhlke, J.K., Bouwman, A.F., Lowrance, R., Peterson, B., Tobias, C., Drecht, G.V., 2006. Denitrification across landscapes and waterscapes: A synthesis. Ecol. Appl. 16, 2064–2090. http://dx.doi.org/10.1890/1051-0761(2006)016[2064:DALAWA]2.0.CO;2.

Sellwood, S.M., Healey, J.M., Birk, S., Butler, J.J., 2005. Direct-push hydrostratigraphic profiling: coupling electrical logging and slug tests. Ground Water. 43, 19 - 29. http://dx.doi.org/10.1111/j.1745-6584.2005.tb02282.x.

References

Semaoune, P., Sebilo, M., Templier, J., Derenne, S., 2012. Is there any isotopic fractionation of nitrate associated with diffusion and advection? Environ. Chem. 9 (2), 158−162. http:dx.doi.org/10.1071/EN11143.

Shao, K., Deng, H.M., Chen, Y.T., Zhou, H.T., Yan, G.X., 2016. Screening and identification of aerobic denitrifiers. IOP Conf. Ser.: Earth Environ. Sci. 39 012049. http://dx.doi.org/10.1088/1755-1315/39/1/012049.

Sheehan, J., Doll, W.E., Mandell, W., 2003. Evaluation of refraction tomography codes for near-surface applications. Extended Abstract, 2003 Annual Meeting of the Society of Exploration Geophysicists, Dallas, Texas, Tulsa, Oklahoma, October 26-31, 2003.

Shehab, G., Mann, R.D., Abbott, B., Minear, J.F., Gillis, D., Kear, G.R., 2008. Array seismic fluid transducer source. U.S. Patent 20050263340, filed May 25, 2004 and published December, 2008.

Shen, J., Crane, J.M., Lorenzo, J.M., White, C.D., 2016. Seismic velocity prediction in shallow (< 30 m) partially saturated, unconsolidated sediments using effective medium theory. J. Environ. Eng. Geophys. 21(2), 67 – 68.

Shen, Y., Chapelle, F.H., Strom, E.W., Benner, R., 2015. Origins and bioavailability of dissolved organic matter in groundwater. Biogeochem. 122(1), 61 - 78. http://dx.doi.org/10.1007/s10533-014-0029-4.

Sigman, D.M., Casciotti, K.L., Andreani, M., Barford, C., Galanter, M., Böhlke, J.K., 2001. A bacterial method for the nitrogen isotopic analysis of nitrate in seawater and freshwater. Anal. Chem. 73, 4145-4153. http://dx.doi.org/10.1021/ac010088e.

Skelton, A., Andren, M., Kristmannsdottir, H., Stockmann, G., Morth, C.-M., Sveinbjornsdottir, A., Jonsson, S., Sturkell, E., Gurunardottir, H.R., Hjartarson, H., Siegmund, H., Kockum, I., 2014. Changes in groundwater chemistry before two consecutive earthquakes in Iceland. Nat. Geosci. 7, 752–756. http://dx.doi.org/ 10.1038/ngeo2250.

Silva, S. R., Kendall, C., Wilkison, D. H., Ziegler, A. C., Chang, C. C. Y., Avanzino, R. J., 2000. A new method for collection of nitrate from fresh water and analysis of the nitrogen and oxygen isotope ratios. J. Hydrol. 228(1-2), 22 – 36. http://dx.doi.org/10.1016/S0022-1694(99)00205-X.

Singh, A., Mishra, S. Ruskauff, G., 2010. Model averaging techniques for quantifying conceptual model uncertainty. Ground Water. 48, 701–715. http://dx.doi.org/10.1111/j.1745-6584.2009.00642.x.

Siontorou, Ch. G., Batzias, F.A., 2012. Managing uncertainty in environmental decision-making within ecological constraints - A model based reasoning approach. Procedia Engineering, 42, 1137-1149. http://dx.doi.org/10.1016/j.proeng.2012.07.506.

Smith, R.L., Baumgartner, L.K., Miller, D.N., Repert, D.A., Böhlke, J.K., 2006. Assessment of nitrification potential in ground water using short term, single-well injection experiments. Microbial Ecol. 51, 22 – 35. http://dx.doi.org/10.1007/s00248-004-0159-7.

Smith, R.L., Howes, B.L., Duff, J.H., 1991. Denitrification in nitrate-contaminated groundwater: Occurrence in steep vertical geochemical gradients. Geochem. Cosmochim. Acta. 55, 1815 - 1825. http://dx.doi.org/10.1016/0016-7037(91)90026-2.

Smolders, A.J.P., Lucassen, E.C.H.E.T., Bobbink, R., Roelofs, J.G.M., Lamers, L.P.M., 2010. How nitrate leaching from agricultural lands provokes phosphorus eutrophication in groundwater fed wetlands: The sulfur bridge. Biogeochem. 98(1-3), 1 – 7. http://dx.doi.org/10.1007/s10533-009-9387-8.

Snider, D. M., Spoelstra, J., Schiff, S. L., Venkiteswaran, J. J., 2010. Stable oxygen isotope ratios of nitrate produced from nitrification: ^{18}O-labeled water incubations of agricultural and temperate forest soils. Environ. Sci. Technol. 44(14), 5358–5364. http://dx.doi.org/10.1021/es1002567.

References

Socco, L.V., Strobbia, C. 2004. Surface wave method for near-surface characterization: A tutorial. Near Surf. Geophys. 2(4), 165–185. http://dx.doi.org/10.3997/1873-0604.2004015.

Sorell, T., McEvoy, K., 2013. Incorporating bioavailability considerations into the evaluation of contaminated sediment sites. Remediation J. 23, 63–72. http://dx.doi.org/10.1002/rem.21338.

Souchez, R., Lorrain, R., 2006. The Environmental significance of deuterium excess in meteoric and non-meteoric Antarctic ice, in: Knight, P.G. (Ed.), Glacier Science and Environmental Change. Blackwell Publishing, Malden, MA. http://dx.doi.org/10.1002/9780470750636.ch35.

Sousa, M.R., Frind, E.O., Rudolph, D.L., 2012. Dealing with uncertainty in source water protection. Proceedings of the IAH Congress, Niagra Falls, Canada, September 16 – 21, 2012, Paper 249.

Spalding, R.F., Exner, M.E., 1993. Occurrence of nitrate in groundwater - A review. J. Environ. Qual. 22, 392 - 402. http://dx.doi.org/10.2134/jeq1993.00472425002200030002x.

Stelzer, R.S., Bartsch, L.A., 2012. Nitrate removal in deep sediments of a nitrogen-rich river network: A test of a conceptual model. J. Geophys. Res. 117, G02027. http://dx.doi.org/10.1029/2012JG001990.

Stemler, A.J., 2002. The bicarbonate effect, oxygen evolution, and the shadow Otto Warburg. Photosynth. Res. 73, 177 – 183. http://dx.doi.org/10.1023/A:1020447030191.

Stenger, R., Barkle, G., Burgess, C., Wall, A., Clague, J., 2008. Low nitrate contamination of shallow groundwater in spite of intensive dairying: the effect of reducing conditions in the vadose zone - aquifer continuum. J. Hydrol.(NZ). 47, 1-24.

Stoddard, J.L., 1994. Long-term changes in watershed retention of nitrogen: Its causes and aquatic consequences. *in*: Baker, L.A. (Ed.), Environmental Chemistry of Lakes and Reservoirs. American Chemical Society, Washington (DC). pp. 223 - 284.

Storck, P., Eheart, J.W., Valocchi, A.J., 1997. A method for the optimal location of monitoring wells for detection of groundwater contamination in three-dimensional heterogeneous aquifers. Water Resour. Res. 33(9), 2081 - 2088. http://dx.doi.org/10.1029/97WR01704.

Stumm, W., Morgan, J.J., 1996. Aquatic Chemistry: Chemical Equilibria and Rates in Natural Waters, third ed. John Wiley & Sons, New York.

Stumpp, C., Klaus, J., Stichler, W., 2014. Analysis of long-term stable isotopic composition in German precipitation. J. Hydrol. 517, 351 – 361. http://dx.doi.org/10.1016/j.jhydrol.2014.05.034, 2014.

Sudicky, E.A., Illman, W.A., 2011. Lessons learned from a suite of CBC Borden experiments. Ground Water. 49, 630 – 648. http://dx.doi.org/10.1111/j.1745-6584.2011.00843.x.

Sundermeyer-Klinger, H., Meyer, W., Warninghoff, B., Bock, E., 1984. Membrane-bound nitrite oxidoreductase of Nitrobacter: Evidence for a nitrate reductase system. Arch Microbiol. 140, 153-158.

Szalai, S., Novák, A., Szarka, L., 2009. Depth of investigation and vertical resolution of surface geoelectric arrays. J. Environ. Eng. Geophys. 14(1), 15 – 23.

Tang, L., Tang, Y., Zheng, G., Zhang, G., Liu, W., Qiu, R., 2014. Spatial heterogeneity effects of Zn/Cd – contaminated soil on the removal efficiency by the hyperaccumulator *Sedum alferdii*. J. Soil Sediments. 14(5), 948 – 954.

Tarantola, A., 2005. Inverse Problem Theory. Methods for Model Parameter Estimation. Soc. of Ind. and Appl. Math, Philadelphia, Pa.

References

Tassone, A., Santomauro, M., Mnichetti, M., Cerredo, M., A., Remesal, M., B., Lippati, H., Lodolo, E., Vilas, J.F., 2010. Imaging subsurface lithological and structural features by resistivity tomography: North Beagle Channel (Tierra del Fuego, Argentina). Revista Mexicana de Ciencias Geológicas, 27(3), 562–572.

Taylor, P.D., Ramsey, M.H., Potts, P.J., 2005. Spatial contaminant heterogeneity: quantification with scale of measurement at contrasting sites. J. Environ. Monit. 7 (12), 1364 – 1370. http://dx.doi.org/10.1039/B511636H.

Telford, W.M., Geldart, L.P., Sheriff, R.E., 1990. Applied Geophysics. Cambridge University Press, Cambridge.

Tetzlaff, D., McDonnell, J. J., Uhlenbrook, S., McGuire, K. J., Bogaart, P. W., Naef, F., Baird, A. J., Dunn, S. M., Soulsby, C., 2008. Conceptualizing catchment processes: simply too complex? Hydrol. Process. 22, 1727–1730. http://dx.doi.org/10.1002/hyp.7069.

Tetzlaff, D., Carey, S.K., Laudon, H., McGuire, K., 2010. Catchment processes and heterogeneity at multiple scales – benchmarking observations, conceptualization and prediction. Hydrol. Process. 24, 2203 – 2208. http://dx.doi.org/10.1002/hyp.7784.

Thacker, B.H., Doebling, S.W., Hemez, F.M., Anderson, M.C., Pepin, J.E., Rodriquez, E.A., 2004. Concepts of model verification and validation. Technical Report, Los Alamos National Lad, Los Alamos, NM, USA (http://www.ltas-vis.ulg.ac.be/cmsms/uploads/File/LosAlamos_VerificationValidation.pdf).

Theis, C.V., 1967. Aquifers and models. In Proceedings of Symposium on Groundwater Hydrology, American Water Resources Asssociation, p. 138.

Thomsen, N.I., Binning, P J., McKnight, U S., Tuxen, N., Bjerg, P L., Troldborg, M., 2016. A Bayesian belief network approach for assessing uncertainty in conceptual site models at contaminated sites. J. Contam. Hydrol. 188, 12-28. http://dx.doi.org/10.1016/j.jconhyd.2016.02.003.

Thornton, S.F., Wealthal, G.P., 2008. Site characterization for the improved assessment of contaminant fate in fractured aquifers. Proceedings of the ICE - Water Manage. 161 (6), 343 – 356. http://dx.doi.org/10.1680/wama.2008.161.6.343.

Thullner, M., Fischer, A., Richnow, H.-H., Wick, L.Y., 2013. Influence of mass transfer on stable isotope fractionation. Appl. Microbial. Biotechnol. 97(2), 441-452. http://dx.doi.org/10.1007/s00253-012-4537-7.

Toledo-Hernandez, C., Ryu, H., Gonzalez-Nieves, J., Huertas, E., Toranzos, G.A., Santo Domingo, J., 2013. Tracking the primary sources of fecal pollution in a tropical watershed: a one year study. Appl Environ Microbiol. 79(5), 1689–1696. http://dx.doi.org/10.1128/AEM.03070-12.

Toomey, D. R., Solomon, S. C., Purdy, G. M., 1994. Tomographic imaging of the shallow crustal structure of the East Pacific Rise at 9°30'N. J. Geophys. Res. 99(B12), 24135–24157. http://dx.doi.org/10.1029/94JB01942.

Topinkova, B., Nesetril, K., Datel, J., Nol, O., Hosl, P, 2007. Geochemical heterogeneity and isotope geochemistry of natural attenuation processes in a gasoline-contaminated aquifer at the Hnevice site, Czech Republic. Hydrogeol J. 15(5), 961–976. http://dx.doi.org/10.1007/s10040-007-0179-8.

Torres, N. V., Santos, G., 2015. The (mathematical) modeling process in biosciences. Frontiers in Genetics. 6, 354. http://dx.doi.org/10.3389/fgene.2015.00354.

Tremblay, L., Lefebvre, R., Paradis, D., Gloaguen, E., 2014. Conceptual model of leachate migration in a granular aquifer derived from the integration of multi-source characterization data (St. Lambert, Canada). Hydrogeol. J. 22 (3), 587 – 608. http://dx.doi.org/10.1007/s10040-013-1065-1.

References

Troldborg, L., Refsgaard, J.C., Jensen, K.H., Engesgaard, P., 2007. The importance of alternative conceptual models for simulation of concentrations in a multi-aquifer system. Hydrogeol. J. 15 (5), 843 - 860. http://dx.doi.org/10.1007/s10040-007-0192-y.

US Environmental Protection Agency (EPA), 2002. Supplemental Guidance for Developing Soil Screening Levels for Superfund Sites, Publication: OSWER 9355.4-24. US EPA, USA (http://www.epa.gov/superfund/health/conmedia/gwdocs/).

Valle Junior, J.R.F., Varandas, S.G.P., Sanches Fernandes, L.F., Pacheco, F.A.L., 2014. Groundwater quality in rural watersheds with environmental land use conflicts. Sci. Total Environ. 493, 812 - 27. http://dx.doi.org/10.1016/j.scitotenv.2014.06.068.

van der Kruk, J., Meekes, J.A.C., Van den Berg, P.M., Fokkema, J.T., 2000. An apparent-resistivity concept for low-frequency electromagnetic sounding techniques. Geophys. Prospect. 48(6), 1033 – 1052. http://dx.doi.org/10.1046/j.1365-2478.2000.00229.x.

Van der Weijden, C.H., Pacheco, F.A.L., 2006. Hydrogeochemistry in the Vouga River basin (central Portugal): Pollution and chemical weathering. Appl. Geochem. 21, 580-613. http://dx.doi.org/10.1016/j.apgeochem.2005.12.006.

van Kessel, M.A.H.J., Speth, D.R., Albertsen, M.; Nielsen, P.H., Op den Camp, H.J.M., Kartal, B., Jetten, M.S.M., Lücker, S., 2015. Complete nitrification by a single microorganism. Nature. 528, 555 - 559. http://dx.doi.org/10.1038/nature16459.

van Rijn, J., Tal, Y., Schreier, H.J., 2006. Denitrification in recirculating systems: Theory and applications. Aquacult. Eng. 34(3), 364 – 376. http://dx.doi.org/10.1016/j.aquaeng.2005.04.004.

Vaudelet, P., Schmutz, M., Pessel, M., Franceschi,M., Guérin, R., Atteia, O., Blondel, A., Ngomseu, C., Galaup, S., Rejiba, F., Bégassat, P., 2011. Mapping of contaminant plumes with geoelectrical methods. A case study in urban context. J. Appl. Geophys. 75(4), 738-751. http://dx.doi.org/10.1016/j.jappgeo.2011.09.023.

Vengosh, A., Keren, R., 1996. Chemical modifications of groundwater contaminated by recharge of treated sewage effluent. J. Contam. Hydrol. 23 (4), 347-360. http://dx.doi.org/10.1016/0169-7722(96)00019-8.

Vengosh, A., 2003. Salinization and saline environments, in: Sherwood Lollar, B. (Ed.), Environmental Geochemistry, Treatise in Geochemistry, vol. 9. Elsevier Science.

Vienken, T., Leven, C., Dietrich, P., 2012. Use of CPT and other direct push methods for (hydro-) stratigraphic aquifer characterization – a field study. Canadian Geotech. J. 49 (2), 197 – 206. http://dx.doi.org/10.1139/t11-094.

Vignoli G., Cassiani G., Rossi M., Deiana R., Boaga J., and Fabbri P., 2012, Geophysical characterization of a small pre-Alpine catchment. J. Appl. Geophys. 80, 32-42. http://dx.doi.org/10.1016/j.jappgeo.2012.01.007.

Vijaya Rao, V., Sain, K., Krishna, V.G., 2007. Modelling and inversion of single-ended refraction data from the shot gathers of multifold deep seismic reflection profiling—an approach for deriving the shallow velocity structure. Geophys. J. Int. 169, 507–514. http://dx.doi.org/10.1111/j.1365-246X.2007.03219.x.

Vitòria, L., Otero, N., Soler, A., Canals, A., 2004. Fertilizer characterization: isotopic data (N, S, O, C and Sr). Environ. Sci. Technol. 38(12), 3254–3262. http://dx.doi.org/10.1021/es0348187.

Vrzel, J., Vuković-Gačić, B., Kolarević, S., Gačić, Z., Kračun-Kolarević, M., Kostić, J., Aborgiba, M., Farnleitner, A., Reischer, G., Linke, R., Paunović, M., Ogrinc, N., 2016. Determination of the sources of nitrate and the microbiological sources of pollution in the Sava River Basin. Sci. Total Environ. 573, 1460-1471. http://dx.doi.org/10.1016/j.scitotenv.2016.07.213.

References

Wainwright, H.M., Flores Orozco, A., Bücker, M., Dafflon, B., Chen, J., Hubbard, S.S., Williams, K. H., 2016. Hierarchical Bayesian method for mapping biogeochemical hot spots using induced polarization imaging. Water Resour. Res. 52, 533–551. http://dx.doi.org/10.1002/2015WR017763.

Walker, W.E., Harremoës, P., Rotmans, J., Van, J.P., der Sluis, M.B.A., Van Asselt, M.B.A., Janssen, P., Krayer von Krauss, M.P., 2003. Defining uncertainty–A conceptual basis for uncertainty management in model-based decision support. Integr. Assess. 4 (1), 5–17. http://dx.doi.org/10.1076/iaij.4.1.5.16466.

Walton, N.R.G., 1989. Electrical conductivity and total dissolved solids – What is their precise relationship? Desalination. 72, 275-292. http://dx.doi.org/10.1016/0011-9164(89)80012-8.

Wang, Y., Ma, L., Mao, Y., Jiang, X., Xia, Y., Yu, K., Li, B., Zhang, T., 2017. Comammox in drinking water systems. Water Res. 116, 332 – 341. http://dx.doi.org/10.1016/j.watres.2017.03.042.

Wankel, S.D., Kendall, C., Paytan, A., 2009. Using nitrate dual isotopic composition ($\delta^{15}N$ and $\delta^{18}O$) as a tool for exploring sources and cycling of nitrate in an estuarine system: Elkhorn Slough, California. J. Geophys. Res. 114, G01011. http://dx. doi.org/10.1029/2008JG000729.

Wankel, S.D., Kendall, C., Pennington, J.T., Chavez, F.P., Payton, A., 2007. Nitrification in the euphotic zone s evidenced by nitrate dual isotopic composition: Observations from Monterey Bay, California. Global Biogeochem. Cycles. 21. http://dx. doi.org/10.1029/2006GB002723.

Ward, A.S., Gooseff, M.N., Fitzgerald, M., Voltz, T.J., Singha, K., 2014. Spatially distributed characterization of hyporheic solute transport during baseflow recession in a headwater mountain stream using electrical geophysical imaging. J. Hydrol. 517, 362 – 377. http://dx.doi.org/10.1016/j.jhydrol.2014.05.036.

Wassenaar, L.I., Hendry, M.J., Harrington, N., 2006. Decadal geochemical and isotopic trends for nitrate in a transboundary aquifer and implications for agricultural beneficial management practices. Environ. Sci. Technol. 40, 4626–32. http://dx.doi.org/10.1021/es060724w.

Watson, D., Doll, W., Jeffrey Gamey, T., Sheehan, J., Jardine, P., 2005. Plume and lithologic profiling with surface resistivity and seismic tomography. Ground Water. 43, 169–177. http://dx.doi.org/10.1111/j.1745-6584.2005.0017.x.

Weaver, J.W., Wilson, J.T., 2000. Diving plumes and vertical migration at petroleum hydrocarbon release sites. LUSTLine Bulletin. 36, 12 - 15 (https://www.clu-in.org/download/contaminantfocus/mtbe/EPA-Plume-Dive-LL36DvPlm.pdf).

Weil, R.R., Brady, N.C., 2017. The colloidal fraction fraction: seat of soil chemical and physical activity. In: Fox, D., Gilfillan, A. (Eds.), The Nature and Properties of Soils, fifteenth ed. Pearson Education, In (Chapter 8).

Wells, N.S., Hakoun, V., Brouyère, S., Knöller, K., 2016. Multi-species measurements of nitrogen isotopic composition reveal the spatial constraints and biological drivers of ammonium attenuation across a highly contaminated groundwater system. Water Res. 98, 363-375. http://dx.doi.org/10.1016/j.watres.2016.04.025.

Wendland, F., Blum, A., Coetsiers, M., Gorova, R., Griffioen, J., Grima, J., Hinsby, K., Kunkel, R., Marandi, A., Melo, T., Panagopoulos, A., Pauwels, H., Ruisi, M., Traversa, P., Vermooten, J.S.A., Walraevens, K., 2008. European aquifer typology: a practical framework for an overview of major groundwater composition at European scale. Environ. Geol. 55, 77 - 85. http://dx. doi.org/10.1007/s00254-007-0966-5.

Wendland, F., Hannappel, S., Kunkel, R., Schenk, R., Voigt, H.J., Wolter, R., 2005. A procedure to define natural groundwater conditions of groundwater bodies in Germany. Water Sci. Technol. 51, 249 - 257.

Wenk, C.B., Zopfi, J., Gardner, W.S., McCarthy, M.J., Niemann, H., Veronesi, M., Lehmann, M. F. 2014. Partitioning between benthic and pelagic nitrate reduction in the Lake Lugano south basin. Limnol. Oceanogr. 59(4), 1421–1433. http://dx. doi.org/10.4319/lo.2014.59.4.1421.

Werner, E., diPretoro, R.S., 2006. Rise and fall of road salt contamination of water-supply springs. Environ Geol. 51(4), 537–543. http://dx.doi.org/10.1007/s00254-006-0350-x..

Wexler, S.K., Goodale, C.L., McGuire, K.J., Bailey, S.W., Groffman, P.M., 2014. Isotopic signals of summer denitrification in a northern hardwood forested catchment. Proc. Natl. Acad. Sci. USA. 111 (46), 16413 - 16418. http://dx.doi.org/10.1073/pnas.1404321111.

Weymann, D., Well, R., Flessa, H., von der Heide, C., Deurer, M., Meyer, K., Konrad, C., Walther, W., 2008. Groundwater N_2O emission factors of nitrate-contaminated aquifers as derived from denitrification progress and N_2O accumulation. Biogeosci. 5, 1215–1226. http://dx.doi.org/10.5194/bg-5-1215-2008.

Whitman, T., Lehmann, J., 2015. A dual-isotope approach to allow conclusive partitioning between three sources. Nat. Commun. 6. http://dx.doi.org/10.1038/ncomms9708.

Whitmire, S.L., Hamilton, S.K., 2005. Rapid removal of nitrate and sulfate in fresh-water wetland sediments. J. Environ. Qual. 34, 2062–2071. http://dx.doi.org/10.2134/jeq2004.0483.

Widory, D, Petelet-Giraud, E., Negrel, P., Ladouche, B., 2005. Tracking the sources of nitrate in groundwater using coupled nitrogen and boron isotopes: a synthesis. Environ. Sci. Technol. 39(2), 539–548. http://dx.doi.org/10.1021/es0493897.

Wilson, J.T., Ross, R.R., Acree, S., 2005. Using direct-push tools to map hydrostratigraphy and predict MTBE plume diving. Ground Water Monitoring & Remediation. 25, 93–102. http://dx.doi.org/10.1111/j.1745-6592.2005.00031.x.

Winderl, C., Anneser, B., Griebler, C., Meckenstock, R.U., Lueders, T., 2008. Depth-resolved quantification of anaerobic toluene degraders and aquifer microbial community patterns in distinct redox zones of a tar oil contaminant plume. Appl. Environ. Microbiol. 74, 792–801. http://dx.doi.org/10.1128/AEM.01951-07.

Wöhling, T., Schöniger, A., Gayler, S. Nowak, W., 2015. Bayesian model averaging to explore the worth of data for soil-plant model selection and prediction. Water Resour. Res. 51, 2825–2846. http://dx. doi.org/10.1002/2014WR016292.

Woll, B., Mack, J., Ellerbusch, F. Vetter, J.R., 2003. Facilitating browfields transactions using Triad and environmental insurance. Remediation J. 13(2), 113-130. http://dx.doi.org/10.1002/rem.10067.

Wolterink, T.J., Williamson, H.J., Jones, D.C., Grimshaw, T.W., Holland, W.F., 1979. Identifying sources of subsurface nitrate pollution with stable nitrogen isotopes. U.S. Environmental Protection Agency, Washington DC (EPA–600/4–79–050).

Wong, W.W., Grace, M.R., Cartwright, I., Cook, P.L.M., 2014. Sources and fate of nitrate in a groundwater-fed estuary elucidated using stable isotope ratios of nitrogen and oxygen. Limnol. Oceanogr. 59, 1493 - 1509. http://dx.doi.org/10.4319/lo.2014.59.5.1493.

Wu, Y., Cheng, Y., Hubbard, C.G., Hubbard, S., Ajo-Franklin, J.B., 2018. Biogenic sulfide control by nitrate and (per) chlorate – A monitoring and modeling investigation. Chem. Geol. 476, 180 – 190. https://doi.org/10.1016/j.chemgeo.2017.11.016.

Wunderlich, A., Meckenstock, R. U., Einsiedl, F., 2013. A mixture of nitrite-oxidizing and denitrifying microorganisms affects the $\delta^{18}O$ of dissolved nitrate during anaerobic microbial denitrification depending on the $\delta^{18}O$ of ambient water. Geochim. Cosmochim. Acta. 119 (15), 31-45. http://dx.doi.org/10.1016/j.gca.2013.05.028.

Wyatt, D.E., Waddell, M.G., Sexton, G.B., 1996. Geophysics and shallow faults in unconsolidated sediments. Ground Water. 34, 326–334. http://dx.doi.org/10.1111/j.1745-6584.1996.tb01892.x.

References

Xue, D., Botte, J., De Baets, B., Accoe, F., Nestler, A., Taylor, P., Van Cleemput, O., Berglund, M., Boeckx, P., 2009. Present limitations and future prospects of stable isotope methods for nitrate source identification in surface - and groundwater. Water Res. 43(5), 1159-1170. http://dx.doi.org/10.1016/j.watres.2008.12.048.

Yan, G., Xing, Y., Xu, L.,Wang, J., Dong, X., Shan, W., Guo, L., Wang, Q. 2017. Effects of different nitrogen additions on soil microbial communities in different seasons in a boreal forest. Ecosphere. 8(7), e01879. http://dx.doi.org/10.1002/ecs2.1879.

Ye, M., Neuman, S.P., Meyer, P.D. , Pohlmann, K., 2005. Sensitivity analysis and assessment of prior model probabilities in MLBMA with application to unsaturated fractured tuff. Water Resour. Res. 41(12), W12429. http://dx.doi.org/10.1029/2005WR004260.

Zarnetske, J.P., Haggerty, R., Wondzell, S. M., Baker, M. A., 2011. Dynamics of nitrate production and removal as a function of residence time in the hyporheic zone. J. Geophys. Res. 116, G01025. http://dx.doi.org/10.1029/ 2010JG001356.

Zarroca, M., Bach, J., Linares, R., Pellicer, X. M., 2011. Electrical methods (VES and ERT) for identifying, mapping and monitoring different saline domains in a coastal plain region (Alt Empordà, Northern Spain). J. Hydrol. 409 (1–2) 407-422. http://dx.doi.org/10.1016/j.jhydrol.2011.08.052.

Zeigler, B.P., 1976. Theory of Modeling and Simulation. Wiley, New York.

Zelt, C. A., Azaria, A., Levander, A., 2006. 3D seismic refraction traveltime tomography at a groundwater contamination site. Geophys. 71(5), H67-H78. http://dx.doi.org/10.1190/1.2258094.

Zelt, C. A., Forsyth, D.A. 1994. Modeling wide-angle seismic data for crustal structure: Southeastern Grenville Province. J. Geophys. Res. 99(B6), 11687–11704. http://dx.doi.org/10.1029/93JB02764.

Zelt, C.A., 1999. Modelling strategies and model assessment for wide-angle seismic traveltime data. Geophys. J. Int. 139 (1),183-204. http://dx.doi.org/10.1046/j.1365-246X.1999.00934.x.

Zhang, Y., Benson, D.A., Meerschaert, M.M., LaBolle, E.M., 2007. Space-fractional advection-dispersion equations with variable parameters: Diverse formulas, numerical solutions, and application to the Macrodispersion Experiment site data. Water Resour. Res. 43, W05439. http://dx.doi.org/10.1029/2006WR004912.

Zhang, D., Li, X.-D., Zhao, Z.-Q., Liu, C.-Q., 2015. Using dual isotopic data to track the sources and behaviors of dissolved sulfate in the western North China Plain. Appl. Geochem. 52, 43-56. http://dx.doi.org/10.1016/j.apgeochem.2014.11.011.

Zheng, C., Gorelick, S. M., 2003. Analysis of solute transport in flow fields influenced by preferential flowpaths at the decimeter scale. Ground Water. 41, 142–155. http://dx.doi.org/10.1111/j.1745-6584.2003.tb02578.x.

Ziegler, C. K., 2006. Using mathematical models to assess sediment stability. Integr Environ Assess Manag. 2, 44–50. http://dx.doi.org/.1002/ieam.5630020109.

Ziegler, P.A. 1990. Geological Atlas of Western and Central Europe (Shell International Petroleum Maatschappij 2nd ed.). Geological Society, London.

Zollo, A., Judenherc, S., Auger, E., D'Auria, L., Virieux, J., Capuano, P., Chiarabba, C., de Franco, R.; Makris, J., Michelini, A., Musacchio, G. 2003. Evidence for the buried rim of Campi Flegrei caldera from 3-d active seismic imaging. Geophys. Res. Lett. 30, 2002. http://dx.doi.org/10.1029/2003GL018173,19.

Zschornack, L., Leven-Pfister, C., 2012. Direct Push Methods for Sampling of Soil, Soil Gas and Groundwater. In: M. Kästner, M., Braeckevelt, G., Döberl, G. Cassiani, M.P., Papini, C. Leven-Pfister, D.

References

Van Ree (Eds.), Model-Driven Soil Probing, Site Assessment and Evaluation – Guidance on Technologies. Sapienza University of Rome, Rome, Italy, pp. 175 – 186.

Zyvoloski, G., Kwicklis, E., Eddebarh, A.A., Arnold, B., Faunct, C., Robinson, B.A., 2003. The site-scale saturated zone flow model for Yucca Mountain: calibration of different conceptual models and their impact on flowpath. J. Contam. Hydrol. 62 – 63, 731 – 750. http://dx.doi.org/10.1016/S0169-7722(02)00190-0.

Appendices

Table A1. Preliminary major ion chemistry of groundwater samples collected depth-specifically between 17 and 18 June, 2014 in an attempt to discern the hotspot of the investigated nitrate plume before the implementation of the conceptual site model approach described in this study. See Figure 3.2 showing sampling locations on the map of the investigated study site.

								Cations[mg/L]				Anions [mg/L]			
Sample Date	Sample ID	Depth ranges below *WT	Longitude [°E]	Latitude [°E]	Elevation [m]	Groundwater EC [µS/m]	Dissolved oxygen [mg/L]	Ca^{2+}	Mg^{2+}	Na^{+}	K^{+}	SO_4^{2-}	HCO_3^-	NO_3^-	Cl^-
17/06/2014	Gw1-2	5.15-5.75 m	8.970277782	48.50037	337.323	2190	4.2	577	70	15	13	1253	391	22	30
17/06/2014	Gw1-1	5.75 -6.35 m	8.970277782	48.50037	337.323	2130	4.6	567	71	16	15	1247	392	22	30
17/06/2014	Gw2-3	6.15-6.75 m	8.972139661	48.49856	336.411	2200	5.2	576	76	13	15	1247	406	21	27
17/06/2014	Gw2-2	6.81-7.41 m	8.972139661	48.49856	336.411	2200	5.4	590	78	13	16	1264	406	21	27
17/06/2014	Gw2-1	7.42-8.02 m	8.972139661	48.49856	336.411	1902	5.1	464	92	15	24	1023	426	29	30
18/06/2014	Gw3-4	5.30-5.90 m	8.976112928	48.49835	335.449	2520	5.7	594	74	19	3.8	1303	392	16	30
18/06/2014	Gw3-3	5.90-6.50 m	8.976112928	48.49835	335.449	2520	5.3	590	76	21	4.7	1287	407	16	32
18/06/2014	Gw3-2	6.45-7.05 m	8.976112928	48.49835	335.449	2440	4.4	547	80	21	5.9	1219	401	17	37
18/06/2014	Gw3-1	7.05-7.65 m	8.976112928	48.49835	335.449	2440	4.2	556	82	20	6.1	1206	394	18	38
18/06/2014	Gw4-3	5.95-6.55 m	8.976997533	48.49975	334.933	2320	4.8	520	77	13	21	1136	404	21	27
18/06/2014	Gw4-2	6.56-7.16 m	8.976997533	48.49975	334.933	2100	4.3	531	77	13	20	1136	414	21	27
18/06/2014	Gw4-1	7.12-7.72 m	8.976997533	48.49975	334.933	2310	5	501	77	13	21	1133	414	21	27

*WT = water table

Table A2 Details of the Schlumberger vertical electrical sounding (VES) data acquisition parameters.

VES Sounding Direction	Longitude	Latitude	Elevation	Location:	Date:
E-W	8.972759	48.50275	337.402 m	Wurlingen, near Tübingen, southeast Germany	19.06.2014
WUR-VES1	AB/2	MN	Full	Half Left	Half Right
1	1.5	1	35.3	24.7	10.7
2	2.5	1	22.8	13.1	9.7
3	4	1	28.8	15.4	13.4
4	6	1	35.3	19.2	16
5	8	1	22.6	11.7	10.7
6	10	1	44.9	23.8	21.3
7	12	1	48.7	25.5	22.9
8	15	1	55.3	28.6	26
9	20	1	65	34.4	30.6
10	25	10	54.9	30.1	25.2
11	25	1	71.5	38.2	33.7
12	30	10	60.5	33.5	27
13	40	10	72.3	41.8	30.2
14	60	10	90.3	58.6	32.1
Operators: Ahamefula Utom; Hao Li; Helko Kotas					

VES Sounding Direction	Longitude	Latitude	Elevation	Location:	Date:
NE-SW	8.973738	48.50254	335.98	Wurlingen, near Tübingen, southwest Germany	19.06.2014
WUR-VES2	AB/2	MN	Full	Half Left	Half Right
1	1.5	1	99.1	59.8	38.2
2	2.5	1	67.4	23.1	44.5
3	4	1	86.8	43.1	44.2
4	6	1	79.7	39.4	40.5
5	8	1	74.8	36.9	38.3
6	10	1	74.1	36.6	37.9
7	12	1	75.4	37.8	38.5
8	15	1	78.4	39.1	39.7
9	20	1	85.6	43.4	42.1
10	25	10	74.8	38.9	36.1
11	25	1	94	47.6	47.1
12	30	10	83.5	42.8	41
13	40	10	101.3	56.2	58.8
14	60	10	113.2	56.2	58.7
Operators: Ahamefula Utom; Hao Li; Helko Kotas					

Table A2 cont'd…

VES Sounding Direction	Longitude	Latitude	Elevation	Location:	Date:
E-W	8.972668	48.50235	336.093	Wurlingen, near Tübingen, southwest Germany	19.06.2014
WUR-VES3	AB/2	MN	Full	Half Left	Half Right
1	1.5	1	87.3	64.5	23.1
2	2.5	1	69.6	42.8	26.8
3	4	1	59.4	31.5	27.9
4	6	1	63.4	33.1	30.4
5	8	1	70.3	36.4	33.9
6	10	1	76.5	40.8	36
7	12	1	80.1	42.6	37.4
8	15	1	86.8	46.3	39.3
9	20	1	98.2	50.5	46.3
10	25	10	74.8	37.3	37.4
11	25	1	109.3	54.3	49.9
12	30	10	82.5	41.3	40.9
13	40	10	97.2	48.6	47
14	60	10	117.7	57.6	60
Operators: Ahamefula Utom; Hao Li; Helko Kotas					

VES Sounding Direction	Longitude	Latitude	Elevation	Location:	Date:
NE-SW	8.971333	48.50221	336.688	Wurlingen, near Tübingen, southwest Germany	19.06.2014
WUR-VES4	AB/2	MN	Full	Half Left	Half Right
1	1.5	1	41.3	25.8	15.6
2	2.5	1	38.4	20.6	17.9
3	4	1	38.4	19.9	18.6
4	6	1	43.9	24.3	19.6
5	8	1	45.6	25.3	20.5
6	10	1	48.7	27.5	21.2
7	12	1	51	29.2	21.9
8	15	1	54.5	31.4	23.5
9	20	1	58.5	33.4	25.4
10	25	10	71.7	39.1	32.8
11	25	1	64.1	38.1	126.6
12	30	10	74.7	40.1	34.4
13	40	10	82.7	46.6	36.5
14	60	10	103.1	60.2	43.7
Operators: Ahamefula Utom; Hao Li; Helko Kotas					

Table A2 cont'd…

VES Sounding Direction	Longitude	Latitude	Elevation	Location:	Date:
NE-SW	8.971243	48.50255	339.19	Wurlingen, near Tübingen, southwest Germany	19.06.2014
WUR-VES5	AB/2	MN	Full	Half Left	Half Right
1	1.5	1	28.3	18.7	9.6
2	2.5	1	15.9	7.8	8.1
3	4	1	16.6	8.8	7.8
4	6	1	19.9	10.79	9.3
5	8	1	23.9	12.7	11.3
6	10	1	27.5	13.5	13.7
7	12	1	32	15.8	16.6
8	15	1	40.7	22.8	17.9
9	20	1	50.7	16.1	22.1
10	25	10	58.4	35.2	23.1
11	25	1	61.9	34.8	29.4
12	30	10	67.7	41.9	25.8
13	40	10	84.7	57.2	28.5
14	60	10	115.1	78.7	40.9
Operators: Ahamefula Utom; Hao Li; Helko Kotas					

VES Sounding Direction	Longitude	Latitude	Elevation	Location:	Date:
NE-SW	8.970604	48.50175	337.181	Wurlingen, near Tübingen, southwest Germany	19.06.2014
WUR-VES6	AB/2	MN	Full	Half Left	Half Right
1	1.5	1	48.7	21.8	26.9
2	2.5	1	41.4	20	21.4
3	4	1	46.2	21.2	25
4	6	1	52.7	25	27.8
5	8	1	56.4	28.9	27.6
6	10	1	58.7	33.3	25.5
7	12	1	62.4	37.9	24.3
8	15	1	70.7	45.6	25
9	20	1	73.6	53.4	21.7
10	25	10	64.9	58.3	20.5
11	25	1	75.1	58.9	14.9
12	30	10	71.3	53.5	17.8
13	40	10	78.2	74.4	3.5
14	60	10	77.3	131.8	52.9
Operators: Ahamefula Utom; Hao Li; Helko Kotas					

Table A2 cont'd…

VES Sounding Direction	Longitude	Latitude	Elevation	Location:	Date:
E-W	8.971074	48.50097	337.833	Wurlingen, near Tübingen, southwest Germany	19.06.2014
WUR-VES7	AB/2	MN	Full	Half Left	Half Right
1	1.5	1	22.4	12.8	9.6
2	2.5	1	14.8	7	7.8
3	4	1	20.1	9.9	10.8
4	6	1	28.2	12.9	15.1
5	8	1	34.2	15.7	19
6	10	1	41.5	18.2	22.4
7	12	1	45.5	18.3	25.2
8	15	1	52.1	21.2	30.2
9	20	1	63.8	28.3	30.2
10	25	10	60.2	28.4	32.2
11	25	1	68.6	30.4	38.9
12	30	10	65.3	30.5	34.8
13	40	10	73.4	33.4	41.7
14	60	10	74.1	26.7	45.5
Operators: Ahamefula Utom; Hao Li; Helko Kotas					

VES Sounding Direction	Longitude	Latitude	Elevation	Location:	Date:
E-W	8.973651	48.50085	336.61	Wurlingen, near Tübingen, southwest Germany	11.06.2014
WUR-VES8	AB/2	MN	Full	Half Left	Half Right
1	1.5	1	16.6	7.4	9.4
2	2.5	1	19.5	8.9	10.6
3	4	1	24.1	10.6	13.8
4	6	1	33	14.1	18.9
5	8	1	40.5	17	23.3
6	10	1	48	20.7	27.3
7	12	1	54.9	23.5	33.1
8	15	1	64.7	27.1	36.5
9	20	1	78.3	34.8	44.7
10	25	10	80.3	38.9	44.4
11	25	1	82.8	38	48.7
12	30	10	92.7	44.6	48.7
13	40	10	107.2	50.2	59
14	60	10	115.4	52.7	67.3
Operators: Ahamefula Utom; Hao Li; Constantin Vogt					

Table A2 cont'd…

VES Sounding Direction	Longitude	Latitude	Elevation	Location:	Date:
N-S	8.973673	48.49994	336.19	Wurlingen, near Tübingen, southwest Germany	11.06.2014
WUR-VES9	AB/2	MN	Full	Half Left	Half Right
1	1.5	1	31	16.2	14.8
2	2.5	1	39.8	20.9	19
3	4	1	53.9	29.4	24.7
4	6	1	76.7	42.4	34.4
5	8	1	92.7	52.2	40.9
6	10	1	103.8	57.7	46.5
7	12	1	111.8	63.4	48.8
8	15	1	119	67.3	52.1
9	20	1	117	64.5	53
10	25	10	94.7	51.8	42.9
11	25	1	113.3	61.9	52.4
12	30	10	89.6	50.4	39.5
13	40	10	83.7	51	32.6
14	60	10	80.2	52.2	28.3
Operators: Ahamefula Utom; Hao Li; Constantin Vogt					

VES Sounding Direction	Longitude	Latitude	Elevation	Location:	Date:
N-S	8.973662	48.49938	336.194	Wurlingen, near Tübingen, southwest Germany	11.06.2014
WUR-VES10	AB/2	MN	Full	Half Left	Half Right
1	1.5	1	46.3	26.9	19.6
2	2.5	1	55.7	28.8	26.9
3	4	1	77.9	39.8	37.8
4	6	1	106.9	54.2	52.3
5	8	1	126.6	64.2	62.5
6	10	1	143.2	70.8	72.9
7	12	1	154.8	73.2	80.7
8	15	1	159.4	76.9	84.9
9	20	1	160.2	70.9	87.4
10	25	10	102.9	45.7	56.9
11	25	1	153.8	71.4	82.1
12	30	10	102.9	45.7	56.9
13	40	10	85.6	36.8	49.2
14	60	10	85.7	38.9	50.8
Operators: Ahamefula Utom; Hao Li; Constantin Vogt					

Table A2 cont'd…

VES Sounding Direction	Longitude	Latitude	Elevation	Location:	Date:
N-S	8.973684	48.49873	336.225	Wurlingen, near Tübingen, southwest Germany	11.06.2014
WUR-VES11	AB/2	MN	Full	Half Left	Half Right
1	1.5	1	41.6	21.7	20.1
2	2.5	1	48.1	24	24
3	4	1	71.8	34.4	36.2
4	6	1	101.7	47	54.4
5	8	1	129.4	60.4	69.8
6	10	1	146.8	68.1	78.5
7	12	1	147.1	61.9	85
8	15	1	162.2	74.9	89.4
9	20	1	158	64.6	89.4
10	25	10	127	65.3	64.1
11	25	1	136.6	51	82
12	30	10	118.9	62.1	57.5
13	40	10	107.1	56.3	51.9
14	60	10	97.1	55.4	42.5
Operators: Ahamefula Utom; Hao Li; Constantin Vogt					

VES Sounding Direction	Longitude	Latitude	Elevation	Location:	Date:
E-W	8.973344	48.49846	335.839	Wurlingen, near Tübingen, southwest Germany	11.06.2014
WUR-VES12	AB/2	MN	Full	Half Left	Half Right
1	1.5	1	49.8	28.5	21.7
2	2.5	1	59.5	31.8	28.4
3	4	1	81.5	43.4	39
4	6	1	113.1	58.5	55.8
5	8	1	137.6	71.6	67.8
6	10	1	158.1	82.5	77.9
7	12	1	170.9	90	81.9
8	15	1	184.2	96.7	89.4
9	20	1	198.5	102.2	91.2
10	25	10	194.3	85.5	77.7
11	25	1	189	112	89.9
12	30	10	154	81.3	74.1
13	40	10	144.3	76.7	69.4
14	60	10	132.2	78.3	54.2
Operators: Ahamefula Utom; Hao Li; Constantin Vogt					

Table A2 cont'd…

VES Sounding Direction	Longitude	Latitude	Elevation	Location:	Date:
E-W	8.972804	48.49848	335.871	Wurlingen, near Tübingen, southwest Germany	11.06.2014
WUR-VES13	AB/2	MN	Full	Half Left	Half Right
1	1.5	1	44	22	22.2
2	2.5	1	52.5	25.8	27.1
3	4	1	69.8	34.3	36
4	6	1	99.5	46.5	53.8
5	8	1	124.9	57	68.5
6	10	1	143.9	65.6	79.7
7	12	1	158.2	70.8	88.1
8	15	1	170.9	73.8	99.1
9	20	1	177.8	80.1	98.3
10	25	10	160.7	74.4	87.2
11	25	1	174.1	72.9	97.1
12	30	10	149.1	70.7	79.5
13	40	10	137.5	60.8	77.5
14	60	10	127	43.6	83.6
Operators: Ahamefula Utom; Hao Li; Constantin Vogt					

VES Sounding Direction	Longitude	Latitude	Elevation	Location:	Date:
E-W	8.972115	48.49851	336.602	Wurlingen, near Tübingen, southwest Germany	11.06.2014
WUR-VES14	AB/2	MN	Full	Half Left	Half Right
1	1.5	1	47.9	29.9	18.3
2	2.5	1	58.4	32.5	26.4
3	4	1	80.6	43.3	38
4	6	1	111.5	59.1	53.2
5	8	1	136.9	72.2	65.8
6	10	1	158.5	81.4	79.2
7	12	1	172.6	87.6	87
8	15	1	187.9	93.5	96
9	20	1	198.2	96.5	104
10	25	10	165.2	79.8	86.7
11	25	1	195	87.1	108.4
12	30	10	165.4	78.1	89.8
13	40	10	149.2	68.7	83.6
14	60	10	133.4	67.1	68.6
Operators: Ahamefula Utom; Hao Li; Constantin Vogt					

Table A2 cont'd…

VES Sounding Direction	Longitude	Latitude	Elevation	Location:	Date:
E-W	8.971354	48.49855	336.442	Wurlingen, near Tübingen, southwest Germany	11.06.2014
WUR-VES15	AB/2	MN	Full	Half Left	Half Right
1	1.5	1	49.65	28.9	17.2
2	2.5	1	59.66	31.5	25.4
3	4	1	83.59	42.2	37
4	6	1	113.72	59	52
5	8	1	138.17	72.1	64.8
6	10	1	156.98	81.4	79.2
7	12	1	170.77	87.6	87
8	15	1	183.69	93.4	96.8
9	20	1	190.23	96.2	103
10	25	10	185.59	79.8	86.7
11	25	1	180.53	87.1	99.4
12	30	10	171.03	77.1	92.3
13	40	10	149.81	67.5	82.6
14	60	10	125.32	67.1	67.6
Operators: Ahamefula Utom; Hao Li; Constantin Vogt					

VES Sounding Direction	Longitude	Latitude	Elevation	Location:	Date:
NW-SE	8.969164	48.49883	338.006	Wurlingen, near Tübingen, southwest Germany	11.06.2014
WUR-VES16	AB/2	MN	Full	Half Left	Half Right
1	1.5	1	42.4	16.5	24.8
2	2.5	1	43	19.8	20.2
3	4	1	65.3	34.1	36.7
4	6	1	89.1	43.9	45.6
5	8	1	109.5	58.2	51.9
6	10	1	124.8	56.9	68.2
7	12	1	135.2	62.1	72.9
8	15	1	138.1	57.2	79.5
9	20	1	131.5	63	76.1
10	25	10	134.5	52.3	85.5
11	25	1	156.3	49.3	102.1
12	30	10	131.2	44.5	88.2
13	40	10	127.3	33.6	92.2
14	60	10	120.3	4.4	116
Operators: Ahamefula Utom; Hao Li; Constantin Vogt					

Table A2 cont'd…

VES Sounding Direction	Longitude	Latitude	Elevation	Location:	Date:
NW-SE	8.968802	48.49912	338.403	Wurlingen, near Tübingen, southwest Germany	10.06.2014
WUR-VES17	AB/2	MN	Full	Half Left	Half Right
1	1.5	1	29.5	18.3	11.3
2	2.5	1	26.4	13.4	13.3
3	4	1	38.3	18.8	19.9
4	6	1	55.9	25.8	30
5	8	1	69.4	31.7	38.1
6	10	1	74.2	31.7	42.9
7	12	1	79	34	45.7
8	15	1	87.7	41.8	46.5
9	20	1	99.2	58.1	44.9
10	25	10	105.6	66.4	39.9
11	25	1	104.8	64.1	36.8
12	30	10	108.2	78.9	28.7
13	40	10	104.9	102	3.6
14	60	10	101.8	174.4	72.1
Operators: Ahamefula Utom; Hao Li; Constantin Vogt					

VES Sounding Direction	Longitude	Latitude	Elevation	Location:	Date:
N-S	8.968464	48.49942	338.815	Wurlingen, near Tübingen, southwest Germany	10.06.2014
WUR-VES18	AB/2	MN	Full	Half Left	Half Right
1	1.5	1	95	34.9	60.2
2	2.5	1	41.1	17.9	23
3	4	1	31.9	14.4	17.8
4	6	1	41	19.6	21.6
5	8	1	51.3	25.8	26.5
6	10	1	60.4	29.7	31.7
7	12	1	66.2	32.2	34.4
8	15	1	77.7	36.8	41
9	20	1	86.4	41.8	48
10	25	10	80.8	41.9	38.4
11	25	1	101.4	40.2	52.5
12	30	10	85.1	44.4	43.7
13	40	10	82.8	41.3	38.1
14	60	10	101.5	87	14
Operators: Ahamefula Utom; Hao Li; Constantin Vogt					

Table A2 cont'd…

VES Sounding Direction	Longitude	Latitude	Elevation	Location:	Date:
E-W	8.969431	48.49944	336.978	Wurlingen, near Tübingen, southwest Germany	10.06.2014
WUR-VES19	AB/2	MN	Full	Half Left	Half Right
1	1.5	1	26	11.6	15.3
2	2.5	1	35.1	16.8	18.5
3	4	1	50	25.5	25
4	6	1	68.2	35.2	33.6
5	8	1	82.2	42.7	40.2
6	10	1	93.9	47.9	46.5
7	12	1	103.5	52.4	52
8	15	1	113.8	56.1	55.3
9	20	1	122.8	60.5	61.8
10	25	10	93.6	46.6	48.5
11	25	1	128.6	64.2	67.3
12	30	10	96.5	49.5	48.5
13	40	10	101.3	53.4	43.9
14	60	10	110.1	71.6	41.9
Operators: Ahamefula Utom; Hao Li; Constantin Vogt					

VES Sounding Direction	Longitude	Latitude	Elevation	Location:	Date:
N-S	8.970349	48.50009	337.065	Wurlingen, near Tübingen, southwest Germany	10.06.2014
WUR-VES20	AB/2	MN	Full	Half Left	Half Right
1	1.5	1	46.1	14.3	18.8
2	2.5	1	35.8	18.7	17.2
3	4	1	45.9	26.4	19.9
4	6	1	57.1	31	26.3
5	8	1	66.2	34.8	32.2
6	10	1	73.3	36.4	36.9
7	12	1	81.3	40.3	41.3
8	15	1	106.4	43.7	46.3
9	20	1	103.8	54.1	51.8
10	25	10	99.7	48.8	49.3
11	25	1	113.8	58.6	53
12	30	10	103.4	50.5	52.2
13	40	10	108.3	54	54.3
14	60	10	113.8	58.4	58.6
Operators: Ahamefula Utom; Hao Li; Constantin Vogt					

Table A2 cont'd…

VES Sounding Direction	Longitude	Latitude	Elevation	Location:	Date:
N-S	8.970376	48.4997	336.963	Wurlingen, near Tübingen, southwest Germany	10.06.2014
WUR-VES21	AB/2	MN	Full	Half Left	Half Right
1	1.5	1	42.9	19.9	23
2	2.5	1	49.5	23.7	26.6
3	4	1	61.1	29.5	32.2
4	6	1	80	39.3	42.6
5	8	1	93.2	45.6	49.4
6	10	1	104.9	49.2	56.5
7	12	1	115	57.5	59.6
8	15	1	125.7	66.2	63.9
9	20	1	142.2	74.6	64.7
10	25	10	112.9	60.9	54.5
11	25	1	148.6	81.6	58.7
12	30	10	117.5	64	52.3
13	40	10	114.5	68.7	49.3
14	60	10	125.4	81.1	43.9
Operators: Ahamefula Utom; Hao Li; Constantin Vogt					

VES Sounding Direction	Longitude	Latitude	Elevation	Location:	Date:
N-S	8.970359	48.49925	337.022	Wurlingen, near Tübingen, southwest Germany	10.06.2014
WUR-VES22	AB/2	MN	Full	Half Left	Half Right
1	1.5	1	46.4	21.8	24.8
2	2.5	1	53.2	24	29.7
3	4	1	69	33.9	35.4
4	6	1	91.6	45.3	47.3
5	8	1	111.2	54	58.6
6	10	1	123.5	59.4	66.1
7	12	1	127.4	63.4	65
8	15	1	134	68.4	68.9
9	20	1	140	62.4	76.5
10	25	10	99.6	50.2	50.4
11	25	1	132.9	55	72.2
12	30	10	102.8	51.1	51.3
13	40	10	102.9	52.8	49.8
14	60	10	96	43.6	49.5
Operators: Ahamefula Utom; Hao Li; Constantin Vogt					

Table A2 cont'd…

VES Sounding Direction	Longitude	Latitude	Elevation	Location:	Date:
N-S	8.972013	48.50031	336.533	Wurlingen, near Tübingen, southwest Germany	10.06.2014
WUR-VES23	AB/2	MN	Full	Half Left	Half Right
1	1.5	1	100.7	34.7	65.8
2	2.5	1	54	28.7	25.6
3	4	1	63.4	32.3	31.5
4	6	1	72.7	35.6	37.4
5	8	1	80.7	38.4	42.9
6	10	1	87.9	41.1	46
7	12	1	88.1	40.5	47.8
8	15	1	92.6	39.1	51.5
9	20	1	88.2	37.5	51.1
10	25	10	67	28.4	38.6
11	25	1	87	31.5	53.7
12	30	10	65.5	27.2	38
13	40	10	65.7	30.7	37.1
14	60	10	74.4	45.7	34.2
Operators: Ahamefula Utom; Hao Li; Constantin Vogt					

VES Sounding Direction	Longitude	Latitude	Elevation	Location:	Date:
N-S	8.972105	48.49967	336.386	Wurlingen, near Tübingen, southwest Germany	10.06.2014
WUR-VES24	AB/2	MN	Full	Half Left	Half Right
1	1.5	1	71.3	37.8	33.8
2	2.5	1	74.4	38.7	36
3	4	1	86.3	43.5	43.5
4	6	1	107.4	52.5	55.7
5	8	1	125.8	60.5	66.5
6	10	1	136	63.3	73
7	12	1	139	63.7	75.5
8	15	1	144.2	64.2	78.1
9	20	1	139.6	55.4	84.8
10	25	10	108.7	44.6	63.3
11	25	1	136.3	54.7	83.7
12	30	10	102.4	39.7	63.7
13	40	10	100	32.9	67.9
14	60	10	106.7	25.7	79.3
Operators: Ahamefula Utom; Hao Li; Constantin Vogt					

Table A2 cont'd…

VES Sounding Direction	Longitude	Latitude	Elevation	Location:	Date:
N-S	8.972131	48.49922	336.327	Wurlingen, near Tübingen, southwest Germany	10.06.2014
WUR-VES25	AB/2	MN	Full	Half Left	Half Right
1	1.5	1	50	32.3	17.7
2	2.5	1	56.3	31.6	25.3
3	4	1	60.8	33.7	27.7
4	6	1	74.7	41.3	34.5
5	8	1	92.2	48	44.3
6	10	1	107.3	55.8	52
7	12	1	114.2	58.2	55.9
8	15	1	124.9	64.1	61.6
9	20	1	131.3	68.3	65.9
10	25	10	125.5	61.9	63.5
11	25	1	134.7	59.1	69.9
12	30	10	121.1	61.5	61.6
13	40	10	115.8	60.4	57.3
14	60	10	110.3	67.7	48.4
Operators: Ahamefula Utom; Hao Li; Constantin Vogt					

VES Sounding Direction	Longitude	Latitude	Elevation	Location:	Date:
N-S	8.972146	48.49878	336.345	Wurlingen, near Tübingen, southwest Germany	10.06.2014
WUR-VES26	AB/2	MN	Full	Half Left	Half Right
1	1.5	1	65.2	33	32.4
2	2.5	1	59.6	27	32.9
3	4	1	71.5	35.7	36.2
4	6	1	99.1	49.9	49.3
5	8	1	122.4	62	60
6	10	1	141.3	73.5	67.3
7	12	1	151.8	76.8	75.3
8	15	1	165.5	81	84.2
9	20	1	173	83.5	88.6
10	25	10	132.5	70.3	63
11	25	1	180.1	72.8	93.5
12	30	10	131.2	72.5	59.9
13	40	10	119.2	52.5	66.3
14	60	10	112.7	42.5	68.9
Operators: Ahamefula Utom; Hao Li; Constantin Vogt					

Table A2 cont'd…

VES Sounding Direction	Longitude	Latitude	Elevation	Location:	Date:
N-S	8.972163	48.49831	336.565	Wurlingen, near Tübingen, southwest Germany	10.06.2014
WUR-VES27	AB/2	MN	Full	Half Left	Half Right
1	1.5	1	71.7	37.6	34.1
2	2.5	1	65.6	33.8	32.1
3	4	1	86.1	43.6	42.5
4	6	1	115	57	58.6
5	8	1	141.9	69	73.3
6	10	1	161.5	81	80.9
7	12	1	179	86.8	94.8
8	15	1	188	89.3	97.6
9	20	1	179.4	79.1	98.3
10	25	10	153.3	74.8	79.8
11	25	1	190	80.1	104.2
12	30	10	148.6	73	74.3
13	40	10	134.4	69.4	72.7
14	60	10	142.2	71.1	61.4
Operators: Ahamefula Utom; Hao Li; Constantin Vogt					

Table A3. Compressional wave traveltimes [s] from reverse vertical seismic profiling recordings (with surface receivers and downhole sources)

Shot Depth	T_oG1	T_oG2	T_oG3	T_oG4	T_oG5	T_oG6	T_oG7	T_oG8	T_oG9	T_oG10	T_oG11	T_oG12
6.05	0.013813	0.013697	0.013115	0.012447	0.012388	0.01172	0.011167	0.010353	0.009509	0.009451	0.009335	**0.009248**
6.25	0.013842	0.013733	0.013174	0.012476	0.012417	0.011778	0.011225	0.010382	0.009538	0.009597	0.009364	**0.009319**
6.45	0.013871	0.013768	0.013203	0.012505	0.012447	0.011807	0.011254	0.010411	0.009568	0.009626	0.009393	**0.009364**
6.65	0.013901	0.013804	0.013232	0.012534	0.012476	0.011836	0.011283	0.01044	0.009597	0.009655	0.009422	**0.009408**
6.85	0.01393	0.013839	0.01329	0.012563	0.012505	0.011865	0.011341	0.010498	0.009626	0.009684	0.009451	**0.009422**
7.05	0.013959	0.013875	0.013348	0.012621	0.012534	0.011894	0.011371	0.010556	0.009655	0.009713	0.009538	**0.009495**
7.25	0.013988	0.01391	0.013406	0.01265	0.012563	0.011923	0.0114	0.010585	0.009684	0.009771	0.009568	**0.009538**
7.45	0.014017	0.013946	0.013464	0.012679	0.012592	0.011981	0.011429	0.010614	0.009713	0.009858	0.009655	**0.009611**
7.65	0.014075	0.013981	0.013523	0.012708	0.01265	0.012039	0.011545	0.010644	0.009771	0.009917	0.009713	**0.009655**
7.85	0.014104	0.014017	0.013552	0.012737	0.012708	0.012068	0.011574	0.010731	0.0098	0.009975	0.009829	**0.009713**
8.05	0.014133	0.014052	0.013581	0.012766	0.012766	0.012098	0.011632	0.010789	0.009946	0.01012	0.009917	**0.009902**
8.25	0.014191	0.014088	0.013639	0.012795	0.012795	0.012185	0.01169	0.010934	0.010062	0.010295	0.010062	**0.01003**
8.45	0.01425	0.014124	0.013813	0.012825	0.012883	0.012301	0.011894	0.011138	0.010265	0.010411	0.010236	**0.010101**
8.65	0.014337	0.014159	0.013842	0.012854	0.012941	0.012388	0.011923	0.011196	0.010382	0.010527	0.010324	**0.010172**
8.85	0.014395	0.014195	0.01393	0.012999	0.013144	0.012476	0.012156	0.011312	0.010527	0.010673	0.010527	**0.010243**
9.05	0.01454	0.01423	0.013959	0.013028	0.013232	0.012534	0.012214	0.011458	0.010673	0.010818	0.010702	**0.010314**
9.25	0.014569	0.014266	0.014017	0.013174	0.013261	0.012592	0.012243	0.011487	0.010702	0.010905	0.010731	**0.010385**
9.4	0.014598	0.014301	0.014075	0.013203	0.01329	0.01265	0.012272	0.011516	0.01076	0.010876	0.01076	**0.010456**
9.55	0.014628	0.014337	0.014104	0.013232	0.013319	0.012679	0.012301	0.011545	0.010789	0.010963	0.01076	**0.010527**

Table A3 cont'd…

Shot Depth	T_oG13	T_oG14	T_oG15	T_oG16	T_oG17	T_oG18	T_oG19	T_oG20	T_oG21	T_oG22	T_oG23	T_oG24
6.05	**0.008739**	0.008753	0.009509	0.009917	0.010469	0.010673	0.010847	0.011603	0.011894	0.012068	0.012476	0.013493
6.25	**0.008802**	0.008817	0.009538	0.009946	0.010527	0.010789	0.010905	0.01169	0.011952	0.012098	0.012534	0.013523
6.45	**0.008841**	0.008881	0.009568	0.009975	0.010556	0.010847	0.010963	0.01172	0.011981	0.012127	0.012563	0.013552
6.65	**0.008884**	0.008945	0.009626	0.010004	0.010585	0.010876	0.010992	0.011778	0.012039	0.012156	0.012577	0.013581
6.85	**0.008928**	0.009009	0.009684	0.010033	0.010614	0.010905	0.011022	0.011807	0.012068	0.012185	0.012621	0.01361
7.05	**0.009**	0.009073	0.009713	0.010091	0.010644	0.010934	0.011051	0.011836	0.012127	0.012214	0.01265	0.013639
7.25	**0.009073**	0.009137	0.009771	0.010149	0.010673	0.010963	0.01108	0.011865	0.012156	0.012243	0.012679	0.013668
7.45	**0.009131**	0.009201	0.009829	0.010178	0.010702	0.010992	0.011109	0.011923	0.012214	0.012272	0.012708	0.013697
7.65	**0.009204**	0.009265	0.009858	0.010236	0.01076	0.011022	0.011138	0.011981	0.012272	0.012301	0.012737	0.013784
7.85	**0.009233**	0.009329	0.009917	0.010324	0.010789	0.011051	0.011196	0.01201	0.012301	0.01233	0.012766	0.013813
8.05	**0.009291**	0.009393	0.010004	0.010411	0.010876	0.011196	0.011312	0.012068	0.01233	0.012388	0.012795	0.013871
8.25	**0.009451**	0.009538	0.010178	0.010527	0.01108	0.011341	0.011371	0.012156	0.012359	0.012447	0.012854	0.01393
8.45	**0.009524**	0.009684	0.010411	0.010702	0.011225	0.011487	0.011545	0.01233	0.012505	0.012534	0.013028	0.014046
8.65	**0.009626**	0.009771	0.010469	0.010818	0.011371	0.011574	0.011661	0.012388	0.012534	0.012592	0.013174	0.014133
8.85	**0.009742**	0.009917	0.010585	0.010905	0.011429	0.01169	0.011778	0.012447	0.012621	0.01265	0.013203	0.01422
9.05	**0.009815**	0.010033	0.01076	0.011051	0.011574	0.011778	0.011865	0.012592	0.012679	0.012825	0.013319	0.014337
9.25	**0.009887**	0.010091	0.010847	0.01108	0.011632	0.011807	0.011894	0.012621	0.012766	0.012854	0.013377	0.014366
9.4	**0.00996**	0.010149	0.010905	0.011138	0.011661	0.011836	0.011923	0.01265	0.012795	0.012883	0.013406	0.014395
9.55	**0.01012**	0.010178	0.010934	0.011196	0.01169	0.011865	0.011952	0.012679	0.012825	0.012912	0.013464	0.014453

Table A4. Direct push soil electrical conductivity logging and lithologic sampling location coordinates and surface elevation.

Location ID	Latitude (°N)	Longitude (°E)	Elevation (m, amsl)
DP soil electrical conductivity logging location coordinate and surface elevation			
EC13	48.50037302	8.973722603	336.192
EC14	48.49990188	8.973706079	336.152
EC15	48.49969892	8.973700097	336.074
EC16	48.49936183	8.973694135	336.137
EC17	48.49899622	8.973691444	336.149
EC7	48.50063366	8.971994154	336.69
EC8	48.50050775	8.972001563	336.49
EC9	48.49985342	8.972051112	336.562
EC10	48.50028324	8.97201482	336.389
EC11	48.49928883	8.97208616	336.403
EC3	48.501896	8.970333	337.617
EC4	48.50208487	8.971432416	336.467
EC5	48.50196805	8.970751273	337.283
EC6	48.50174	8.97372108	335.77
EC18	48.49874	8.970403	336.442
EC19	48.49970106	8.970375538	336.963
EC20	48.49854608	8.971353929	336.442
DP soil lithologic sampling location coordinate and surface elevation			
SS13	48.5004404	8.973725178	336.178
SS15A	48.49993005	8.973704522	336.202
SS15A	48.49955041	8.973697197	336.121
SS17	48.49905233	8.973690772	336.17
SS13	48.5004404	8.973725178	336.178

Table A5. Direct push multilevel groundwater sampling location coordinates and surface elevation.

Location ID	Latitude (°N)	Longitude (°E)	Elevation (m, amsl)
Gw8	48.50040898	8.972007199	336.446
Gw11	48.49928883	8.97208616	336.403
Gw13	48.50037302	8.973722603	336.192
Gw15	48.49969892	8.973700097	336.074
Gw17	48.49883538	8.973687492	336.071

Table A6. Representative results of hydrogeochemical analysis on groundwater samples collected from the studied aquifer.

Sample ID	Depth ranges below *GS	Temp [°C]	pH [-]	DO [mg/L]	EC [µS/m]	Eh [mv]	Ca^{2+} [mg/L]	Mg^{2+} [mg/L]	Na^{+} [mg/L]	K^{+} [mg/L]	SO_4^{2-} [mg/L]	HCO_3^{-} [mg/L]	NO_3^{-} [mg/L]	$**NO_2^{-}$ [mg/L]	Cl^{-} [mg/L]	Mn^{2+} [mg/L]	NH_4^{+} [mg/L]	Fe^{2+} [mg/L]	DOC [mg/L]
Gw17-1	6.75-7.25 m	13.7	6.72	4.07	2340	114.9	566	64.9	11.6	11.6	1291	431.09	16.6	-0.02	19.2	0.057	0.06	0.05	5.09
Gw17-2	6.5 -7.00 m	14.7	6.94	3.58	2390	117.1	535	59.4	11.2	11.2	1316	417.97	16.4	-0.02	18.8	0.038	<0.03	0.04	3.00
Gw17-3	6.25-6.75 m	15.5	6.81	3.62	2370	105.1	542	66.3	11.4	11.7	1283	417.97	16.2	0.02	18.8	0.07	<0.03	<0.04	5.09
Gw17-4	6.00-6.50 m	16.8	6.95	3.38	2370	98.6	532	65.7	11.1	11.1	1260	410.04	15.8	0.03	18.2	0.068	<0.03	<0.04	3.25
Gw17-5	5.75-6.25 m	16.8	6.91	3.01	2390	97.4	547	65.2	10.5	10.8	1273	411.26	16.7	-0.02	18.4	0.044	0.03	<0.04	5.58
Gw15-1	9.50-10.00 m	17.6	6.89	1.83	2670	9.8	516	61.9	9.92	4.85	1509	353.59	42.8	0.43	27.1	0.15	<0.03	0.08	<1,0
Gw15-2	9.25-9.75 m	15.8	6.94	1.33	2470	2.1	596	82.1	10.9	5.88	1336	374.95	41.3	0.53	33.4	0.183	0.16	0.08	<1,0
Gw15-3	8.75-9.25 m	15.2	7	0.14	2410	6.4	558	83.1	10.4	8.77	1317	389.29	37.3	0.48	26.5	0.198	0.06	<0.04	7.95
Gw15-4	8.25-8.75 m	17.4	7	0.3	2400	5.2	547	83.4	10	8.3	1277	392.95	36.9	0.47	29.8	0.17	<0.03	0.25	4.74
Gw15-5	7.75-8.25 m	16.9	7	0.43	2390	49.5	508	78.6	9.44	10.5	1235	398.75	29.1	0.38	23.9	0.092	0.03	0.14	3.27
Gw15-6	7.25-7.75 m	19.4	7	1.28	2450	58.9	607	71	11.1	8.17	1379	408.82	16.9	0.10	19.6	0.161	<0.03	0.11	8.06
Gw15-7	6.75-7.25 m	17.1	7.1	2.58	2470	37.9	616	63	10.7	4.52	1317	410.65	13	0.02	16.4	0.03	<0.03	0.19	8.30
Gw15-8	6.25-6.75 m	16.9	6.94	2.6	2480	33.2	608	62.8	10	4.17	1373	403.63	13.3	-0.02	16.7	0.017	<0.03	0.21	5.03
Gw15-9	5.75-6.25 m	16.6	6.98	2.5	2500	22.3	610	62.5	11	4.57	1391	408.21	13.5	-0.02	17.1	0.023	0.03	0.52	3.19
Gw13-1	6.80-7.30 m	16.3	6.99	2.05	2500	51.7	615	63.1	11.8	4.48	1373	410.04	12.5	0.03	19.4	0.044	<0.03	0.1	3.12
Gw13-2	6.30-6.80 m	17.2	6.88	1.9	2500	101.2	609	61.4	11.2	3.33	1399	417.36	12.4	-0.02	18.6	0.014	<0.03	0.06	2.84
Gw13-3	5.80-6.30 m	17.7	6.8	1.82	2500	67.7	626	62.8	11.3	3.5	1366	412.48	12	-0.02	18.2	0.036	<0.03	0.24	<1,0
Gw8-1	12.10-12.60 m	16.1	7	1.1	2490	-16.3	581	84.4	11.1	9.25	1407	404.54	19.4	0.11	18.8	0.09	0.05	0.51	4.30
Gw8-2	9.90-10.40 m	17.2	7.2	1.42	2330	21.5	575	69.1	9.33	4.79	1308	403.93	15.5	0.05	16.4	0.036	0.03	1.86	12.4
Gw8-3	9.10-9.60 m	20.4	7	0.16	2360	-109.6	482	110	12.2	11.5	1285	380.75	30.5	0.29	21.1	0.123	0.05	<0.04	8.38
Gw8-4	8.60-9.10 m	18.8	7.02	1.18	2440	33.2	575	82.8	11.4	9.09	1305	395.09	16.7	0.09	17.6	0.066	<0.03	0.05	9.48
Gw8-5	8.10-8.60 m	18.1	7.2	1.36	2450	29.6	545	78.5	11.3	9.09	1376	404.54	15	0.04	17.1	0.103	0.03	0.05	11.4
Gw8-6	7.60-8.10 m	18.5	7.1	1.37	2460	34.9	571	75.1	10.1	7.67	1360	402.71	14.3	0.04	16.7	0.074	0.03	<0.04	8.42
Gw8-7	7.10-7.60 m	15.6	7.1	1.62	2480	51.8	605	69.7	10.1	5.81	1370	403.32	13.5	0.02	16	0.049	<0.03	<0.04	11.2
Gw8-8	6.10-6.60 m	16.5	7	1.69	2490	46.8	611	63.6	9.73	4.09	1413	410.04	12.7	-0.02	15.8	0.011	<0.03	0.24	3.15
Gw11-1	6.00-6.50 m	18.9	7.05	1.33	2350	38.2	544	66.2	12.3	13.8	1239	415.83	19	-0.02	22.3	0.015	<0.03	<0.04	2.83
Gw11-2	5.50-6.00 m	18.5	6.99	1.27	2420	29.7	553	67	10.8	11.6	1250	419.80	19.2	-0.02	22.4	0.029	<0.03	<0.04	8.19

*GS = ground surface; ** The negative signs in the NO_2^{-} values indicate those values that are below the detection limit of 0.02 mg/L as plotted in Figure 4.24

Table A7. Representative results of multi ('dual')-isotope data of collected groundwater samples.

Sample ID	$\delta^{18}O\text{-}H_2O$	$\delta^{2}H\text{-}H_2O$	d-excess	$\delta^{34}S\text{-}SO_4^{2-}$	$\delta^{18}O\text{-}SO_4^{2-}$	$\delta^{15}N\text{-}NO_3^{-}$	$\delta^{18}O\text{-}NO_3^{-}$
Gw17-1	-8.7	-62.5	6.7	16.1	14.0	7.8	3.1
Gw17-2	-8.6	-62.2	6.5	15.9	13.2	7.4	3.9
Gw17-3	-8.7	-62.1	7.1	15.8	13.1	7.4	3.9
Gw17-4	-8.6	-62.3	6.6	16.3	13.4	7.2	4.0
Gw17-5	-8.5	-62.3	6.0	15.5	13.7	8.1	4.6
Gw15-1	-8.6	-61.9	6.5	16.2	13.8	14.2	12.6
Gw15-2	-8.5	-61.5	6.1	16.0	13.1	15.4	13.0
Gw15-3	-8.4	-61.7	5.3	16.2	13.1	15.1	12.5
Gw15-4	-8.5	-61.8	6.2	15.3	13.2	14.6	12.2
Gw15-5	-8.4	-61.7	5.6	16.1	13.4	14.2	12.4
Gw15-6	-8.5	-61.3	6.8	16.1	13.4	10.6	5.8
Gw15-7	-8.5	-62.4	5.6	16.0	13.4	6.7	3.4
Gw15-8	-8.5	-62.3	5.7	16.3	12.9	6.9	3.5
Gw15-9	-8.5	-62.3	6.1	16.1	12.8	6.8	3.5
Gw13-1	-8.6	-62.1	7.0	16.1	13.2	7.4	6.0
Gw13-2	-8.6	-62.4	6.0	16.2	13.4	6.4	4.5
Gw13-3	-8.6	-62.5	6.4	16.3	13.5	6.7	4.8
Gw8-1	-8.5	-61.8	6.2	16.3	13.7	14.5	11.3
Gw8-2	-8.5	-61.9	6.2	16.2	13.4	10.7	8.4
Gw8-3	-8.3	-62.2	4.6	15.8	13.2	17.9	15.0
Gw8-4	-8.4	-61.3	5.8	15.8	13.5	13.2	11.8
Gw8-5	-8.4	-61.4	5.4	15.5	12.9	11.0	8.1
Gw8-6	-8.3	-61.5	4.9	15.6	12.8	8.0	4.7
Gw8-7	-8.4	-62.1	5.3	15.4	13.5	7.3	3.5
Gw8-8	-8.4	-62.2	5.2	15.2	13.0	6.9	2.4

Figure A1. Direct push soil electrical conductivity (EC) logs and their location coordinate on the map across the study site. Locations of the vertical electrical sounding survey centres are also shown on the map and marked with the VES notation.